38th NOAA Climate Diagnostics and Prediction Workshop
Special Issue


College Park, MD

Climate Prediction S&T Digest

February 2014

NWS Science & Technology Infusion Climate Bulletin Supplement

Inside this issue:

NOAA's National Weather Service

Office of Science and Technology
1325 East West Highway
Silver Spring, MD 20910

Climate Prediction Center
5830 University Research Court
College Park, MD 20740

Although the skill of current operational climate prediction is limited and the research on the topic presents many challenges, there are promises of improvement on the horizon. To accelerate advancement in climate services, an effective mechanism of S&T infusion from research to operation for application is much needed. This bulletin has been established to clarify science-related problems and relevant issues identified in operation, helping our partners in the research community to understand which R&D activities are needed to "shoot arrows at the target".

Science and Technology Infusion Climate Bulletin
http://www.nws.noaa.gov/ost/climate/STIP/index.htm

National Weather Service
National Oceanic and Atmospheric Administration
U.S. Department of Commerce

PREFACE

It is with great pleasure that the Climate Prediction Center and the Office of Science and Technology offer you this synthesis of the 38th Climate Diagnostics and Prediction Workshop. The CDPW remains a must attend workshop for the climate monitoring and prediction community. As is clearly evident in this digest, considerable progress is being made both in our ability to monitor and predict climate. The purpose of this digest is to ensure that climate research advances are shared with the broader community and also transitioned into operations. This is especially important as NOAA works to enhance climate services both across the agency and with external partners. We hope you find this digest to be useful and stimulating. And please drop me a note if you have suggestions to improve the digest.

I would like to thank Dr. Jiayu Zhou of the Office of Science and Technology / NWS, for developing the digest concept and seeing it through to completion. This partnership between OST and CPC is an essential element of NOAA climate services.

Michael Halpert

Mike Halpert
Acting Director, Climate Prediction Center
National Centers for Environmental Prediction
NOAA's National Weather Service

CONTENTS

OVERVIEW

NOAA's 38th Climate Diagnostics and Prediction Workshop was held in College Park, Maryland, on 21-24 October 2013. It was hosted by the Climate Prediction Center (CPC) of National Centers for Environmental Prediction (NCEP) and the Cooperative Institute for Climate and Satellites (CICS) of University of Maryland; and co-sponsored by NOAA Climate Program Office (CPO) Modeling, Analysis, Predictions and Projections (MAPP) Program, and the Climate Services Division (CSD) of National Weather Service (NWS). The American Meteorological Society (AMS) was a cooperating sponsor.

To accelerate improvements in NOAA operational products and datasets, and delivery of climate information, this workshop brought NCEP and the broader climate community together to address the following themes:

1. Exploring potential sources of predictability on intra-seasonal to interannual (ISI) time scales;
2. Realizing prediction skill by improving forecast tools and techniques through dynamical models and statistical methods, forecaster practices and protocols, data quality and assimilation, and scientific best practices;
3. Enhancing monitoring and timely attribution and assessment of recent high impact weather, water, and climate events;

4. Improving the forecast evaluation process, including verification techniques, performance metrics, evaluating existing forecast tools, the process of phasing out old tools and implementing new forecast tools, and engaging users in the evaluation process;
5. Developing applications that enhance NOAA climate services by improving understanding of user needs and delivering the best available climate information for the NOAA societal challenges in water, coasts, extremes, and marine ecosystems.

This Digest is a collection of extended summaries of the presentations contributed by participants. The workshop is continuing to grow and expected to provide a stimulus for further improvements in climate monitoring, diagnostics, prediction, applications and services.

1. EXPLORING POTENTIAL SOURCES OF PREDICTABILITY ON ISI TIME SCALES

Science and Technology Infusion Climate Bulletin
NOAA's National Weather Service
38th NOAA Annual Climate Diagnostics and Prediction Workshop
College Park, MD, 21-24 October 2013

Observed Linkages between the Northern Annular Mode/North Atlantic Oscillation, Cloud Incidence, and Cloud Radiative Forcing

Ying Li and David W. J. Thompson
Department of Atmospheric Science, Colorado State University
Fort Collins, Colorado, U.S.A.

Yi Huang and Minghong Zhang
Department of Atmospheric and Oceanic Sciences, McGill University
Montreal, Quebec, Canada

1. Introduction

The northern annular mode/North Atlantic Oscillation (NAM/NAO) is the dominant pattern of climate variability in the Northern Hemisphere extratropical circulation (*e.g.*, Hurrell 1995; Thompson and Wallace 2000; Hurrell *et al.*, 2003). The NAM/NAO is associated not only with significant changes in the zonal wind but also in the mean meridional circulation and thus presumably the vertical structure of cloud incidence. The objective of this study is to examine and interpret the signature of the NAM/NAO in the horizontal and vertical structures of cloud incidence and cloud radiative forcing using nearly five years of CloudSat/CALIPSO data.

2. Data and methodology

2.1 Data

We use the cloud fraction data obtained from the combined radar and lidar retrievals 2B- GEOPROF-LIDAR product (version P2R04; Mace *et al.* 2009). The results are presented in terms of "cloud incidence", which provides a quantitative estimate of the likelihood of a cloud within a given volume sensed by the satellite (Verlinden *et al*., 2011; Li and Thompson 2013; Li *et al.* 2014). The analyses here are based on ~5 years of CloudSat observations from June 2006 through April 2011.

Various fields are also derived from monthly-mean output from the European Centre for Medium Range Weather Forecasts (ECMWF) Interim Reanalysis (ERA-Interim) (Simmons *et al.* 2007). The ERA-Interim is used to calculate the surface temperature, atmospheric temperature, specific humidity, surface albedo, top of the atmosphere (TOA) radiation fluxes anomalies associated with the NAM/NAO. It is also used to supplement the satellite derived cloud incidence.

2.2 Decomposition of radiation anomalies associated with NAM/NAO

We apply the radiative kernel method (Huang *et al.* 2007; Soden *et al.* 2008; Shell *et al.* 2008) to diagnose variations in TOA radiative fluxes associated with the NAM/NAO. The longwave radiative flux anomalies are decomposed into contributions from changes in surface and atmospheric temperature, atmospheric water vapor, and cloud; the shortwave radiative flux anomalies are decomposed into contributions from changes in surface albedo, atmospheric water vapor, and cloud.

Taking the longwave radiation anomalies as an example, the clear- and all-sky anomalies are decomposed as:

$$\Delta R^{clear} = \Delta R_T^{clear} + \Delta R_q^{clear} + Z^{clear} \quad (1)$$

$$\Delta R^{all} = \Delta R_T^{all} + \Delta R_q^{all} + \Delta R_{cloud} + Z^{all} \quad (2)$$

Correspondence to: Ying Li, Department of Atmospheric Science, Colorado State University, Fort Collins, Colorado; E-mail: yingli@atmos.colostate.edu.

where ΔR denotes the TOA longwave radiation anomalies associated with the NAM/NAO, ΔR_T, ΔR_q and ΔR_{cloud} represent contributions from change in surface and atmospheric temperature, atmospheric water vapor, and cloud, respectively. Z is the residual term, which provides a measure of the fidelity of the linear decomposition assumption.

The non-cloud contributions are calculated as follows:

$$\Delta R_T = \frac{\partial R}{\partial T}\Delta T; \quad \Delta R_q = \frac{\partial R}{\partial q}\Delta q \tag{3}$$

where $\frac{\partial R}{\partial T}$ and $\frac{\partial R}{\partial q}$ are the pre-calculated global radiative kernels based on the Geophysical Fluid Dynamics Laboratory (GFDL) general circulation model (GCM) (Soden *et al.* 2008); ΔT and Δq correspond to regression anomalies in surface and atmospheric temperature and atmospheric water vapor, respectively, associated with the NAM/NAO.

The cloud contribution is derived by combining equations (1) and (2):

$$\begin{aligned}\Delta R_{cloud} &= \left(\Delta R^{all} - \Delta R^{clear}\right) - \left(\Delta R_T^{all} - \Delta R_T^{clear}\right) - \left(\Delta R_q^{all} - \Delta R_q^{clear}\right) \\ &= \left(\Delta R^{all} - \Delta R^{clear}\right) - \left(\frac{\partial R^{all}}{\partial T} - \frac{\partial R^{clear}}{\partial T}\right)\Delta T - \left(\frac{\partial R^{all}}{\partial q} - \frac{\partial R^{clear}}{\partial q}\right)\Delta q\end{aligned} \tag{4}$$

Note that the cloud radiative forcing (CRF) is defined as the difference between all- and clear- sky radiative anomalies ($CRF \equiv \Delta R^{all} - \Delta R^{clear}$) so that ΔR_{cloud} obtained by adjusting the CRF for the impacts of changes in T and q is often referred to as *adjusted* CRF (Shell *et al.* 2008; Soden *et al.* 2008).

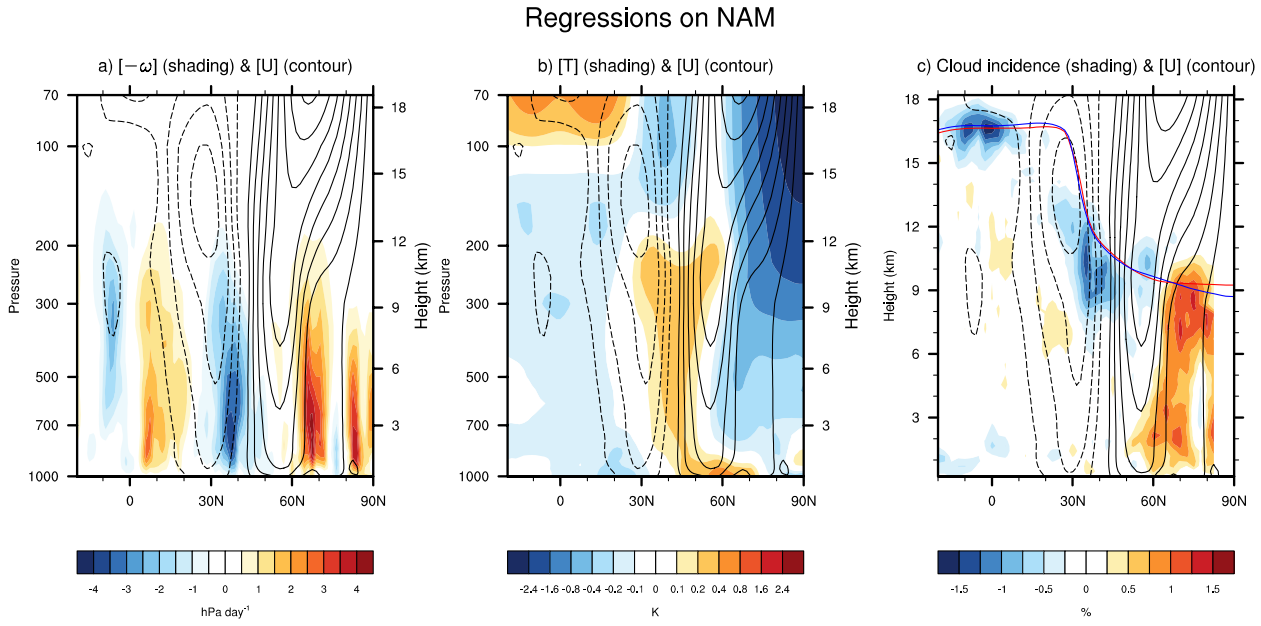

Fig. 1 Regressions of zonal-mean (a) pressure vertical motion (shading; ω has been multiplied by −1 so that positive values correspond to upward motion) and zonal wind (contour), (b) temperature (shading) and zonal wind (contour), and (c) cloud incidence (shading) and zonal wind (contour) onto standardized monthly-mean values of the anomalous NAM/NAO index. Results are based on October–March data from June 2006–April 2011. The seasonal cycle has been removed from the data. Units are K (temperature), hPa day^{-1} (pressure vertical motion) and % (cloud incidence). Contour interval of zonal wind is 0.5 m s^{-1} (dashed contours indicate negative values). The red and blue lines in (c) indicate the climatological-mean tropopause height plus and minus the regression of tropopause height onto the standardized NAM/NAO index, respectively. Tropopause height is identified using the WMO lapse rate definition.

3. Results

3.1 . Zonally averaged circulation

Figures 1 reviews key aspects of the signature of the NAM/NAO in the zonal-mean circulation (Figs. 1a and b), and corresponding changes in cloud incidence (Fig. 1c). The positive polarity of the NAM/NAO is characterized by increases in zonally averaged cloud incidence north of ~60ºN, decreases between ~25–50ºN, and increases in the subtropics (Figure 1c). For the most part, the largest anomalies in upper tropospheric cloud incidence coincide with the largest changes in vertical motion: downward anomalies in vertical motion at middle latitudes overlie decreases in cloud incidence; upward anomalies in vertical motion at high latitudes overlie increases in cloud incidence.

Figure 2 quantifies the zonal-mean downwelling TOA longwave radiation anomalies associated with the NAM/NAO. The very close agreement between the solid (calculated directly from the ERA-Interim reanalysis) and dashed lines (calculated from radiative kernel method) in panel a and c indicates that the residual terms in equations (1) and (2) are very small, and thus that the linear decomposition of TOA radiation

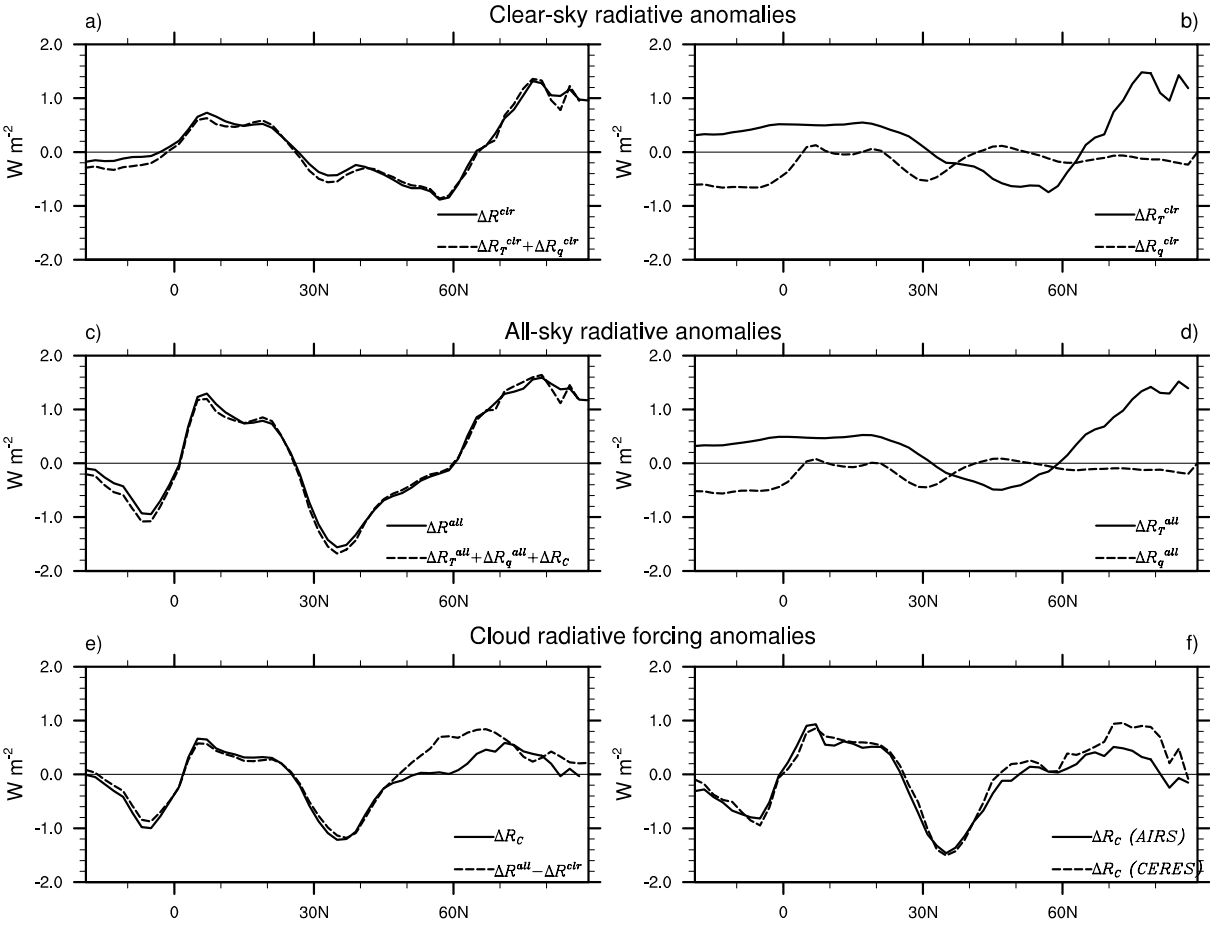

Fig. 2 (a) Zonal-mean TOA downwelling longwave clear-sky radiation anomalies associated with the NAM/NAO calculated directly from the ERA-Interim reanalysis (solid line) and derived from the sum of the contributions from various physical factors using the radiative kernel method (see Eq. 1; dashed line). (b) downwelling longwave radiation anomalies contributed from changes in temperature (solid line) and water vapor (dashed line). (c)-(d) As in (a)-(b), but for all-sky conditions. (e) adjusted cloud radiative forcing (CRF) estimated using the radiative kernel method [solid line, see Eq. 4)], and CRF anomalies estimated as the simple difference between the all- and clear-sky radiative fluxes (dashed line). (f) adjusted CRF based on AIRS (solid line) and CERES EBAF (dashed line) observations.

anomalies by the kernel method is robust. The non-cloud contributions to the net changes in longwave forcing are dominated by the changes in surface and atmospheric temperature (solid lines in panels b and d).

Figure 2e shows the changes in longwave CRF (dashed) and adjusted longwave CRF (solid) associated with variability in the NAM/NAO. Both results indicate: 1) longwave warming due to clouds north of ~60°N, where the NAM/NAO is associated with increases in cloud incidence; and 2) longwave cooling due to clouds between ~25–50ºN, where the NAM/NAO is associated with decreases in cloud incidence. The difference between the two longwave estimates within the latitude band ~50-70°N is centered over Northern Eurasia (not shown), where the large surface warming associated with the NAM/NAO is accompanied by strong cooling in the troposphere, and thus a large increase in the temperature lapse rate. As noted in Huang and Ramaswamy (2009), such a large change in the lapse rate may be mistaken for a cloud radiative effect in simple differences between all- and clear-sky radiation.

3.2 North Atlantic sector

Variations in the NAM/NAO are marked by a range of cloud incidence anomalies over the North Atlantic sector. A key result of Figure 3 is that the changes in upper tropospheric cloud incidence indicated by CloudSat are reproducible in the ERA-Interim reanalysis (compare Figure 3b and 3c), and they are qualitatively consistent with the attendant changes in anomalous vertical velocity (compare Figure 3a and 3b).

Figure 4 shows the geographical distribution of the downwelling TOA radiation anomalies associated with the NAM/NAO. The large contributions of the TOA longwave radiation anomalies due to changes in surface and atmospheric temperature are found over the continental areas, and are consistent with the negative Planck and lapse rate feedbacks.

The longwave cooling due to clouds peaks in a region extending eastward from the east coast of the U.S. to eastern Europe (Figure 4b), and is coincident with the decreases in high cloud incidence found over those locations (Figures 3b, c). The longwave warming due to clouds peaks over the subtropical North Atlantic and the subpolar North Atlantic (Figure 4b), and is coincident with the increases in high cloud incidence found over those regions (Figures 3b, c). The spatial consistency between the longwave adjusted CRF and the anomalous high cloud incidence from two independent datasets further corroborates the robustness of our estimate of variations in cloud radiative forcing due to variability in the NAM/NAO.

The shortwave adjusted CRF is negligible over high latitudes where the incident solar radiation is very weak during winter. Over the North Atlantic mid/low latitudes, the shortwave adjusted CRF is still a factor of 2–3 smaller in magnitude than that due to the longwave forcing. Thus, the total adjusted CRF associated with the NAM/NAO is dominated by the longwave component (Figure 4c).

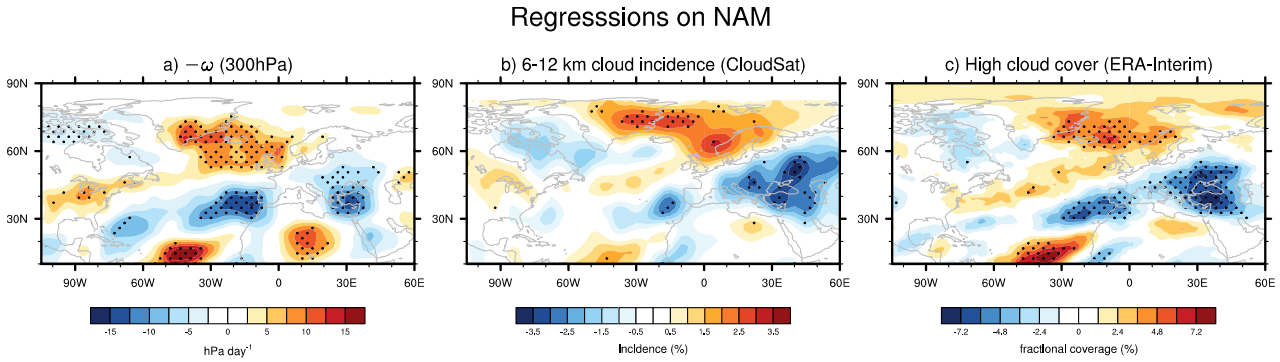

Fig. 3 Regressions of monthly-mean (a) pressure vertical motion (upward motion is positive) at 300 hPa, (b) cloud incidence averaged between 6–12 km based on CloudSat/CALIPSO dataset and (c) high-cloud fractional coverage based on ERA-Interim reanalysis onto standardized monthly-mean values of the anomalous NAM/NAO index. Stippling indicates results that exceed 95% confidence level based on a two-tailed test of the t-statistic, with the effective degrees of freedom computed given by equation (31) in Bretherton *et al.* (1999). The results in (a) and (b) have been smoothed with a NCAR Command Language (NCL) built-in 9-point smoothing function for the purpose of display only.

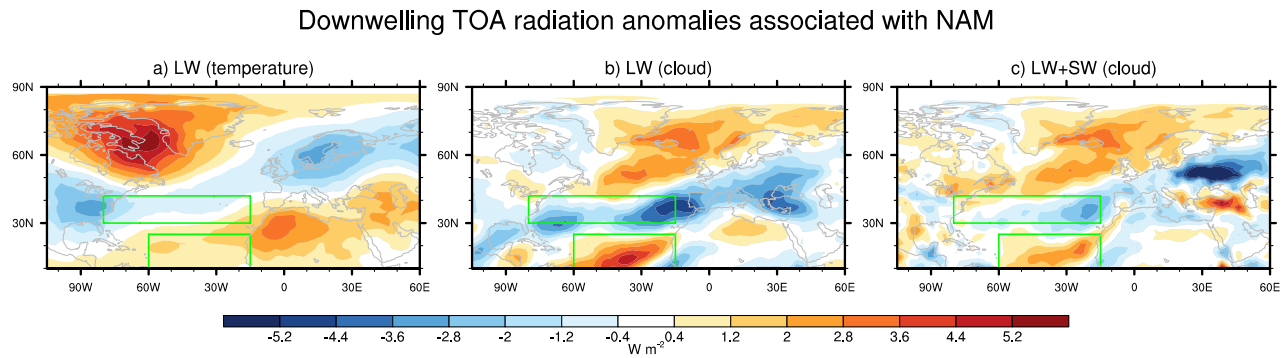

Fig. 4 TOA downwelling radiation anomalies associated with the NAM/NAO contributed from (a) temperature (longwave), (b) cloud (longwave), and (c) cloud (longwave+shortwave). Green boxes indicate example regions where the radiation forcing anomalies due to the changes in temperature and clouds coincide with each other (see text for detail).

4. Concluding remarks

We have explored the signature of the NAM/NAO in the vertical and horizontal distribution of clouds and adjusted CRF in both CloudSat/CALIPSO data and ERA-Interim reanalysis. The positive polarity of the NAM/NAO is marked by coherent and robust changes in cloud incidence that largely mirror its attendant changes in vertical motion. The changes in cloud incidence associated with the NAM/NAO, in turn, lead to marked anomalies in adjusted CRF. Over the North Atlantic, the anomalies in net adjusted CRF are due primarily to changes in the fluxes of longwave radiation, and are comparable in amplitude to the changes in radiative flux due to the NAM/NAO-related temperature anomalies. The primary cloud incidence and adjusted CRF anomalies associated with the NAM/NAO were found to be reproducible in independent data sources and using different analysis techniques (Figure 2e and compare Figure 3b and c).

In the absence of land-sea contrasts, the adjusted CRF anomalies associated with annular variability might be expected to shorten the timescale of the attendant temperature anomalies. For example: Regions of large-scale ascent and cooling are marked by increases in cloud incidence, and the resulting positive anomalies in longwave adjusted CRF should act to shorten the timescale of the negative atmospheric temperature anomalies (e.g., north of 60ºN in Figure 1 and 2e).

In the presence of large land-sea contrasts, the temperature anomalies associated with the NAM/NAO are dominated by horizontal temperature advection (as opposed to vertical motion). Over the high latitudes of the North Atlantic, the cloud and temperature radiative forcing anomalies associated with the NAM/NAO do not clearly coincide with each other (compare Figure 4a and 4c). Over the mid/low latitudes of the North Atlantic, the TOA adjusted CRF anomalies generally reinforce those due to the changes in temperature (*e.g.*, see green boxes of Figure 4). Hence over the mid/low latitudes of the North Atlantic, the adjusted CRF should act to shorten the timescale of the mid/low latitude temperature anomalies associated with the NAM/NAO. The importance of cloud and temperature radiative feedbacks in determining the timescale of large-scale atmospheric phenomena will be examined in a companion study.

References

Bretherton, C. S., M. Widmann, V. P. Dymnikov, J. M. Wallace, and I. Bladé, 1999: The effective number of spatial degrees of freedom of a time-varying field. *J. Climate*, **12**, 1990–2009.

Huang, Y., and V. Ramaswamy, 2009: Evolution and trend of the outgoing longwave radiation spectrum, *J. Climate*, **22**, 4637–4651, doi:10.1175/2009JCLI2874.1.

Huang, Y., V. Ramaswamy, and B. Soden, 2007: An investigation of the sensitivity of the clear-sky outgoing longwave radiation to atmospheric temperature and water vapor, *J. Geophys. Res.*, **112**, D05,104, doi:10.1029/2005JD006906.

Hurrell, J., Y. Kushnir, M. Visbeck, and G. Ottersen, 2003: An Overview of the North Atlantic Oscillation, in The North Atlantic Oscillation: Climatic Significance and Environmental Impact. *Geophys. Monogr. Ser.*, **134**, pp. 1–35, Amer. Geophys. Union, Washington D.C.

Hurrell, J. W., 1995: Decadal trends in the North Atlantic Oscillation regional temperatures and precipitation. *Science*, **269**, 676–679.

Li, Y., and D. W. J. Thompson, 2013: The signature of the stratospheric Brewer-Dobson circulation in tropospheric clouds. *J. Geophys. Res.*, **118**, 3486–3494.

Li, Y., D. W. J. Thompson, G. L. Stephens, and S. Bony, 2014: A global survey of the instantaneous linkages between cloud vertical structure and large-scale climate. *J. Geophys. Res.*, revised.

Mace, G. G., Q. Zhang, M. Vaughn, R. Marchand, G. Stephens, C. Trepte, and D. Winker, 2009: A description of hydrometeor layer occurrence statistics derived from the first year of merged CloudSat and CALIPSO data. *J. Geophys. Res.*, **114**, D00A26.

Shell, K. M., J. T. Kiehl, and C. A. Shields, 2008: Using the radiative kernel technique to calculate climate feedbacks in NCAR's Community Atmospheric Model. *J. Climate*, **21**, 2269–2282.

Simmons, A., S. Uppala, D. Dee, and S. Kobayashi, 2007: ERA-Interim: New ECMWF reanalysis products from 1989 onwards. *ECMWF Newsletter*, **110**, 25–35, ECMWF, Reading, United Kingdom..

Soden, B. J., I. M. Held, R. Colman, K. M. Shell, J. T. Kiehl, and C. A. Shield, 2008: Quantifying climate feedbacks using radiative kernels. *J. Climate*, **21**, 3504–3520.

Stephens, G. L., 2005: Feedbacks in the climate system: A critical review. *J. Climate*, **18**, 237–273.

Thompson, D. W. J., and J. M. Wallace, 2000: Annular modes in the extratropical circulation. Part I: Month-to-month variability. *J. Climate*, **13**, 1000–1016.

Verlinden, K. L., D. W. J. Thompson, and G. L. Stephens, 2011: The three-dimensional distribution of clouds over the Southern Hemisphere high latitudes. *J. Climate*, **24**, 5799–5811.

Science and Technology Infusion Climate Bulletin
NOAA's National Weather Service
38th NOAA Annual Climate Diagnostics and Prediction Workshop
College Park, MD, 21-24 October 2013

Towards Filling the Gap in NOAA's Seamless Suite of Forecast Products; Prospects of "Useful" Predictions for Weeks 3 & 4?

Muthuvel Chelliah

Climate Prediction Center, NCEP/NWS/NOAA, College Park, MD

1. Introduction

In the operational NOAA's seamless suite of weather and climate forecast products that are now issued to the public, there are products on "almost" all time scales ranging from minutes (in the form of alerts and warnings) to seasons and years (as guidance and outlooks). The Climate Prediction Center is responsible for forecast products beyond a week. At present, as can be seen from Fig.1, there are no official forecast products in the weeks 3-4 time frame, sometimes referred to as the 'black hole' in the forecast suite. In fact this "hole" has remained unfilled, even though NWS started issuing 5-day mean forecasts (circa 1940), monthly (early 1950s) and seasonal (early 1970s) climate outlooks a long time ago. In the early 1990s, while analyzing the Dynamical Extended Range Forecast (DERF) experiments' products data at former NMC (now NCEP), Huug van den Dool (1994) showed that there was very little forecast skill in the anomaly correlations of NMC's operational model's forecasts of daily mean 500mb geopotential height during weeks 3-4 (Fig. 2). About fifteen years later in Europe, Weigel *et al.* (2008) showed that the time averaged weeks 3 and 4 temperature forecasts skill remained still low with anomaly correlations hovering only between 0.1 and 0.2 all through the year for Northern/Southern Hemisphere or for Tropics. (Fig. 3).

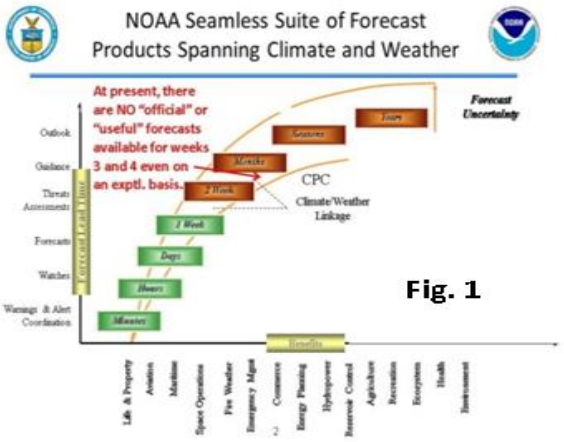

Fig. 1

Then recently at NCEP (Saha *et al.* 2013), a large dataset was created of 45-day forecasts, made 4 times a day (now 16) for about 12 years (1999-2010), using the latest state of the art data assimilation system and coupled ocean-sea ice-atmosphere climate forecast system (CFSv2) model. The schematic is shown in Fig. 4.

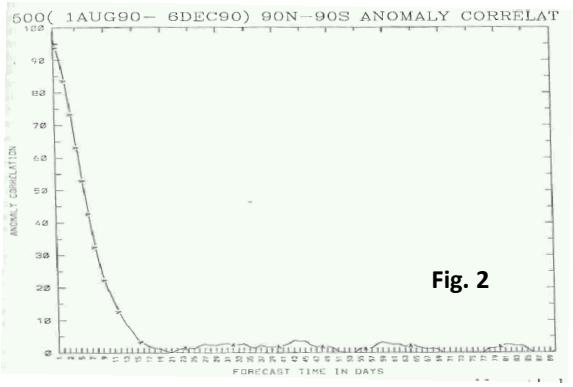

Fig. 2

Using this recent CFSv2 data set, we again evaluated the skill of week 3 (purple) and week 4 (light green) mean forecasts of 500 mb Geopotential height, and it is shown in Fig. 5 for the globe (top panel) and for a rectangular region over the continental US (bottom panel). To place the skill of weeks 3 and 4 in perspective, for comparison purposes, we also show the skill for days 1, 2, 5, wk1P (dys 6-10), and week 2. But weeks 3 and 4 forecasts still remain very low.

So the question becomes, when will the forecast skill of weeks 3-4 time scale improve? Do we just wait and hope the skill improves sometime in the future? Or do we need to think differently about the way we want to issue forecasts or the metrics we use for weeks 3-4 forecasts, since this time period is beyond weather time scale (up to 7-10 days) and less than climate time scale (month-season)?

Correspondence to: Muthuvel Chelliah, Climate Prediction Center, NCEP/NWS/NOAA, College Park, MD 20742;
E-mail: muthuvel.chelliah@noaa.gov.

While it is clear that for weather time scale, the future state of the atmosphere is sensitive mainly to the initial conditions of the "fast atmosphere", and for the longer climate time scales (month-season) the future climate is sensitive to the initial condition of the "slow ocean" as well as the intermediate land surface components, it is not even clear exactly what to call the weeks 3, and 4. Is it weather or climate?

Also note that the metric that was used in Figs. 2, 3 and 5 is the traditional anomaly correlation coefficient, where the anomalies for weeks 3 and 4 are computed as departures from some long term climatology. That is, we are treating this period as "climate". Is it really climate? Is this really the metric we want to use for this time scale? Is this why our forecast skill score as noted in Figs. 2, 3, and 5 has not improved over the last few decades in spite of the great advances and understanding in weather prediction and climate? Note that the typical weather forecast for tomorrow, the next few days up to a week (up to ten days in weather.com, or in accuweather.com) is NOT anomalies but the actual (total) temperature or precipitation amount.

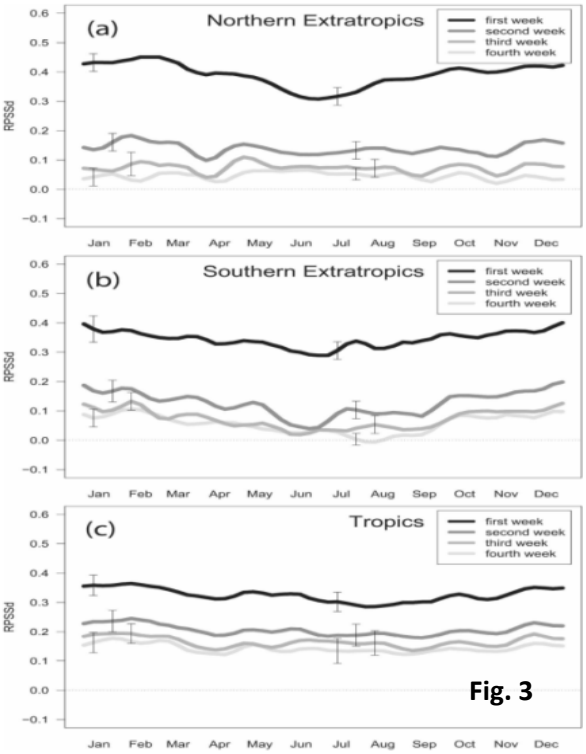

Fig. 3

Since the weeks 3-4 time period is neither weather, nor climate, we need a 'paradigm shift' in the way we look at forecasts for weeks 3 and 4. As this period is "weather-to-climate" transition period, why don't' we look at forecasts of "something new", that is neither the total field (weather) nor anomaly from a traditional long term mean climatology (climate)?

2. Propsal and discussion

I propose that on any given day, while issuing forecasts for weeks 3 and 4, we use terminology such as 'departure' from 'yesterday' or the 'past week's mean average conditions (see Fig. 4), since most likely people will remember how 'yesterday's weather was like, or the immediately previous week's weather was like. Such as, if it was too hot or cold. Was it dry or was it rainy? Is the general public more likely to remember this than some climatology? This kind of information will definitely be 'useful guidance' to the public regarding upcoming weeks 3 and 4 weather/climate conditions, with reference to something they experienced very recently. In Figs. 6 and 7 below, we show respectively the forecast skill score results for Weeks 1P, 2, 3 and 4 for Global 500 mb Heights and T2m respectively.

In Figs. 6 and 7, the top right panel shows results for week 3 forecast and bottom right panel is for week 4 forecast. Also shown for reference and comparison are week 1P (days 6-10) and week 2 forecast in top left and bottom left panels. The different lines are the average skill scores for the 1999-2010 period by different methods.

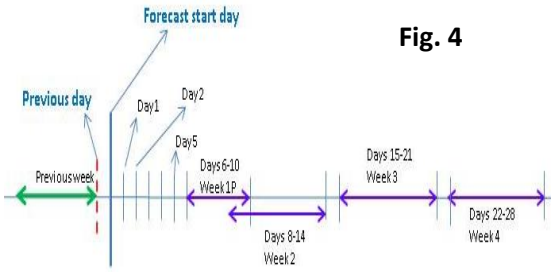

Fig. 4

In each panel, the blue line, all the way at the bottom, corresponding to the traditional anomaly correlation method (cf. Figs. 2, 3, and bottom 2 lines in both panels of Fig. 5), the skill is expectedly low. The yellow/orange line at the top is for the 'null' forecast, where the observed climatology (1999-2010 mean) itself is prescribed as forecast for each appropriate period in years 1999, 2000, … 2010. The black line near the top is the spatial 'correlation' among the full fields (not anomaly).

Here, as expected the skill is high since the fields are dominated by climatology. It is interesting however, that 'on average' using climatology for forecast (yellow line) is better than the black line. The red line is the correlation between the observed (analysis) and the forecast for week 3 (or week4, etc.) after subtracting the "previous 7 day mean" from both the verifying analysis and forecast fields. Note in both Figs. 6 and 7, the distance/difference between the blue and red lines gradually increases as we move farther out from wk1p forecast (top left panel) to week 4 (bottom right) forecast, thus showing how the 'traditional' skill score falls rapidly from wk1p to wk4. One criticism with the red line being so high is the presence of the residual effect of climatology among the correlated fields. To remove this effect from the red line, we further remove the 'climatology difference or tendency', - that is the climatology of the future verifying period minus the climatology of the previous 7 day mean - from the correlated fields. This result is shown in the green curve, which is below the red line. Forecasts for weeks 3-4 mean as departures from 'previous 1-day mean' (purple) are also shown. The correlation skill of the forecasts, if thought of as departures from previous 7-day or 1-day means, is quite high. It is hoped that this kind of guidance will be useful to public and industry alike.

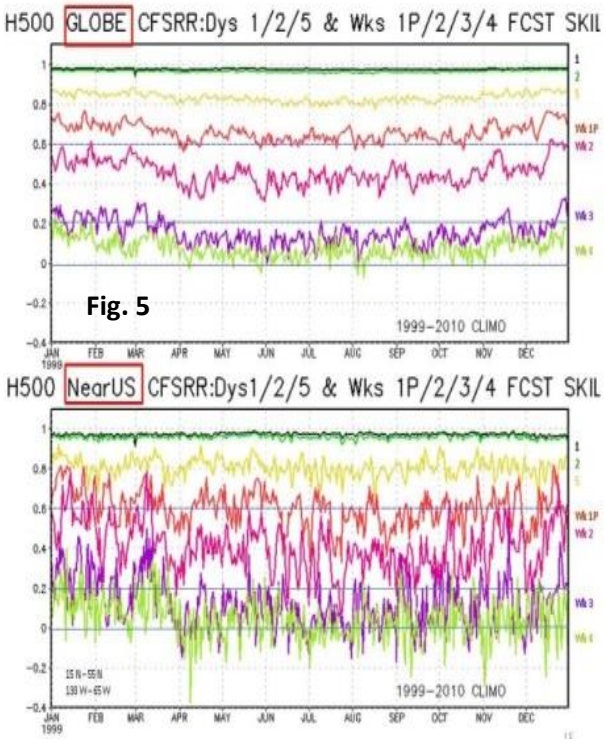

Fig. 5

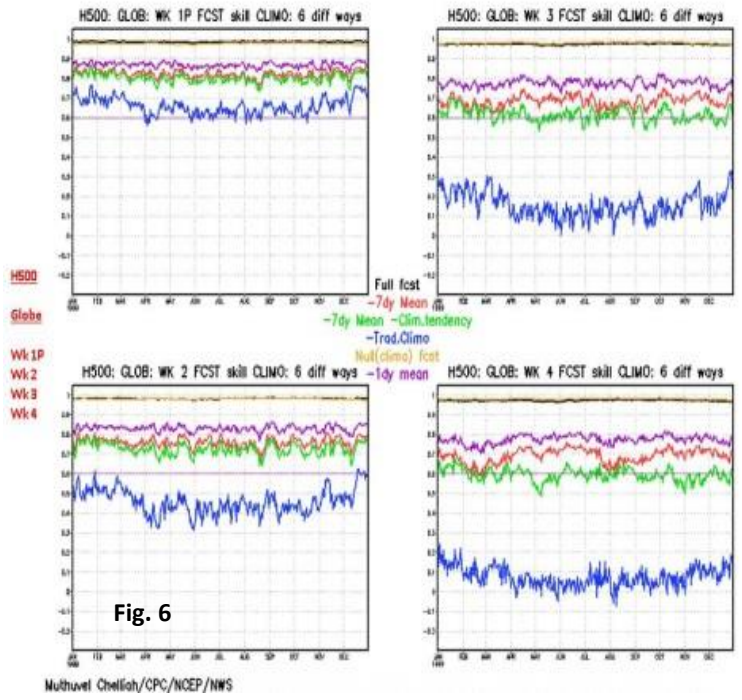

Fig. 6

3. Summary

At present we do not have any official forecast products (or even guidance) in the weeks 3-4 time frame. Based on the traditional anomaly (from a long term climatology) correlation skill metric, the forecast skill of operational models have remained very low (below 0.2) over the past 2-3 decades in spite of great improvements in other weather and climate prediction. Weeks 3-4 period is neither weather nor climate. This study proposes that we think differently about issuing weeks 3-4 forecast guidance to the public. Instead of treating weeks 3-4 as "climate" by evaluating the forecast anomaly as departures from some long term climatology, and then computing the correlations, which stil remains low, it is suggested that we treat the anomalies of weeks 3-4 as departures from most recent 1-day or 7-day means, which people are most likely to remember. In other words, we forecast the 'tendencies'. These tendencies in weeks 3 and 4 have much higher skill (~0.6 or higher) throughout the year even after accounting for and subtracting the "climatology tendency". It is hoped that forecasts for weeks 3-4 presented this way, will be useful to the public and industries alike.

References

Van den dool, H., 1994: Long range weather forecasts through numerical and empirical methods. *Dyn. of Atm.and Oceans*, **20**, 247-270.

Weigel, A.P., D. Baggenstos, M.A. Liniger, F. Vitart, and C. Appenzeller, 2008: Probabilistic verifitation of monthely temperature forecasts. *Mon.Wea. Rev.*, **136**, 5162-5182.

Saha, S., S. Moorthi, X. Wu, J. Wang, S. Nadiga, P. Tripp, D. Behringer, Y. Hou, H. Chuang, M. Iredell, M. Ek, J. Meng, R. Yang, M. Peña Mendez, H. van den Dool, Q. Zhang, W. Wang, M. Chen, and E. Becker, 2013: The NCEP Climate Forecast System Version 2. *J. Climate*. doi: 10.1175/JCLI-D-12-00823.1, in press.

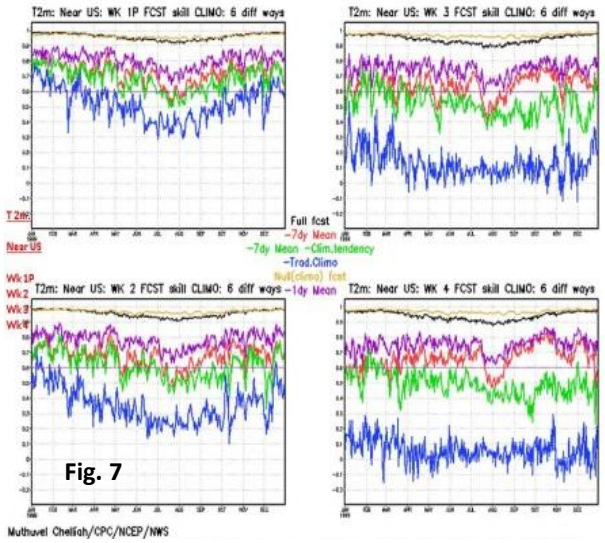

Fig. 7

Science and Technology Infusion Climate Bulletin
NOAA's National Weather Service
38th NOAA Annual Climate Diagnostics and Prediction Workshop
College Park, MD, 21-24 October 2013

Mechanisms for the Onset and Evolution of North American Monsoon

Ehsan Erfani[1, 2] and David L. Mitchell[1]

[1]*Desert Research Institute, Reno, Nevada*
[2] *University of Nevada, Reno, Nevada*

ABSTRACT

The North American Monsoon (NAM) is a seasonal shift in the large-scale circulation that supplies summertime precipitation in northwestern Mexico and US southwest. An understanding of the NAM's major governing processes is necessary to improve global and regional climate modeling, including the NAM's remote impacts on the summer circulation, precipitation and drought over North America.

In this study, we suggest a partial mechanistic understanding of the NAM. In the local scale, this mechanism helps to explain how the low-level moisture from the Gulf of California (GC) fuels the NAM rainfall. The proposed hypothesis is supported by satellite observations, ship soundings launched over the GC, and regional model (WRF) simulations.

North American Monsoon Experiment (NAME) field campaign in summer 2004 provides unique enhanced observational data such as multi network composite rainfall and Multiplatform-Merged (MPM) SST for evaluation of the model. WRF simulations show that warmer GC SSTs tend to enhance low-level moisture during this period and as a result more precipitation occurs over the foothills of Sierra Madre Occidental (SMO) and over US southwest. However, predicted inversions are stronger than those observed. This discrepancy may represent an opportunity to improve WRF performance over North America during summer.

1. Introduction

The North American Monsoon (NAM) provides about 60% - 80%, 45% and 35% of the annual precipitation for northwestern Mexico, New Mexico (NM) and Arizona (AZ), respectively (Douglas *et al.* 1993; Higgins *et al.* 1999). An intercomparison of regional climate models by Mearns *et al.* (2012) has shown that summer precipitation prediction over North America is the poorest in the NAM region. NAM rainfall is relevant to the amplification and northward shift of the upper level anticyclone over the southwestern US, called the monsoon anticyclone or monsoon high (Carleton *et al.* 1990; Higgins *et al.* 1999).

Several studies investigated the importance of GC SSTs on NAM rainfall. An empirical study of six monsoon seasons by Mitchell *et al.* (2002) indicated that no monsoon precipitation was observed in the

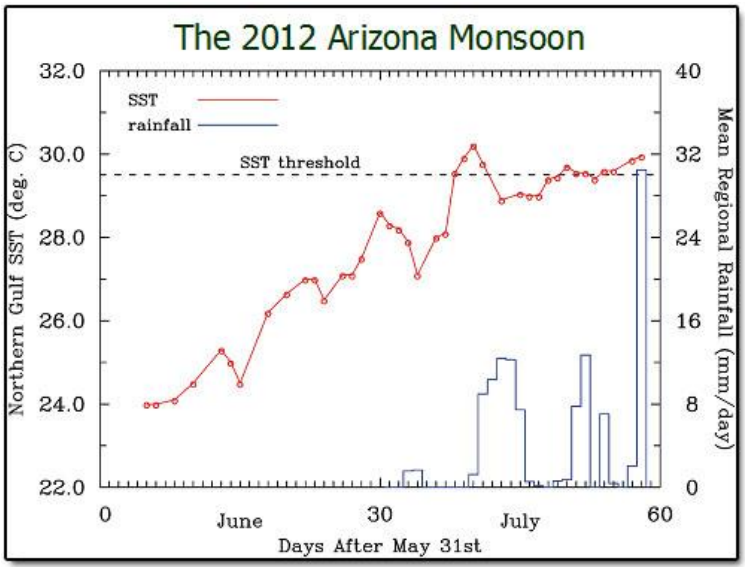

Fig. 1 Temporal evolution of Arizona rainfall rates and N. GC SST in June and July 2012. Similar results were seen in Mitchell *et al.* (2012) for five June–August seasons.

Correspondence to: Ehsan Erfani, Desert Research Institute and University of Nevada, Reno, Nevada;
E-mail: ehsan.erfani@dri.edu.

NAM region when GC SSTs did not exceed 26°C. They also showed that 75% of June-August precipitation in Arizona-New Mexico region occurred 0-7 days after the northern GC SSTs exceeded 29.5°C.

Although various observational and modeling studies showed some characteristics of the NAM, a mechanistic understanding of the NAM is still elusive. In this study, we offer a partial mechanism that addresses mesoscale processes. Section 2 discusses the relationship between GC SSTs, inversion cap and relative humidity based on both observations and numerical simulations. Conclusions are presented in section 3.

2. Results

In this research, we utilized sea surface temperature (SST) and rainfall amount observed from satellite, temperature and moisture profiles from ship soundings launched over the GC, and regional scale model simulation over the NAM region by WRF.

Following Mitchell *et al.* (2002), we have analyzed three other monsoon seasons at higher resolution regarding SST and AZ rainfall amounts, resulting in similar findings. Figure 1 shows the most recent example. All these findings indicate rainfall begins after the northern GC SST exceeding a threshold of 29.5°C. The mechanism for this relates to the marine boundary layer (MBL) over the northern GC (Figure 2). For SSTs < 29°C, the air over GC is capped by a strong inversion of ~ 50-200 m above the surface, restricting moisture to MBL in GC. The inversion generally disappears once SSTs exceed 29°C, allowing MBL moisture to mix with air in free troposphere. This results in a deep, moist layer that can be advected inland to produce thunderstorms.

A set of carefully designed simulations using WRF is conducted to investigate the dependence of NAM precipitation and onset on SSTs in the GC. WRF is able to simulate low level jet (LLJ) parallel to the GC axis during the 2004 monsoon onset. In agreement with observations, WRF simulations show that warmer GC SSTs tend to weaken the inversion that caps the GC MBL and increase low-level moisture

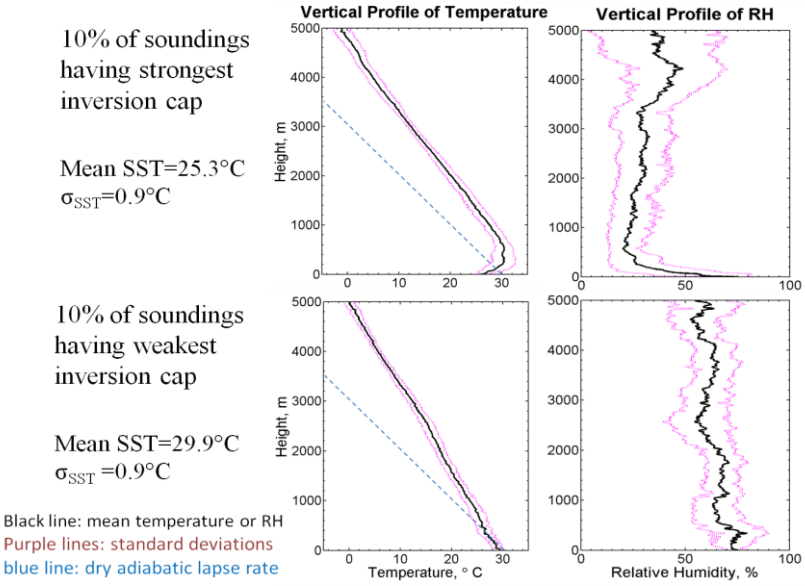

Fig. 2 Vertical profile of temperature (left panels) and relative humidity (RH) (right panels) for 10% of soundings having the strongest inversion cap over GC (upper panels) and for 10% of data having the weakest inversion cap over GC (lower panels) based on RV balloon sounding.

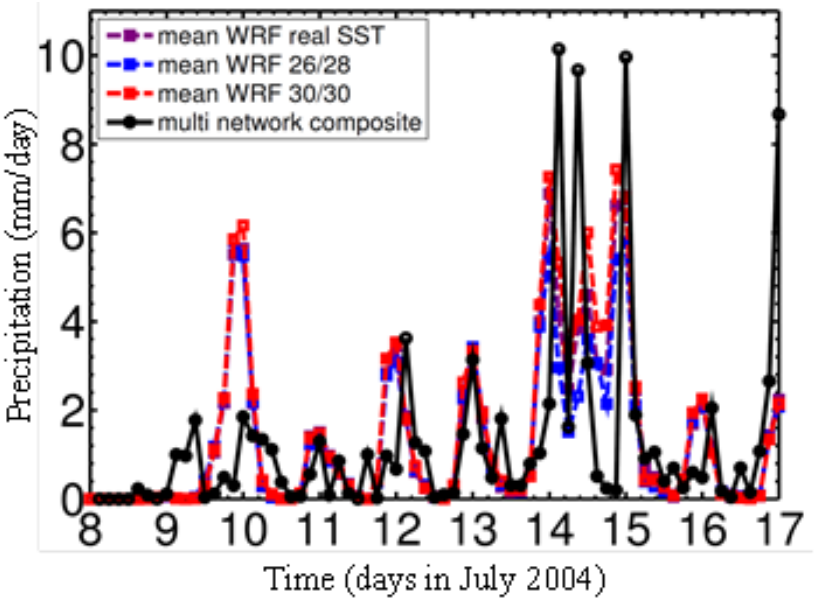

Fig. 3 Time series of precipitation rate in Arizona region for both observations and WRF simulations from 8 to 17 July 2004.

during this period. This leads to the rainfall enhancement in AZ region (Figure 3). However, WRF simulates a stronger inversion compared to observational soundings and as a result, moisture profiles in WRF simulations are drier compared to observational soundings (figure not shown). This might explain the underestimation of rainfall in WRF simulations compared to observations as shown in figure 3.

3. Conclusions

We suggest a mechanism to physically understand key processes governing NAM. The mechanism at the local scale is related to the MBL over northern GC. The strong low-level inversion, capping the top of shallow MBL, weakens with increasing SST and generally disappears once SSTs exceed 29°C, which allows the trapped MBL moisture to mix with free tropospheric air. This leads to a deep, moist, well-mixed layer that can be transported inland to form thunderstorms. WRF simulations generally agree with the observations, however overestimate the inversion and underestimate the moisture profile and rainfall. This discrepancy may represent an opportunity to improve WRF performance during summer over North America.

References

Carleton, A.M., D.A. Carpenter, and P.J. Wesser, 1990: Mechanisms of interannual variability of the southwest United States summer rainfall maximum. *J. Climate,* **3,** 999–1015.

Douglas, M.W., R.A. Madox, and K. Howard, 1993: The Mexican monsoon. *J. Climate*, **6,** 1665-1677.

Higgins, R.W., Y. Chen, and A.V. Douglas, 1999: Interannual variability of the North American warm season precipitation regime. *J. Climate,* **12,** 653-680.

Mearns, L.O., and Coauthors, 2012: The North American Regional Climate Change Assessment Program: Overview of Phase I Results. *Bull. Amer. Meteor. Soc.*, **93**, 1337–1362.

Mitchell, D.L., D.C. Ivanova, R. Rabin, T. J. Brown, and K. Redmond, 2002: Gulf of California sea surface temperatures and the North American monsoon: Mechanistic implications from observations. *J. Climate,* **15**, 2261-2281.

Science and Technology Infusion Climate Bulletin
NOAA's National Weather Service
38th NOAA Annual Climate Diagnostics and Prediction Workshop
College Park, MD, 21-24 October 2013

Coupling of Bay of Bengal Tropical Cyclones with the Myanmar Monsoon Onset

Boniface Opoku Fosu, and Shih-Yu Wang

Department of Plants, Soils, and Climate, Utah State University, Logan, UT

1. Introduction

The Madden-Julian Oscillation (MJO) greatly modulates the onset and intensity of the South Asian summer monsoon (*e.g.* Wu and Schubert 1999). The MJO also modifies the large-scale environment that leads to tropical cyclone (TC) development, such as those in the Bay of Bengal (BoB); (Kikuchi and Wang 2010). However, the extent to which the MJO affects monsoon onset and TC activity collectively and/or concurrently has not been analyzed. This study shows the extent to which certain MJO events provide favorable conditions for springtime (pre-monsoon) TCs in the BoB to occur concurrently with the monsoon onset in Myanmar.

Having only recently opened to the western world after years of civil unrest and political instability, Myanmar employs 65 percent of its active labor force in agriculture, an industry that is heavily reliant on monsoon rainfall. This country is also very vulnerable to TCs, such as Cyclone Nargis in May 2008 that killed about 126,000 people. The purpose of this study was to provide insight into predicting the Myanmar monsoon onset and to aid in disaster planning.

2. Data and methodology

The identification of yearly monsoon onset dates over Myanmar was focused on western and central Myanmar (16-23°N and 92-97°E). The APHRODITE gridded daily precipitation dataset (Yatagai *et al.* 2012) available on a 0.5° resolution was used from 1979-2010. In order to deal with the strong seasonal variability associated with the monsoon, we used the 5-days running mean of rainfall to define onset. The procedure is as follows: beginning April 1, the onset selection criterion was met on a day from which the accumulated rainfall of the preceding 14 days was less than the accumulated rainfall of the following 14 days. To ensure the difference between the two totals was substantial, as is expected for monsoon onsets, it had to be greater than a third of the total May precipitation (Fig 1). Using the selected onset dates, a composite rainfall evolution was constructed based on the relative day of onset in each year. The evolution starts with composites of rainfall sixty days prior to each onset, up until 40 days afterwards resulting in a 101-days composite of monsoon evolution. Day 0 is the composite onset, or May 20 on average.

Next, the European Centre for Medium Range Forecasts reanalysis dataset available on a 1.5° by 1.5° latitude and longitude grid (Dee *et al.* 2011), was used to derive 850-hPa streamfunction (ψ and velocity potential (χ).

Based on the 101-days evolution, two ψ fields were composited and averaged over longitude 80 -100°E: 1) total (shaded) and 2) 30-60 day band passed (contours, to depict the MJO signal). Furthermore, we made composites of χ using 30-60 days band passed fields. But unlike ψ, these composites were based on springtime cyclogenesis dates (*e.g.* Ventrice *et al.* 2011).

Lastly, empirical orthogonal functions (EOFs) of daily band passed VP fields were constructed from May 1 to June 30. The corresponding principal components (PCs) of the first two modes were used to construct phase-space diagrams. The PCs were normalized with their variances as a way to gauge the strength of the MJO at any time.

The tropical cyclone data was obtained from UNISYS (http://weather.unisys.com/hurricane/n_indian/index.php). Genesis day was defined when a disturbance was

Correspondence to: S.-Y. Simon Wang, Department of Plants, Soils, and Climate, Utah State University, Logan, Utah; E-mail: simon.wang@usu.edu.

first classified as a tropical depression in the North Indian Ocean (NIO). The tropical cyclogenesis days are plotted relative to the composite onset in Fig. 2, at the same latitude they occurred.

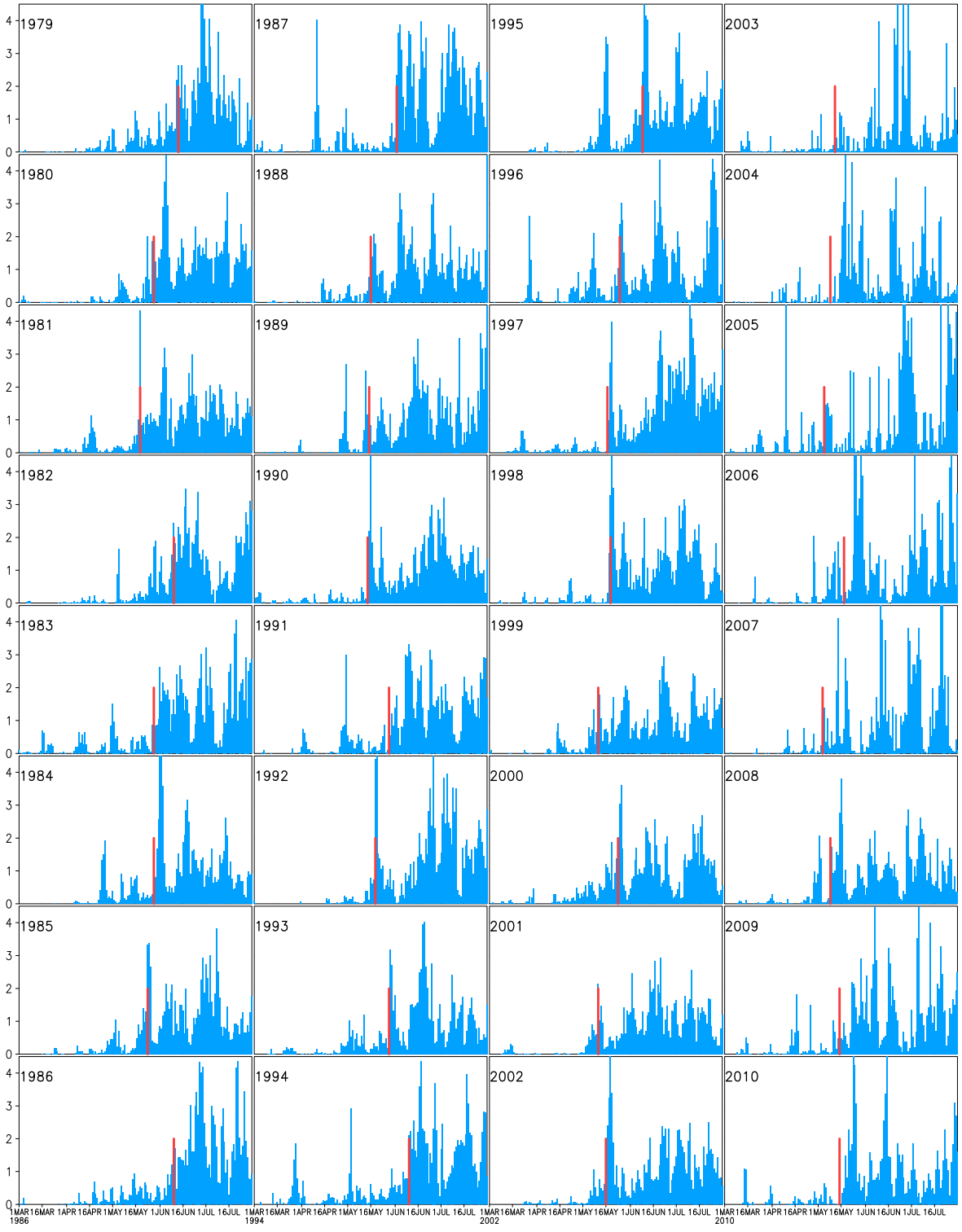

Fig. 1 Histograms of the mean daily 5-days running mean precipitation from March-July averaged over 16-23°N and 92-97°E (1979 to 2010). Each year is normalized with its corresponding mean May precipitation. The red lines show the onset dates.

3. Results and discussion

Fig. 2 shows the composite onset lies within the positive MJO phase. In the analysis, 26 out of the 32 onsets occurred during the positive phase of the MJO (not shown). This phase of the MJO enhances rising motion and acts to induce lower tropospheric convergence that leads to the intensification of the monsoon trough, as opposed to the dry phase, which suppresses rising motion. The monsoon is not a constant deluge of rainfall but it is characterized by regular breaks that have been associated with the negative phase of the MJO, otherwise known as monsoon breaks. Fig. 2 also shows the monsoon break occurs within the negative phase of the MJO. In addition, 11 of the 27 cyclogenesis cases are clustered around the composite onset, coinciding with the positive phase of the MJO. The large-scale positive circulation patterns of the MJO provide favorable conditions for tropical cyclogenesis, and also modulate the onset and breaks of the monsoon. It is now apparent that monsoon precipitation of western and central Myanmar is very sensitive to the phasing of the MJO with respect to the seasonal cycle. In general, the onsets (breaks) are associated with an increase (decrease) in cyclonic vorticity and a decrease (increase) in surface pressure over the central monsoon trough region, and a subsequent deepening (weakening) of the low level trough caused by the enhanced (suppressed) convection tendencies of the MJO positive (negative) phase.

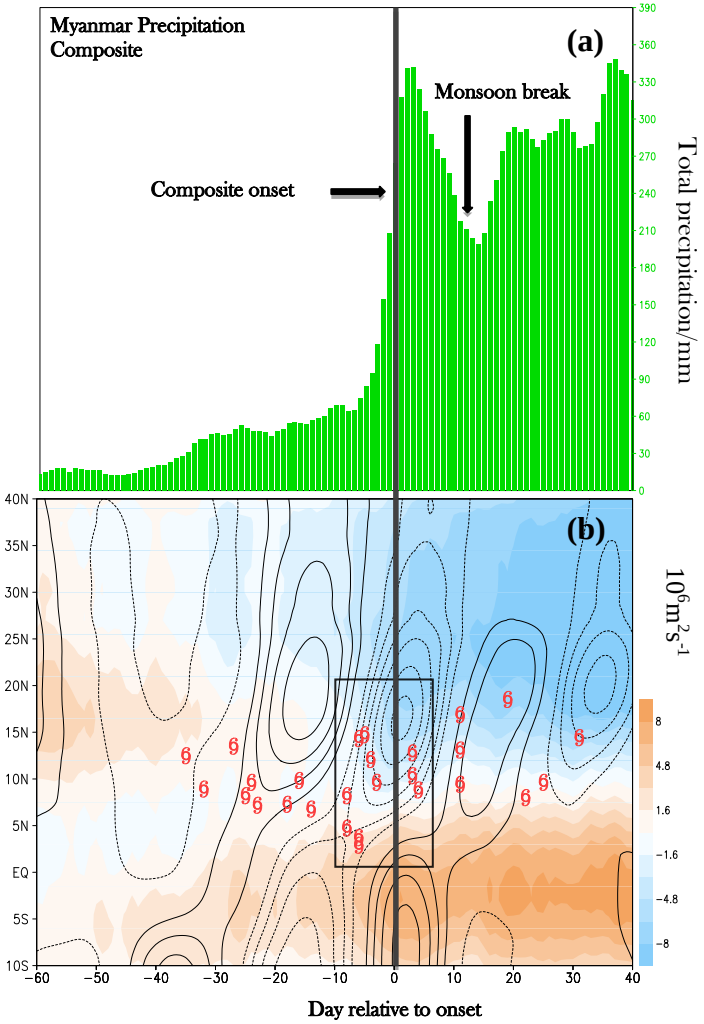

Fig. 2 (a) Evolution composite of rainfall accumulated averaged over western/central Myanmar (16-23°N and 92-97°E; 1979-2010. The composite onset day is May 20 (day 0, black line). (b) Evolution composite of 850-hPa total SF fields (raw data, shaded); superimposed with 30-60 days band passed streamfunction (SF, contours), averaged over longitude 80-100°E; and the locations of tropical cyclogenesis (red marks) relative to the onset from 1979-2010. The black box shows coupled onset-cyclogenesis events.

It is possible to see the relationship between TCs and the MJO in Fig. 2; however, the interpretation is different since those composites were made relative to the evolution composite of rainfall. By treating the TC genesis itself as part of a stochastic process that is driven by large-scale intraseasonal variability, and employing a composite χ method that averages all 27 TCs together as shown in Fig. 3, we are able to depict the synoptic convective and divergent variations associated with the eastward propagating MJO and bring out the large-scale environmental features favorable for TC formation in five-day increments.

The results so far illustrate how the MJO modulates the Myanmar monsoon onset and the majority of TC geneses in the BoB. But why did some TCs occur with the onset whiles others did not? In an attempt to explain this relationship, we analyze two groups of the EOF phase space diagrams and spatial plots: the coupled group comprises years where with TC and the Myanmar monsoon onset are coupled within 10 days of occurrence of one from the other. The other, which we will call the "decoupled group", was the years having no observed coupling (Fig 4). Comparisons of the two groups reveal that the coupled group has well

defined tracks of sequential days, which signifies a strong and systematic eastward propagation of the MJO. The second group shows the opposite for most years. We see weak MJO activity as rather random motions near the origin in most of those years. As we have already mentioned, since 1979, 11 out of the 27 monsoon onsets were coupled with TC genesis in the BoB within 10 days of formation, with at least 8 of them occurring earlier than the onset (Fig. 2b).

It appears when the tropical storm is formed (especially the stronger ones), the associated latent heating contributes to the intensification of the lower tropospheric westerlies. Together with the warm ocean waters in the NIO at this time, a low-level cyclonic circulation and an upper level anticyclone are formed, enhancing local cyclonic vorticity. As the positive phase of the MJO coincides with the emerging westerlies, the disturbances act to enhance local convection, westerly surface winds and low level cyclonic rotation that initiates the Myanmar monsoon onset. Thus the MJO helps the TC to form with the tendency of tracking eastwards toward Myanmar (Wang *et al.* 2013). The storm then releases substantial latent heating that concurrently, together with the MJO acts to intensify local convection and the emerging westerlies leading to the beginning of the onset over western and central Myanmar.

4. Concluding remarks

The work presented here suggests strong MJO events favor the coupling of spring TCs in the BoB with the Myanmar monsoon onset. It does so by modifying large-scale environmental features that favor TC geneses that subsequently initiate or intensify the monsoon onset over western and central Myanmar.

We have also showed that the large-scale circulation patterns of the MJO provide favorable conditions for tropical cyclogenesis, and in the meantime also modulate the onset of the Myanmar monsoon.

These results may provide guidance for seasonal and/or short-term prediction during the spring and early summer season in the BoB.

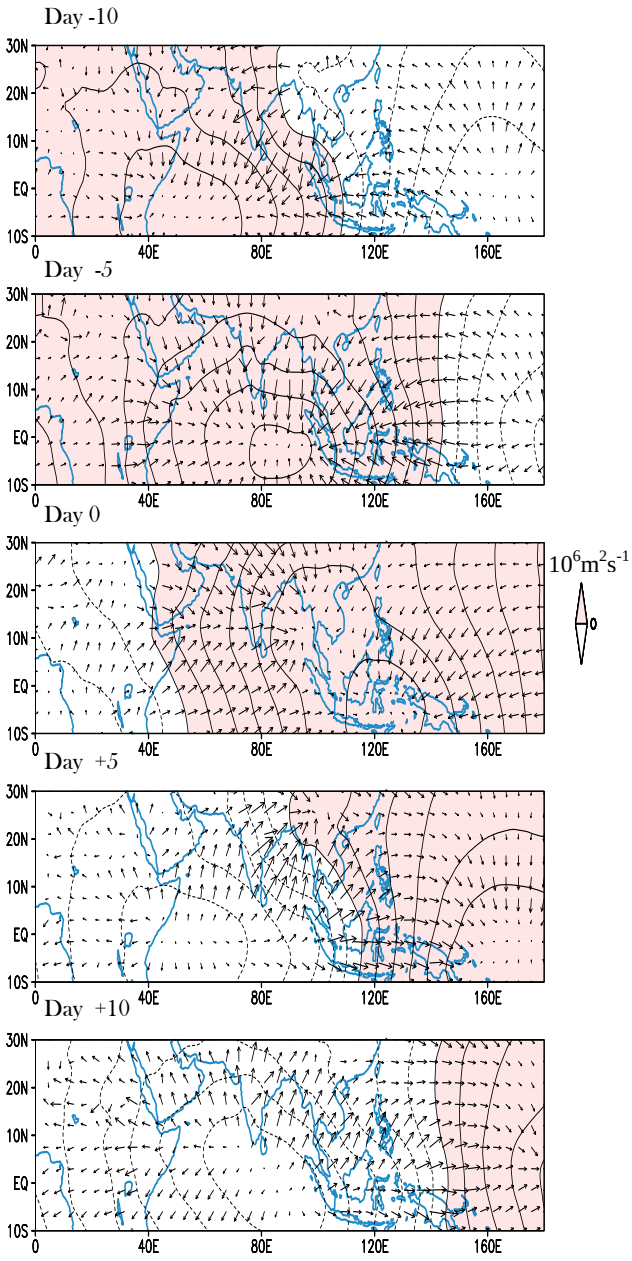

Fig. 3 Composite mean of bandpassed χ at 850-hPa based on 27 spring tropical cyclogenesis (1979-2010).Vectors represent divergent winds. Positive anomalies are shown with contours in shade. The data has been band passed within a frequency of 30-60 days to isolate the MJO signal associated with TC development.

References

Dee, D. P., S. M. Uppala, A. J. Simmons, P. Berrisford, P. Poli, S. Kobayashi, U. Andrae, M. A. Balmaseda, G. Balsamo, P. Bauer, P. Bechtold, A. C. M. Beljaars, L. van de Berg, J. Bidlot, N. Bormann, C. Delsol, R. Dragani, M. Fuentes, A. J. Geer, L. Haimberger, S. B. Healy, H. Hersbach, E. V. Hólm, L. Isaksen, P.

Kållberg, M. Köhler, M. Matricardi, A. P. McNally, B. M. Monge-Sanz, J.-J. Morcrette, B.-K. Park, C. Peubey, P. de Rosnay, C. Tavolato, J.-N. Thépaut, and F. Vitart, 2011: The ERA-Interim reanalysis: configuration and performance of the data assimilation system. *Q.J.R. Meteorol. Soc.*, **137**, 553–597. doi: 10.1002/qj.828.

Kikuchi K, B. Wang, 2010: Formation of tropical cyclones in the Northern Indian Ocean associated with two types of tropical intraseasonal oscillation modes. *J Meteorol Soc Jpn*, **88**, 475–496.

Ventrice, M. J., C. D. Thorncroft, and P. E. Roundy, 2011: The Madden–Julian oscillation's influence on African easterlywaves and downstream tropical cyclogenesis. *Mon. Wea. Rev.*, **139**, 2704–2722.

Wang, S.-Y., B. M. Buckley, J.-H. Yoon, and B. Fosu, 2013: Intensification of premonsoon tropical cyclones in the Bay of Bengal and its impacts on Myanmar, *J. Geophys. Res.*, **118**, 4373–4384. doi:10.1002/jgrd.50396.

Wu, M. C., S. Schubert, and N. E. Huang, 1999: The development of the South Asian summer monsoon and the intraseasonal oscillation. *J. Climate*, **12**, 2054.

Yatagai, A., K. Kamiguchi, O. Arakawa, A. Hamada, N. Yasutomi, and A. Kitoh, 2012: APHRODITE: constructing a long-term daily gridded precipitation dataset for Asia based on a dense network of rain gauges, *Bull. Amer. Meteor. Soc.*, doi:10.1175/BAMS-D-11-00122.1. http://weather.unisys.com/hurricane/n_indian/index.phphow

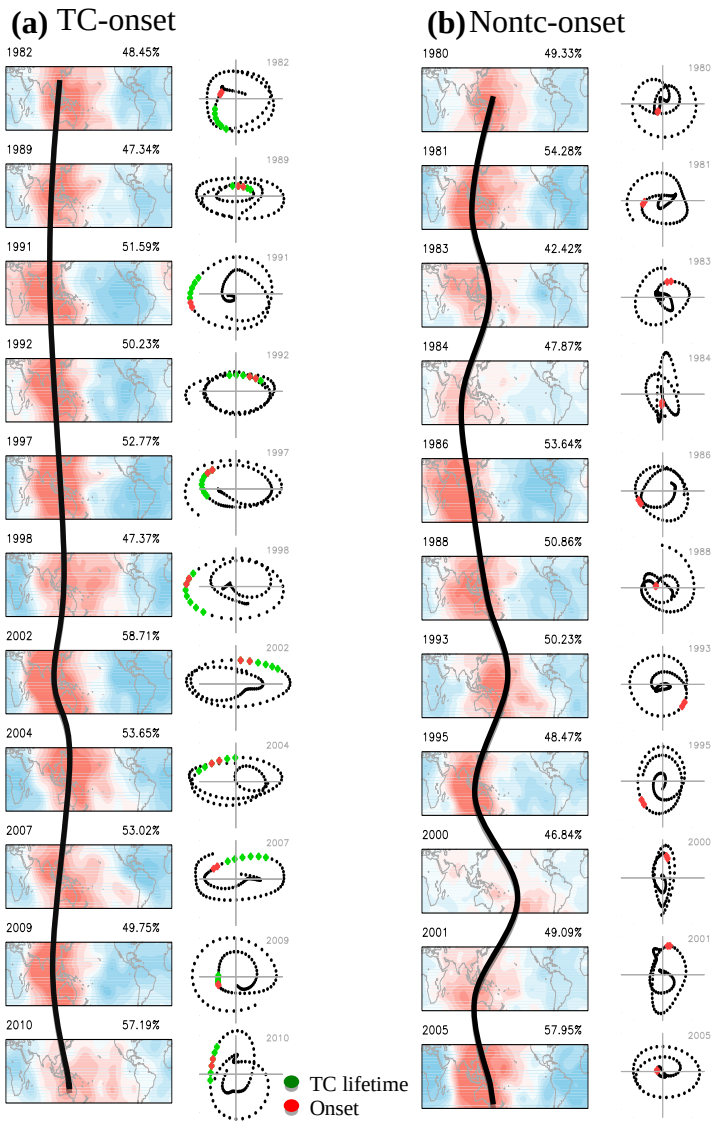

Fig. 4 EOF one loading patterns of bandpassed χ at 850-hPa for (a) coupled onset-cyclogenesis events and (b) uncoupled onset-cyclogenesis periods, along with yearly phase space points for all available days in May and June, using PC1 and PC2. The black lines join centers of enhanced convergence. Each field is normalized by its explained variance (shown above on right). The red dots show monsoon onset whiles the green dots show the spring tropical cyclone lifetime.

2. REALIZING PREDICTION SKILL

Science and Technology Infusion Climate Bulletin
NOAA's National Weather Service
38th NOAA Annual Climate Diagnostics and Prediction Workshop
College Park, MD, 21-24 October 2013

Developing a More Reliable and Usable ENSO Prediction Plume

Anthony G. Barnston and Michael K. Tippett
International Research Institute for Climate and Society,
The Earth Institute at Columbia University, Lamont Campus, Palisades, NY

Huug van den Dool and David A. Unger
Climate Prediction Center, NCEP/NWS/NOAA, College Park, MD

1. Introduction

Since early 2002, the International Research Institute for Climate and Society (IRI) has issued, each month, a collection of the forecasts from a large number of ENSO forecasting institutions, in the form of an ENSO prediction plume (Fig. 1). The forecasts predict the Nino3.4 index in the tropical Pacific (SST averaged over 5ºN-5ºS, 120º-170ºW).

In late 2011 this forecast plume became a product of both IRI and the NOAA Climate Prediction Center (CPC). Although the product has been popular and frequently viewed on the Web, it has had several significant problems:

- The forecast producers do not form their anomalies with respect to the same 30-year base periods as encouraged, and IRI/CPC does not correct for such (usually minor) deviations.
- The forecast spread within individual models, indicative of model uncertainty, is ignored and only the mean forecast is shown.
- Model biases, evident upon examination of hindcasts, are not corrected; and some forecasts are from models that lack hindcasts.
- No attempt is made to provide a final forecast probability distribution; users see the spread of the model forecasts and are left to surmise the uncertainty on their own.

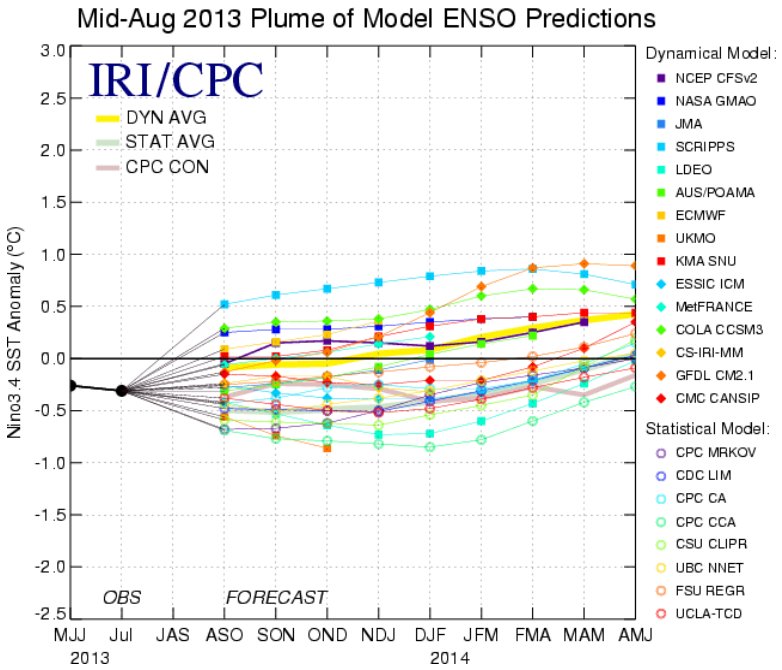

Fig. 1 Example of an IRI/CPC ENSO prediction plume product, issued in mid-August 2013.

Of the four problems listed above, the third one appears most serious, because some of the dynamical models are known to have substantial (>0.5ºC) biases. Hence, some of the spread in the model forecasts shown in Fig. 1, even at very short lead times, may well be due to differing model biases. The ENSO forecast plumes posted on the CPC Web site from the North American Multi-model Ensemble (NMME) project (Kirtman *et al.* 2014) have undergone hindcast-based bias correction by start month and lead time, and the resulting plume is noticeably less wide than the IRI/CPC plume at short leads. The NMME plume also shows all ensemble members of all models, forming a very dense cluster of lines on the plot.

Correspondence to: Anthony G. Barnston, International Research Institute for Climate and Society, The Earth Institute at Columbia University, Lamont Campus, Palisades, NY 10964; E-mail: tonyb@iri.columbia.edu.

The current work attempts to develop a protocol for selecting and processing the incoming forecasts for the IRI/CPC plume so as to eliminate or greatly reduce each of the problems identified above. Because the most serious problem (lack of bias correction) requires a multidecadal hindcast history to evaluate bias, it appears that forecasts from models lacking an adequate hindcast history will not qualify for a higher quality version of the plume.

This work uses as test cases a set of 6 models from the NMME project, because those models all have 29-year hindcast data that is conveniently available. The 6 models include (1) NCAR/Univ. Miami CCSM3 (6 members), (2) NOAA/NCEP CFSv2 (24 members), (3) Canada CMC#1 (10 members), (4) Canada CMC#2 (10 members), (5) NOAA GFDL model (10 members), and (6) NASA model (11 members). All 6 models have a 1982-2010 hindcast period. Models' maximum lead times vary from 9 to 12 months. Besides looking at the forecast characteristics of each model, those of the combined forecast (our MME) are studied. The MME is formed by combining the individual ensemble members of all of the models. Because some models have many more members than others, the number of members acts as an effective weighting system: *e.g.*, the NOAA/NCEP CFSv2 has 4 times as many ensemble members as the NCAR /Univ. Miami CCSM3, so it will exert 4 times the weight of CCSM3 in forming the MME forecast. Here, we forecast 1-month mean SST rather than seasonal mean SST as done in the IRI/CPC plume.

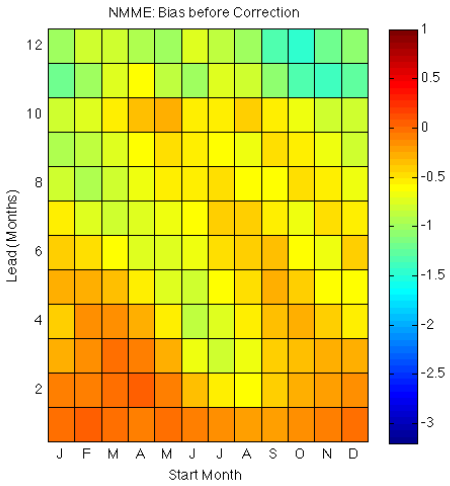

Fig. 2 Bias of the MME in forecasts of Nino3.4 SST, by start month (from Jan to Dec along x-axis) and lead time (from 1 to 12 from bottom to top along y-axis).

2. Results

The basic discrimination skill of each of the 6 models is examined using the temporal correlation (or "anomaly correlation") between Nino3.4 SST hindcast and observation for each start month and each lead time up to 12 months lead. Although the model skill profiles differ from one another in their details, all are seen to have acceptable profiles with the expected seasonal distribution (not shown). However, an examination of mean bias indicates major differences in bias among the models, both in general severity and in distribution over start months and leads. It is clear that each model should be bias-corrected prior to being shown on an improved ENSO prediction plume. The net bias of the MME, shown in Fig. 2, lacks the severity of the biases of individual models due to some bias cancellation, but still reveals a moderate negative bias at long leads and at intermediate leads for some times of the year.

Another kind of bias that individual models may carry is forecast amplitude bias. The interannual standard deviation of the forecasts should not be larger than that warranted by the model's correlation skill, which would be approximately that of the observations multiplied by the skill (Hayes 1973). Such a prescription for the amplitude of the ensemble mean forecast would minimize mean squared errors and produce probabilistically reliable forecasts. However, each model has its "own world", with signal-to-noise ratios that may not agree with that of the real world. It turns out that the amplitude of the MME forecast does not deviate greatly from the ideal amplitude, so that correction of the amplitude by start month and lead does not greatly change the performance of the forecasts. Figure 3 shows the root-mean-square error (RMSE) skill score, defined as $1 - (\mathrm{RMSE}_{\mathrm{fct}} / \mathrm{RMSE}_{\mathrm{cli}})$ where fct refers to the forecasts and cli refers to perpetual climatology forecasts (*i.e.*, zero anomaly). Figure 3 shows that the RMSE is generally substantially improved with bias correction, and only slightly more by forecast amplitude correction.

Although amplitude correction does not change the RMSE skill score dramatically, the amplitude corrections are not minor. Figure 4 shows the MME forecast-to-observation standard deviation ratio before and after correction for the amplitude, and it is clear that the forecasts tend to have too high a standard deviation before correction, especially at intermediate and long leads. While the standard deviation of individual ensemble members is expected to be comparable to that of the observations for all start times at all

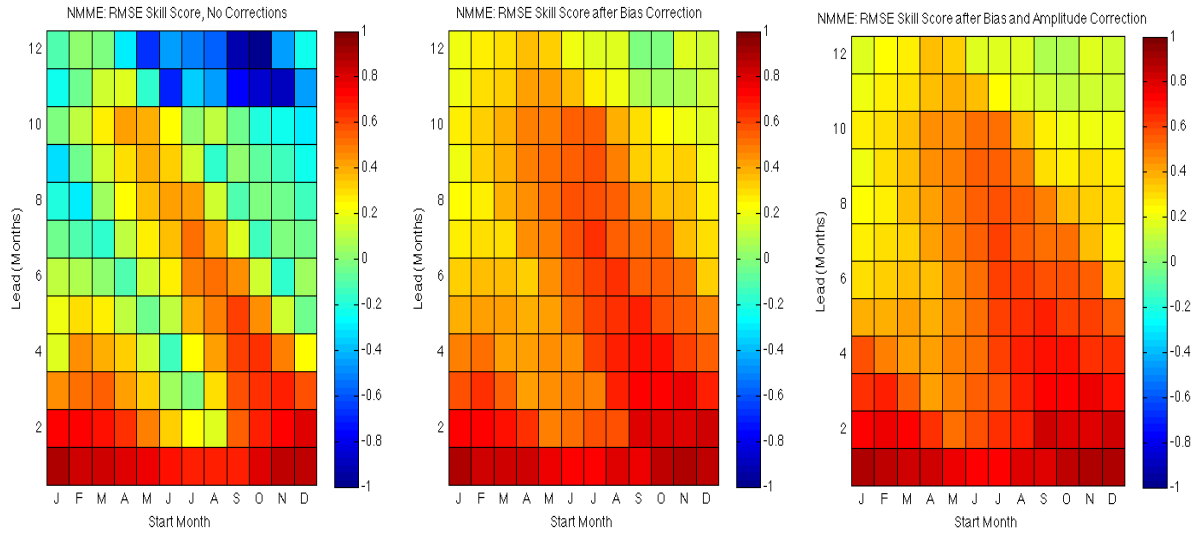

Fig. 3 RMSE skill score for the MME forecasts, by start month (x-axis) and lead time (y-axis). See the text for the definition of the score. The left panel shows skills without any corrections, the middle panel with individual model bias corrections, and right panel with both bias and amplitude corrections.

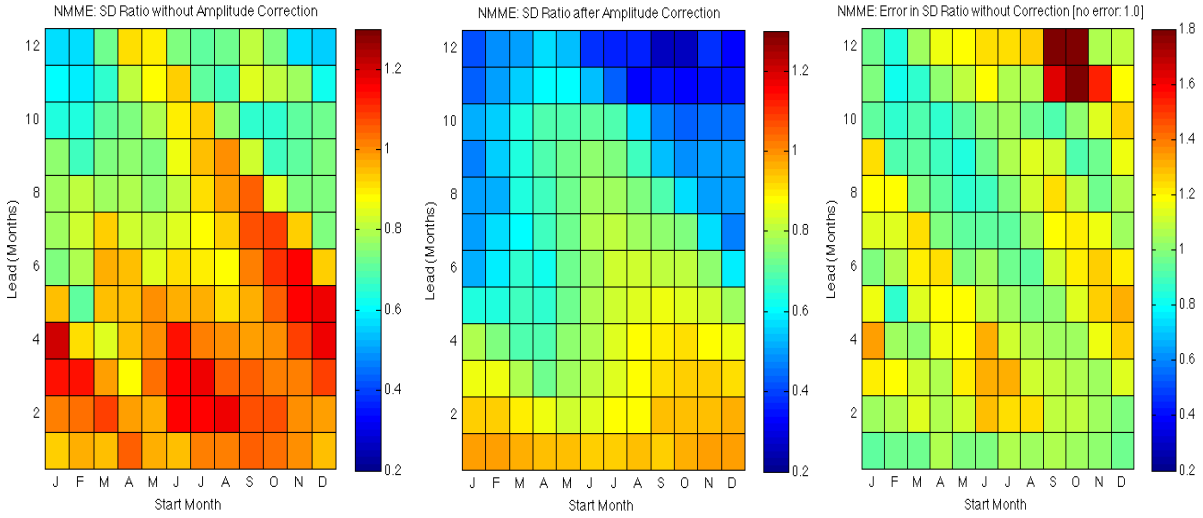

Fig. 4 Standard deviation ratio of MME forecasts versus observations. Left panel shows ratios without amplitude correction, middle panel with amplitude correction, and right panel the ratio of the values without correction to those with correction (note the different scale for the right panel).

leads, that of the ensemble means should be in proportion to the lack of predictability. Although predictability within each model's world is estimated by its signal-to-noise ratio (interannual standard deviation of ensemble mean forecast versus ensemble spread), the actual predictability is better estimated by the correlation between the forecasts and observations. It is this latter measure of realized predictive skill that should govern the interannual standard deviation of the forecasts.

The most appropriate interannual standard deviation for each start month and lead time is determined by the actual temporal correlation skill of the hindcasts with observations, such that a correlation of 0.5 would imply an ideal MME forecast standard deviation of 0.5 that of the observations. Using this indirect way to set the forecast amplitude corrects for model signal-to-noise ratios that do not properly reproduce that in nature.

An important characteristic of a forecast is its uncertainty. For individual forecasts, uncertainty is ideally expressed by the spread of the ensemble members. Even the shape of the distribution of the member forecasts may occasionally be meaningful if it is based on the physics at play in the forecast rather than just accidental

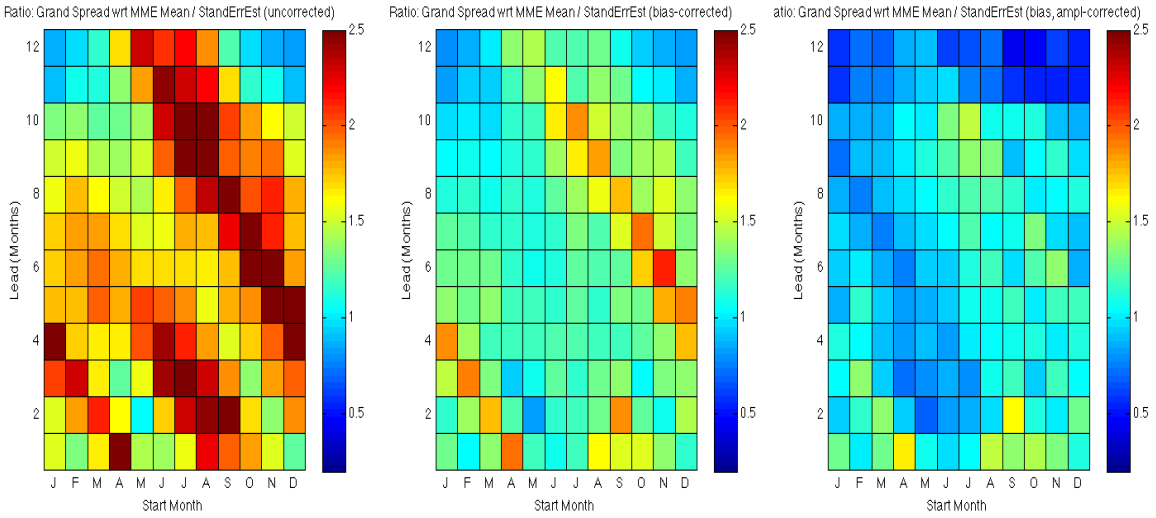

Fig. 5 Ratio of the MME spread (across all model members) to the actual hindcast skill-based standard error of estimate. Left panel shows the ratio for no corrections, middle panel for only bias corrections, and right panel for both bias and amplitude corrections. The ideal ratio is 1.

sampling variability in the finite set of ensemble members. A check for a reasonable magnitude of ensemble spread is the standard error of estimate, based again on the actual correlation skill of the MME forecasts over the hindcast period, by start month and lead time. The standard error of estimate (SEE) is defined by

$$SEE = SD_y\sqrt{1-cor_{xy}^2}$$

The above formula implies that high-skill forecasts should have a smaller spread than lower-skill forecasts. Is this formula followed to first order in the MME hindcasts? Figure 5 shows the ratio of the MME spread (across all model members) and the skill-based SEE for the cases of no corrections, only bias corrections, and bias and amplitude corrections. The ratios in Fig. 5 indicate far too much spread in model members without bias correction, and a much more realistic spread after bias correction. Further improvement of the ratio (toward 1) occurs with amplitude correction.

One contribution to the spread of the MME forecasts is that among the members of each model with respect to its own ensemble mean, while a second contribution is that of the differing ensemble means across the models. We ask how much the first component of the spread is contributing to the total spread. Figure 6 shows this aggregated "internal" member spread before and after amplitude correction. The internal spread after the amplitude correction is generally

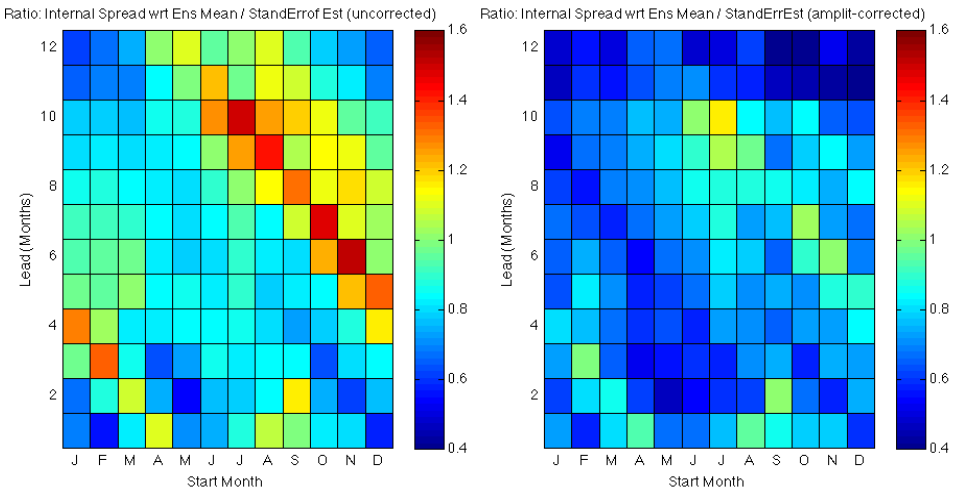

Fig. 6 Spread of the MME forecasts coming from the variation of the members of each model with respect to its own ensemble mean ("internal" model spread). Left panel shows internal spread before amplitude correction, right panel following amplitude correction.

well below the level that is compatible with the SEE.

Figure 7 illustrates an example of the effects of the bias and amplitude corrections in an individual forecast case—here, for forecasts from June 2009 for what turned out to be a moderate strength El Niño during late 2009 and early 2010. Without any correction, the MME forecast substantially underestimates the strength of the event, and the uncertainty is overestimated (especially at short lead times) due to the differing biases of the ensemble means of the various models. Note that the ensemble mean forecasts of the different models differ greatly without any correction. Correction of the mean biases leads to a much improved MME forecast (middle panel) and more realistic width of the uncertainty distribution. Correction for the amplitude as well as the bias results in slight underestimation of the strength of the event, and some underestimation of the amount of uncertainty at short leads. The strength underestimation may be partly a result of the more conservative forecast amplitude following amplitude correction.

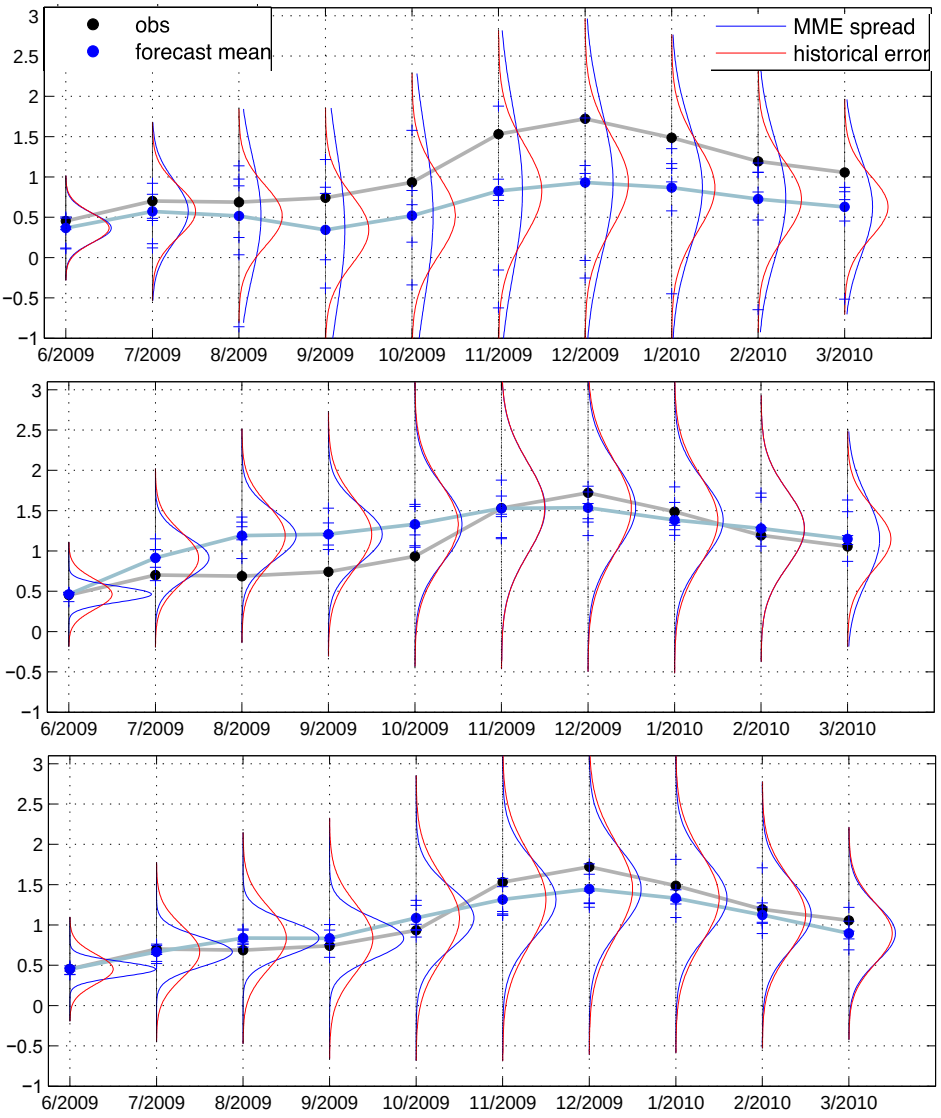

Fig. 7 MME forecasts from June 2009 for the period of the 2009/2010 El Niño event. Top panel shows forecasts without any corrections, middle panel after bias correction, and bottom panel after bias and amplitude correction. The blue line and solid dots show the MME mean forecasts; the black line and dots show the observations. The horizontal ticks on the vertical line for each month show individual model ensemble mean forecasts. The thin blue vertical vertical Gaussian distribution curves show forecast uncertainty based on the MME spread, and the thin red vertical distribution curves show uncertainty based on the hindcast skill-based standard error of estimate.

3. Summary and discussion

Findings from this study so far are as follows:

Multi-model ensemble spread is considerably larger than the SEE-based (more likely realistic) spread when the models' differing biases are uncorrected. The ratio between the two spreads is about 1.5 to 1.8 before bias correction, and about 1.2 to 1.4 after individual model bias corrections.

The ratio of internal spread around individual model ensemble means (i.e., the spread of individual model ensemble members) to the standard error of estimate is in 0.8 – 1.0 range, showing slightly too tight an ensemble distribution. This result is expected in view of individual models having their own universe, and often (not always) recognizing less noise in that universe than there is in the real world.

Correcting forecasts so that the ratio of their interannual SD equals that of observations multiplied by their correlation skill (i.e., amplitude correction) makes less difference in the RMSE of the MME forecasts than model bias correction, but brings the spread of the MME forecasts within the neighborhood of that indicated by the skill-based SEE for intermediate and long leads. For shortest leads, the MME spread becomes smaller than the SEE-based spread.

A clear conclusion is that individual model biases should be corrected before the merging into a MME is done:

Correction of model amplitude biases should also be done. It reduces the interannual variability of the MME forecasts to be lower than that of the observations, to minimize squared errors and to create probabilistic reliability (lack of overconfidence). The lower the hindcast-based skill, the smaller the interannual variability of the MME forecasts should become.

A final thought concerns best way to display the forecast plume for users. Both the mean of the MME and the associated uncertainty must be shown in an easily understood and usable way.

References

Hayes, W. L., 1973: Statistics for the Social Scientists, Second Edition. Holt, Rinehart and Winston, Inc.

Kirtman, B. P., D. Min, J. M. Infanti, J. L. Kinter, D. A. Paolino, Q. Zhang, H. van den Dool, S. Saha, M. P. Mendez, E. Becker, P. Peng, P. Tripp, J. Huang, D. G. DeWitt, M. K. Tippett, A. G. Barnston, S. Li, A. Rosati, S. D. Schubert, Y.-K. Lim, Z. E. Li, J. Tribbia, K. Pegion, W. Merryfield, B. Denis and E. Wood, 2014: The US national multi-model ensemble for intra-seasonal to interannual prediction. *Bull. Amer. Meteor. Soc.*, **95**, in press.

Science and Technology Infusion Climate Bulletin
NOAA's National Weather Service
38th NOAA Annual Climate Diagnostics and Prediction Workshop
College Park, MD, 21-24 October 2013

Sea Ice in the NCEP Climate Forecast System Reanalysis

Xingren Wu[1, 2], and Robert Grumbine[1]

[1]*Environmental Modeling Center, NCEP/NWS/NOAA*

[2]*I.M. Systems Group, Inc., Rockville, MD*

ABSTRACT

The NCEP climate forecast system (CFS) reanalysis (CFSR) was recently completed using the NCEP coupled atmosphere-ocean-land surface-sea ice system. This paper describes the sea ice concentration data used and how sea ice concentration is assimilated in the CFSR. The near record minimum of Arctic sea ice is clearly shown in the CFSR output. Because of the realistic sea ice distribution, there have been many improvements in the CFSR compared to the previous NCEP/NCAR Reanalysis-1 and NCEP-DOE Reanalysis-2. For instance, the surface air temperature improved in the fall over the Arctic Ocean.

1. Introduction

Sea ice is known to play a significant role in the global climate system. Realistic representation of sea ice is essential for good performance of atmospheric and oceanic data assimilation models over the polar regions in the CFSR. Global climate modeling studies show that sea ice concentration has a strong impact on the climate over the Antarctic regions (*e.g.*, Simmonds and Budd 1991; Simmonds and Wu 1993). Recent studies (*e.g.*, Overland and Wang 2010; Screen and Simmonds 2010; Liu *et al.* 2012) demonstrate that the declining Arctic sea ice has a significant impact on the atmospheric circulation, surface latent heat flux and winter snowfall. We note that, there was no sea ice concentration in the previous NCEP reanalysis, the NCEP/NCAR Reanalysis-1 (R1) (Kalnay *et al.* 1996) and NCEP-DOE Reanalysis-2 (R2) (Kanamitsu *et al.* 2002), although sea ice concentration data from analysis were used to present the sea ice coverage in R1 and R2 with 55% cutoff (*i.e.* when sea ice concentration is greater than 55% it is considered as 100% sea ice coverage). The new CFSR at NCEP (Saha *et al.* 2010) allows us to add sea ice concentration from analysis into the reanalysis system, which leads to more realistic interactions between sea ice and atmosphere in the polar regions. This paper describes the sea ice data used in the CFSR, how sea ice concentration is assimilated, and discusses the implications for improvement in the products of the CFSR.

2. The sea ice concentration analysis

The sea ice analysis produces a global record of sea ice concentration for the CFSR for all points that may freeze anywhere in the globe. This is done daily on a grid of 0.5 degree latitude-longitude resolution throughout the period of the CFSR. When there are discontinuities in the production of the data set, newer data sets and newer methods are used.

From 1979 to 1996, the sea ice concentrations for most of the globe are regridded from Cavalieri *et al.* (1996, updated 2007) (GSFC Ice), except for (i) possibly ice-covered regions that lie outside that grid, (ii) large Canadian lakes, (iii) the Great Lakes, and (iv) sea surface temperature-based filtering of erroneous ice in the analysis. For the Great Lakes, the data used are Assel *et al.* (2002) from 1979 through the end of the data set in Spring, 2002, and passive microwave thereafter. Those grids are available 1-3 times per week throughout the period they are available. Concentrations were linearly interpolated between the observation dates, and those interpolated values are used here, averaged on to the target 0.5 degree grid from the native 2.55 km Mercator projection. For large lakes in Canada, the Canadian Ice Service (CIS, personal

Correspondence to: Xingren Wu, Environmental Modeling Center, NCEP/NWS/NOAA, 5830 University Research Court, College Park, MD 20740-3818; Email: Xingren.Wu@noaa.gov

communication) analyses were used for all lakes which were analyzed from November 1995 through October 29, 2007 (initially 34, in November, 1995, increasing to 137 by October, 2007). From October 30, 2007 onwards, the concentrations are the operational NCEP passive microwave sea ice concentration analyses.

There are regions which may freeze but lie outside the domain analyzed in GSFC Ice. These large water bodies were analyzed by proxy over 1979-1996, as was done for portions of the North American Regional Reanalysis (Mesinger *et al.* 2006). Proxies were generated anew for the CFSR as the domain is much larger, and more data are available. During the period 1 January 1997 - 30 June 2006 when both NCEP ice and GSFC ice were available, the NCEP ice analysis was used to identify points (one by one) which lay inside the GSFC ice domain and which had high correlation to concentrations analyzed for points outside the GSFC ice domain - but still inside the NCEP domain. This includes large lakes such as Lake Ladoga, Lake Onega, and the Caspian Sea. Due to changes in sea surface temperature (SST) sources for filtering sea ice concentration analyses, some regions such as the Aral Sea, Lakes Balkhash, and Hulun Nur could not be consistently analyzed and were assigned zero ice concentration. Some lakes were assigned land flags in the CFSR when they could not be observed strictly by modern passive microwave due to land contamination issues and the lack of available data; these lakes include Lake Athabasca, Lake of the Woods, Lake Nipigon (outside the period of CIS data), Iliamna Lake, and Lake Vanern.

From January 1997-February 2000, the global ice concentration analysis was the NCEP operational ice analysis (Grumbine 1996) (outside the Great Lakes and Canadian Lakes). From 1 March 2000 to 29 October 2007, the sea ice analysis is the newer NCEP sea ice analysis system applied to archived passive microwave data for DMSP F-13, F-14, and F-15. The old NCEP system was based on the NASA Team1 algorithm (Cavalieri 1992) as was the GSFC ice. The newer system is based on the Team2 algorithm (Markus and Cavalieri 2000). In the newer NCEP system, the sea ice concentration for each day is computed by regression of the Stokes-like parameter $(T85V^2 - T85H^2)^{0.5}$ (where T85V is the 85 GHz brightness temperature at vertical polarization, and T85H is likewise for the horizontal polarization) against the Team2-derived concentration - for those points that are greater than 100 km from land, and are poleward of 60 degrees latitude. The regression provides an unbiased estimator, and, due to the small footprint of the 85 GHz channel, a higher resolution estimate, permitting analysis closer to the coast and inside smaller lakes than would otherwise be possible with the pure Team2 algorithm. This operational system used the SSMI (Special Sensor Microwave/Imager) instruments on DMSP F-13, F-14, and F-15 while those were all available. F-14 stopped providing data in October 2008. F-15 suffered progressively more severe corruption of the 22 GHz channel in late 2008 and was removed from NCEP sea ice production 5 March, 2009. AMSR-E was added to the operational sea ice system on 13 May 2009, using the AMSR-E Team2 algorithm with January, 2009 tie points as described in Markus and Cavalieri (2009). That date was concurrent with a data flow outage from AMSR-E and data corruption in F-13. This simultaneous failure degraded the quality of the sea ice analysis in May 2009. Sea ice data were reprocessed for the CFSR using F-13 and AMSR-E from February to April. The passive microwave weather filters are imperfect, meaning that ice concentrations can be reported from the microwave for reasons other than ice being on the surface, so that an SST filter is also used (Grumbine 1996). The sea ice concentrations were in general produced before the SST analyses used for the CFSR. Therefore, an a posteriori filter was used for retrospective analyses through 29 October 2007 (Grumbine 2009). The usual SST filtering was also done using AVHRR-Only analysis (Reynolds *et al.* 2007) for 4 January 1985-10 February 2000. The real-time global (RTG) low resolution analysis (Thiebaux *et al.* 2003) was used 11 Feb 2001 through 29 October 2007 and RTG high resolution analysis (Gemmill *et al.* 2007) thereafter.

3. The coupled model

The model used for the CFSR is the NCEP coupled atmosphere-ocean-land surface-sea ice model. The atmospheric model is based on the previous NCEP operational global forecast system (GFS) model with improvements including new radiation and physics (Saha *et al.* 2010). The horizontal resolution is T382 with 64 hybrid vertical layers. The ocean model is from GFDL Modular Ocean Model version 4p0d (MOM4, Griffies *et al.* 2004), with 40 vertical layers. The zonal resolution of MOM4 is $1/2^o$. The meridional resolution is $1/4^o$ between 10^oS and 10^oN, gradually increasing through the tropics becoming $1/2^o$ poleward of 30^oS and 30^oN. The ocean model uses a tripolar grid north of 65^oN. The land surface model is the NOAH land surface

model (Ek *et al.* 2003), which is imbedded in the GFS. The sea ice model is described below. Full details of the model description for the atmosphere, ocean, and land surface can be found in Saha *et al.* (2010).

4. The sea ice model

The sea ice model is from GFDL Sea Ice Simulator with slight modifications. Similar to the ocean model, sea ice model components use a tripolar grid north of 65°N, *i.e.*, a grid that has "poles" located in the land masses of northern Canada and northern Russia, in addition to the normal South Pole. There are three layers for the sea ice model, including two equal layers of sea ice and one (optional) layer of snow with five categories of sea ice thickness (0-0.1, 0.1-0.3, 0.3-0.7, 0.7-1.1, and the category greater than 1.1 m). The snow has no heat capacity, the upper ice layer has sensible and latent heat capacity (*i.e.* a variable temperature/ salinity dependent), and the lower ice layer has only sensible (fixed) heat capacity. The base of ice is fixed at the (salinity dependent) seawater freezing temperature. Sea ice dynamics is based on Hunke and Dukowicz (1997) using the elastic-viscous-plastic technique to calculate ice internal stress. The ice strength follows that of Hibler (1979). Ice thermodynamics is based on Winton (2000). It is possible for ice to be transferred conservatively between the snow layer and the two ice layers when there is snowfall, evaporation, freezing, or melting. When sea ice forms over the ocean, it releases latent heat and salt to the ocean. Details can be found in Griffies *et al.* (2004).

5. The assimilation of sea ice concentration in the CFSR

Due to the lack of observations of sea ice thickness and motion covering the CFSR period starting 1979, a sea ice merging scheme is used in the CFSR to add sea ice concentration into the system. The 6-hour model guess field and the analyzed sea ice concentration are used to produce a

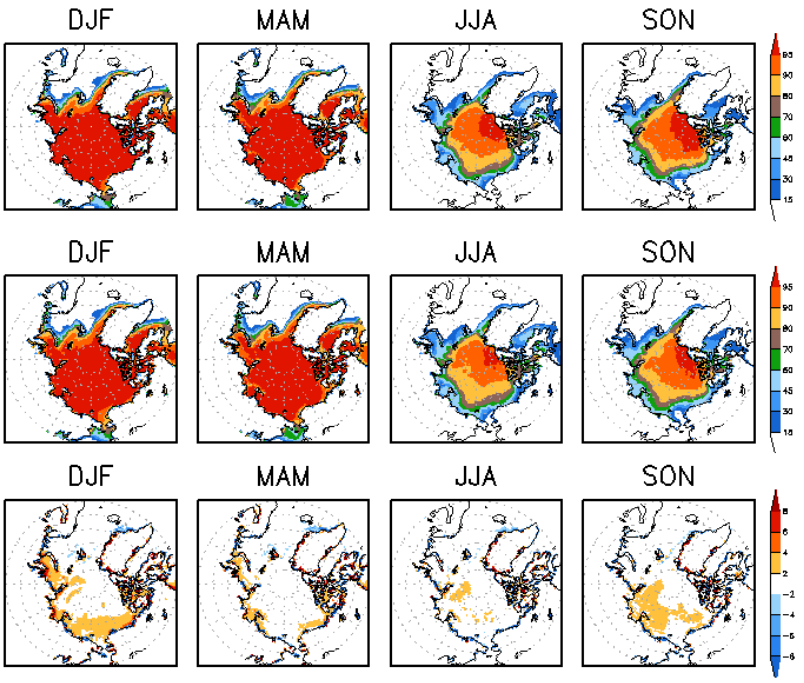

Fig. 1 Sea ice concentration (%) in the Arctic averaged from 1979 to 2010 for December-January-February (DJF), March-April-May (MAM), June-July-August (JJA) and September-October-November (SON) from the CFSR (top), the analysis (middle) and the difference between the CFSR and the analysis (bottom). The contours are 15/30/45/60/70/80/90/95 for the sea ice concentration and -8/-6/-4/-2/2/4/6/8 for the difference.

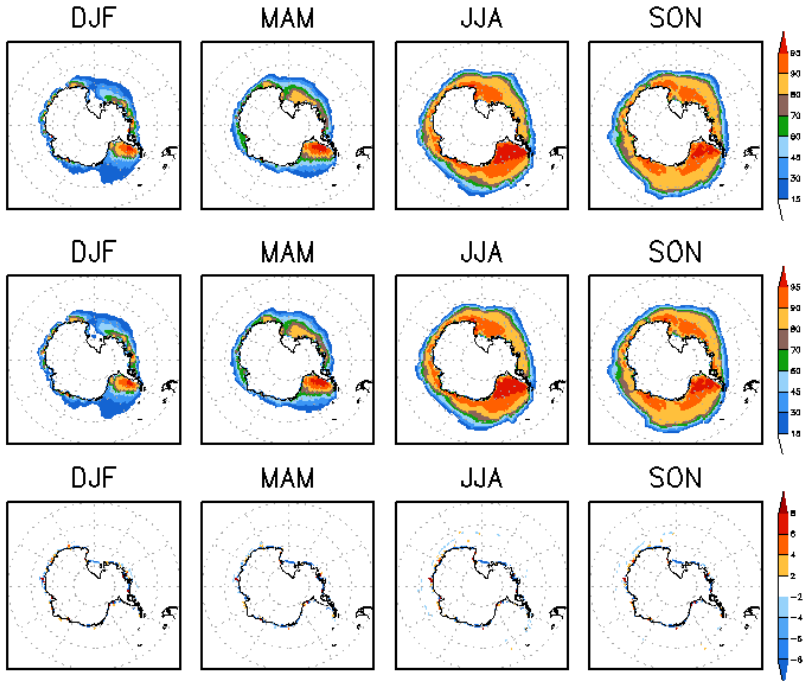

Fig. 2 As in Fig. 1 but for the Antarctic.

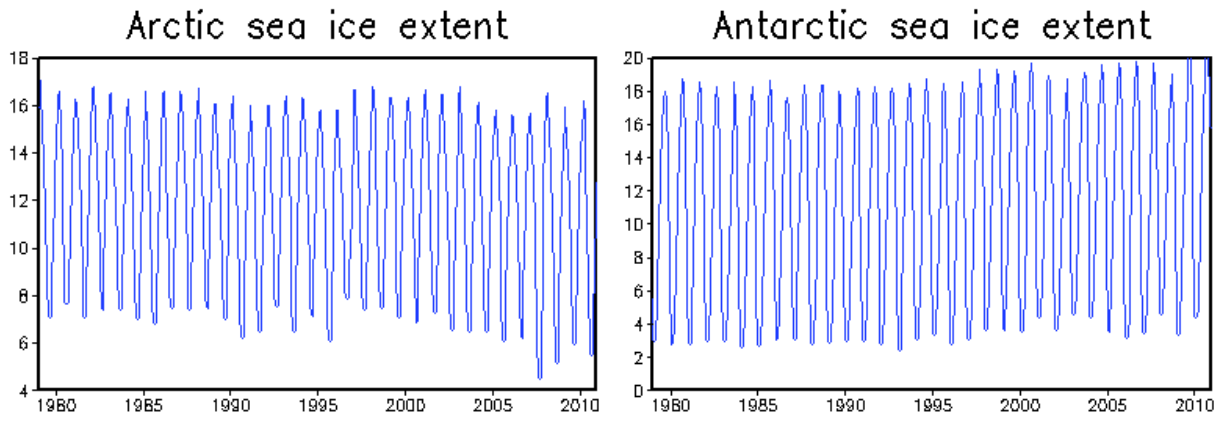

Fig. 3 Monthly mean sea ice extent (10^6 km^2) for the Arctic (left) and Antarctic (right) from the CFSR.

new initial condition. During the merging process, a quality control is applied to prevent the failure when there is a feedback between the ice analysis and the SST analysis. This is done on the sea ice model grid after the interpolation (regridding) is performed for SST and sea ice concentration. When the SST from the analysis is warmer than 275.3 K, or the sea ice concentration from the analysis is less than 15%, no sea ice is allowed to exist, so sea ice is removed from the CFSR initial condition. When the sea ice concentration from the analysis is greater than (or equal to) 15% and the SST is not warmer than 275.3 K, the CFSR initial sea ice concentration is reset to the analyzed value. If the model guess contains more sea ice, thin ice is removed first before thicker ice. In summer, the melt pond effect on ice albedo is considered1, which is done for the Arctic sea ice cover north of 70^{o}N only. When there are serious problems for sea ice concentration data from analysis, we only use model predictions. This happens for May 1-13, 2009.

6. Sea ice in the CFSR

Because sea ice concentration has been "assimilated", there is no doubt that the ice field is very close to the observations for sea ice concentration and ice coverage. Figure 1 shows the sea ice concentration averaged from 1979-2010 in the CFSR for December-January-February (DJF), March-April-May (MAM), June-July-August (JJA), and September-October-November (SON) for the Arctic, the corresponding analysis, and the difference between the CFSR and the analysis. It can be seen that the difference is very small and mostly along the coast. The Antarctic sea ice concentration for each season from the CFSR and the analysis is shown in Figure 2 with the difference given. The difference over the Antarctic is even smaller and almost negligible.

The Arctic region sea ice reaches its maximum coverage in late February or early March and minimum

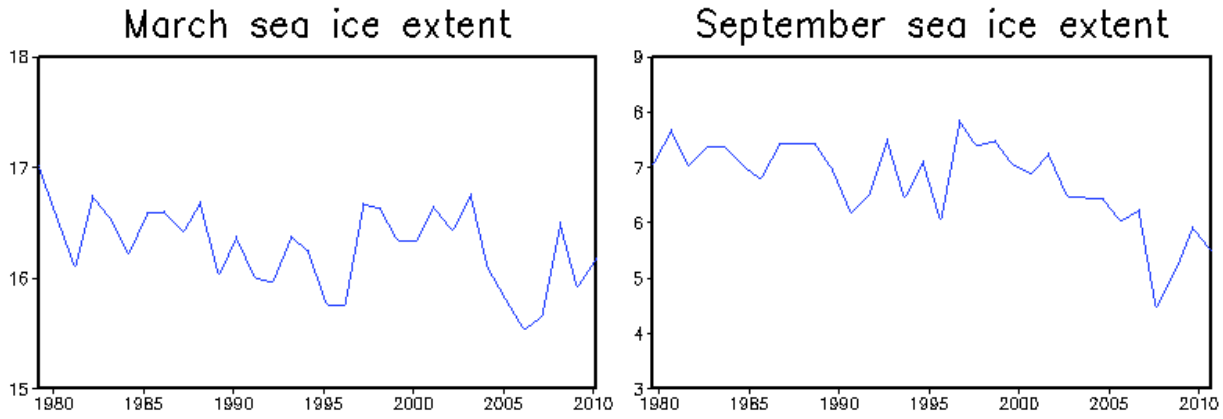

Fig. 4 Arctic sea ice extent (106 km^2) from the CFSR in March (left) and September (right).

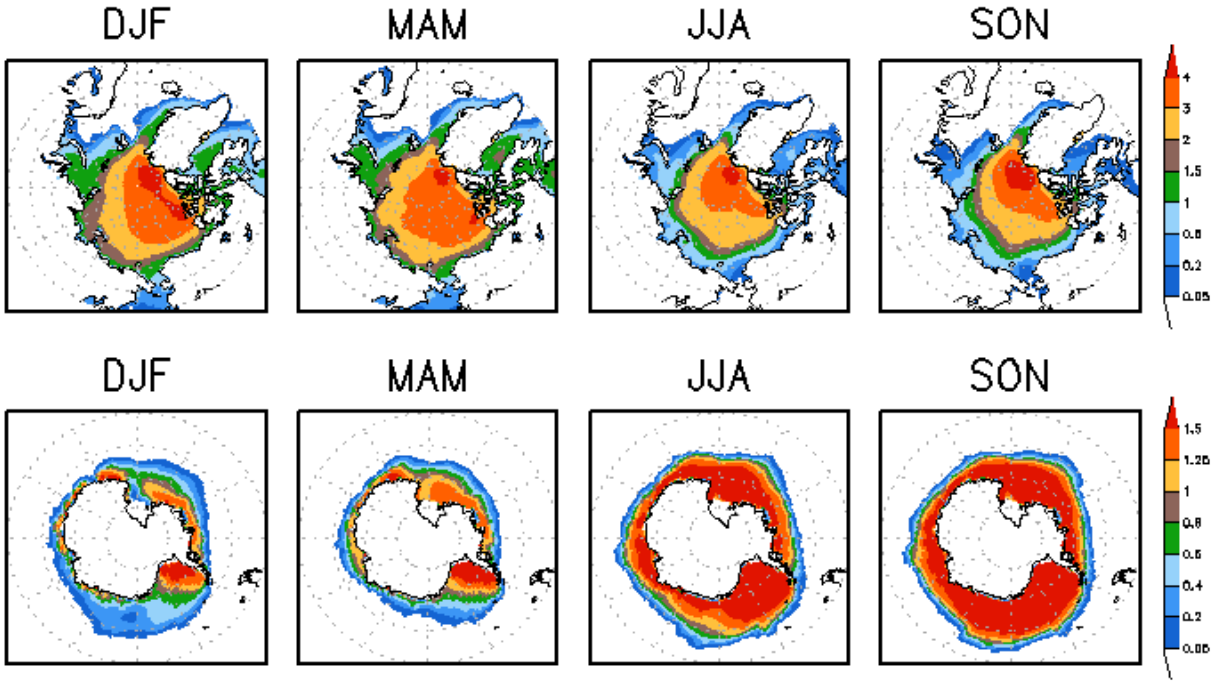

Fig. 5 Sea ice thickness (m) in the Arctic (top) and Antarctic (bottom) averaged from 1979 to 2010 for DJF, MAM, JJA and SON from the CFSR. The contours are 0.05/0.2/0.5/1/1.5/2/3/4 for the Arctic and 0.05/0.2/0.4/0.6/0.8/1/1.25/1.5 for the Antarctic.

coverage in September. From November to June, sea ice covers 90% of the Arctic Ocean, where the open water region is very small. The Antarctic sea ice reaches its maximum coverage in September and minimum coverage in February. Much larger seasonal variation of sea ice exists in the Antarctic than in the Arctic. Sea ice extent, which is defined as the total area with sea ice present (including open water) for which each grid cell has at least 15% sea ice, is shown in Figure 3. It can be seen that the maximum sea ice extent is about three times the minimum sea ice extent for the Arctic, but it is about nine times for the Antarctic. Large reductions in sea ice are obvious in the CFSR for both summers of 2007 and 2008 over the Arctic. Inter-annual variability for the total sea ice extent is relatively small for both hemispheres but regional inter-annual variation for the marginal sea ice zone is very large (not shown). The overall trend over the 32-year period is slightly positive for the Antarctic and negative for the Arctic, which is consistent with previous studies (*e.g.*, Comiso and Nishio 2008; Parkinson 2006). The March and September Arctic sea ice extent is shown in Figure 4. This is comparable to that from Stroeve *et al.* (2007), in particular for the sea ice trend for September. The plots in Stroeve stopped at 2006, whereas our CFSR data includes 2007-2010.

The seasonal sea ice thickness for the 32-year mean is shown in Figure 5. Sea ice is much thicker over the Arctic than over the Antarctic. The averaged sea ice thickness in the CFSR is reasonable in the Arctic for the first 20 years but it is too thick for the last decade; it might also be too thick in the Antarctic

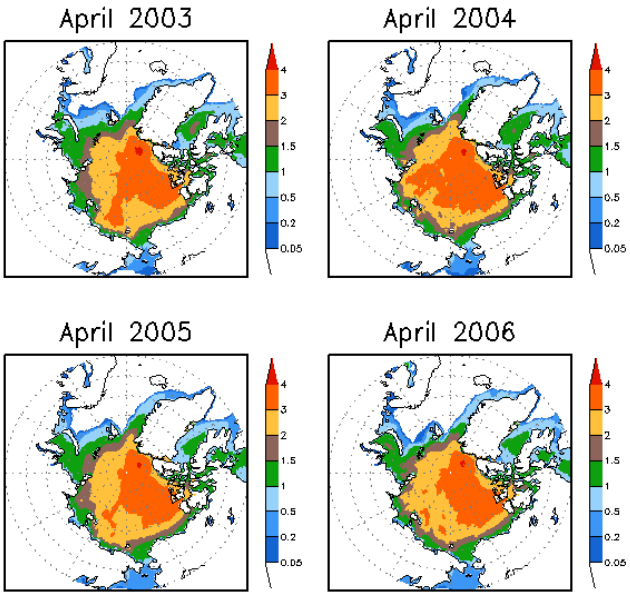

Fig. 6 Sea ice thickness (m) for April from 2003 to 2006 in the Arctic from the CFSR. The contours are 0.05/0.2/0.5/1/1.5/2/3/4.

as the observed Antarctic sea ice is mostly less than 1 m (*e.g.*, Wadams *et al.* 1987; Worby *et al.* 1994). Maslanik *et al.* (2007) showed a large interannual variation of Arctic spring sea ice thickness between 2003 and 2006. The sea ice thickness for April from the CFSR is shown here (Fig. 6) for 2003-2006. The interannual variation from the CFSR is not as large as the observations shown in Maslanik *et al.* (2007). The sea ice thickness errors can result from deficiencies in any component of the coupled atmosphere-ocean-land surface-sea ice model and their interactions. One example is the downward shortwave radiation. When the CFSR model is used to do seasonal forecast there is a cold SST bias in the Tropics, leading to an El Nino/Southern Oscillation variability that is too weak (Saha *et al.* 2014). Nevertheless, the CFSR is able to simulate the large reduction in sea ice over the past 20 years. Figure 7 shows the sea ice concentration and thickness for September of 1987 and 2007 for the Arctic. Record minimum Arctic sea ice cover was observed in September 2007 (*e.g.* Comiso *et al.* 2008), which was broken again in 2012. The sea ice thickness in the CFSR also shows a large reduction from 1987 to 2007.

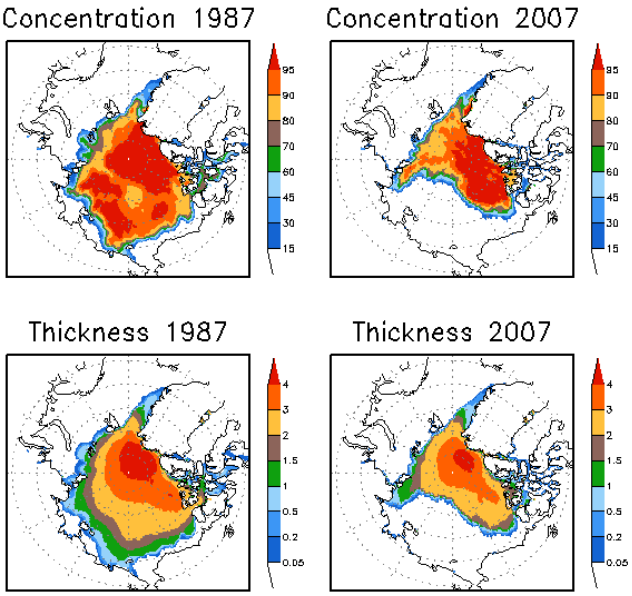

Fig. 7 Sea ice concentration (%) and thickness (m) for September 1987 and 2007 from the CFSR for the Arctic.

8. Summary

We have described the sea ice data used in the NCEP CFSR and how sea ice is assimilated. This is the first reanalysis at NCEP where sea ice concentration is assimilated into the reanalysis system. Because of the realistic sea ice distribution and other improvements in the CFSR, it is expected that the coupled reanalysis has been improved in many aspects over the polar regions compared with the previous R1 and R2 (*e.g.* Wang *et al.* 2010). Figure 8 shows the difference in surface air temperature (SAR) among CFSR and R1, R2, and ERA40 (ECMWF Re-Analysis System, Uppala *et al.*, 2005) for the Arctic in September. It can be seen that, due to the lack of open water in the sea ice zone in R1 and R2, the surface air temperatures from R1 and R2 are colder than CFSR in September, but there is good agreement between CFSR and ERA40. Large and Yeager (2004) showed that the mean SAR in R1 for September during 1979-1998 north of 70°N is about 1.7°C colder than observations. For our case during 1979-2009, CFSR is 1.8°C warmer than R1 over the same region, 1.3°C warmer than R2, and 0.2°C warmer than ERA40. This cold bias in R1 for September has been completely removed in the CFSR.

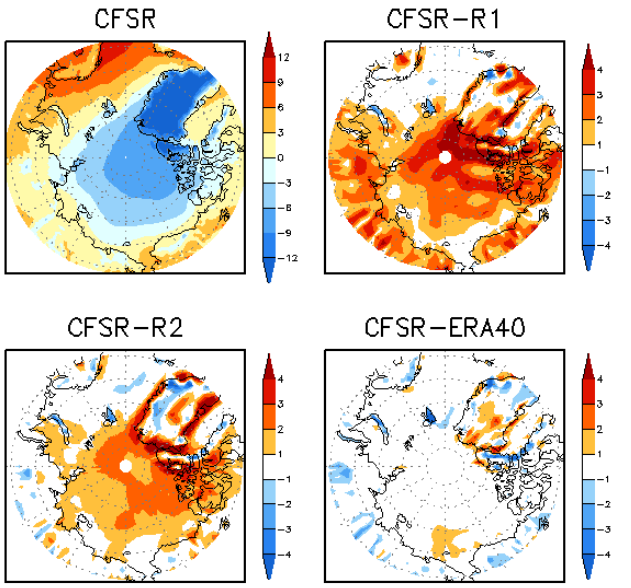

Fig. 8 Mean surface air (2m) temperature (°C) averaged 1979-2009 for September from the CFSR for the Arctic (top left), and the difference among CFSR and R1, R2 and ERA40. The surface air temperatures from R1 and R2 are also averaged over 1979-2009, but averaged over 1979-2001 for ERA40.

Acknowledgements. We acknowledge all members of the CFSR team at NCEP.

References

Assel, R. A., David C. Norton, and K. C. Cronk, 2002: A Great Lakes ice cover digital data set for winters 1973-2000, *NOAA Technical Memorandum GLERL-121*, 46 pp.

Cavalieri, D. J., 1992: Sea ice algorithm. NASA sea ice validation program for the Defense Meteorological Satellite Program Special Sensor Microwave Imager: Final Report. *NASA Technical Memorandum 104559*, 25-31.

Cavalieri, D. J., C. L. Parkinson, P. Gloersen, and H. J. Zwally, 1996: Sea ice concentrations from Nimbus-7 SMMR and DMSP SSM/I-SSMIS passive microwave data, 1978-1996. Boulder, Colorado USA, NASA DAAC at the National Snow and Ice Data Center. Digital Media. Updated 2007.

Comiso, J. C., and F. Nishio, 2008: Trends in the sea ice cover using enhanced and compatible AMSR-E SSM/I, and SMMR data. *J. Geophys. Res.*, **113**, C02S07, doi:10.1029/2007JC004257.

Comiso, J. C., C. L. Parkinson, R. Gersten, and L. Stock, 2008: Accelerated decline in the Arctic sea ice cover. *Geophys. Res. Lett.*, **35**, L01703, doi:10.1029/2007GL031972.

Ek, M. B., K. E. Mitchell, Y. Lin, E. Rogers, P. Grunmann, V. Koren, G. Gayno, and J. D. Tarplay, 2003: Implementation of the Noah land-use model advances in the NCEP operational mesoscale Eta model. *J. Geophys. Res.*, **108**, 8851, doi:10.1029/2002JD003296.

Gemmill, W., B. Katz, and X. Li, 2007: Daily real-time, global sea surface temperature, a high-resolution analysis: RTG_SST_RH. *NOAA/NWS/NCEP/MMAB Technical Notes 260*, 39 pp.

Griffies, S. M., M. J. Harrison, R. C. Pacanowski, and A. Rosati, 2004: A technical guide to MOM4. *GFDL Ocean Group Technical Report No. 5*, NOAA/Geophysical Fluid Dynamics Laboratory, Available online at http://www.gfdl.noaa.gov/~fms.

Grumbine, R. W., 1996: Automated passive microwave sea ice concentration analysis at NCEP. *NOAA/NWS/NCEP/OMB Technical Note 120*, 13 pp.

Grumbine, R. W., 2009: A posteriori filtering of sea ice concentration analyses. *NOAA/NWS/NCEP/MMAB Techical Notes 282*, 7 pp.

Hibler, W. D. III, 1979: A dynamic thermodynamic sea ice model, *J. Phys. Oceanogr.*, **9**, 815-846.

Hunke, E. C., and J. K. Dukowicz, 1997: An elastic-viscous-plastic model for sea ice dynamics. *J. Phys. Oceanogr.*, **27**, 1849-1867.

Kalnay, E., M. Kanamitsu, R. Kistler, W. Collins, D. Deaven, and Co-authors, 1996: The NCEP/NCAR 40-Year Reanalysis Project. *Bull. Amer. Meteor. Soc.*, **77**, 437-471.

Kanamitsu, M., W. Ebisuzaki, J. Woollen, S. K. Yang, J. J. Hnilo, M. Fiorino, and G. L. Potter, 2002: NCEP-DOE AMIP-II Reanalysis (R-2). *Bull. Amer. Meteor. Soc.*, **83**, 1631-1643.

Large, W. G., and S. G. Yeager, 2004: Diurnal to decadal global forcing for ocean and sea-ice models: The data sets and flux climatologies. *NCAR Technical Note, NCAR/TN-460+STR*, 105pp.

Liu, J., J. A. Curry., H. Wang, M. Song, and R. M.Horton, 2012: Impact of declining Arctic sea ice on winter snowfall. *Proceeding of the National Academy of Sciences of the United States of America*, **109**, 4074-4079.

Markus, T., and D. J. Cavalieri, 2000: An enhancement of the NASA team sea ice algorithm. *IEEE Transactions on Geoscience and Remote Sensing*, **38**, 1387-1398.

Markus, T., and D. J. Cavalieri, 2009: The AMSR-E NT2 sea ice concentration algorithm: Its basis and implementation. *Journal of the Remote Sensing Society of Japan*, **29**, 216-225.

Maslanik, J. A., C. Fowler, J. Stroeve, S. Drobot, J. Zwally, D. Yi, and W. Emery, 2007: A younger, thinner Arctic ice cover: Increased potential for rapid, extensive sea-ice loss. *Geophys. Res. Lett.*, **34**, L24501, doi:10.1029/2007GL032043.

Mesinger, F., G. DiMego, E. Kalnay, K. Mitchell, P. C. Shafran, W. Ebisuzaki, D. Jović, J. Woollen, E. Rogers, E. H. Berbery, M. B. Ek, Y. Fan, R. Grumbine, W. Higgins, H. Li, Y. Lin, G. Manikin, D. Parrish,

and W. Shi, 2006: North American Regional Reanalysis. *Bull. Amer. Meteor. Soc.*, **87**, 343–360, doi: 10.1175/BAMS-87-3-343.

Overland, J. E., and M. Wang, 2010: Large-scale atmospheric circulation changes associated with the recent loss of Arctic sea ice. *Tellus*, **62A**, 1-9.

Parkinson, C. L., 2006: Earth's Cryosphere: Current state and recent changes. *Review of Environment and Resources*, **31**, 33-60.

Reynolds, R. W., T. M. Smith, C. Liu, D. B. Chelton, K. S. Casey, and M. G. Schlax, 2007: Daily high-resolution-blended analyses for sea surface temperature. *J. Climate*, **20**, 5473-5496.

Saha, S., S. Moorthi, H.-L. Pan, X. Wu, J. Wang, S. Nadiga, P. Tripp, and Co-authors, 2010: The NCEP Climate Forecast System Reanalysis. *Bull. Amer. Meteor. Soc.*, **91**, 1015-1057.

Saha, S., S. Moorthi, X. Wu, J. Wang, S. Nadiga, P. Tripp, and Co-authors, 2014: The NCEP Climate Forecast System version 2. *J. Climate*, (in press).

Screen, J. A., and I. Simmonds, 2010: The central role of diminished sea ice in recent Arctic temperature amplification. *Nature*, **464**, 1334-1337, doi:10.1038/nature09051.

Simmonds, I., and W. F. Budd, 1991: Sensitivity of the southern hemisphere circulation to leads in the Antarctic pack ice. *Q. J. R. Meteorol. Soc.*, **117**, 1003-1024.

Simmonds, I., and X. Wu, 1993: Cyclone behaviour response to changes in winter southern hemisphere sea-ice zone. *Q. J. R. Meteorol. Soc.*, **119**, 1121-1148.

Stroeve, J., M. M. Holland, W. Meier, T. Scambos, and M. Serreze, 2007: Arctic sea ice decline: Faster than forecast. *Geophys. Res. Lett.*, **34**, L09501, doi:10.1029/2007GL029703.

Thiébaux, J., E. Rogers, W. Wang, and B. Katz, 2003: A new high-resolution blended real-time global sea surface temperature analysis. *Bull. Amer. Meteor. Soc.*, **84**, 645–656, doi: 10.1175/BAMS-84-5-645.

Uppala, S. M., and Co-authors, 2005: The ERA-40 re-analysis. *Q. J. R. Meteorol. Soc.*, **131**, 2961-3012.

Wadhams, P., M. A. Lange, and S. F. Ackley, 1987: The ice thickness distribution across the Atlantic sector of the Antarctic Ocean in midwinter. *J. Geophys. Res.*, **92**, 14535-14552.

Wang, W., P. Xie, S.-H. Yoo, Y. Xue, A. Kumar, and X. Wu, 2010: An assessment of the surface climate in the NCEP Climate Forecast System Reanalysis. *Clim. Dyn.*, **37**, 1601-1620.

Winton, M., 2000: A reformulated three-layer sea ice model. *J. Atmos. Oceanic Technol.*, **17**, 525-531.

Worby, A. P., W. F. Weeks, M. O. Jeffries, K. Morris, and R. Jana, 1994: Late winter-sea-ice-thickness and snow-thickness distribution in the Bellingshausen and Amundsen Seas. *Antarctic Journal of the United States*, **29**, 13-15.

Science and Technology Infusion Climate Bulletin
NOAA's National Weather Service
38th NOAA Annual Climate Diagnostics and Prediction Workshop
College Park, MD, 21-24 October 2013

Sensitivity Study of the Skill of the CPC Week-2 Reforecast Tool to Reforecast Sampling

Melissa Ou, Mike Charles, Dan Collins, and Emily Riddle

Climate Prediction Center, NCEP/NWS/NOAA, MD

1. Introduction

This study assess the impact of reducing the number of years, number of ensemble members, and frequency of reforecasts on the skill of week-2 calibrated surface temperature and precipitation forecasts using the current Global Ensemble Forecast System (GEFS) model reforecasts. These week-2 forecasts are referred to as the week-2 'Reforecast Tool' and are evaluated over the Contiguous United States (CONUS) for this assessment.

Previously, the NOAA Earth System Research Laboratory (ESRL) had been producing reforecasts, which the Climate Prediction Center (CPC) has used to create 6-10 and 8-14 days calibrated (week-2) forecasts. However, ESRL will no longer be generating these reforecasts, and it was proposed to be created by the Environmental Modeling Center (EMC) at the National Centers for Environmental Prediction (NCEP) therefore enabling reforecasts to be updated more frequently with the real-time GEFS. The EMC requested input from the CPC regarding what they deemed necessary (for CPC's forecast timescales) in terms of the amount of reforecasts that would be produced in the future by EMC.

To evaluate the sensitivity of week-2 reforecast tool skill to reforecast sampling, 11 configurations (cases) of reforecast sampling are selected to produce skill scores of calibrated week-2 forecasts. The goal is to determine how the skill of the week-2 reforecast tool varies based on various reforecast configurations to help determine what would be considered a sufficient number of reforecasts needed without a significant loss in skill. A lower configuration of reforecasts would require less computational resources on behalf of EMC to produce these reforecasts.

TABLE 1 Explanation of cases used in the study.

Case #	# Training Years	# Ensemble Members	Model Run Frequency
0	1985-2010 (26 yrs)	11	daily
1	2001-2010 (10 yrs)	11	daily
2	1985-2010 (26 yrs)	6	daily
3	1985-2010 (26 yrs)	11	once every 3-4 days (2/week, Mon and Thurs)
4	1985-2010 (26 yrs)	11	once every 7 days (every Thurs)
5	1985-2010 (26 yrs)	6	once every 7 days (every Thurs)
6	2001-2010 (10 yrs)	11	once every 7 days (every Thurs)
7	2001-2010 (10 yrs)	6	once every 7 days (every Thurs)
8	1993-2010 (18 yrs)	6	once every 7 days (every Thurs)
9	1985-2010 (26 yrs)	3	once every 7 days (every Thurs)
10	2001-2010 (10 yrs)	3	once every 7 days (every Thurs)
11	1985-2010 (26 yrs)	1	once every 7 days (every Thurs)

Correspondence to: Melissa Ou, Climate Prediction Center, NCEP/NWS/NOAA, 5830 University Research Court, College Park, MD 20740-3818; E-mail: Melissa.Ou@noaa.gov.

Three different parameters are evaluated with varying configurations of reforecasts to calculate the statistics used to "train" the reforecast tool – the number of training years, the number of ensemble members, and the model run frequency. The model run frequency is the number of times a week a reforecast dataset is used in the statistics calculation for training the reforecast tool.

2. Data and methodology

The reforecasts used in this study are from the Global Ensemble Forecast System (GEFS) with physics operational during 2012, provided by ESRL. The reforecast dataset includes daily reforecasts for 26 years (from 1985-2010) with 11 ensemble members (including a control run). 16 months of real-time GEFS data (from Feb 26, 2012 to June 11, 2013), with physics also operational in 2012 are used in the calibration. Forecasts are formatted as probabilities of three different categories, below-normal, above-normal, and near-normal. The observations used to calculate the skill scores are station-based 5 and 7 day means of CPC's U.S. station-based daily precipitation and temperature data. About 200 stations of data are utilized.

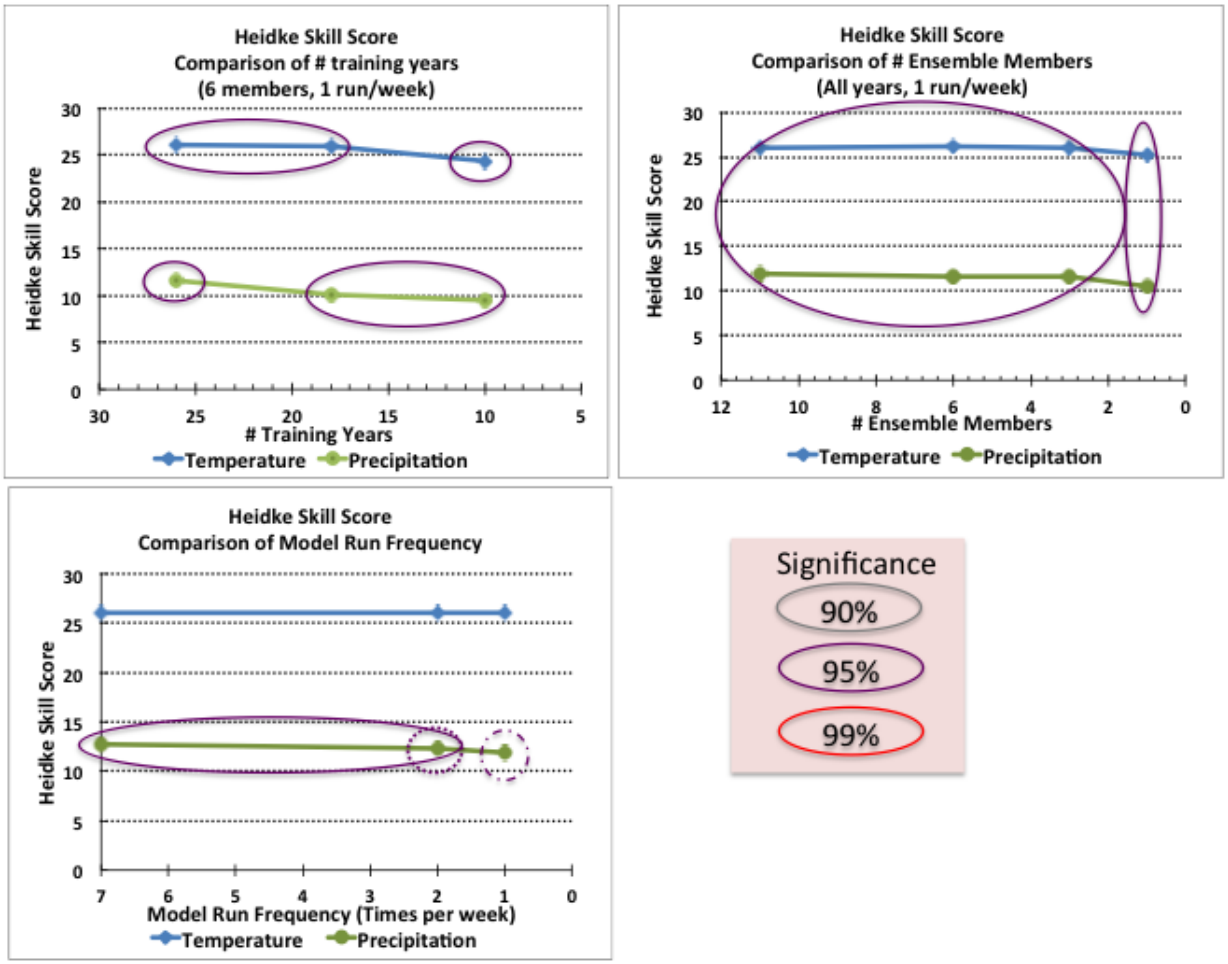

Fig. 1 Line plots of Heidke Skill Score for various configurations of reforecast sampling for 3 different parameters for temperature and precipitation. Pairs of skill scores that have a value difference significant to the 90% level or greater are circled in matching colors. Multiple points in one circle on a plot with a matching circle of point(s) of the same color denotes the skill value difference at significance levels >= 90% for the same variable. The pink box indicates the colors of circles and the associated significance level. For example, in the plot for the # training years (top left), the difference in skill of both 26 and 18 years compared to the skill value of 10 years have a significance >= 95%.

To create forecasts, for each of the cases, first statistics are generated by using the reforecasts and associated observations. The model analysis fields from the reforecasts are used as the "observations" in the

calibration to train the model. It should be noted that using an actual observation dataset did not greatly alter verification results, so the model analysis is used for the statistics calculation.

Next, these statistics are used to calibrate the real-time ensemble forecasts (2012-2013) using the ensemble linear regression method (Unger, 2009). This produces tercile probabilistic forecasts of temperature and precipitation. The three categories of the forecast are above-normal, below-normal, and near-normal. Finally, skill scores are generated using CPC's verification system. These steps are done for each of the cases, by sampling the reforecast dataset according to the configuration specified by each case to calculate the statistics that go into the calibration step.

This study is designed so that there are a reasonable number of cases to evaluate the skill to capture a sufficient range of reforecast sample configurations, while keeping the number of cases to a minimum due to the significant computational time it would take to step through the process to create skill scores. 11 cases were created with differing combinations of the three parameters being evaluated. Case 0 represents the maximum configuration, with all 26 years, 11 ensemble members, and daily reforecasts used per week. Subsequent cases use sub-samples of the pool of available reforecasts. Table 1 shows the details of each of these configurations.

Three skill scores are used in this evaluation, including the Heidke Skill Score (HSS), Rank Probability Skill score (RPSS), and the Reliability Skill Score. The HSS and RPSS are calculated by aggregating over the CONUS for each time step of the 16 months of available forecasts, then the mean skill from these time series of scores are computed. A 1-tail two-sample t-test was performed for testing the significance of the mean skill differences from each of the different cases.

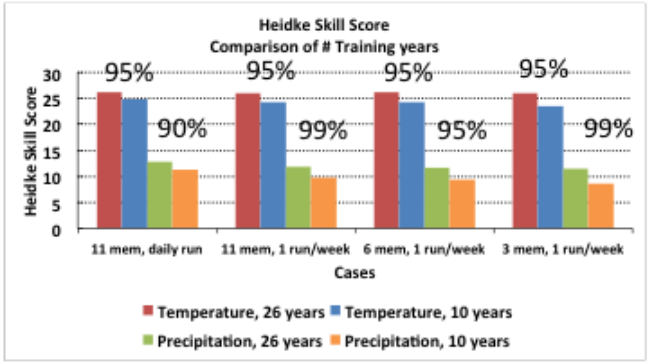

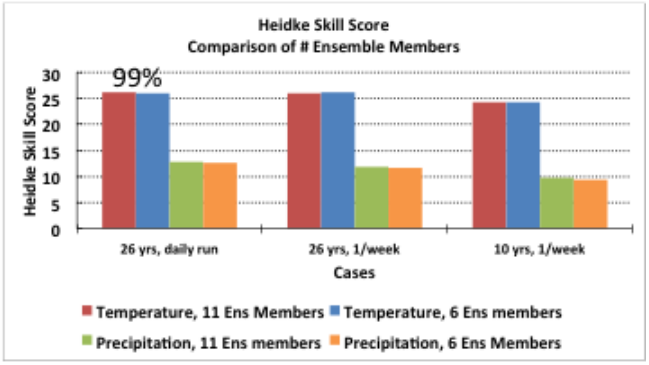

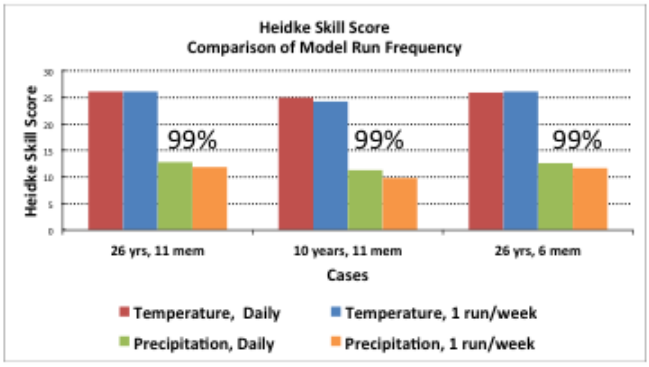

Fig. 2 Bar histograms of Heidke Skill Score for 2 different configurations of reforecast sampling for temperature and precipitation. Differences between two compared values that have significance levels >= 90% are printed above the two skill values being compared.

3. Results

The cases selected for each chart are based on ease of comparing cases isolating impacts by changing each of the parameters. Line plots and reliability diagrams in this study shows how skill of forecasts change with decreasing configurations of each of the three parameters, while keeping the other 2 parameters constant at a selected case. The caveat of using these types of charts is that the skill associated with the decreasing configurations of the changed parameter only reflect one case of the other 2 fixed parameters (*e.g.* changing training years for 26, 18, and 10 years, while keeping the members and model runs constant at 6 and 1,

respectively). Bar histograms are also created for Heidke and RPSS, which allows multiple cases of the 2 fixed parameters to be compared but for only 2 different configurations of the changing parameter (*e.g.* for changing the number of training years, 26 *vs.* 10 years are compared for 11 members/daily model run, 11 members/1 run/week, *etc.*).

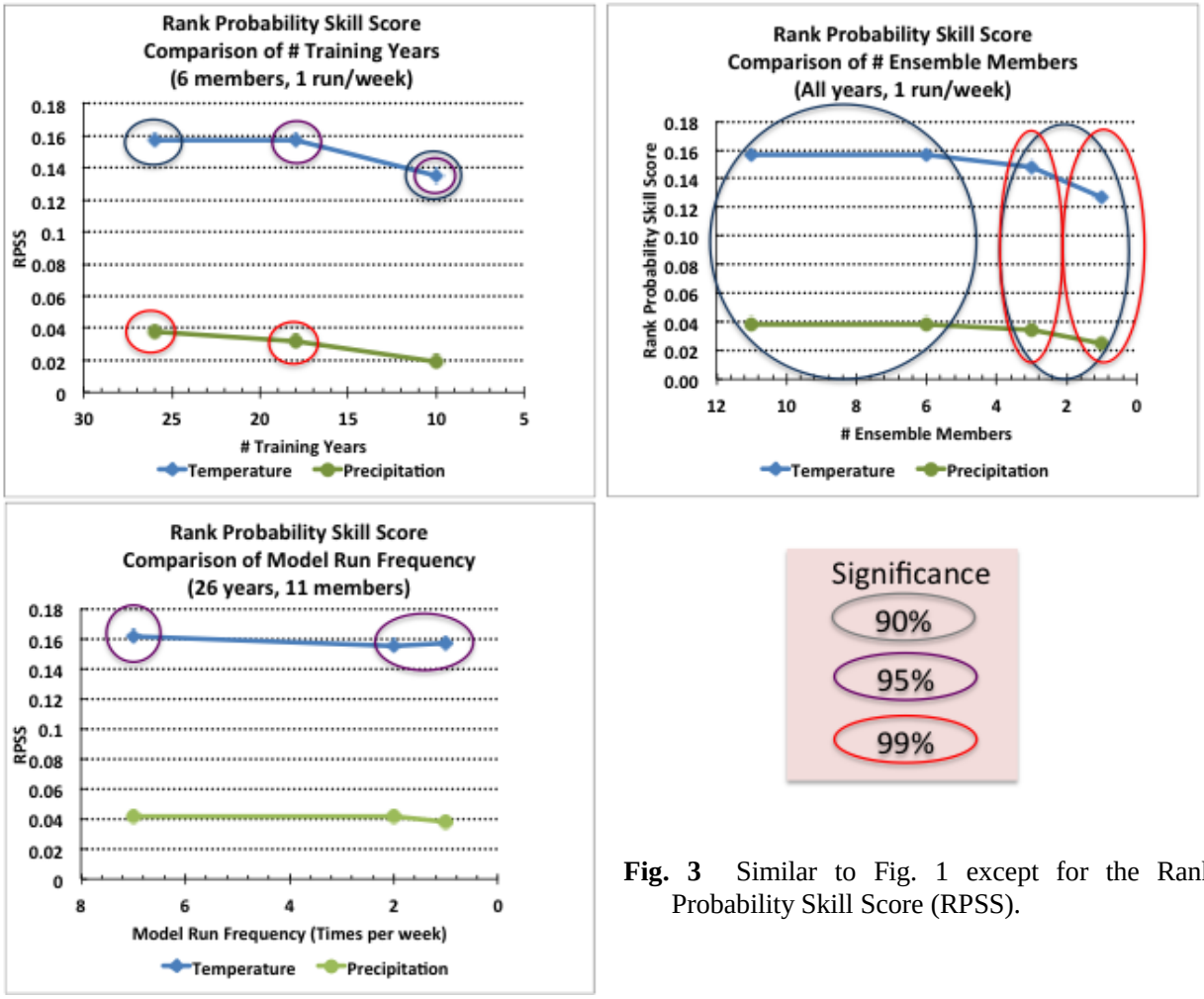

Fig. 3 Similar to Fig. 1 except for the Rank Probability Skill Score (RPSS).

Analysis of line plots of HSS (Fig. 1) shows the most significant drop in skill by changing the number of training years used in the reforecast sample and the least loss of skill from changing the model frequency, for both temperature and precipitation for the shown cases. For temperature, the significant drop in skill (with 6 members and 1 model run/week) occurs when using 10 years instead of 18 (HSS decreases by 1.2), whereas for precipitation the drop occurs when dropping from 26 years to 18 years (HSS decreases by 1.4). These skill differences have a significance level of 95% or greater.

For the selected line plot cases, changing the number of ensemble members only causes a significant drop in skill when using only one member (control run only) for both temperature and precipitation. The model run frequency only causes a noticeable drop in skill when going from 2 runs/week to 1 run/week for precipitation. The HSS of temperature is not greatly impacted by changing the number of ensemble members.

Bar histograms of HSS (Fig. 2) show similar results as the line plots of HSS, with the number of training years impacting the skill most and the number of ensemble members the least. The model run frequency impacts the skill of precipitation forecasts slightly more than temperature. In general, the line plots and

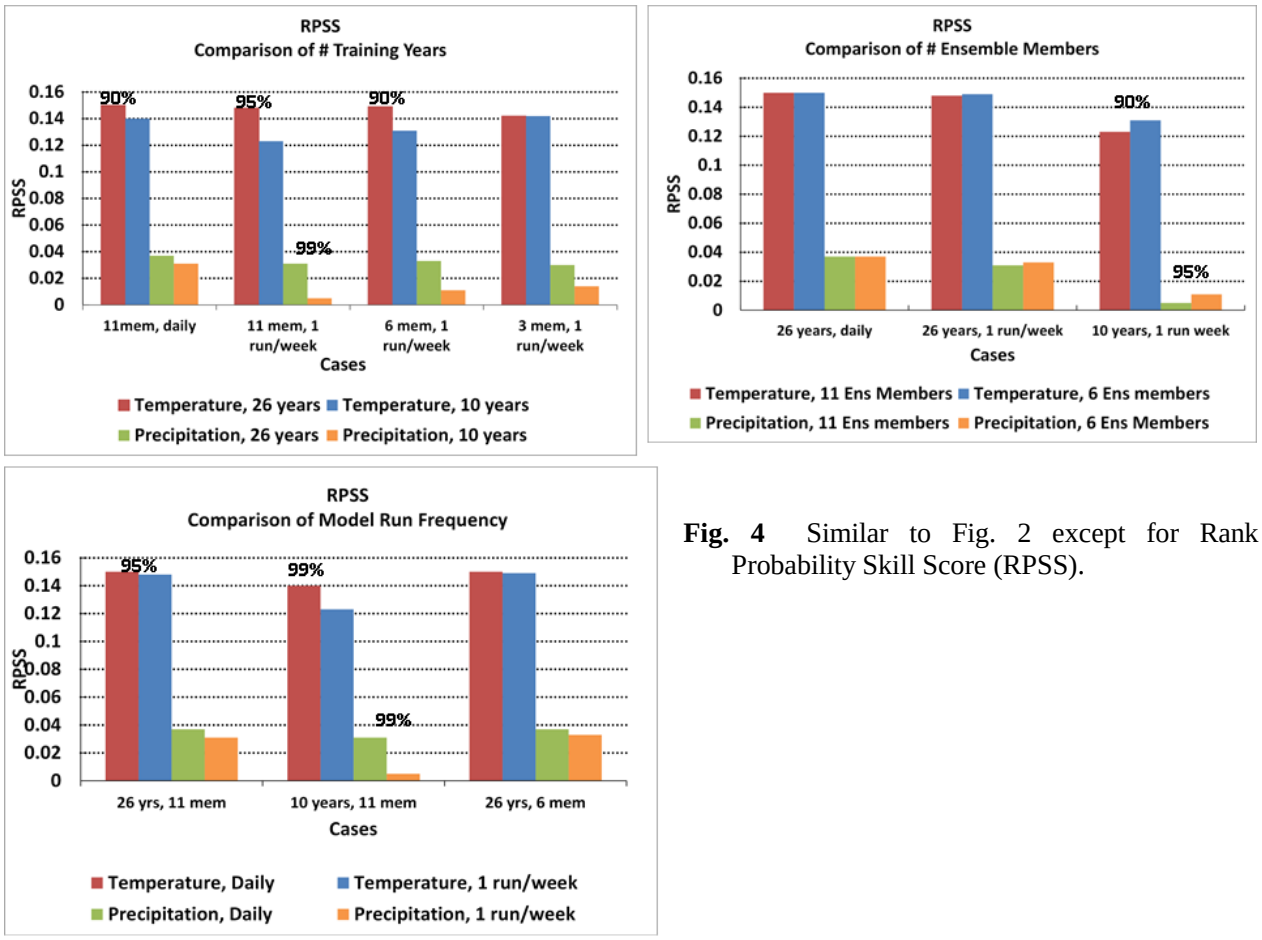

Fig. 4 Similar to Fig. 2 except for Rank Probability Skill Score (RPSS).

histograms of HSS show skill loss of about 2 when using 10 years instead of 26 for both temperature and precipitation.

An interesting feature of the results is that for some cases, a lower configuration of some parameters led to an increase in skill. For temperature, using 6 ensemble members instead of 11 for the case with 26 years and 1 run/week shows a small increase in skill. This is also true for using 1 run/week instead of daily runs (also for temperature). However, these examples do not have a high significance, although some examples shown later on do.

Like the line plots of HSS, the line plots of RPSS also show that the greatest loss in skill results from lower configurations of the number of training years and the least skill loss from changing the model run frequency. Similar to the HSS temperature line plots, the drop in skill occurs when using only 10 years. For precipitation, using 18 years instead of 26 caused a significant decrease in skill. Interestingly, the number of ensemble members shows a noticeable decrease in RPSS when dropping down to 3 members instead of just 1 in the case of the HSS. This would indicate that even though using 3 members does not greatly impact the hit-based aspect of skill assessing the number of correctly forecast, it does affect the ability of the forecast to properly issue the probabilities associated with the forecast.

The bar histograms of RPSS also show the greatest decrease in skill associated with the number of training years. Across the shown cases, the drop in skill from using 10 training years instead of 26 is about 0.02 for both temperature and precipitation. Precipitation has a more varied skill response amongst cases than temperature. Similar to the RPSS line plots, using 6 instead of 11 members across 3 different cases does not yield a significant difference in skill. The impact of model run frequency on skill in the line plot cases was not impressive, although, the cases in the histogram show varying results. The variance of skill difference is especially noticeable for precipitation, where the case of 26 years and 11 members yields a RPSS drop of

0.004 (case shown on line plot) but for 10 years and 11 members, there is a skill drop of 0.025. This exemplifies the importance of evaluating the impact of skill on decreasing training data configurations across various cases, varying the fixed parameters in different ways.

For the case where 10 training years and 1 run/week are used, using 6 ensemble members instead of 11 actually increases the skill by a small amount for temperature and precipitation (0.006 for temperature, 0.004 for precipitation). These results are significant to the 90% level for temperature, and 95% level for precipitation. Improvements in skill by lowering the reforecast sampling configuration would likely be due to overfitting of data, meaning that it is potentially useful to select a lower configuration to improve skill. Doing so, however, may impact the skill in different ways depending on the verification metric or method, such as scoring by separate categories, the type of score, *etc*.

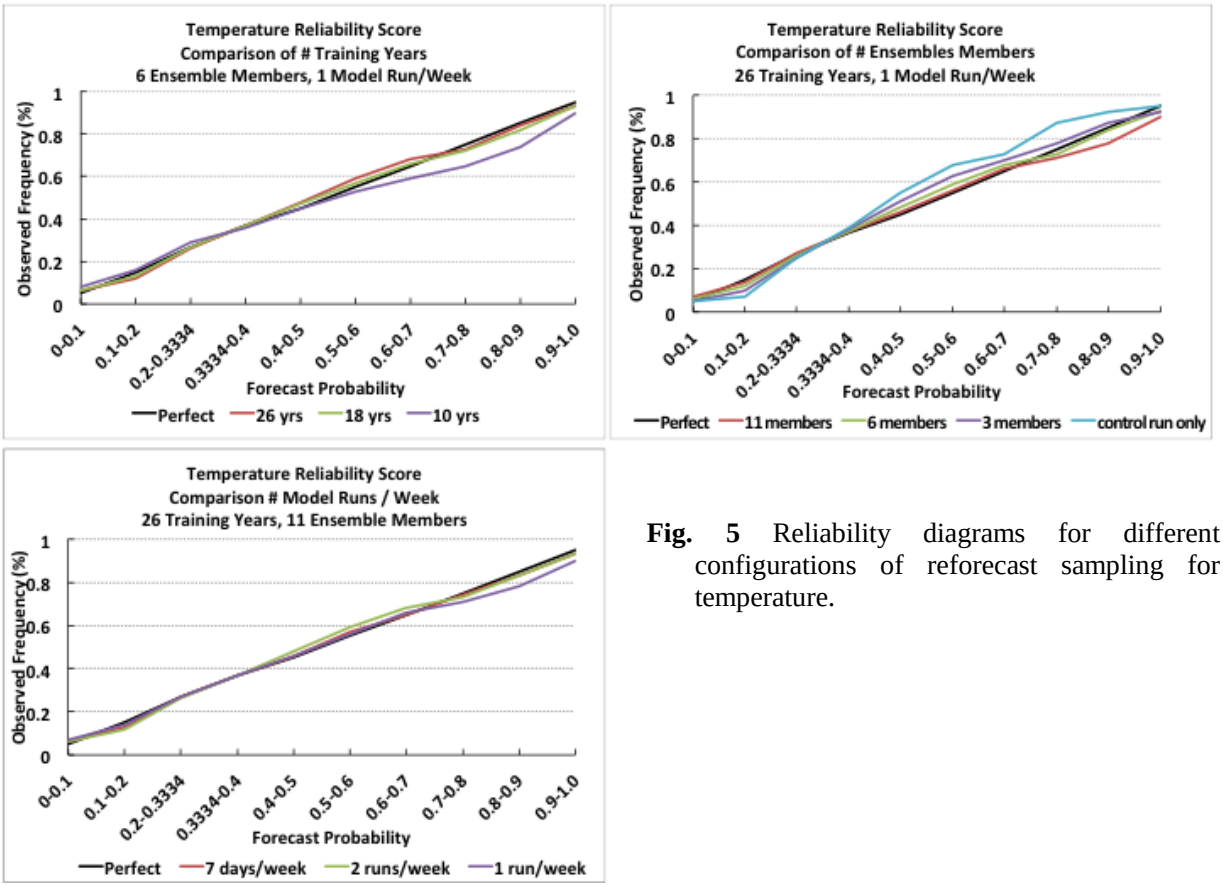

Fig. 5 Reliability diagrams for different configurations of reforecast sampling for temperature.

Reliability diagrams are shown for temperature (Fig. 5) and precipitation (Fig. 6) with the same cases as the line plots. These cases show that temperature forecasts have generally good reliability. The cases that cause the lowest reliability is using one ensemble member only (the control run) and using 10 training years. Using only the control run leads to forecast probabilities that are too low (for forecast probabilities 40% or greater) and using 10 years leads to forecast probabilities that are too high (for forecast probabilities of 60% or greater). The forecast probabilities that are too low or high are reflected by curves on the reliability diagram that lie above and below the perfect skill line, respectively.

Overall, the reliability of the precipitation forecasts (for the selected cases) show worse reliability than temperature, which is to be expected due to the inherent nature of it being a harder quantity to forecast. There is greater spread amongst the precipitation reliability curves across the cases compared to temperature, indicating that precipitation is more sensitive to reforecast sampling than temperature. These diagrams indicate the greatest decrease in skill results from using only 10 members and only the control run, while the model run frequency impacts skill the least, which is similar to the behavior of the reliability scores of temperature.

It is evident that the reliability curves start deviating from the perfect score line at lower probabilities in precipitation than temperature which may indicate that there is a greater range of forecast probabilities that are less reliable for precipitation. Regardless of these differences, the overall behavior of the skill seems to react in a similar manner for both temperature and precipitation when changing the parameters of the reforecast sampling.

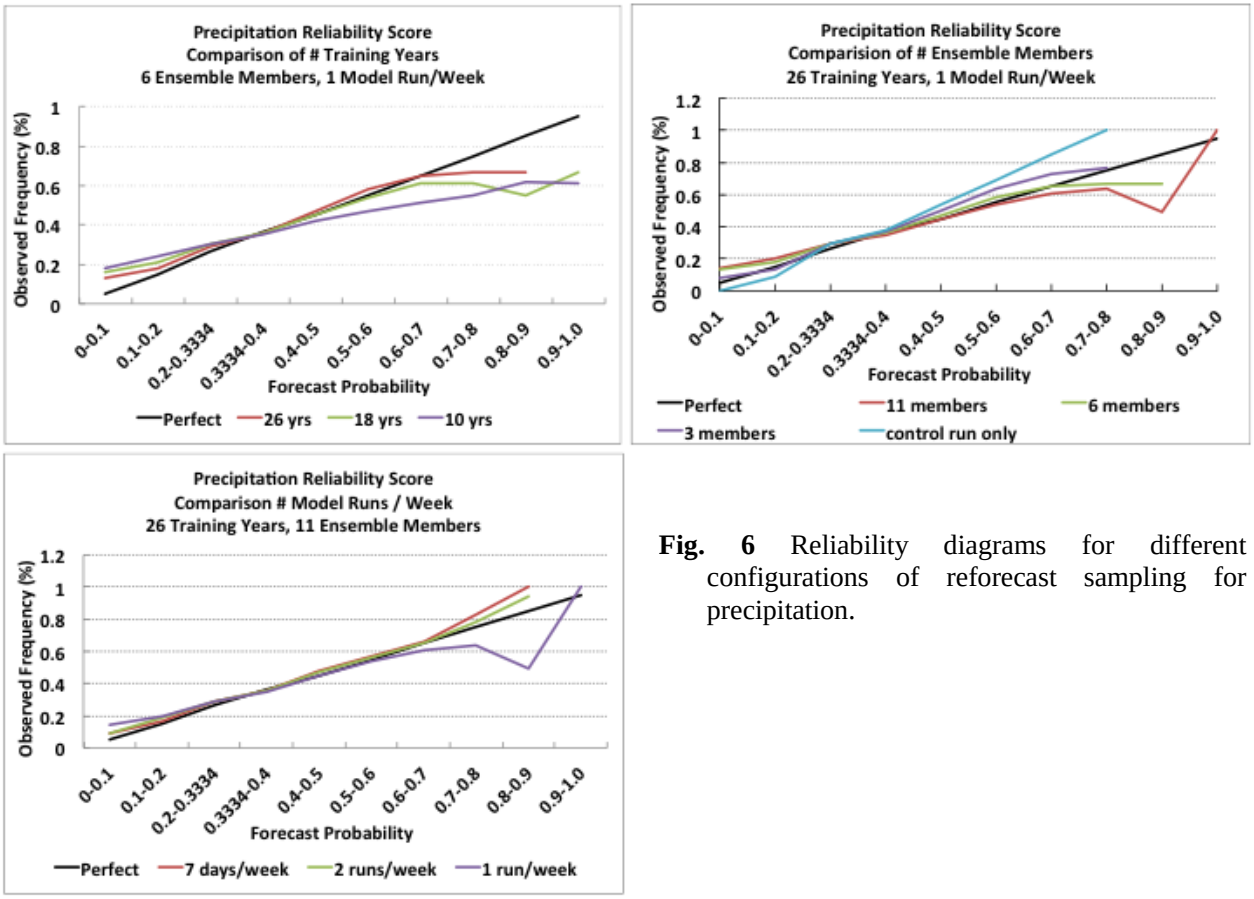

Fig. 6 Reliability diagrams for different configurations of reforecast sampling for precipitation.

4. Conclusions

Evaluation of skill scores of the week-2 reforecast tool indicate that temperature and precipitation forecasts are most sensitive to the number of training years of reforecasts used in the calibration and the least sensitive to the model run frequency. In general, precipitation forecasts are more sensitive to decreasing configurations of reforecasts than temperature.

It is important to assess the skill of forecasts using different score types. Skill metrics that assess forecast quality based on probabilities were impacted differently than those that assess the number of correctly guessed forecasts. Using 3 members or less of reforecasts did not impact the Heidke skill score, but it did noticeably decrease the RPSS.

The skill of precipitation forecasts is more sensitive to decreasing configurations of reforecasts than temperature, especially when evaluating the probabilistic aspect of skill. This shows that the forecast skill of different atmospheric variables may be sensitive to the configuration of different reforecast parameters. Therefore, determining the minimum required reforecasts for reforecast production should be driven by the atmospheric variable (of the variables desired to be forecast) that exhibits the most skill sensitivity to changing configurations of reforecast sampling. Despite the differences between temperature and precipitation regarding skill sensitivity, the type of impact to each are similar (*e.g.* using the control run only leads to forecast probabilities that are too low and using only 10 training years produces probabilities that are too high).

Even though decreasing the configuration of reforecasts may lead to some forecasts' decrease in skill, it is also evident that selective lower configurations can still produce skillful week-2 forecasts with minimal skill loss. Dropping down from 11 members to 6 and daily reforecasts to 1 model run per week only causes a minor decrease in skill, if sufficient training years are used.

CPC's recommendation for a lower configuration of reforecast sampling without significant week-2 forecast skill loss is to produce as many years as possible with 6 ensemble members and 1 run/week (weekly). In this case, the maximum years available for this study was 26 years, but 30 years would be desirable since it would be consistent with the standard CPC follows for their climatology and may allow forecasts to see further improvements in skill than the reforecast tool currently has. This configuration seems optimal from these evaluations based on significantly reducing the required resources needed to produce reforecasts without causing a great drop in skill for week-2 temperature and precipitation forecasts. Compared to real-time ensemble forecasts with 21 members per cycle and 4 cycles per day, weekly 6 member (5 members plus control run) reforecasts for 30 years would cost approximately 26% of the computing of the real-time ensemble reforecasts.

References

Unger, David A., Huug van den Dool, Edward O'Lenic, Dan Collins, 2009: Ensemble Regression. *Mon. Wea. Rev.*, **137**, 2365–2379.

Science and Technology Infusion Climate Bulletin
NOAA's National Weather Service
38th NOAA Annual Climate Diagnostics and Prediction Workshop
College Park, MD, 21-24 October 2013

Prediction of Short Rains over Equatorial East Africa Using Multi-Model Ensemble

T. k. Bahaga[1, 2], F. Kucharski[2], G. Mengistu Tsidu[1], and Hongwei Yang[3]

[1]*Addis Ababa University, Department of Physics, Addis Ababa, Ethiopia*

[2]*The Abdus Salam International Center for Theoretical Physics, Earth System Physics Section, Trieste, Italy*

[3]*APEC Climate Center, Busan, Republic of Korea*

1. Introduction

In this study the performance of dynamical seasonal forecast systems is evaluated for the prediction of short rain anomalies over equatorial East Africa. The evaluation is based on observational data and the Asia-Pacific Climate Center (APCC) Ocean-Atmosphere coupled Multi-Model Ensemble (MME) hindcasts. The ensembles of individual models and their MME mean are evaluated. Hindcasts initialized on 1st August for 24 years covering 1982-2005 periods alone are considered, as these are the most relevant to short rain predictions. This study is motivated by the desire to use the output of best seasonal forecasts over East Africa.

The climate of equatorial Eastern Africa is dominated by March to May (long rains) and September to November (short rains). Interannual variability of short rains over equatorial East Africa is dominated by changes on the large-scale with a clear link to tropical ocean-atmosphere variability. The Indian Ocean Dipole (IOD) and its influence on climate variability over surrounding regions have been reported by Saji *et al.* (1999). After the discovery of this mode, several studies focused on the Indian Ocean to understand variability of the short rains over East Africa (Black *et al.* 2003; Behera *et al.* 2005; Ummenhofer *et al.* 2009; Bahaga *et al.* 2013). These studies indicated that SON rainfall over East Africa (Indonesia) is increased (decreased) during positive IOD events.

2. Data, models and evaluation methods

2.1 Verification data

The observed rainfall data used in this study are derived from Climate Prediction Center (CPC) Merged Analysis of Precipitation (CMAP) (Xie and Arkin 1996). The observational SST data are obtained from

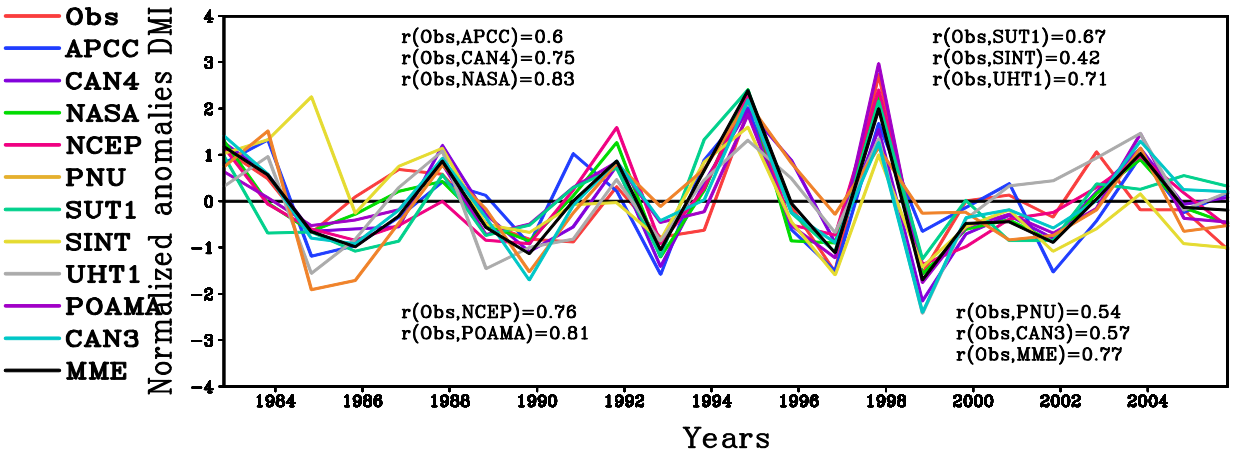

Fig. 1 Year-to-year variation of IOD derived from observation, Individual coupled models ensemble mean and MME mean hindcast SST anomalies normalized by standard deviation along with their correlation coefficient with respect to verification data.

Correspondence to: Titike Kassa Bahaga, Addis Ababa University, Department of Physics, Addis Ababa, Ethiopia.; Email: tkkassa@gmail.com, tbahaga@ictp.it.

improved Extended Reconstruction SST (ERSSTv3b, which includes satellite data) of Smith *et al.* (2006). This data was downloaded from http://www.ncdc.noaa.gov/ersst/ and is available from 1871 to present.

2.2 Coupled forecast models

The coupled models that are examined in this study are ten state-of-the-art fully coupled atmosphere-ocean-land seasonal prediction systems and are obtained from operational seasonal prediction models participating in the APCC MME seasonal forecast (Sohn *et al.* 2012).

2.3 Forecast quality measures

To measure the quality of a deterministic forecast, MME mean prediction was constructed using the simple average of ten models ensemble means. The metrics used to measure and evaluate prediction skill of individual coupled models ensemble mean and MME mean forecasts includes the spatial map of anomaly correlation coefficient (ACC) and simple correlations. Calculation of these quantities is standard (*e.g.*, Wilks 1995) and uses anomaly data, whereby the observed seasonal cycle and the hindcast climatology are removed from the observations and forecasts, respectively.

3. Results

3.1 IOD prediction in coupled models and MME

Bahaga *et al.* (2013) has shown that the IOD in the SST dipole mode index has high prediction skill for the variations of short rains. Here we consider SON mean SST anomalies for hindcast verification, which is the peak season in the evolution of IOD. In addition, IOD and equatorial East Africa short rains have strong contemporaneous relations at this time of the year.

Figure 1 show the forecast of interannual variation of SON season mean Dipole mode index (DMI) normalized by the corresponding standard deviation and derived from ten coupled models ensemble mean and MME mean hindcast initialized on the 1st of August. It is seen from Figure 1 that there is a large skill of IOD predictions for almost all models and their MME mean, as reflected in the large significant correlation of predicted SST anomalies with observation.

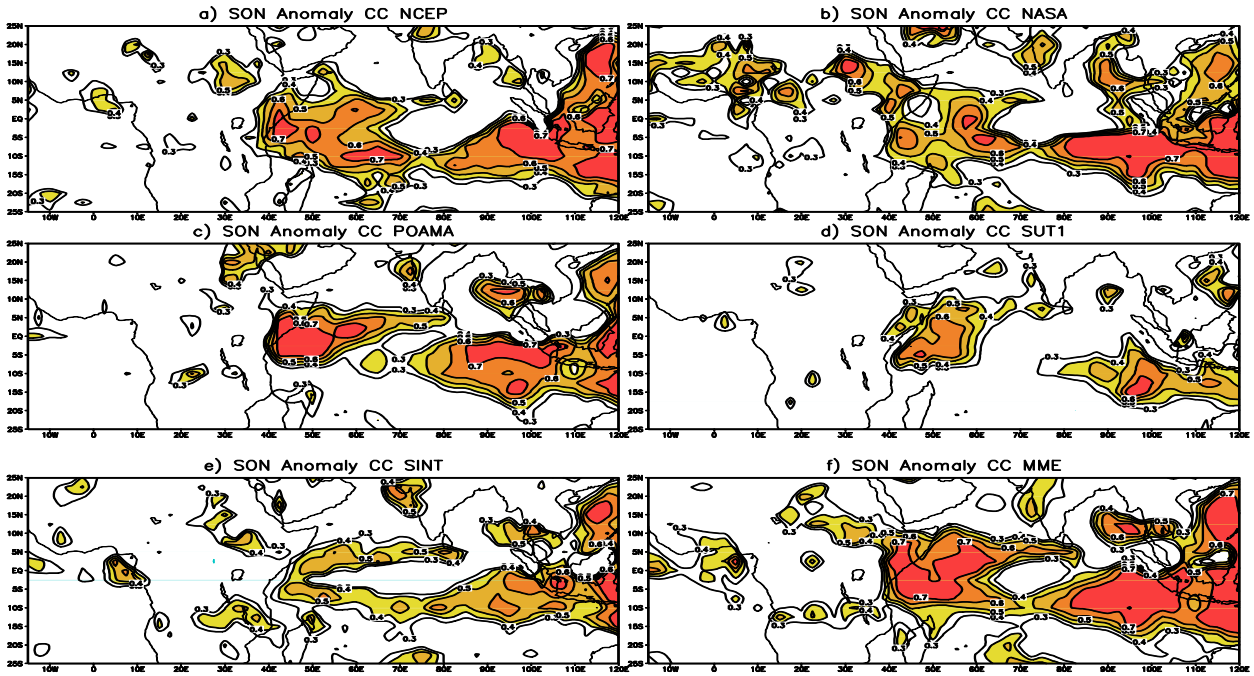

Fig. 2 Anomaly correlation coefficient (ACC) between SON observed rainfall and forecast rainfall derived from coupled models ensemble and MME mean during the period of 1982-2005 with a) NCEP, (b)NASA, (c) POAMA, (d) SUT1, (e) SINT, and (f) MME. Shaded positive values are significant at 95% confidence level.

The forecast skill for the SST anomalies in almost all models exhibits skill greater than 0.5 and also highly significant above 99.9% level, except for the SINT model (with a correlation of only 0.42). Models with high DMI forecast skill are NCEP, NASA, POAMA ensemble mean and MME mean. On the other hand, SUT1, PNU, and CANCM3 are characterized by relatively lower correlation. Moreover, DMI prediction shows very good skills with the major positive IOD events like 1982, 1994 and 1997 captured well in nearly all forecasts (Figure 1). In general, it can be concluded that the APCC coupled models and MME mean initialized on 1st August produce excellent predictions of the temporal behavior of the SST anomalies over the Indian Ocean.

3.2 Equatorial East Africa short rain prediction

Previous studies have demonstrated that IOD is the source of predictability for East African short rains (Behera *et al.* 2005; Bahaga *et al.* 2013). The skill of SON rainfall anomaly forecast is evaluated based on the Anomaly Correlation Coefficient (ACC) between the observation and coupled models forecast over Indian Ocean basin (Figure 2). Overall there is little or no skill found over most of land points, with the exception of the coast of East Africa and countries east of tropical Indian Ocean region where significant skill can be identified. A similar lack of rainfall predictability over most land regions has also been reported by Wang *et al.* (2009). On the other hand, most coupled models and MME mean show significant skill over ocean points in the south eastern Indian Ocean and western Indian Ocean (Figure 2a-f).

3.3 Short rain forecast skill

The interannual variation of equatorial East Africa rainfall index (EEARI) (5ºS-5ºN, 35-45ºE) and the correlation between observed and each coupled models ensemble and MME mean is shown in Figure 3. The figure illustrates that five coupled models predict equatorial East Africa rainfall with statistically significant skill. NCEP prediction giving the strongest correlation of all and SUT1, UHT, POAMA and CANCM3 also show significant skill. The other models have relatively lower skill and are unable to produce significant correlations. Despite insignificant skill in some individual models, MME mean produce the fourth largest significant correlation at 95% confidence level.

3.4 MME mean forecast skill improvements by model selection

Finally we consider improvements of forecast skill in the MME mean hindcasts of SON equatorial East Africa rain-fall by selecting five good models according to their correlation skill in predicting the EEARI index (Figure 3). Only models that show at least 90% statistically significant correlations are selected. The resulting models are UHT1, NCEP, POAMA, SUT1 and CANCM3. Such a selection should be revisited once more hindcast data is available. The correlation between observed and ensemble mean of EEARI for the selected coupled models and their MME mean is shown in Figure 4. The 90% significant level is indicated by

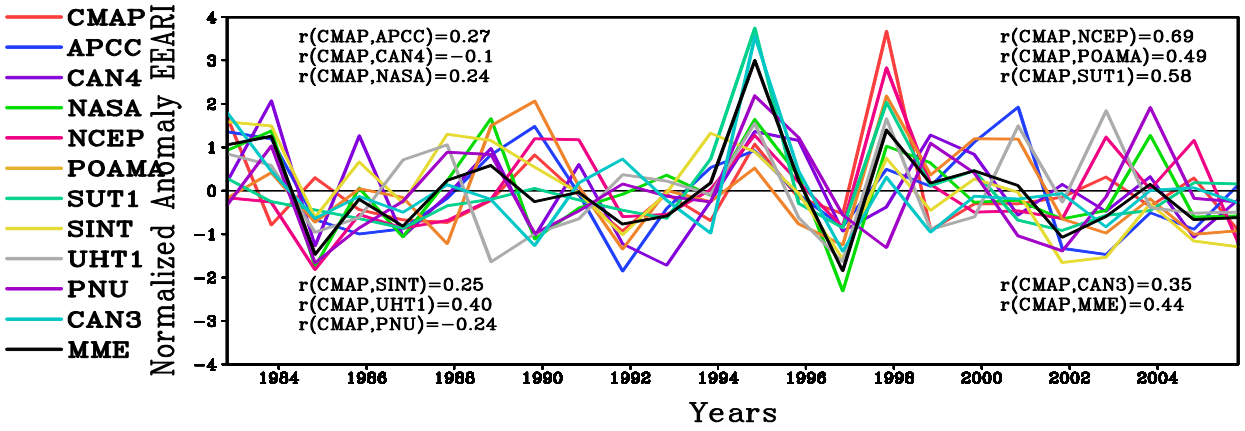

Fig. 3 Interannual variation of SON normalized anomaly over equatorial East Africa in APCC coupled models hindcast and MME mean verified against observation along with the spatial correlation between observed and predicted SON equatorial East Africa rainfall index (EEARI) (5ºS-5ºN, 35-45ºE) for a period of 1982-2005.

the horizontal dashed line. Thus the skill of the MME based on this model selection improves its skill from 0.44 for all models to 0.67.

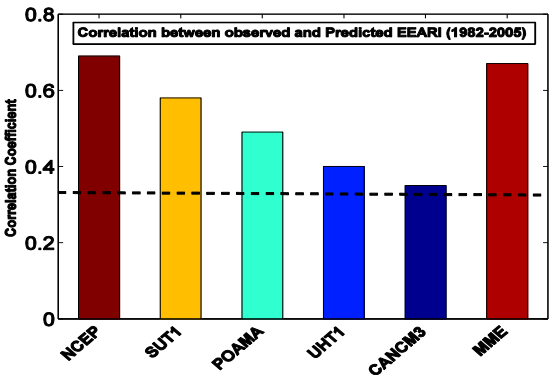

Fig. 4 Correlation between observed and predicted SON Equatorial East Africa rainfall for hindcasts in APCC coupled models dataset for a period 1982-2005, the correlation is calculated for the same index.

4. Conclusions

Hindcast experiments from 10 APCC coupled models ensemble mean and their MME mean were analyzed regarding their predictive skill of East African rainfall. Coupled model hindcast also evaluated for prediction of SST anomalies over tropical Indian Ocean. Nearly all models and MME mean shows statistically high significant skill in forecasting the peak phase of the IOD in the boreal autumn season, which is typically when the IOD is best defined and most climatically important. Furthermore, out of ten models five coupled models and MME mean show statistically significant skill in predicting equatorial East Africa short rains. The results of this study reveal an encouraging potential for real time forecasts of East African rainfall with about one month lead time. Such forecasts would be of substantial societal importance.

References

Bahaga, T. K, G. M. Tsidu, F. Kucharski, and G.T. Diro, 2013: Potential predictability of the SST-Forced Equatorial East African short rain interannual variability in the 20th century. *Q. J. R. Meteorol. Soc.*, DOI: 10.1002/qj.2338, in press.

Behera, S. K., J.J. Luo, S. Masson, P. Delecluse, S. Gualdi, A. Navarra, and T. Yagamata, 2005: Paramount impact of the Indian Ocean dipole on the East African short rains: A CGCM study. *J. Climate*, **18**, 4514–4530.

Black E., J. M. Slingo, and K. R. Sperber, 2003: An observational study of the relationship between excessively strong short rains in coastal East Africa and Indian Ocean SST. *Mon. Wea. Rev.*, **131**, 74–94.

Saji, N. H., B. N. Goswami, P. N. Vinayachandran, and T. Yamagata, 1999: A dipole mode in the tropical Indian Ocean. *Nature*, **401**, 360–363.

Smith, T. M., R. W. Reynolds, T. C. Peterson, and J. Lawrimore, 2006: Improvements to NOAA's historical merged land ocean surface temperature analysis. *J. Climate*, **21**, 2283–2296

Sohn, S. J., Y. M. Min, J. Y. Lee, C. Y. Tam, I. S. Kang, B. Wang, J. B. Ahn, and T. Yamagata, 2012: Assessment of the long-lead probabilistic prediction for the Asian summer monsoon precipitation (1983 - 2011) based on the APCC multimodel system and a statistical model. *J. Geophys. Res.*, **117**, DOI: 10.1029/2011JD016308.

Ummenhofer, C. C., A. S. Gupta, M. H. England, and C. J. C. Reason, 2009: Contributions of Indian Ocean sea surface temperatures to enhanced East African rainfall. *J. Climate*, **22**, 993–1013.

Wang, B., J.-Y. Lee, I.-S. Kang, and Co-authors, 2009: Advance and prospectus of seasonal prediction: Assessment of the APCC/CLI PAS 14-model ensemble retrospective seasonal prediction (1980 - 2004). *Clim. Dyn.*, **33**, 93–117.

Wilks, D. S., 1995: Statistical methods in the atmospheric sciences: An introduction. *Academic Press*.

Xie, P., P. A. Arkin, 1996: Analysis of global monthly precipitation using gauge observations, satellite estimates, and numerical model predictions. *J. Climate*, **9**, 840–858.

Science and Technology Infusion Climate Bulletin
NOAA's National Weather Service
38th NOAA Annual Climate Diagnostics and Prediction Workshop
College Park, MD, 21-24 October 2013

Meteorological Drought Prediction Using a Multi-Model Ensemble Approach

Li-Chuan Chen[1], Kingtse Mo[2], Qin Zhang[2], and Jin Huang[2]

[1] *Earth System Science Interdisciplinary Center/Cooperative Institute for Climate and Satellites, University of Maryland, College Park, MD*

[2] *Climate Prediction Center, NCEP/NWS/NOAA, College Park, MD*

1. Introduction

In the United States, drought is among the costliest natural hazards, with an annual average of 6 billion dollars in damage (NCDC 2013). Drought prediction from monthly to seasonal time scales is of critical importance to disaster mitigation, agricultural planning, and multi-purpose reservoir management. Started in December 2012, NOAA Climate Prediction Center (CPC) has been providing operational Standardized Precipitation Index (SPI) Outlooks using the North American Multi-Model Ensemble (NMME) forecasts, to support CPC's monthly drought outlooks and briefing activities. The current NMME system consists of six model forecasts from U.S. and Canada modeling centers, including the CFSv2, CM2.1, GEOS-5, CCSM3.0, CanCM3, and CanCM4 models (Kirtman *et al.* 2013). Detailed information about the NMME project and forecasts can be found on CPC website (http://www.cpc.ncep.noaa.gov/products/NMME). In this study, we conduct an assessment of the meteorological drought predictability using the retrospective NMME forecasts for the period from 1982 to 2010. The standardized precipitation index, which measures precipitation deficits over a period of time, is used to predict meteorological drought.

2. Methodology

The current NMME SPI prediction framework is similar to the CFSv2 SPI prediction system that developed by Yoon *et al.* (2012). For each model, monthly-mean precipitation (P) forecasts were first bias corrected and spatially downscaled (BCSD) to regional grids of 0.5-degree resolution over the contiguous United States based on the probability distribution functions (PDFs) derived from the hindcasts. As a result, BCSD scheme corrects both the climatological mean and standard deviation of the hindcasts. Specifically, for each month and lead time, the PDF at each grid point is computed based on model hindcasts excluding the target year. The bias-corrected percentile for the target year is then obtained from the inverse PDF of the P analysis based on the percentile calculated from the PDF of the hindcasts. The BCSD method was applied to each member and each lead of the P hindcasts. The corrected P forecasts were then appended to the CPC Unified Precipitation Analysis (Chen *et al.* 2008) to form a P time series for computing 1-month, 3-month, 6-month, and 12-month SPIs. The NMME-ensemble SPI forecasts are the equally weighted mean of the six model forecasts. Two performance measures, the anomaly correlation coefficient (ACC) and root-mean-square errors (RMSE) against the observations, are used to evaluate forecast skill. In this study, CPC Unified Precipitation Analysis is used as the observations for forecast evaluation.

3. Results and discussions

Figure 1 shows the relation of SPI forecast skill to lead time for January and July. In this figure, color lines are for model forecasts and the bold black line is for the ensemble forecasts. The values plotted in the figure are the averages over the continental U.S. For 3-month SPI (SPI3), skill quickly drops and is very close to the P forecast skill after Lead 3, when observations are no longer included in the 3-month window. Similar results are observed for 6-month SPI (SPI6). When P observations are no longer included in the 6-month window at Lead 6, SPI6 forecast skill converges to the P forecast skill. We also notice that when there are more observations include in the time window, for example, Month-1 SPI6 forecasts include 5 months of observations, its skill is higher than Month-1 SPI3 forecasts, which include 2 months of observations. Therefore, P observation is a dominant factor contributed to the SPI forecast skill and the small differences

Correspondence to: Li-Chuan Chen, ESSIC/CICS-MD, University of Maryland, 5830 University Research Court, College Park, MD 20740, U.S.A.; Email: LiChuan.Chen@noaa.gov.

among models. Similar results are observed for using ACC and RMSE as performance measures and for different months.

Another thing we notice from this figure is that for both SPI3 and SPI6, the ensemble forecasts, which are on top of most model forecasts in the ACC plots and on the lower end of most model forecasts in the RMSE plots, have higher skill than that from individual models, but the differences are not large. If we use 0.5 as a threshold for ACC and 0.8 as a threshold for RMSE to determine skillful forecasts, both ACC and RMSE suggest similar results that SPI6 forecasts are skillful out to four months.

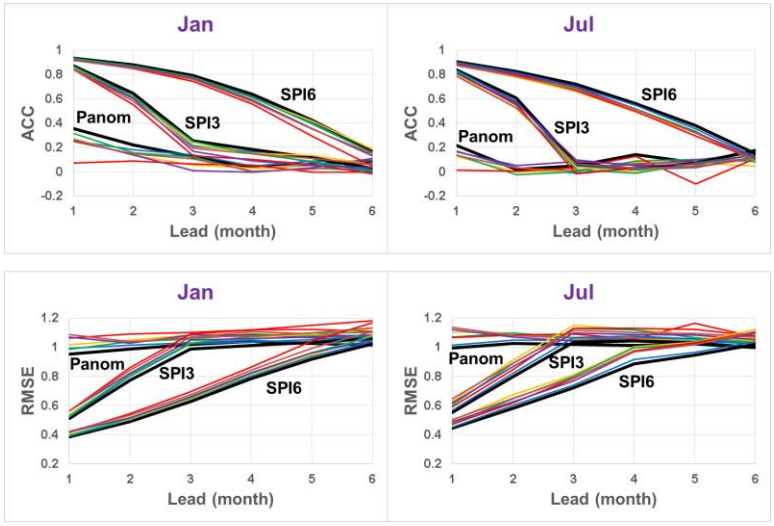

Fig. 1 Relation of SPI forecast skill to lead time for January and July.

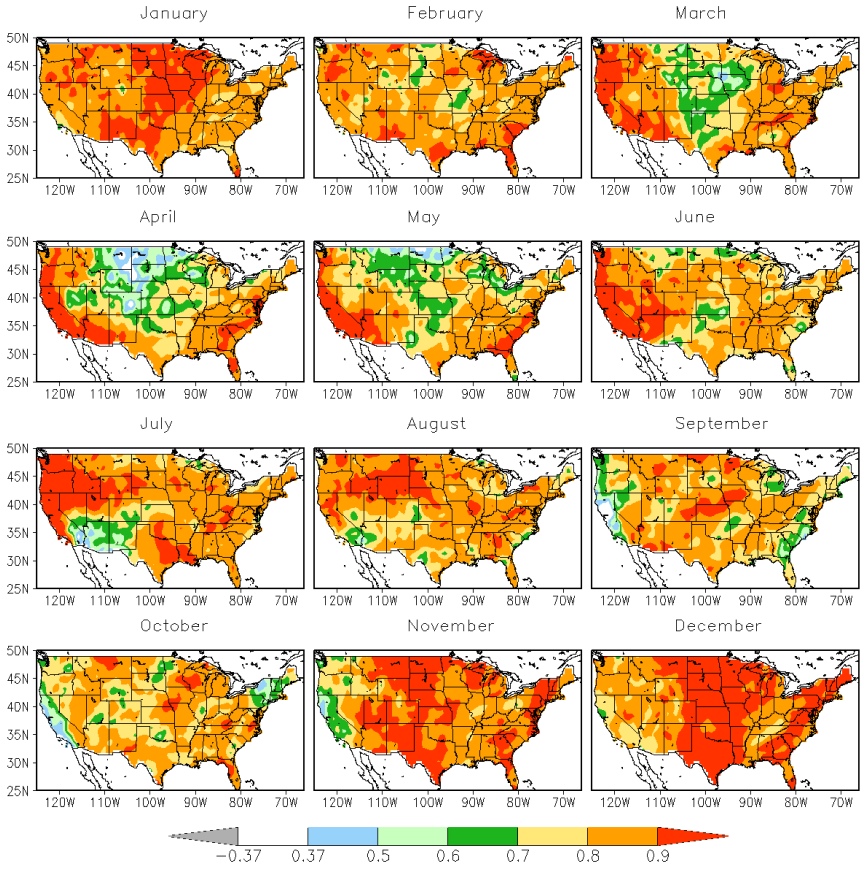

Fig. 2 ACC maps of Month-1 SPI3 forecasts for all 12 months.

Figure 2 shows the ACC maps of Month-1 SPI3 forecasts for all 12 months. We can see that predictive skill is seasonally and regionally dependent. Skill generally is higher for the winter season (*e.g.*, January) and lower in the Spring (*e.g.*, April). Areas with high forecast skill in the month generally correspond to the dry climatology in the region. For example, over central U.S. for January and along the West Coast in July. Areas with low forecast skill in the month generally correspond to the wetter climatology in the region. For example, springtime over the central U.S. is the time of rain showers, and July over the Southwest is their monsoon season.

4. Conclusions

For P forecasts (figures not shown), errors vary among models and predictive skill generally is low after the second month. All model P forecasts have higher skill in winter and lower skill in summer. BCSD improves RMSE for both P and SPI forecasts, but the differences in ACC between with and without BCSD are marginal (and not statistical significant). Most RMSE improvements are over the western mountainous regions and along the Great Lake. Although P forecast skill is not large and quickly drops after one month, SPI predictive skill is high and the differences among models are small. Generally, model with lower P forecast skill has lower SPI forecast skill. The skill mainly comes from the P observations appended to the model forecasts. This

factor also contributes to the similarity of SPI prediction among the six models. Still, NMME SPI ensemble forecasts have higher skill than those based on individual models or persistence.

Overall, SPI predictive skill is regionally and seasonally dependent, and NMME SPI6 forecasts are skillful out to four months. SPI forecast skill at a region corresponds to local rainfall climatology and variability. Dynamical models improve SPI predictive skill from baseline skill when and where P forecasts are skillful. The improved skill of SPI prediction during the wet seasons spanning roughly late autumn to early spring over the Southwest and Gulf Coast region is attributed to the known impacts of ENSO signals on these regions' cold-season precipitation, which is consistent with the findings by Quan *et al.* (2012) from CFSv2 SPI prediction.

References

Chen, M., W. Shi, P. Xie, V. B. Silva, V. E. Kousky, R. W. Higgins, and J. E. Janowiak, 2008: Assessing Objective Techniques for Gauge-Based Analyses of Global Daily Precipitation, *J. Geophys. Res.*, **113**, D04110. doi:10.1029/2007JD009132.

Kirtman, B. P., and Coauthors, 2013: The North American Multi-Model Ensemble (NMME): Phase-1 Seasonal to Interannual Prediction, Phase-2 Toward Developing Intra-Seasonal Prediction. *Bull. Amer. Meteor. Soc.* doi: 10.1175/BAMS-D-12-00050.1, in press.

National Climatic Data Center (NCDC), 2013: Billion Dollar U.S. Weather Disasters, 1980-2012. Available online at http://www.ncdc.noaa.gov/ol/reports/billionz.html.

Quan, X.-W., M. P. Hoerling, B. Lyon, A. Kumar, M. A. Bell, M. K. Tippett, H. Wang, 2012: Prospects for Dynamical Prediction of Meteorological Drought. *J. Appl. Meteor. Climatol.*, **51**, 1238–1252. doi: 10.1175/JAMC-D-11-0194.1.

Yoon, J.-H., K. C. Mo, and E. F. Wood, 2012: Dynamic-Model-Based Seasonal Prediction of Meteorological Drought over the Contiguous United States. *J. Hydrometeor.*, **13**, 463–482. doi: 10.1175/JHM-D-11-038.1.

Science and Technology Infusion Climate Bulletin
NOAA's National Weather Service
38th NOAA Annual Climate Diagnostics and Prediction Workshop
College Park, MD, 21-24 October 2013

Recent Science Advancement in Seamless Weather to Climate Modeling and Prediction

Jiayu Zhou, S&TI Climate Mission, Office of Science and Technology, NWS/NOAA
Wayne Higgins, Climate Program Office, OAR/ NOAA
Mike Halpert, Climate Prediction Center, NCEP/NWS/NOAA

1. Overview

The climate-weather-water connection is a grand challenge for NOAA. The weather to climate continuum demands a unified modeling and seamless prediction framework. Since the predictability of long-term climate is largely uncertain and demands increased basic research, the service is advised to put the emphasis on short-term climate applications, by expanding the current weather service to provide much needed weather-climate services, incorporating short-term climate monitoring and prediction with reliable and skillful information.

2. Long-term climate is what you get

a. Correction on weather-climate classification

According to an analysis of observed variability characterized by spectral composites (Lovejoy and Schertzer 2013), only the average of short-term climate/macroweather (10 days to 10-30 years) converges to normal, so that products of probabilistic prediction with shallow uncertainty are well justified for application uses. However, long-term climate processes (10-30 years to 100,000 years) are "weather-like", of which the variability grows with an increase of time scale.

This important characteristic is known to be missing in current Earth system model simulations due to a lack of internal long-term processes that interact with boundary conditions and are coupled with external forcings (Lovejoy, Schertzer and Varon 2013).

b. Profound uncertainties in long-term projection

Natural long-term climate change at any time or place is (qualitatively and quantitatively) unexpected in very much the same way that the weather is unexpected due to the variability growing with time. Most people understand the greenhouse effects of anthropogenic greenhouse gases. The real problem is the projection of future long-term climate, for which greenhouse gases are only one of the players. The others and interactions among all players with chaotic internal dynamics are far from well explored and understood, which brings out concerns about the reliability of current long-term climate projection products and present a barrier to clear-cut policy and decision making.

i) Climate change on hold?

Recent CO_2 emissions have actually risen even more steeply than people feared. As a result, according to most climate models, the temperature should have risen about 0.25°C over the past 10 years. However, the increase over the last 15 years was just 0.06°C. Model deficiencies are increasingly getting the attention of climate scientists as to what could be the fundamental problems (von Storch et al. 2013).

ii) Warming of deep ocean

Warming really means heating that could be felt in many ways. Recent observational studies show ongoing warming of deep oceans at an alarming rate (Balmaseda 2013), which could be related to the slowdown of global surface air temperature rising. This part of the energy imbalance induced by the greenhouse gases was not observed throughout previous record.

Correspondence to: Jiayu Zhou, Office of Science and Technology, NOAA's National Weather Service, Silver Spring, MD 20910; E-mail: jiayu.zhou@noaa.gov.

iii) Cooling in near future?

Though greenhouse gases play a role in the earth's energy balance by trapping energy and radiating it back to earth, the ultimate heat source of the Earth-atmosphere system is incoming solar radiation. By analyzing the average annual balance of the thermal budget, it has been demonstrated that the negative energy balance that has occurred since the 90's (Abdussamatov 2012), will likely continue during the next a few 11-year solar cycles.

3. Toward unified probabilistic modeling for reliable weather-climate seamless prediction

No forecast can be considered reliable without an accurate assessment of forecast uncertainty. With the power law behavior for atmospheric energy, uncertainties in subgrid processes propagate upscale by nonlinear dynamical effects. The errors with conventional numerical algorithms based on deterministic closures, which represent subgrid processes by the bulk-average effect of some putative large ensemble, appear to lead to substantial biases and considerable uncertainty in simulating climate. With increasing resolution, the convergence to the 'true' underlying equations is exceptionally slow.

The development of explicitly probabilistic weather and climate models, in which the inherent uncertainty is recognized explicitly without scale separation (Palmer 2012), gives more reliable estimates of uncertainty that pave the way for significant advancement of weather-climate prediction.

4. Guidance for effective development

a. Embrace seamless prediction and unified modeling framework

The seamless prediction concept, which emphasizes the interdependency in predictability between weather and climate, is increasingly recognized as a critical paradigm. In particular, a unified modeling framework for seamless prediction is required not only to optimize the usage of NOAA modeling resources but also accelerate improvement of the weather-climate model performance.

b. Meet challenges

NOAA is facing considerable challenges in continuously improving its operational Climate Forecast System, finding the resources needed to develop multiple climate models with high resolution and full physics, and at the same time running large ensemble integrations from states initialized with contemporary observations. To be successful, the agency is reorganizing to mobilize all positive factors by remove obstacles, *e.g.* fragmentation etc. (Rood 2013).

References

Abdussamatov, H.I., 2012: Bicentennial decrease of the total solar irradiance leads to unbalanced thermal budget of the Earth and the Little Ice Age. *Appl. Phys. Res.*, **4**, 178-184.

Balmaseda, M.A., K.E. Trenberth, and E. Källén, 2013: Distinctive climate signals in reanalysis of global ocean heat content. *Geophys. Res. Lett.*, **40**, 1754–1759.

Lovejoy, S., 2013: What is climate? *Eos*, Transactions, AGU, **94**, 1-2.

Lovejoy, S., D. Schertzer, and D. Varon, 2012: Do GCMs predict the climate ... or macroweather? *Earth Syst. Dynam.*, **4**, 439–454.

Palmer, T.N., 2012: Towards the probabilistic Earth-system simulator: a vision for the future of climate and weather prediction. *Q. J. R. Meteorol. Soc.*, **138**, 841-861.

Rood, R.B., 2013: To be the best in weather forecasting: Why Europe is beating the U.S. Capital Weather Gang blog (03/08), *Washington Post*.

Von Storch, H., A. Barkhordarian, K. Hasselmann, and E. Zorita, 2013: Can climate models explain the recent stagnation in global warming? *Academia.edu*, https://www.academia.edu/4210419/Can_climate_models_explain_the_recent_stagnation_in_global_warming

Science and Technology Infusion Climate Bulletin
NOAA's National Weather Service
38th NOAA Annual Climate Diagnostics and Prediction Workshop
College Park, MD, 21-24 October 2013

National Earth System Prediction Capability Project

Daniel P. Eleuterio
Office of Naval Research, Arlington, VA
Jessie C. Carman
NOAA's Office of Oceanic and Atmospheric Research, Silver Springs, MD

1. Background

The national Earth System Prediction Capability (ESPC) initiative arose from an agreement between DoD (Navy, Air Force) and NOAA leaders signed in 2010 to design and build the next generation global environmental analysis and prediction capability, covering time scales from days to decades. Due to the research needed, the effort was expanded in 2012 to include DoE, NASA, and NSF to improve communication and synergy for global prediction of weather, ocean, and sea ice conditions and for coordination of research-to-operations at weather to short-term climate variability timescales.

By coordinating efforts across agencies, ESPC hopes to develop a U. S. national research agenda that will lead to improved operational prediction across time scales. While acknowledging separate agency missions and requirements, this research agenda will encourage a common core capability based on common prediction requirements, interoperability, and forecast model standards; and lead to a global coupled air-sea-land-ice prediction capability based on multi-model ensembles.

In a series of articles in a special issue of the Bulletin of the American Meteorological Society, an international group of scientists put forth a strong argument for rationalizing investment in numerical prediction and accelerating capability to meet current and emerging requirements. Shapiro et al. (2010) calls for a holistic approach to NWP, linking observations, models, assimilation and analysis systems, and high-performance computing. Brunet et al. (2010) calls for a seamless weather-to-climate prediction system with special focus on the need for improvement of the representation of processes, particularly tropical convection, to improve prediction. The National Earth System Prediction Capability intends to meet these needs by fostering connections among the various modeling agencies and computing advances, taking a unified view across time scales.

2. National ESPC goals

The next-generation national operational environmental prediction system will use coupled model development to advance computational and environmental numerical prediction science and technology, and implement a computation suite across partner operational prediction centers. The system will use guided, focused process studies to enhance our understanding of the complex interactions of the earth environmental system that influence predictability at these longer time scales. The system will provide better quantification and display of uncertainty and forecast risk through probabilistic prediction techniques, and will improve assessments of predictive capability with better skill scores and metrics appropriate for the longer time scales. In this way ESPC's goal is to better inform public and private safety and policy decisions for the United States in an increasingly complex and changing global human enterprise.

3. Programmatic strategy

ESPC builds on the past successes achieved by interagency efforts. Notable among these successes is the Hurricane Forecast Improvement Program (HFIP) (Gall *et al.* 2013), which is providing rapid improvement in research-to-operations for both US (via NOAA) and global (via Navy) tropical cyclone track and intensity

Correspondence to: Daniel P. Eleuterio, Office of Naval Research, Arlington, VA;
E-mail: Daniel.eleuterio@navy.mil.

prediction capability. HFIP uses a distributed computing concept to leverage the resources of multiple agencies.

Another interagency success on which to build is the National Unified Operational Prediction Capability (NUOPC) (Sandgathe *et al.* 2011), which is using multi-model ensembles to improve medium-range (5-16 day) forecasts and provide probabilities of specific events. NUOPC also uses the distributed computing concept by combining the operational model output from several prediction centers to improve the medium-range capability.

ESPC also benefits from the National Multi-Model Ensemble (NMME) (Kirtman *et al.* 2013), which provides guidance out to 12 months using multi-model ensembles of climate models from both operational and research agencies and offices. NMME began as a proof-of-concept research initiative; even though the models are run at sub-optimal resolution leaving room for skill improvement with resolution, the project has quickly found a much-needed niche and will develop to better meet forecast needs over this time scale. Expanding on the other interagency efforts, NMME distributes computing and maintenance across not just operational but also research facilities.

In building the interagency "system of systems" ESPC will rely on existing collaborative community models to characterize parts of the earth environment. The Hybrid Coordinate Ocean Model (HYCOM) (Bleck 2002) and its data assimilation system have been developed to provide daily, weekly, and extended forecasts of global ocean conditions at high (~3km) horizontal resolution. WaveWatch III (Tolman *et al.* 2011) provides surface wave growth, decay, refraction and other properties of the wave fields. Both HYCOM and WaveWatch III are used extensively in academia for continued research. Additionally, the Los Alamos Sea Ice Model (CICE) was developed for coupling to various global and regional models, including those participating in the Fourth and Fifth Assessment reports of the Intergovernmental Panel on Climate Change. Land models such as NASA's Land Information System and NOAA's Noah Land Model permit partners to access the latest model improvements. The Naval Research Laboratory is in the process of integrating these models into a short to medium range (0-90 days) Earth system coupled prediction capability that has shown good progress in initial case studies and sensitivity tests (Metzger *et al.* 2014).

To improve coupling and sharing across component models, ESPC relies on the Earth System Prediction Suite (ESPS) common model architecture (Collins *et al.* 2005). ESPS is a collection of earth system component models and interfaces that are interoperable, documented, and available for community use. With a focus on coupled modeling systems across weather and climate scales, ESPS is intended to formalize code preparation for cross-agency use, establishing plug-and-play capabilities via the NUOPC interoperability layer and simplify toolkit code selection for the broader research community. By increasing interoperability, ESPS is intended to leverage the legacy investments from NASA, NOAA, NSF, DOE, and Navy.

4. Scientific strategy

a. Coupled Modeling

Coupling between Earth system components improves predictive skill across time scales. While this is relatively well established at climate scales and in highly forced mesoscale conditions such as in tropical cyclones, recent UKMO work[1] identifies ocean coupling as an important way to improve model fidelity significantly even in the 5-15 day time range. A recent National Academy Press study (NRC. 2010) elaborated on the importance of exploiting low-order modes and sources of predictability within the climate system, to create intraseasonal to interannual predictions of the weather-climate system.

For short range prediction, tropical cyclone intensity and track is dependent on upper ocean heat content, i.e. the temperature and the thickness of the near-surface warm layer, which either provides available heat to fuel convection, or curtails convection if wind-driven ocean mixing penetrates to deeper cold layers, bringing them to the surface. Weather prediction in the littoral and coastal zones depend greatly on air-ocean temperature contrasts for land-breeze, sea-breeze, fog and stratus phenomena; additionally the strong currents

[1] https://www.godae-oceanview.org/files/download.php?m=documents&f=130221160735-AbstractJohnsTopic3.pdf

and temperature gradients associated with western boundary currents such as the Gulf Stream or Kuroshio can enhance surface winds and seas particularly during cold air surges.

For medium range prediction, phenomena such as monsoon onset and intensity as well as monsoon breaks are dependent on the interaction of heat storage over the continent vs. the ocean. Active tropical convection regimes such as the Madden-Julian Oscillation (MJO) depend on the interaction of atmospheric dynamics and ocean properties. Outside of the tropics, blocking patterns in the jet stream produce surface heat waves, droughts, and neighboring regions of intense flooding. Also, intense polar low pressure systems share some similarities with hurricanes in that they derive considerable energy from the ocean heat source.

For long range prediction, interacting modes of the air-ocean system drive such phenomena as the MJO, el Nino-Southern Oscillation (ENSO), Pacific Decadal Oscillation (PDO), the North Atlantic Oscillation (NAO), and others; these phenomena drive teleconnections affecting weather and ocean properties throughout the globe.

b. Multi-model Ensembles

Multi-model ensembles provide a practical approach to estimating and understanding forecast uncertainty due to initial conditions and observation errors, model formulation, and numerical uncertainties. Ensembles of a single model can reduce error due to initial conditions, but these single model ensembles are often over-confident (have a low spread) and may have persistent error modes and biases. By combining the ensemble results of several models, the community can reduce these errors, obtain a better assessment of uncertainty, and leverage the distributed computing resources of various agencies to obtain a larger total number of ensemble members.

c. Predictability Demonstration Projects

Model fidelity at these time scales is presently less than desirable for decision-making. To foster improvements, ESPC has established a set of five Demonstration Projects to focus and coordinate inter-agency research efforts and demonstrate the predictability (or causes of lack thereof) for five phenomena distributed across the air-ocean system. These five projects consist of:

1) Extreme Weather Events: Predictability of Blocking Events and Related High Impact Weather at Lead Times of 1-6 Weeks
2) Seasonal Tropical Cyclone Threat: Predictability of Tropical Cyclone Likelihood, Mean Track, and Intensity from Weekly to Seasonal Timescales
3) Arctic Sea Ice Extent and Seasonal Ice Free Dates: Predictability from Weekly to Seasonal Timescales
4) Coastal Seas: Predictability of Circulation, Hypoxia, and Harmful Algal Blooms at Lead Times of 1-6 Weeks
5) Open Ocean: Predictability of the Atlantic Meridional Overturning Circulation (AMOC) for Improved Weather and Climate Forecasts

The projects do not represent a complete set of phenomena necessary for prediction across time scales, but rather a distributed subset of separate (interacting) phenomena for which correct representation is a prerequisite for forecast fidelity. A goal of these projects is to improve model representation of these conditions and provide those model improvements to the operational and research modeling centers.

d. National Ocean Partnership Program (NOPP) project

Global earth system coupled modeling at extended time scales is computationally intensive, particularly as model resolutions and ensemble numbers increase. Emerging heterogeneous computational architectures such as NVidia's Graphics Processing Unit (GPU) and Intel's Many Integrated Core (MIC) show promise in meeting the computation need, although existing codes need to be optimized to fully exploit the architecture . A NOPP project on Advancing Air-Ocean-Land-Ice Global Coupled Prediction on Emerging Computational Architectures has been initiated in FY13. The selected projects focus on:

1) Accelerated Prediction of the Polar Ice and Global Ocean (APPIGO)
2) An Integration and Evaluation Framework for ESPC Coupled Models
3) RRTMGP: A High-Performance Broadband Radiation Code for the Next Decade
4) NPS-NRL-Rice-UIUC Collaboration on Nonhydrostatic Unified Model of the Atmosphere (NUMA) Coupled Models on Many- Core Computer Architectures

Further information on these projects can be found at http://coaps.fsu.edu/aoli/projects .

5. Summary: towards a National ESPC

Federal partnering between agencies has the potential to leverage the efforts of many programs to improve adoption of research breakthroughs from the wider community into the national operational capability. Previous interagency programs such as HFIP, NUOPC, and NMME have shown great benefit to operational national forecast skill over short, medium, and long range weather by both leveraging the research efforts of the agencies as well as exploring a paradigm of using distributed computing for operations.

The National ESPC project's goals are to leverage community models for transition from research to operations of regional and global air-sea-wave-ice coupled models; to foster adoption of ESMF standards through the ESPS initiative; and to extend and improve the multi-model ensemble approach flexible enough to meet sub-seasonal and seasonal timescales through an NMME capable of transitioning research to operations.

References

Bleck, R. 2002: An Oceanic General circulation model framed in hybrid isopycnic-Cartesian coordinates. *Ocean Modelling*, **4**, 55-88.

Brunet, G., and Co-authors, 2010: Collaboration of the weather and climate communities to advance subseasonal-to-seasonal prediction. *Bull. Amer. Meteor. Soc*., **91**, 1397-1406. doi: 10.1175/ 2010BAMS3013.1

Collins, N., and Co-authors, 2005:. Design and implementation of components in the Earth System Modeling Framework. *The International Journal of High Performance Computing Applications*, **19**, 341-350. doi: 10.1177/1094342005056120

Gall, R., and Co-authors, 2013: The Hurricane Forecast Improvement Project. *Bull. Amer. Meteor. Soc*. **94**, 329-343. doi: 10.1175/BAMS-D-12-00071.1

Kirtman, B. and Co-Authors, 2013: The North American Multi-Model Ensemble (NMME): Phase-1 seasonal to interannual prediction, Phase-2 Toward developing intra-seasonal prediction. *Bull. Amer. Meteor. Soc.* doi: 10.1175/BAMS-D-12-00050.1

Metzger, E. J., and Co-authors, 2014: Operational implementation design for the Earth System Prediction Capability (ESPC): A first-look. *NRL Technical Report 7320--13-9498*. Available from http://www7320.nrlssc.navy.mil/pubs.php.

NRC, 2010: Assessment of intraseasonal to interannual climate prediction and predictability. *National Academies Press*, Washington, D.C.

Sandgathe, S., and Co-authors, 2011: National Unified Operational Prediction Capability initiative. *Bull. Amer. Meteor. Soc.*, **92**, 1347-1351. doi: 10.1175/2011BAMS3212.1

Shapiro, M., and Co-authors, 2010: An Earth-system prediction initiative for the twenty-first century. *Bull. Amer. Meteor. Soc.*, **91**, 1377-1388. doi:10.1175/2010BAMS2944.1

Tolman, H.L., and Co-authors, 2011: The NOPP Operational Wave Model Improvement Project. *JCOMM Technical Report No. 67,* http://www.jcomm.info/images/stories/2011/12thWaves/Papers/kona11_tolman _banner_kaihatu.pdf.

3. ENHANCING MONITORING AND TIMELY ATTRIBUTION AND ASSESSMENT

Science and Technology Infusion Climate Bulletin
NOAA's National Weather Service
38th NOAA Annual Climate Diagnostics and Prediction Workshop
College Park, MD, 21-24 October 2013

Could the 2012 Drought Have Been Anticipated? – A NASA NEWS Initiative

S.-Y. Simon Wang*, Danny Barandiaran, Kyle Hilburn, Paul Houser, Bob Oglesby, Ming Pan, Rachel Pinker, Joe Santanello, Siegfried Schubert, and Hailan Wang

NASA Energy and Water Cycle Study (NEWS) Working Group on Extremes

1. Introduction

The 2012 drought that engulfed most of North America set many records, surpassing by most measures even the severity of the 1988 drought (Kimery 2012). Numerous press and governmental resources have documented the extent and tremendous impact of the 2012 drought in the United States[1]. An assessment report of the NOAA Drought Task Force (Hoerling *et al*. 2013) summarized that the drought – primarily that covering the central Great Plains during May-August of 2012 (Fig. 1a) – resulted mostly from natural atmospheric variations. They concluded: "neither ocean states nor human-induced climate change appeared to play significant roles" and so, the drought could not have been predicted.

Here we ask: If not predictable, could the 2012 drought nonetheless have been "anticipated"? In other words, we examine in a comprehensive manner – *i.e.* beyond just the forecast schemes – how this drought developed and whether or not there were signs that could foretell such drought.

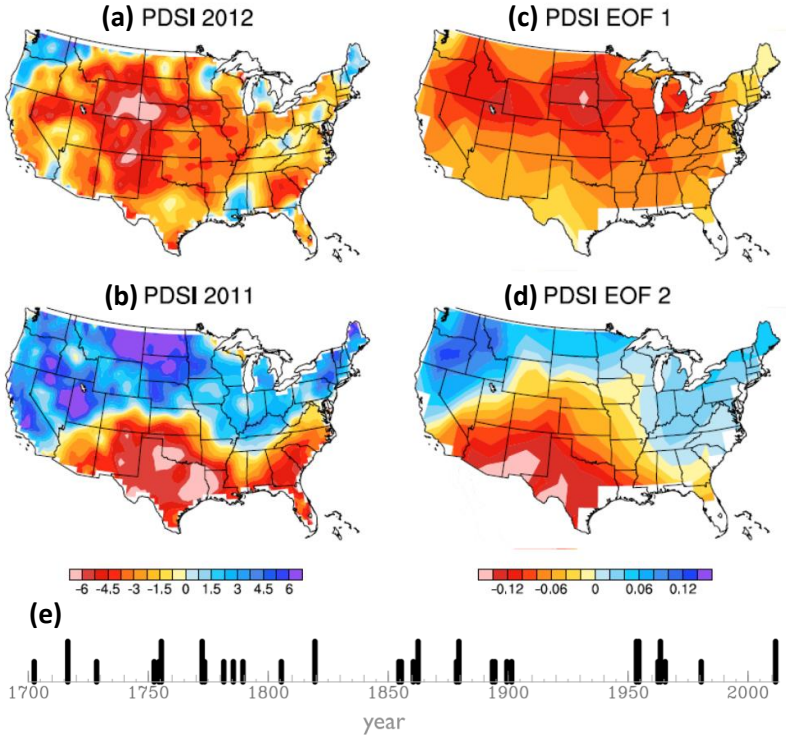

Fig. 1 May-July (MJJ) PDSI during (a) 2012 and (b) 2011, in comparison with (c) EOF1 and (d) EOF2 of the MJJ PDSI from 1900 to 2012. (e) The occurrence of which PC2 is followed by PC1 when both PCs exceed two (one) standard deviation plotted as long (short) sticks, based upon the North American Drought Atlas tree-ring data.

This paper summarizes relevant research efforts by members of the NASA NEWS Working Group on Extremes. These efforts examine the 2012 drought from several key aspects: (a) the large-scale pattern and its recurrence over North America; (b) precipitation and synoptic regimes over the Great Plains; (c) the contributions of ocean surface temperatures, land processes, and radiative forcing in drought formation and

[1] New York Times - http://topics.nytimes.com/top/news/science/topics/drought/
USDA - http://www.ers.usda.gov/topics/in-the-news/us-drought-2012-farm-and-food-impacts.aspx#.UqD-RWRDtLs
The Economist – http://www.economist.com/node/21559381

* Group members in alphabetic order after S. Wang.
Correspondence to: S.-Y. Simon Wang Utah Climate Center/Dept. Plants, Soils, and Climate, Utah State University, Logan, Utah; E-mail: simon.wang@usu.edu.

prolongation; (d) the role of ET fluxes, and our ability to simulate them accurately; and (e) potential predictability and model scenarios for drought recovery. These studies, in hindsight, suggest that factors leading to the 2012 drought did reveal signs that could have helped anticipate its occurrence.

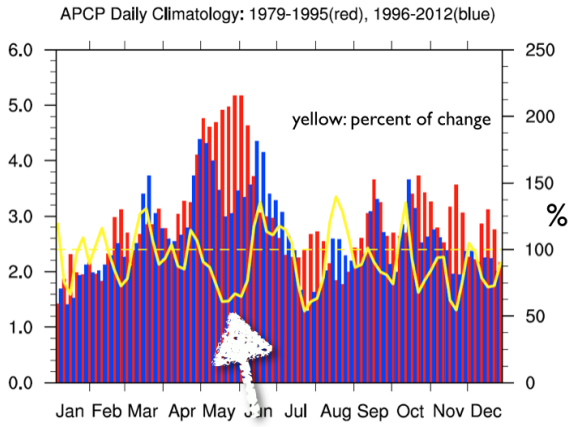

Fig. 2 5-day mean precipitation over the Oklahoma-Texas region for the period 1979-1995 (red) versus 1996-2012 (blue), and the percent difference between the two periods (yellow line). Note the large decline in May.

2. Results and Discussion

a. Drought pattern and recurrence

A unique aspect of the 2012 drought is that it evolved from the 2011 drought that devastated the southern Great Plains (Fig. 1a, b). This precursor drought was associated with La Niña (Seager *et al.* 2013). The central Great Plains therefore experienced consecutive drought conditions from 2011 to 2012 (which continued at least through March 2013). First, the Empirical Orthogonal Function (EOF) analysis of the Palmer Drought Severity Index (PDSI) (Dai *et al.*, 2004) for the period of 1900-2012 indicated that the first two leading patterns of drought are similar to the recent ones – *i.e.* EOF1 with a widespread pattern (Fig. 1c) corresponds to the 2012 drought, while EOF2 with the dipole pattern (Fig. 1d) resembles the 2011 drought. The apparent correspondence between the EOFs and the recent droughts suggests that a drought evolution similar to that occurring from 2011 to 2012 may not be unique. To examine further, we plotted the occurrence of when the second principal component (PC2) leads the PC1 – in the sense that the 2011 drought led the 2012 one. The dataset used here is the PDSI derived from tree rings (the North American Drought Atlas; Cook et al., 2004). The result is shown in Figure 1e with the long (short) bars indicating that both PC1 and PC2 are positive and both exceed two (one) standard deviation. It appears that the evolution of droughts like the 2011-2012 succession did occur sporadically in the past (Fig. 1e).

b. Recent trends in precipitation and LLJ

Over the central U.S., the warm-season precipitation migrates from the southern Great Plains in spring to the upper Midwest in summer, providing crucial growing-season water along its path. Both rainfall and convective storm activity reach their maximum in May and June in the southern Great Plains forming a precipitation center over the Oklahoma-Texas region (Wang and Chen 2009). This rainfall maximum is depicted in Figure 2 by the elevated spring precipitation peaking in May. Observations indicate, however, that over the past three decades the amount of spring precipitation has declined. Figure 2 shows time series of pentad precipitation averaged for Oklahoma-Texas over the period

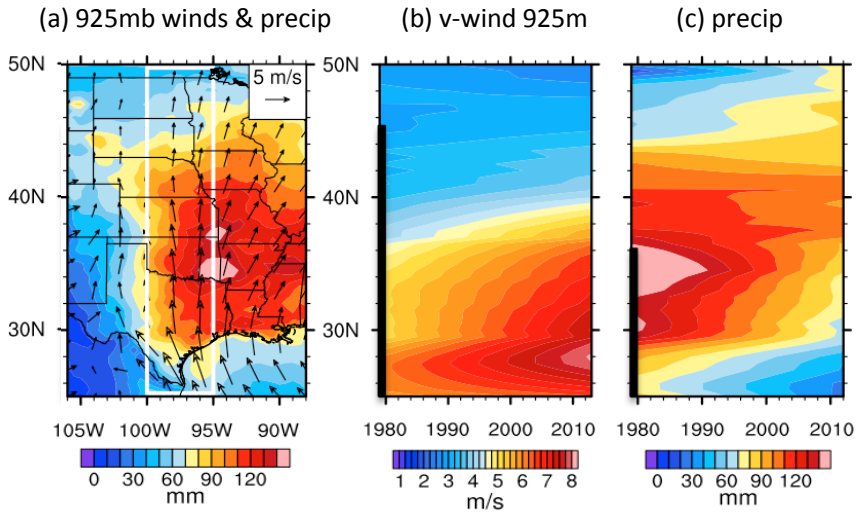

Fig. 3 a) May climatology for precipitation (shaded) and 925mb wind field (vectors) and Latitude-time Hovmöller trend plots for b) 925mb v-wind, c) total precipitation. Latitudes in which the regression coefficient is significant at 95% confidence are indicated along the y-axis. (After Barandiaran *et al.* 2013)

1979-1995 versus that for 1996-2012, along with the percent difference between the two periods. There is a clear reduction in April-June (AMJ) rainfall, particularly the entire month of May during which deficits of as much as 50% are observed (Barandiaran *et al.* 2013). This rainfall reduction suggests decline of a vital water source during the rainy season in the Oklahoma-Texas region, and also makes the region more susceptible to drought during the summer.

A key atmospheric circulation systems closely connected to the region's seasonal precipitation is the Great Plains Low-Level Jet (GPLLJ), which is primarily a transient pattern of nocturnal strong winds just above the surface. The GPLLJ transports abundant amounts of water vapor from the Gulf of Mexico and provides moisture convergence at its northern edges, facilitating the formation of convective precipitation. Focusing on May, Figure 3a depicts the climatological precipitation overlaid with 925-mb wind vectors for geographical reference; the white box indicates the sub-region over which averages are calculated in subsequent panels. The trend for all latitudes is calculated using linear least-squares regression for 6-hourly 925mb v-wind strength of each month (Fig. 3b) and monthly total precipitation (Fig. 3c). There is an apparent increase in the strength of the v-wind between 30°N-35°N including the Gulf of Mexico (*i.e.* upstream of the GPLLJ). North of 40°N the increasing trend becomes very small, to near zero. These v-wind changes accompany a northward migration of the maximum gradient of v-wind speed, and the resultant convergence at the exit region of the GPLLJ. Correspondingly, the changes in total precipitation reveal a northward migration, leading to drying in the central and southern Great Plains (Barandiaran *et al*. 2013).

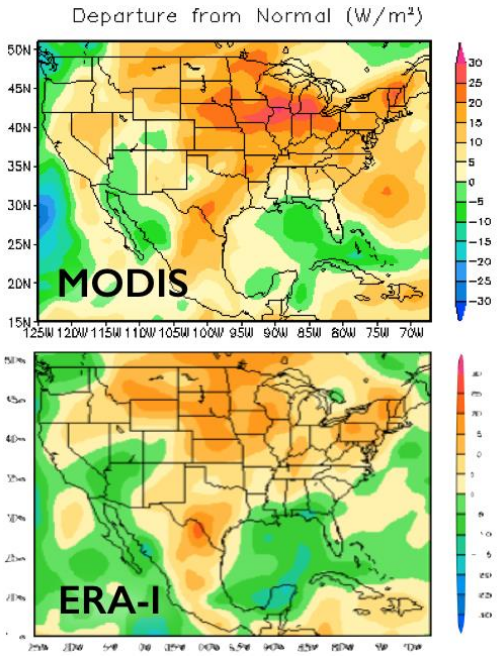

Fig. 4 (top) May-August shortwave radiation anomaly from MODIS (from 10 year mean); (bottom) shortwave radiation anomaly from ERA-Interim reanalysis.

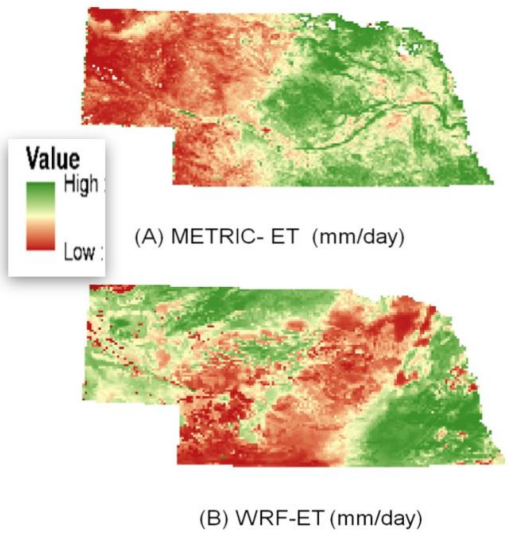

Fig. 5 Surface ET simulated for two days in August 2012 by (A) MODIS-METRIC model that includes irrigation, and (B) WRF-CLM model without irrigation leading to drying in farmed areas.

c. Forcings that initiate/enhance drought

[Radiative forcing] Another unique feature associated with the 2012 drought is its rapid development in early summer, coined "flash drought" by the NOAA report (Hoerling *et al.* 2013). In particular, the drought over the Northern Plains expanded rapidly during June and quickly formed dry to exceptional drought conditions. As shown in Figure 4, the rapid development of 2012 drought is associated with enhanced shortwave radiation input, as depicted by MODIS data and also seen in the ERA-I surface shortwave fluxes. The timing of intensive shortwave radiation anomalies coincides with the seasonal maximum of shortwave radiation, and the area is closely associated with the rainfall deficits (Wang and Chen 2009).

[Land forcing] Santanello *et al.* (2013) diagnosed the process and impacts of local land–atmosphere coupling during dry and wet extreme conditions in the U.S. southern Great Plains, through an evaluation of nine different land–planetary boundary layer (PBL) schemes coupled in a high-resolution regional model. Results show that the sensitivity of land–air coupling is stronger toward the land during dry conditions, while the PBL scheme coupling becomes more important

during the wet regime. In other words, soil moisture impacts are felt via land-PBL interactions, where the atmosphere is more sensitive to dry soil anomalies while deep, dry PBL growth can lead to a persistent positive feedback on dry soils. Hubbard *et al.* (2013) meanwhile found that dry soil moisture conditions could strongly enhance the effects of remote SST forcing. Comparing remote sensing and modeling data, Ozturk *et al.* (2013) found that the evapotranspiration (ET) effect, which is linked to irrigation in the Northern Plains; this also feedbacks on drought intensity. Figure 5 demonstrates that, when it is dry, more irrigation is needed to grow the crops; then if the drought persists, the crop fails and less irrigation takes place on the dying plants. So, early in the drought irrigation modulates some of the land-air coupling impact of the drought; later on, the lack of irrigation does the opposite and land-air feedbacks can dominate.

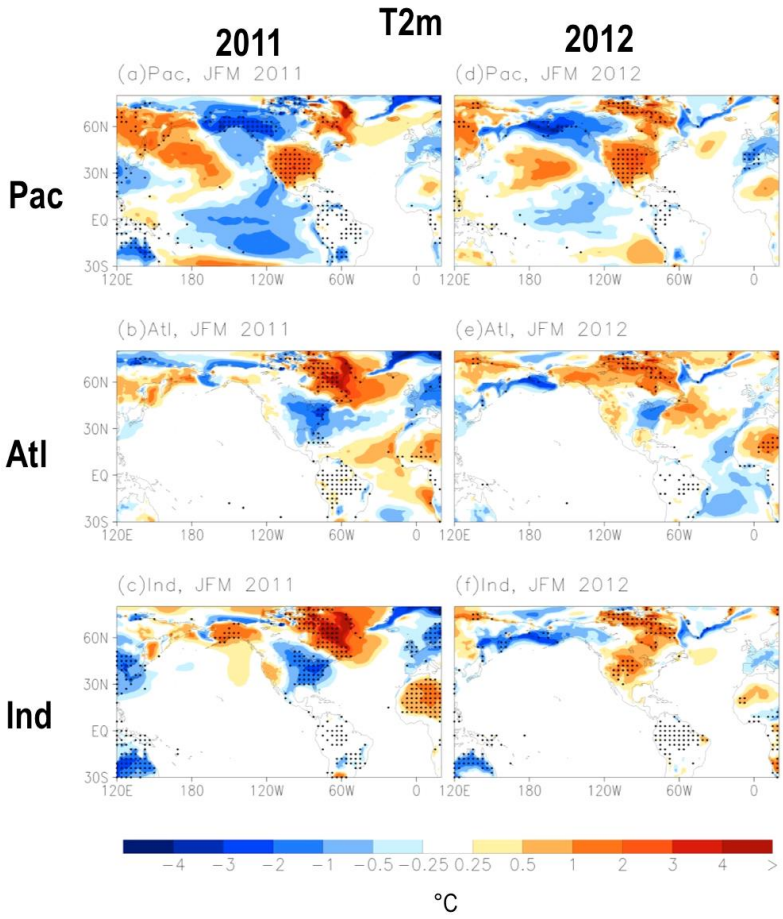

Fig. 6 JFM ensemble mean T2m response to SST forcing in individual ocean basins based on GEOS-5 ensembles initialized in November of the previous year, for SST in (top-bottom) for Pacific, Atlantic, and Indian Ocean. (From H. Wang *et al.* 2013)

[Teleconnection forcing] As was noted in the NOAA Drought Task Force report, the 2012 drought lacked substantial ocean forcing in the tropical Pacific given the ENSO neutral status. Using the NASA GEOS-5 model, H. Wang *et al.* (2013) found that the winter-spring response over the U.S. to the Pacific SST is remarkably similar for years 2011 and 2012 (Fig. 6a, d) despite substantial differences in the tropical Pacific SST. The pronounced winter and early spring temperature differences between the two years (warmth confined to the south in 2011 and covering much of the continent in 2012) primarily reflect differences in the contributions from the Atlantic and Indian Oceans, with both acting to cool the east and upper mid-west during 2011 (Fig. 6b, c), while during 2012 the Indian Ocean reinforced the Pacific-driven continental-wide warming and the Atlantic played a less important role (Fig. 6e, f). During early summer the development of a stationary Rossby wave over the North Pacific – an atmospheric process – produced the record-breaking precipitation deficits and heat in the Central Plains in the middle of summer. S.-Y. Wang *et al*. (2013) further indicated that, particularly in July, the seasonal pattern of stationary Rossby waves has changed since 1979 in a way that favors the type of short-wave circulation anomalies that produce heat and dry conditions over the Northern Plains. This latter finding coincides with the climatological maximum of radiative forcing in July.

d. Potential predictability

The modeling study by H. Wang *et al.* (2013) suggested that the 2012 drought would not have benefited from long-lead prediction, as the full extent of the event was not forecasted until one month prior. This implies that the stationary Rossby waves that reinforce the drought occurred at intra-seasonal timescales. Such forcing of Rossby waves is triggered by submonthly vorticity transients (Schubert *et al.* 2011) and varies month-by-month (S.-Y. Wang *et al.* 2013), hence the difficulty in predicting them at longer than these relatively short lead times. However, once the Rossby waves develop, the perturbation downstream would

establish and frequently last for an extensive period of time, about 2-6 weeks (Schubert *et al.* 2011). In other words, short-term climate prediction from 2 weeks to 2 months may be the only remedy for predicting "flash drought" such as that of 2012. H. Wang *et al.* (2013) have demonstrated the potential of Rossby waves in providing early-warning of heat waves in the U.S. during the 2012 drought.

e. Drought recovery

An often overlooked question concerns the processes by which drought recovers. Drought management would benefit greatly if more risk-based information is available on how a region in drought may recover, *e.g.*, the likelihood of recovery under different precipitation scenarios and the related uncertainty. As discussed earlier, several factors such as the initial moisture condition, the amount and timing of precipitation, and the temperature control the recovery process. In view of the aforementioned limit in forecast skills of the 2012 drought, Pan *et al.* (2013) proposed a probabilistic framework to assess drought recovery that is based on the joint distribution between cumulative precipitation (which is the main driver for recovery) and a soil moisture–based drought index.

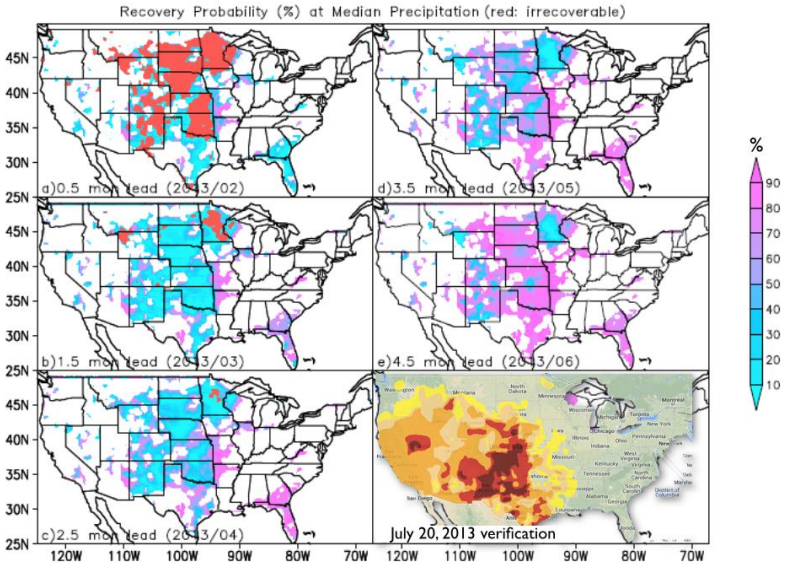

Fig. 7 Maps of the probability of drought recovery under the median (p = 50%) cumulative precipitation scenario. Red colored areas are those unable to recover from drought under any cumulative precipitation scenario, and empty colored areas are those not in drought ($\theta > \theta_{\text{drought}}$) as of 1 February 2013. (a–e) The results for lead times of 0.5–4.5 months. (From Pan *et al.* 2013)

Figure 7 shows maps of recovery probability under the median cumulative precipitation scenario staring in February 2013. The smaller the value, the less likely it is to recover and the higher the probability (risk) that the area remains in drought. At one-month lead, large parts of Central and Northern Plains are irrecoverable, and the recovery probability is very low. Most areas start to be recoverable from the 1.5 month onward (Fig. 7b), but the recovery probability is low (10%–20%). The recovery probability increases at 2.5 and 3.5 months until it reaches the 80% level at the 4.5 month lead (very likely to recover if median cumulative precipitation is received for 6 months). As shown in the lower right corner (verification), by July 2013 most of the Northern Plains has indeed recovered from drought, although the southwestern states remained in drought. The results suggest that a probabilistic analysis for drought recovery can provide indispensable risk information for drought managers.

3. Concluding Remarks

The 2012 drought was unique in terms of the rapidity, with which it developed, the lack of "classic" oceanic forcing patterns, and the association with record heat waves in the Central U.S. Through our collective efforts it was found that the 2012 drought did, however, show signs of precursors, albeit without a long lead time. First, the succession of a "dipole" drought pattern like that in 2011 followed by the widespread drought pattern like that in 2012 is not unprecedented; in fact it has repeatedly occurred over the past 300+ years. Model experiments suggested that the tropical Atlantic and Indian Ocean status (instead of the Pacific) helped initiate drought conditions in spring 2012. Second, since 1979 the GPLLJ has strengthened making the critical spring/rainy season over the central and southern part of the Great Plains drier than ever. Third, the timing of the drought development in June and heat wave in July coincides with the seasonal drying in the Central Plains, enhancing shortwave radiation while reducing ET; this further

exacerbated the drought as it persists towards the middle of summer. Fourth, the state of the soil moisture can precondition, enhance, and prolong drought conditions. Human activities such as irrigation may partially offset this. Finally, a standing pattern of stationary Rossby short waves developed in the late spring/early summer season, producing the anticyclone anomaly that later occupied the Central U.S. for the rest of summer.

Although it is difficult to foresee the initiation of a specific stationary Rossby wave pattern, once it develops the standing pattern of short waves did persist for an extensive period of time, thus providing potential sources for short-term/intraseasonal climate prediction – *i.e.* early warning. In summary, prediction of the 2012-like drought is not without hope but more emphasis will need to be on intraseasonal timescales. Furthermore, predicting the recovery of drought is equally important and this has been shown to be feasible.

References

Barandiaran, D.A., S.-Y. Wang and K. Hilburn, 2013: Observed trends in the Great Plains low-level jet and associated precipitation changes in relation to recent droughts. *Geophys. Res. Lett.*, in press.

Cook, E.R., C.A. Woodhouse, C.M., Eakin, D.M. Meko, and D.W. Stahle, 2004: Long-term aridity changes in the western United States, *Science*, **306**, 1015-1018.

Dai, A., K.E. Trenberth, and T. Qian, 2004: A global data set of Palmer Drought Severity Index for 1870-2002: Relationship with soil moisture and effects of surface warming, *J. Hydrometeor.*, **5**, 1117-1130. doi: 10.1175/JHM-386.1.

Kimery, A., 2011: Dealing with the drought, *HSToday*, 8:12, 38-41.

Hoerling, M., and Co-authors, 2013: An interpretation of the origins of the 2012 central Great Plains drought – Assessment report. http://www.drought.gov/media/pgfiles/2012-Drought-Interpretation-final.web-041013_V4.0.pdf .

Hubbard, T.J., Y. Zhang, R.J. Oglesby, S. Feng, Q.S. Hu, A. Kilic, D. Ozturk, 2013: Quantifying the relative roles of local versus remote effects on North American summertime drought. GC11A-0968, AGU Fall Meeting, San Francisco, CA, 9-13 December 2013.

Ozturk, D., A. Kilic, R.J. Oglesby, Q.S. Hu, and T.J. Hubbard, 2013: Evaluation of ET in regional climate models with remotely sensed data. A33E-0285, AGU Fall Meeting, San Francisco, CA, 9-13 December 2013.

Pan, M., X. Yuan, and E.F. Wood, 2013: A probabilistic framework for assessing drought recovery. *Geophys. Res. Lett.*, **40**, 3637–3642. doi: 10.1002/grl.50728.

Santanello, J.A., C.D. Peters-Lidard, A. Kennedy, S.V. Kum, 2013: Diagnosing the nature of land-atmosphere coupling: a case study of dry/wet extremes in the U.S. Southern Great Plains. *J. Hydrometeor.*, **14,** 3-24. doi: 10.1175/JHM-D-12-023.1.

Schubert, S., H. Wang and M. Suarez, 2011: Warm season subseasonal variability and climate extremes in the Northern Hemisphere: The role of stationary Rossby waves. *J. Climate*, **24**, 4773–4792. doi: 10.1175/JCLI-D-10-05035.1.

Seager, R., L. Goddard, J. Nakamura, N. Henderson, and D.E. Lee, 2013: Dynamical causes of the 2010/11 Texas-northern-Mexico drought. *J. Hydrometeor.*, in press.

Wang, H., S. Schubert, R. Koster, Y.-G. Ham and M. Suarez, 2013: On the role of SST forcing in the 2011 and 2012 extreme U.S. heat and drought: A study in contrasts. *Submitted to J. Hydrometeor*.

Wang, S.-Y. and T.-C. Chen, 2009: The late-spring maximum of rainfall over the U.S. Central Plains and the role of the low-level jet. *J. Climate*, **22**, 4696-4709, doi: 10.1175/2009JCLI2719.1.

Wang, S.-Y., R.E. Davies and R.R. Gillies, 2013: Identification of extreme precipitation threat across mid-latitude regions based on short-wave circulations. *J. Geophys. Res*, doi: 10.1002/jgrd.50841.

Science and Technology Infusion Climate Bulletin
NOAA's National Weather Service
38th NOAA Annual Climate Diagnostics and Prediction Workshop
College Park, MD, 21-24 October 2013

The Surprisingly Quiet 2013 Atlantic Basin Hurricane Season

Philip Klotzbach

Department of Atmospheric Science, Colorado State University

1. Introduction

The Atlantic basin hurricane season was much less active than anticipated by Atlantic basin seasonal hurricane forecasts issued by Colorado State University (CSU), the National Oceanic and Atmospheric Administration (NOAA), Tropical Storm Risk, and the UK Met Office, among others. For example, NOAA's outlook issued on May 23 called for 13-20 named storms, 7-11 hurricanes and 3-6 major hurricanes, while CSU's outlook issued on June 3 called for 18 named storms, 9 hurricanes and four major hurricanes. While the 2013 Atlantic hurricane season had near-average named storm activity, with 13 named storms forming, only two hurricanes and no major hurricanes formed. This is the fewest hurricanes to occur in a season since 1982. This manuscript attempts to analyze, with the benefit of hindsight, what climate conditions caused this year's hurricane season to be much weaker than anticipated. Section 2 describes the data utilized, while Section 3 examines the climate features present during the 2013 Atlantic hurricane season. Section 4 concludes the manuscript. A much more detailed discussion of the 2013 Atlantic hurricane season can be found with the Tropical Meteorology Project's 2013 verification located online at http://tropical.atmos.colostate.edu.

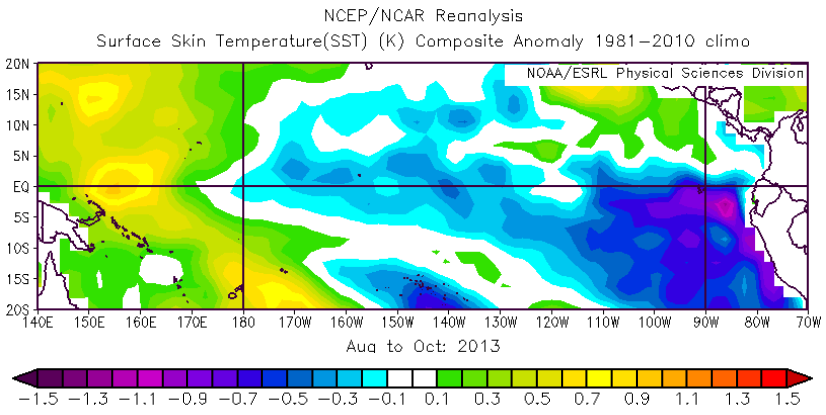

Fig. 1 August-October SST anomalies across the tropical Pacific.

2. Data

Tropical cyclone statistics were calculated from the operational b-decks created by the National Hurricane Center. Large-scale climate fields were calculated from the NCEP/NCAR Reanalysis (Kistler *et al*. 2001).

3. Climate features present during the 2013 Atlantic hurricane season

El Niño has been documented in many previous studies to have a detrimental impact on Atlantic basin tropical cyclone activity through alterations in vertical wind shear, mid-level moisture, upper-tropospheric temperature and static stability (Tang and Neelin, 2004; Klotzbach, 2011a). Figure 1 displays sea surface temperature (SST)

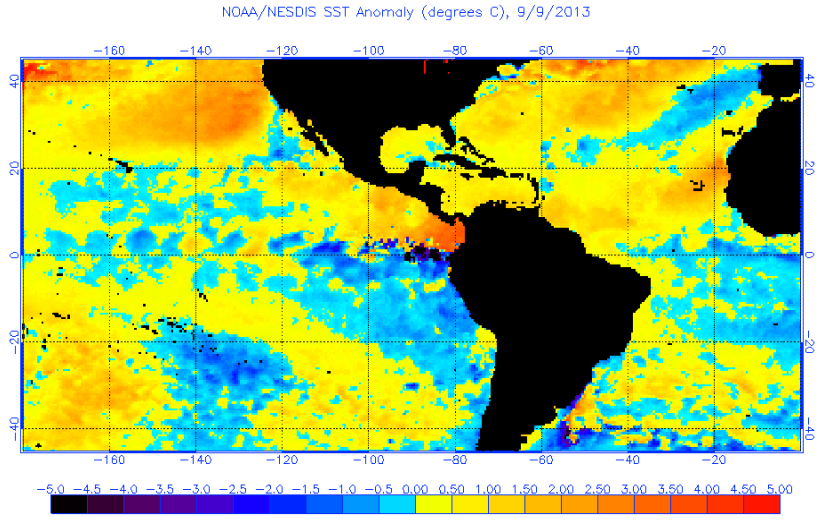

Fig. 2 Western Hemisphere SST anomalies on September 9, 2013.

Correspondence to: Philip Klotzbach, Department of Atmospheric Science, Colorado State University, Fort Collins, CO; E-mail: philk@atmos.colostate.edu.

anomalies across the central and eastern tropical Pacific averaged over August-October 2013. Anomalies were generally slightly cooler than normal, indicating cool neutral El Niño-Southern Oscillation (ENSO) conditions. Consequently, ENSO is not thought to have played a significant detrimental role in this year's hurricane season.

Another area that shows strong correlations with Atlantic basin hurricane activity is Atlantic basin SSTs. While tropical Atlantic SSTs were warmer than normal, cool anomalies were evident in the subtropical eastern Atlantic. This area has been shown in several studies including Klotzbach (2011b), to be a critical area for Atlantic hurricane activity. Cold anomalies in this region tend to generate stronger-than-normal baroclinicity, thereby contributing to cold upper-level lows, which enhance African easterly wave recurvature in the eastern part of the basin. As a general rule, the farther east that African easterly waves recurve, the less likely they are to intensify into hurricanes. Figure 2 displays SST anomalies across the Western Hemisphere around the peak of the Atlantic hurricane season.

The primary reason why the Atlantic basin storm season was likely so much less active than forecast was due to a combination of copious amounts of dry air and mid-level sinking that occurred.

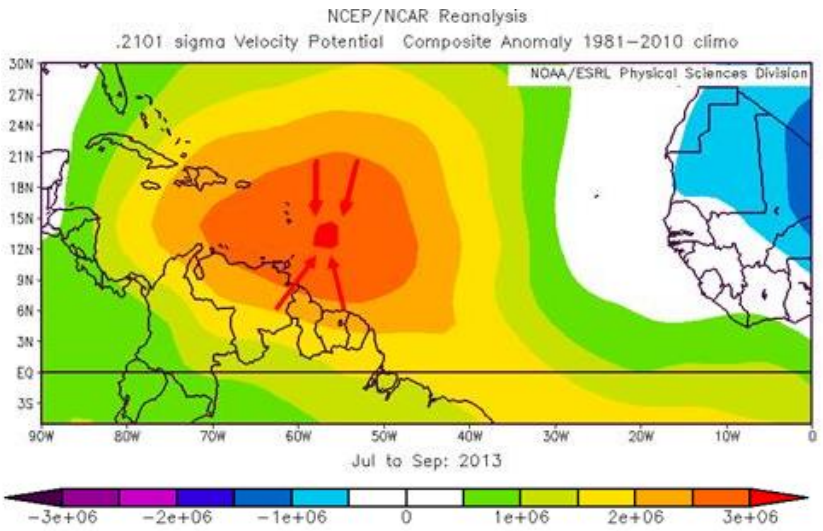

Fig. 3 Upper-level velocity potential anomalies in July-September 2013. Note the positive velocity potential anomalies that occurred during the months, indicating upper-level convergence (as demarked by the red arrows) and sinking motion.

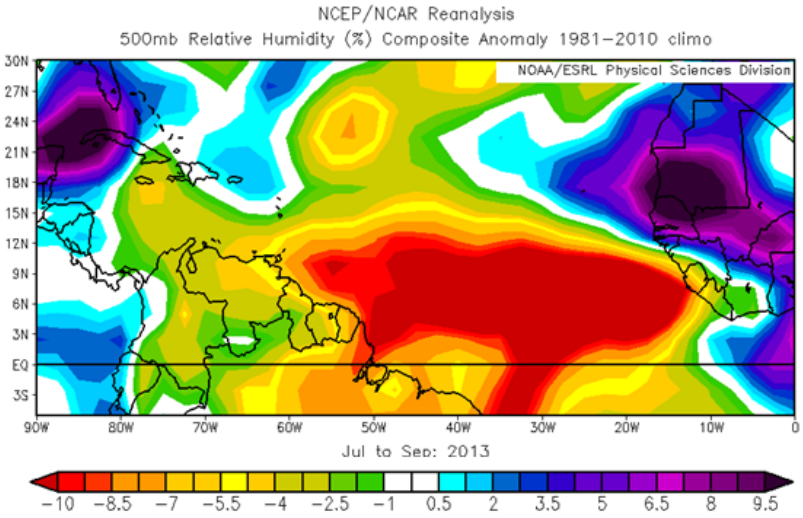

Fig. 4 July-September 2013 500-mb RH anomalies. Note the anomalous dryness across the Atlantic MDR this year.

The mid-level sinking that occurred during July-September 2013 is quite pronounced across the tropical Atlantic, especially when looking at velocity potential anomalies (Figure 3). Positive velocity potential anomalies at upper levels are associated with upper-level convergence and consequently sinking and drying at the middle levels of the atmosphere.

The anomalous dryness that persisted across the tropical Atlantic was also quite pronounced throughout the peak months of MDR formation from July-September. By October, TC formation tends to shift westward towards the Caribbean. NCEP/NCAR Reanalysis moisture values seem reasonable since the late 1970s (*e.g.*, no unusual trends). Table 1 displays relative humidity and specific humidity compared with other years from 1979-2012. A ranking of one indicates the driest during the time period. Note the anomalous dryness that occurred throughout the three-month period. It seems like this dry air was one of the critical reasons why the season was very quiet.

Figure 4 displays anomalous 500-mb relative humidity during the three-month period from July-September 2013. RH was quite low across the MDR, with even drier anomalies noted to the south of MDR.

One of the primary reasons why several of the seasons since 1995 have been very active was due to a pronounced and northward shifted Intertropical Convergence Zone (ITCZ) in the eastern tropical Atlantic (Klotzbach and Gray 2006). A stronger than normal ITCZ is associated with strong cross-equatorial flow which provides increased moisture flux into the tropical Atlantic and provides pre-existing cyclonic vorticity that helps spin up easterly waves. Anomalous meridional flow in July-September 2013 in the eastern tropical Atlantic was strongly out of the north, indicating a suppressed ITCZ and anomalous moisture divergence out of the tropical Atlantic (Figure 5).

Specific Humidity

	300-mb	500-mb	700-mb
July 2013	5	9	16
August 2013	12	2	6
September 2013	2	2	14

Relative Humidity

	300-mb	500-mb	700-mb
July 2013	5	8	11
August 2013	7	14	1
September 2013	2	2	8

Table 1 Specific humidity and relative humidity rankings for July 2013, August 2013 and September 2013 at 300-mb, 500-mb and 700-mb across the MDR (7.5-22.5°N, 20-75°W). Note that a ranking of one implies the driest (or most enhanced downward motion) across the MDR, while a ranking of 35 would imply the wettest (or most enhanced vertical motion) month of the last 35 years across the MDR.

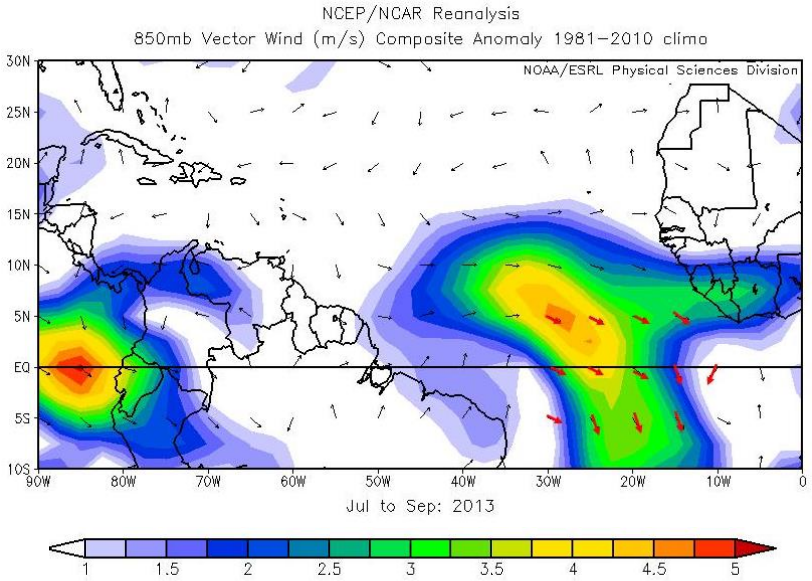

Fig. 5 Anomalous vector wind anomaly from July-September 2013. Note the anomalous northerly flow in the tropical Atlantic which likely was one of the reasons why there was such significant dryness in the tropical Atlantic this year.

4. Summary

This paper briefly discusses the reasons behind the much quieter than expected 2013 Atlantic basin storm season. While ENSO did not appear to play a significant role, it seems like a combination of cooler-than-normal subtropical Atlantic SSTs (and concomitant formation of upper-level lows), anomalously strong upper- and mid-level subsidence, and anomalous upper- and mid-level dryness were the likely culprits that restricted TC formation in the Atlantic in 2013. A much more thorough explanation of the reasons for the 2013 Atlantic hurricane season forecast bust are described in the Tropical Meteorology Project's end-of-season forecast verification located online at http://tropical.atmos.colostate.edu.

References

Kistler, R., and Co-Authors, 2001: The NCEP-NCAR 50-year reanalysis: Monthly means CD-ROM and documentation. *Bull. Amer. Meteor. Soc.*, **82**, 247-267.

Klotzbach, P. J., 2011a: El Niño – Southern Oscillation's Impact on Atlantic Basin hurricanes and U.S. landfalls. *J. Climate*, **24**, 1252-1263, doi:10.1175/2010JCLI3799.1

Klotzbach, P. J., 2011b: A simplified Atlantic basin seasonal hurricane prediction scheme from 1 August. *Geophys. Res. Lett.*, **38**, L16710, doi:10.1029/2011GL048603.

Klotzbach, P. J. and W. M. Gray, 2006: Causes of the unusually destructive 2004 Atlantic basin hurricane season. *Bull. Amer. Meteor. Soc.*, **87**, 1325-1333.

Tang, B. H., and J. D. Neelin, 2004: ENSO influence on Atlantic hurricanes via tropospheric warming. *Geophys. Res. Lett.*, **31**, L24204, doi:10.1029/2004GL021072.

Science and Technology Infusion Climate Bulletin
NOAA's National Weather Service
38th NOAA Annual Climate Diagnostics and Prediction Workshop
College Park, MD, 21-24 October 2013

Why Were Some La Niñas Followed by Another La Niña?

Zeng-Zhen Hu[1], Arun Kumar[1], Yan Xue[1], and Bhaskar Jha[1,2]

[1]*Climate Prediction Center, NCEP/NWS/NOAA*

[2] *WYLE Science, Technology and Engineering Group, Houston, Texas, USA*

ABSTRACT

This paper investigates why some La Niña events are followed by another La Niña and some others are not. We propose two preconditions that result in continuation of a La Niña. The first one is that La Niña must be a strong event (a major La Niña). This ensures that the reflected Rossby wave signal at the eastern boundary of the Pacific has a strong westward propagating cold ocean temperature anomaly over the off-

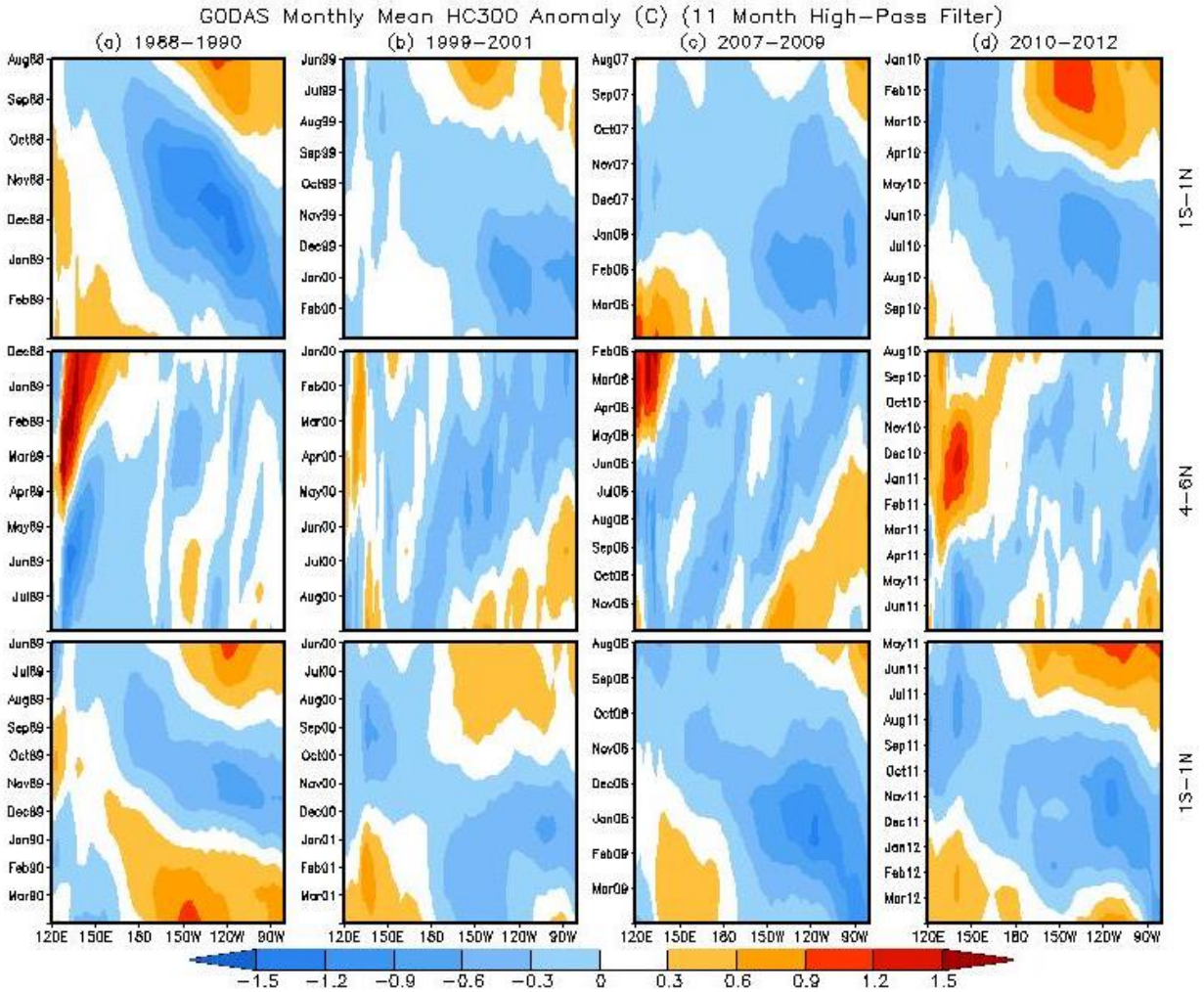

Fig. 1 Monthly mean HC300 anomalies averaged in 1°S-1°N (top and bottom panels) and in 4-6°N (middle panel) in the Pacific during (a) 1988-90, (b) 1999-2001, (c) 2007-09, and (d) 2010-12. An 11 month high-pass filter is applied to suppress the interannual and longer time scale variations.

Correspondence to: Zeng-Zhen Hu, Climate Prediction Center, NCEP/NWS/NOAA, 5830 University Research Court, College Park, MD 20740-3818; Email: Zeng-Zhen.Hu@noaa.gov

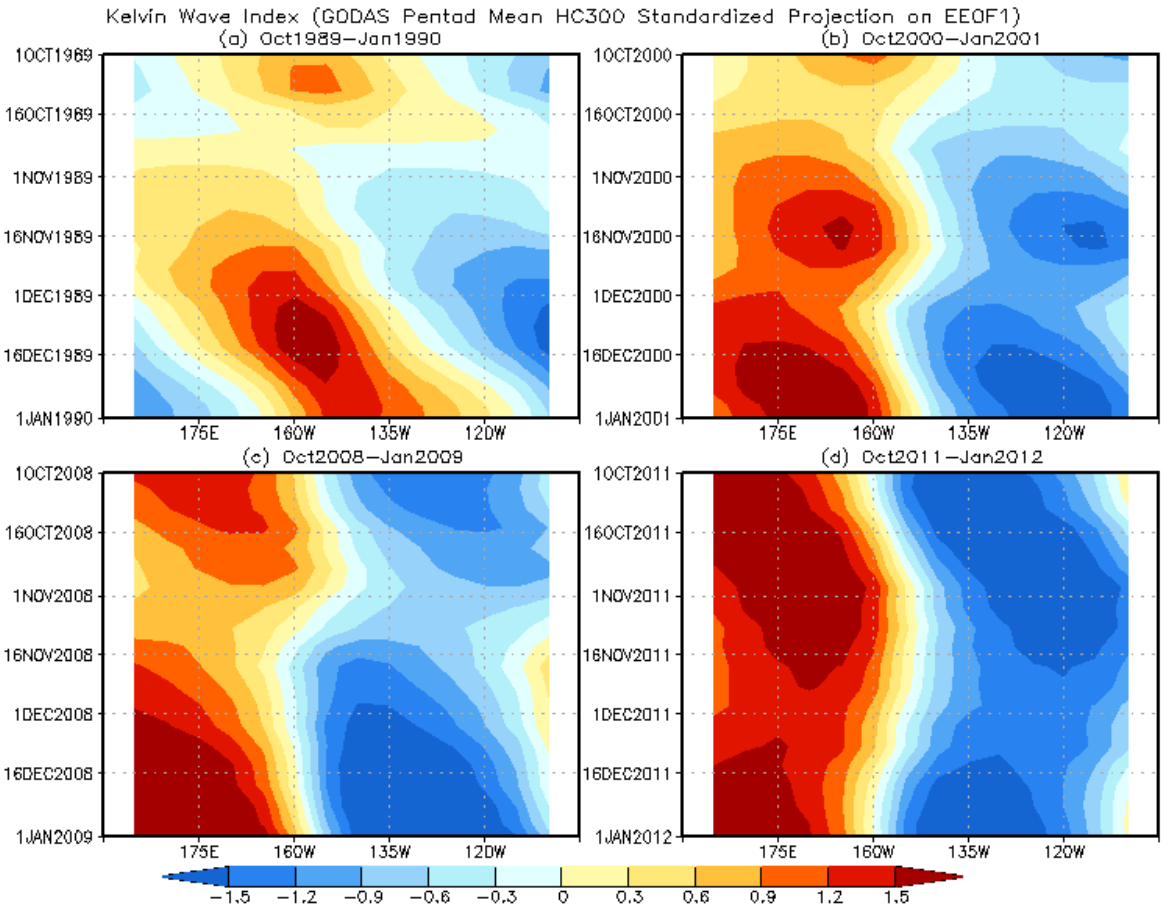

Fig. 2 Standardized projection of pentad mean OTAs along the equator onto 1st mode of EEOF in (a) Oct 1989-Jan 1990, (b) Oct 2000- Jan 2001, (c) Oct 2008-Jan 2009, and (d) Oct 2011-Jan 2012. X-axis represents the longitude location of maximum positive loading in the 14 contiguous pentad OTAs of 1st EEOF. See Seo and Xue (2005) for the details of the EEOF calculation.

equatorial region (Fig. 1). The off-equator cold anomaly may not be conducive to the equatorial recharge process, and as a result, may favor the persistence of cold ocean subsurface temperature anomaly and prevent the transition from La Niña to El Niño.

The second precondition is whether there are eastward propagating downwelling Kelvin waves during the decay phase of a major La Niña (Fig. 2). Eastward propagating downwelling Kelvin waves could lead to demise for a tendency for a follow-up La Niña. The equatorial Kelvin wave activities are associated with fluctuations of surface wind in the equatorial far-western Pacific. The analysis suggests that both the surface wind in the equatorial far-western Pacific and the recharge/discharge of the equatorial Pacific are indicators for occurrence or no occurrence of a follow-up La Niña event.

This work has been published in Climate Dynamics in 2014.

References

Hu, Z.-Z., A. Kumar, Y. Xue, and B. Jha, 2014: Why were some La Niñas followed by another La Niña? *Clim. Dyn.*, **42** (3-4), 1029-1042. DOI 10.1007/s00382-013-1917-3.

Seo, K., and Y. Xue, 2005: MJO-related oceanic Kelvin waves and the ENSO cycle: A study with the NCEP Global Ocean Data Assimilation System. *Geophys. Res. Lett.*, **32**, doi: 10.1029/2005GL022511. ISSN: 0094-8276.

Science and Technology Infusion Climate Bulletin
NOAA's National Weather Service
38th NOAA Annual Climate Diagnostics and Prediction Workshop
College Park, MD, 21-24 October 2013

Observed Trends in the Great Plains Low-level Jet and Associated Precipitation Changes in Relation to Recent Droughts

Daniel Barandiaran[1], Shih-Yu Wang[1, 2], and Kyle Hilburn[3]

[1]*Department of Plants, Soils and Climate, Utah State University, Logan, Utah*
[2]*Utah Climate Center, Utah State University, Logan, Utah*
[3]*Remote Sensing Systems, Santa Rosa, California*

ABSTRACT

Recent drought over the Great Plains has had significant impacts on agriculture and the economy, highlighting the need for better understanding of any ongoing changes in the regional hydroclimate. The Southern Plains peak rainfall season is in the spring (Fig.1 a-b), and the period 1996-present has been much drier than 1979-1995 in the highlighted region (Fig. 1c).

Trends in the Great Plains low-level jet (GPLLJ) during the months April-June (AMJ) and associated precipitation are analyzed using the North American Regional Reanalysis (NARR) for the period 1979-2012. Linear trends computed for meridional winds and precipitation intensity, frequency and total across the Great Plains (Fig. 2) show that (1) the GPLLJ has strengthened and expanded northward and (2) precipitation has decreased substantially in the Southern Plains while increasing in the Northern Plains. Particularly in May, the rainy season in the Oklahoma-Texas region, precipitation has migrated northward in correspondence to the shifted northern edge of the GPLLJ, leading to near 50% declines in precipitation since 1979. These observed changes are discussed in the context of recent droughts and projected climate for the region.

This work has been published in Geophysical Research Letters in 2013.

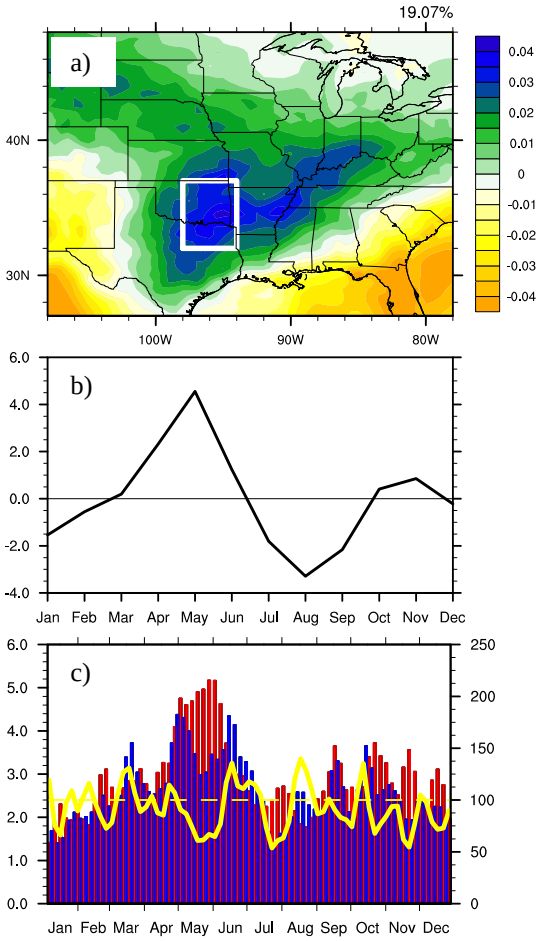

Fig. 1 a) EOF 2 of precipitation climatology for Central U. S. White box highlights center of action, and is used for calculations for panel c. b) PC2 of precipitation climatology for Central U.S., showing the springtime peak of rainfall for the region. c) Climatology of average pentad precipitation within averaged over the box shown in panel a. Red bars are for the period 1979-1995, blue bars are for the period 1996-2012. Yellow line indicates percent difference between the two time periods.

References

Barandiaran, D., S.-Y. Wang and K. Hilburn, 2013: Observed trends in the Great Plains low-level jet and associated precipitation. *Geophys. Res. Lett.*, DOI: 10.1002/2013GL058296

Correspondence to: S.-Y. Simon Wang, 4825 Old Main Hill, Logan, UT 84322;
E-mail: simon.wang@usu.edu

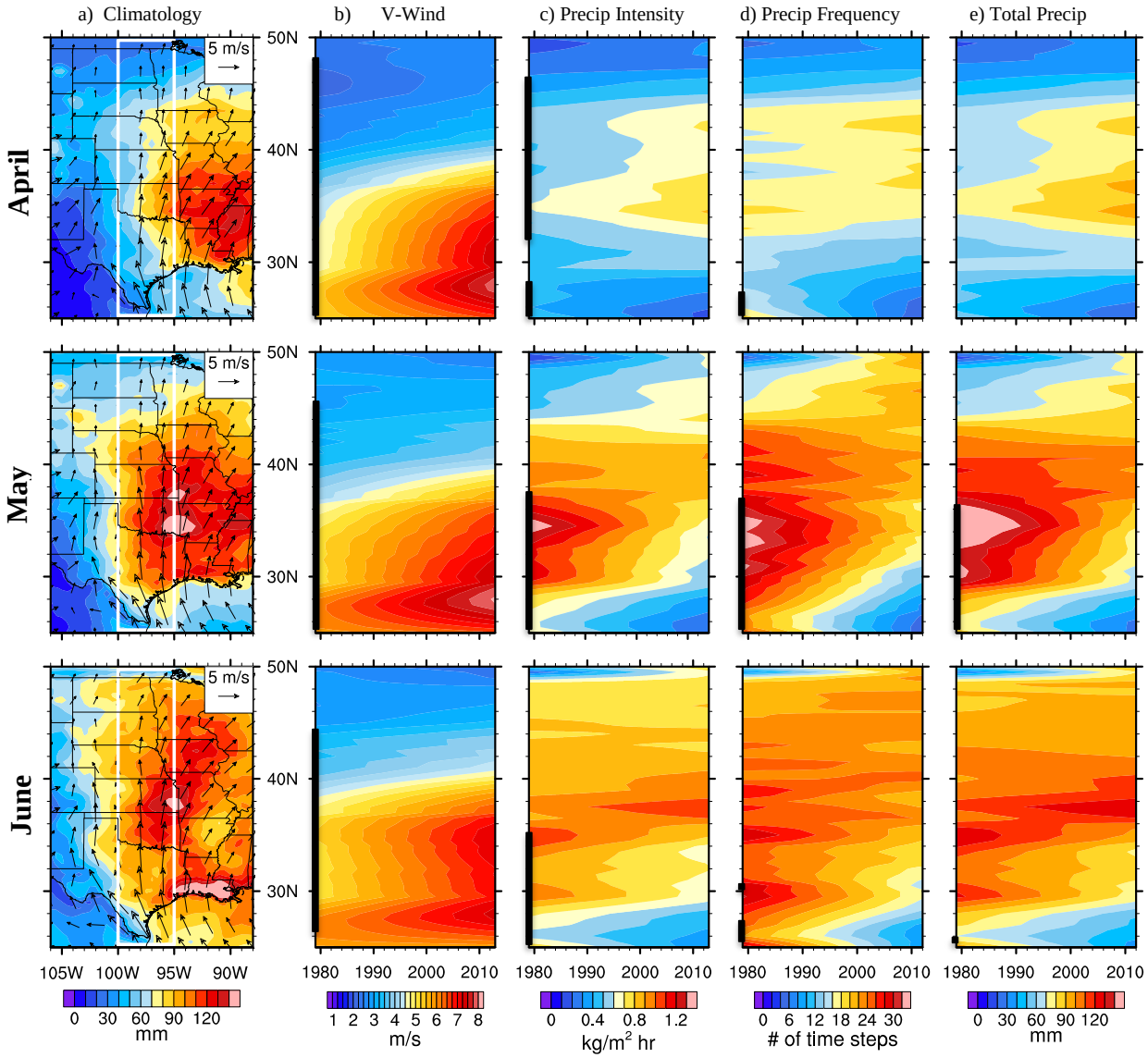

Fig. 2 a) Monthly climatology for precipitation (shaded) and 925 mb wind field (vectors) and Latitude-time Hovmöller trend plots for b) 925 mb v-wind, c) precipitation intensity, d) precipitation frequency and e) monthly total precipitation, zonally averaged along the longitude range indicated by the white boxes within monthly climatology plots. Data plotted consists of regressed linear trend added to climatological mean. Thick bars along latitude axis on trend plots indicate latitudes for which regression coefficients are statistically significant at 95% confidence.

Science and Technology Infusion Climate Bulletin
NOAA's National Weather Service
38th NOAA Annual Climate Diagnostics and Prediction Workshop
College Park, MD, 21-24 October 2013

Climate Monitoring from Space – Architecture for Sustained Observations

John J. Bates

National Climatic Data Center, NOAA/NESDIS, Asheville NC

1. Overview

The task of climate monitoring has requirements that extend beyond the current paradigm of one-time research missions and operational satellite systems in existence today. Recognizing these needs, international research and operational Space Agencies, the Committee on Earth Observation Satellites (CEOS) and Coordination Group for Meteorological Satellites (CGMS), have formed a new Working Group on Climate that has defined an architecture that ensures delivery of sustained observations over the time frames required for analysis of the Earth's climate system. An architecture typically describes the structure of a system, as reflected in its building blocks, their relationships to each other, and to the environment. The descriptive format of the architecture is generally tailored to the particular needs of the users/stakeholders and makes use of common definitions and standards in its construction.

2. Why is an architecture needed?

Based on discussions within the various climate monitoring working groups and related meetings, two main needs/usage scenarios for an architecture have emerged:

1. To promote a common understanding, amongst the various stakeholders, of the implementation implications of meeting the various climate monitoring requirements. To support such a usage, the architecture should depict, in a structured and readily-accessible format, the functions, information flows and dependencies of the processes necessary to satisfy the relevant requirements and support the verification by the originators/owners of the requirements that they have been correctly interpreted. While this should encompass the end-to-end climate monitoring processes (*e.g.* from sensing right through to decision-making), the initial emphasis is expected to be placed on representing the upstream processes (*i.e.* sensing and climate data record creation).

2. To support an assessment of the degree to which the current and planned systems meet the requirements, and the generation of an action plan to address any identified shortfalls/gaps. It is anticipated that such an action plan would help promote the fulfilment of user needs through the coordinated implementation of activities across agencies.

Based on the two identified usage scenarios, an architec¬ture with two main "views" is proposed:

- A Logical View;
- A Physical View.

The logical view serves the first usage scenario (Fig. 1). It represents the functional and data-flow implications of the requirements baseline as a set of interlinked functions and associated data-flows. Leaving aside performance considerations (*e.g.* accuracy, uncertainty, stability, coverage *etc.*), the logical view could be considered as the "target" for a climate monitoring system and, in the sense that it is applicable to all Climate Data Records, this representation is generic. As this view is intimately tied to the requirements baseline (and not to the physical implementation of a climate monitoring system) this view is as stable as the requirements baseline and, once established, should only need to be updated when the functional aspects of the requirements change.

In contrast, the purpose of the physical view, which supports the second usage scenario, is to describe the current and planned implementation arrangements for each essential climate variable, including how the

Correspondence to: John J. Bates, National Climatic Data Center, NOAA/NESDIS, Asheville NC;
E-mail: John.J.Bates@noaa.gov.

various functions of the logical view are/will be physically implemented. As this physical view tracks the evolving implementation of the climate monitoring system, it will need to be regularly updated (*e.g.* once a year).

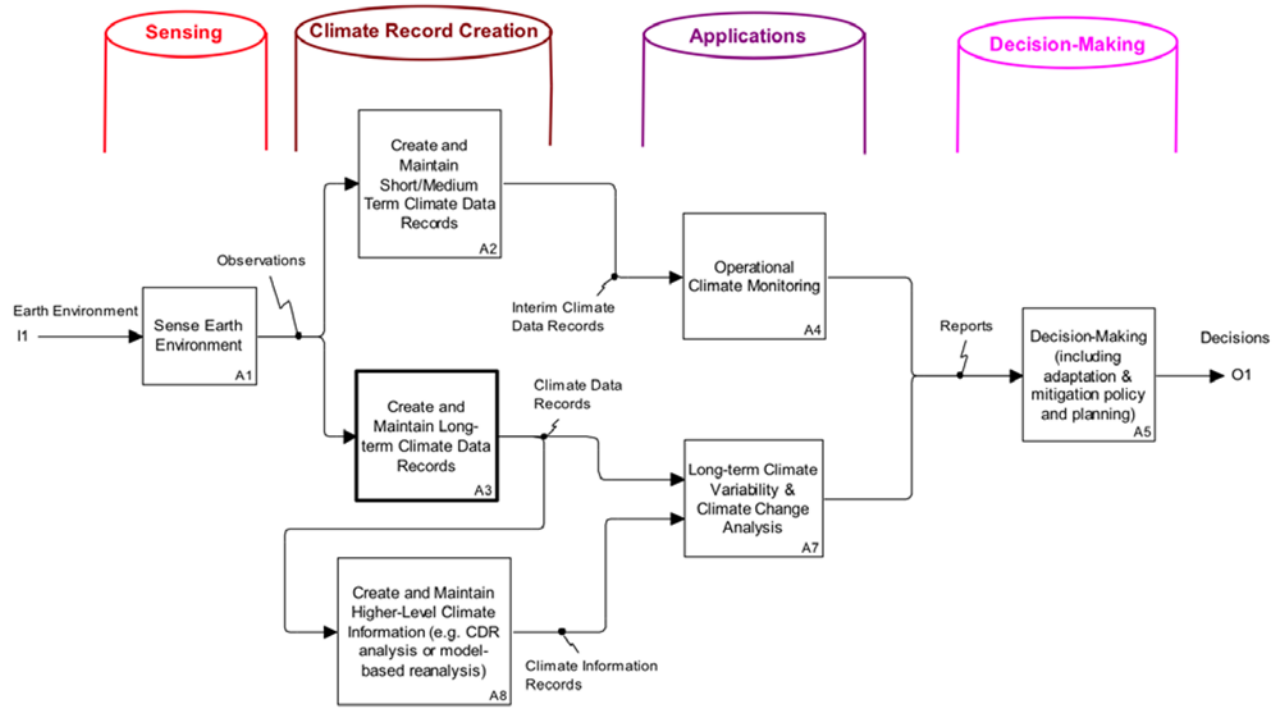

Fig. 1 Schematic of the Logical Architecture for climate monitoring including the four pillars required for monitoring and decomposition steps for creation and applications.

3. Conclusions

A new Space Agency Working Group on Climate has written and released a report on a 'Strategy Towards and Architecture for Climate Monitoring from Space'. The report establishes a framework for international collaboration to address critical issues such as:

- In general, current observing systems have not been primarily designed with a climate perspective, therefore, inventories are needed to document the contributions of current and planned observing systems for climate purposes.
- Requirements for mission continuity and contingency need improvement through international collaboration of space agencies.
- Sustained Climate Data Record (CDR) programs will provide an avenue to replace heritage algorithms and data sets with improved versions once they are successfully demonstrated, validated and available.
- There is an imperative to ensure traceability along harmonized practices.
- It is hoped that the report will help establish a basis for sustained and routine climate monitoring from space similar to the World Weather Watch. The full report can be found at:

  http://www.ceos.org/images/strategy_towards_architecture_hig_rez_V10_high_rez.pdf.

4. IMPROVING FORECAST EVALUATION PROCESS

Science and Technology Infusion Climate Bulletin
NOAA's National Weather Service
38th NOAA Annual Climate Diagnostics and Prediction Workshop
College Park, MD, 21-24 October 2013

Validation of CFSv2 Model Behavior – Land-Atmosphere Interactions and the Hydrologic Cycle

Paul A. Dirmeyer[1,2] and Ahmed Tawfik[2]

[1]*Department of Atmospheric, Oceanic and Earth Sciences, College of Science*
[2]*Center for Ocean-Land-Atmosphere Studies*
George Mason University, Fairfax, VA

1. Introduction

Recent multi-model results from the second Global Land-Atmosphere System Study (GLACE-2; Koster *et al.* 2010, 2011; Guo *et al.* 2011, 2012) suggest that realistic initialization of land surface states (namely soil moisture) in subseasonal-seasonal climate forecasts can improve the skill of temperature and precipitation predictions over some parts of the globe. However, not all models show this improvement. While there is theory to suggest the locations of the world where the effects should be largest correspond to "hotspots" of land atmosphere coupling (*e.g.*, Koster et al. 2004, Guo *et al.* 2006, Dirmeyer *et al.* 2009), some models seem to lack critical aspects of the feedback loop. The NCEP CFSv2 appears to be such a model (Dirmeyer 2013).

In this study, operational forecasts and retrospective forecasts from NCEP CFSv2 as well as Global Land Data Assimilation System (GLDAS; Rodell et al. 2004) output from the land surface component (Noah v2.7.1) are assessed with regard to metrics of land atmosphere coupling to gauge model behavior, with particular emphasis on the simulation of the water cycle.

2. Models and Data

The current CFSv2 model is described by Saha *et al*. (2013). Saha *et al.* (2010) describe the CFSv2 reforecasts in detail. The Noah land surface model is described by Ek *et al.* (2003). Operational data come from the four-times-a-day four-member operational ensemble forecast six-hourly output from 2013, aggregated to daily means. Reforecast data are monthly from 1982-2008. GLDAS-2 data from Noah run offline are from the same period as the CFSv2 reforecast and used at both daily and monthly time scales for comparison to the coupled products, as the time interval affects certain calculations such as

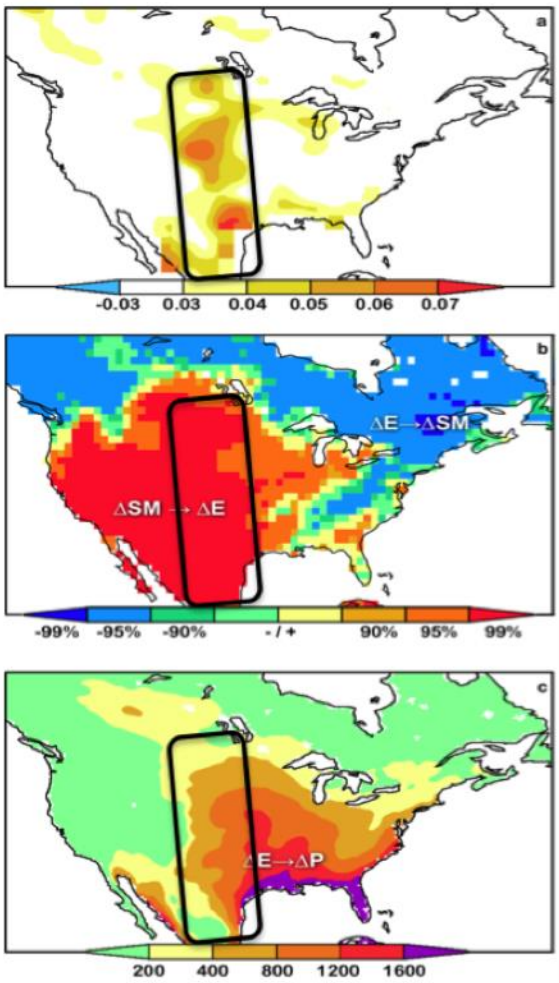

Fig. 1 Multi-model coupling strength from GLACE (top); correlation significance between soil moisture and evaporation from GSWP (middle) and mean CAPE from NARR (J/kg, bottom). All data are for the JJA season.

Correspondence to: Paul A. Dirmeyer, Department of Atmospheric, Oceanic and Earth Sciences, College of Science, George Mason University, Fairfax, VA; E-mail: pdirmeye@gmu.edu.

variances and correlations, but not seasonal means.

3. Theory

Variations at the land surface are translated into atmospheric responses through numerous interconnected non-linear pathways (*e.g.*, van Heerwaarden *et al.* 2010). These land-atmosphere connections can be divided into two segments, a terrestrial and an atmospheric component (Dirmeyer *et al.* 2012). The terrestrial segment describes the sensitivity of surface energy fluxes to changes in the land surface state (Dirmeyer 2011). When surface fluxes respond to soil moisture, the terrestrial segment provides a necessary but not a sufficient condition for the land surface to exert control on the properties of the atmospheric boundary layer. These may be brought to bear through the water or energy cycles.

The atmospheric segment relates the sensitivity of boundary layer development, cloud formation and precipitation to surface fluxes such as evapotranspiration or sensible heat flux (*e.g.*, Betts et al. 1996, Ek and Holtslag 2004). When both segments are operating, feedbacks occur.

Predictability in the physical climate system on time scales beyond those of deterministic weather phenomena can be greatly aided by knowledge of the surface state, precisely because it is a slow manifold compared to the atmosphere (Shukla 1998). This is, of course, predicated on properly representing the mechanisms involved in land-climate interactions. Soil moisture, in particular, has been shown to have a "memory" based on lagged autocorrelations on the order of months (*e.g.*, Schlosser and Milly 2002) and observationally-based land surface initialization extends the predictability of sub-seasonal to seasonal climate in global models (Koster *et al.* 2011, Guo *et al.* 2012).

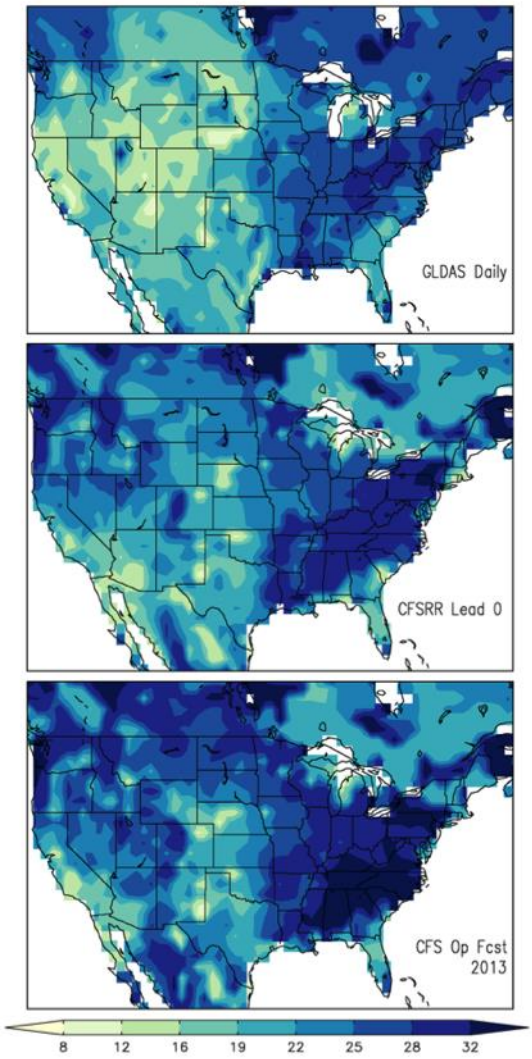

Fig. 2 10-40cm soil wetness (%) for JJA from the indicated sources.

Much of this land surface-driven predictability is associated with "hot spots" of land-atmosphere coupling around the globe (Koster *et al.* 2004) where both terrestrial and atmospheric segments show the proper relationships and adequate strength to complete the feedback loop (Guo *et al.* 2006). The sensitivity of surface fluxes to soil moisture, most readily indicated by a positive correlation between anomalies of soil moisture and evaporation on daily to monthly time scales, is most prevalent in arid and semi-arid regions. On the other hand, the sensitivity of precipitation to variations in surface fluxes skews towards more humid areas, where the atmosphere is typically in a state of conditional instability. Hotspots appear around the transitions between arid and humid zones, where both terrestrial and atmospheric segments exhibit some strength. Figure 1 illustrates this relationship over North America combining three independent data sets (Guo *et al.* 2006, Dirmeyer *et al.* 2006, Mesinger *et al.* 2006).

4. Results

The ability of CFSv2 to simulate climate sensitivity to soil moisture states over the Great Plains of North America has been shown to be weak (Zhang *et al.* 2011), and appears to be the result of several factors. First of all, the model exhibits a somewhat peculiar pattern of mean soil moisture over the central and western parts of the continent. Fig 2 shows the mean JJA soil moisture from the Noah land surface model driven offline by observationally constrained meteoro¬logical forcing, and in the coupled reforecasts at a lead forecast of 0-months (initialization ranging from 30 days prior to 7 days into the forecast month). In GLDAS, the driest

soil is not over the desert Southwest but rather areas of the inter-mountain west and the Great Plains. In CFSv2 reforecasts, the western and southwestern regions are even wetter, and the driest zone is over the central and southern High Plains. The irregularity is even stronger in the operational forecasts (7-10 days lead shown). As a result, the Great Plains area is insensitive to drought because conditions are already so dry.

Figure 3 shows the pattern of latent and sensible heat fluxes for JJA in the CFSv2 operational forecasts, with superposed circles showing observed values from a distribution of FLUXNET sites across the United States (Baldocchi *et al.* 2001). There is a distinct negative bias in Bowen ratio over most areas.

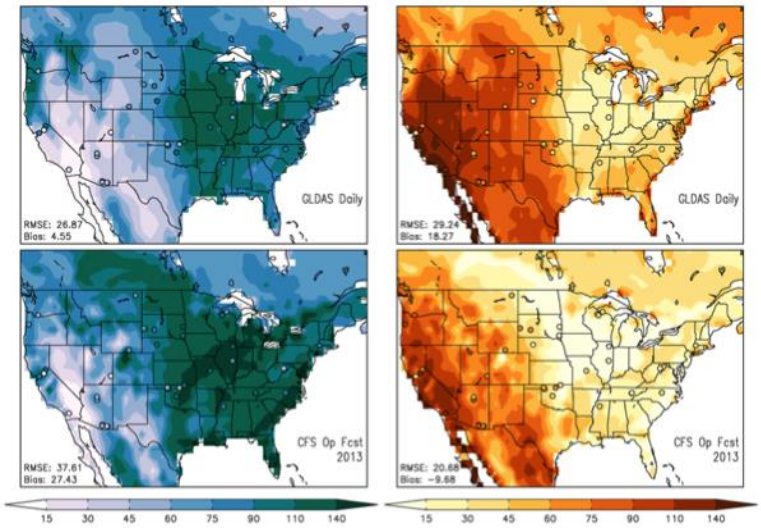

Fig. 3 JJA mean latent (left) and sensible (right) heat flux (Wm^{-2}) from the indicated sources. Dots are values from FLUXNET sites.

The positive bias in latent heat flux (LHF) is over 27 Wm-2 across the flux sites for the operational CFSv2 model, but only +4 Wm^{-2} for Noah in GLDAS. Meanwhile there is nearly a 10 Wm^{-2} deficit in sensible heat flux (SHF) in CFSv2, indicating not only a problem in partitioning net energy, but also an excess of net radiation at the surface in the coupled model. This led to a positive temperature bias in CFSRR, which was addressed by extending the root depth in Noah to tap soil moisture in all four model layers (M. Ek, pers. comm.). This reduced temperature biases through increased evaporation, but exacerbated other problems.

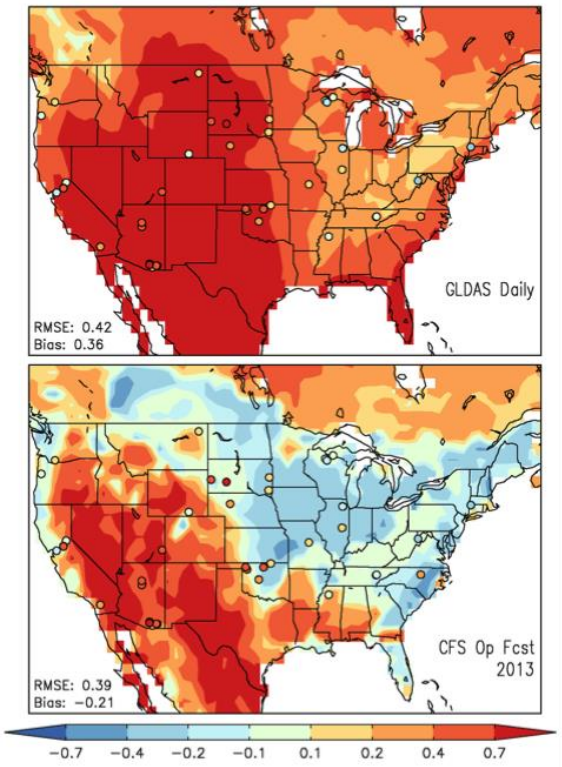

Fig. 4 Correlation between daily soil moisture and latent heat flux during JJA from the indicated sources.

The bias is particularly strong over the agricultural areas, with the lowest Bowen ratios outlining clearly the crop vegetation types over the eastern and northern Great Plains well into southern Canada. This profligate evaporation renders the remainder of the GLACE hot spot immune to soil moisture variations. Thus, a combination of atmospheric and land surface model errors and biases appear to compound, weakening land-atmosphere coupling strength.

The degree to which coupling intensifies these problems can be seen in Fig 4. Correlation of surface fluxes with soil moisture in GLDAS is seen to have a pattern consistent with Fig 1, but somewhat too strong compared with in situ observations. This excessive strength is characteristic of offline land model simulations and is not in itself an indicator of a problem with Noah. However, this strength is completely eradicated over the Great Plains in the coupled CFSv2, where positive correlations between latent heat fluxes and soil moisture are lost.

This also severely affects the development of the daytime atmospheric boundary layer and the height of the lifting condensation level (LCL) over the central and northern Great Plains. Cloud bases in this area are much too low, and day-to-day variability is nearly zero (not

shown). As a result, both the terrestrial and atmospheric segments of the coupled feedback loop are absent over all but the extreme southern Great Plains. Figure 5 shows coupling indices – the terrestrial coupling index (top) is the standard deviation of daily LHF (Wm^{-2}) times the correlation between LHF and soil moisture. For the atmosphere, it's the standard deviation of the height of the LCL (m) times the correlation between SHF and LCL.

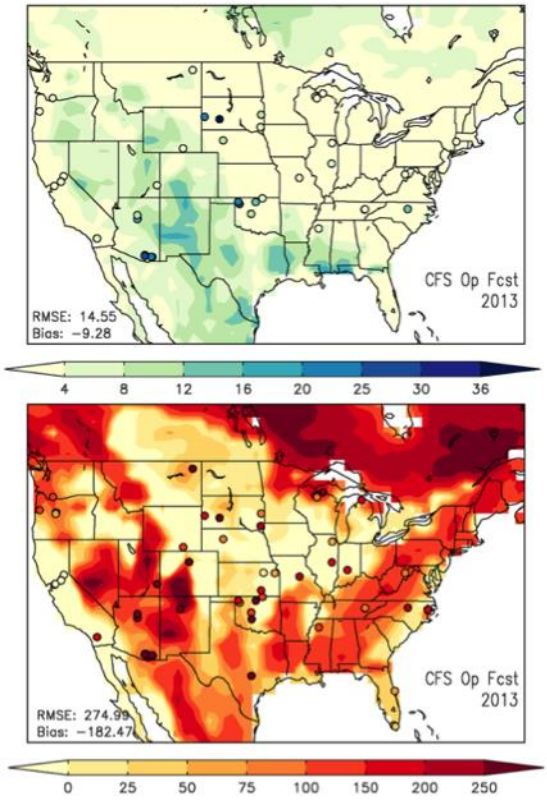

Fig. 5 Terrestrial (top; Wm^{-2}) and atmospheric (bottom; m) coupling indices for CFSv2 operational forecasts during JJA. See text for full description.

5. Conclusions and discussion

A variety of metrics based on state variables and fluxes indicated the behavior of the coupled land-atmosphere system in CFSv2 is considerably different than for the land surface model (Noah) alone driven by observed meteorology, or metrics based on FLUXNET stations. All biases trend toward excessive weakness in land surface feedbacks on the atmosphere, weakening the potential predictability and prediction skill to be gained by the operational NCEP forecast model from realistic land surface initialization (namely for soil moisture). Experiments with other models from GLACE-2 indicate that some models can benefit from realistic land initial states – and these models possess stronger coupling. Thus, this should be a correctable problem if addressed as a coupled land-atmosphere model development effort, resulting in potential increases in forecast skill over the Great Plains, and possibly neighboring areas, during the warm season. Such gains may be extendable to other "hot spot" regions as well, such as the Sahel region of Africa, Eastern Europe to central Asia, western India and Pakistan, much of South America and Australia.

References

Baldocchi, D., and coauthors, 2001: FLUXNET: A new tool to study the temporal and spatial variability of ecosystem-scale carbon dioxide, water vapor and energy flux densities. *Bull. Amer. Meteor. Soc.*, **82**, 2415-2434.

Betts, A. K., J. H. Ball, A. C. M. Beljaars, M. J. Miller, and P. A. Viterbo, 1996: The land surface-atmosphere interaction: A review based on observational and global modeling perspectives. *J. Geophys. Res.*, **101**, 7209-7225.

Dirmeyer, P. A., X. Gao, M. Zhao, Z. Guo, T. Oki and N. Hanasaki, 2006: The Second Global Soil Wetness Project (GSWP-2): Multi-model analysis and implications for our perception of the land surface. *Bull. Amer. Meteor. Soc.*, **87**, 1381-1397, doi: 10.1175/BAMS-87-10-1381.

Dirmeyer, P. A., C. A. Schlosser, and K. L. Brubaker, 2009: Precipitation, recycling and land memory: An integrated analysis. *J. Hydrometeor.*, **10**, 278–288, doi: 10.1175/2008JHM1016.1.

Dirmeyer, P. A., 2011: The terrestrial segment of soil moisture-climate coupling. *Geophys. Res. Lett.*, **38**, L16702, doi: 10.1029/2011GL048268.

Dirmeyer, P. A., and coauthors, 2012: Evidence for enhanced land-atmosphere feedback in a warming climate. *J. Hydrometeor.*, **13**, 981-995, doi: 10.1175/JHM-D-11-0104.1.

Dirmeyer, P. A., 2013: Characteristics of the water cycle and land-atmosphere interactions from a comprehensive reforecast and reanalysis data set: CFSv2. *Climate Dyn.*, **41**, 1083-1097, doi: 10.1007/s00382-013-1866-x.

Ek, M., K. E. Mitchell, Y. Lin, E. Rogers, P. Grunmann, V. Koren, G. Gayno, and J. D. Tarpley, 2003: Implementation of Noah land-surface model advances in the NCEP operational mesoscale Eta model. *J. Geophys. Res.*, **108**, 8851, doi:10.1029/2002JD003296.

Ek, M. B., and A. A. M. Holtslag, 2004: Influence of soil moisture on boundary layer cloud development. *J. Hydrometeor.*, **5**, 86-99.

Guo, Z., and coauthors, 2006: GLACE: The Global Land-Atmosphere Coupling Experiment. 2. Analysis. *J. Hydrometeor.*, **7**, 611-625, doi: 10.1175/JHM511.1.

Guo, Z., P. A. Dirmeyer, and T. DelSole, 2011: Land surface impacts on subseasonal and seasonal predictability. *Geophys. Res. Lett.*, **38**, L24812, doi:10.1029/2011GL049945.

Guo, Z., P. A. Dirmeyer, and T. DelSole, and R. D. Koster, 2012: Rebound in atmospheric predictability and the role of the land surface. *J. Climate*, **25**, 4744-4749, doi: 10.1175/JCLI-D-11-00651.1.

Koster, R. D., and coauthors, 2004: Regions of strong coupling between soil moisture and precipitation. *Science*, **305**, 1138-1140.

Koster, R., and coauthors, 2010: The contribution of land surface initialization to subseasonal forecast skill: first results from the GLACE-2 project. *Geophys. Res. Lett.*, **37**, L02402, doi:10.1029/2009GL041677.

Koster, R. D., and coauthors, 2011: The second phase of the Global Land-Atmosphere Coupling Experiment: Soil moisture contributions to subseasonal forecast skill. *J. Hydrometeor.*, **12**, 805–822, doi: 10.1175/2011JHM1365.1.

Mesinger, F., and 18 co-authors, 2006: North American Regional Reanalysis. *Bull. Amer. Meteor. Soc.*, **87**, 343-360.

Rodell, M., P. R. Houser, U. Jambor, J. Gottschalck, K. Mitchell, C.-J. Meng, K. Arsenault, B. Cosgrove, J. Radakovich, M. Bosilovich, J. K. Entin, J. P. Walker, C. Lohmann, and D. Toll, 2004: The global land data assimilation system. *Bull. Amer. Meteor. Soc.*, **85**, 381-394.

Saha, S., and coauthors, 2010: The NCEP Climate Forecast System reanalysis. *Bull. Amer. Meteor. Soc.*, **91**, 1015–1057, doi: 10.1175/2010BAMS3001.1.

Saha, S., and coauthors, 2013: The NCEP Climate Forecast System version 2. *J. Climate*, **27**, (early release), doi: JCLI-D-12-00823.1.

Schlosser, C. A., and P. C. D. Milly, 2002: A model-based investigation of soil moisture predictability and associated climate predictability. *J. Hydrometeor.*, **3**, 483-501.

Shukla, J., 1998: Predictability in the midst of chaos: A scientific basis for climate forecasting. *Science*, **282**, 728-731.

van Heerwaarden, C. C., J. Vilà-Guerau de Arellano, A. Gounou, F. Guichard, and F. Couvreux, 2010: Understanding the Daily Cycle of Evapotranspiration: A Method to Quantify the Influence of Forcings and Feedbacks, *J. Hydrometeorol.*, **11(6)**, 1405–1422, doi:10.1175/2010JHM1272.1.

Zhang, L., P. A. Dirmeyer, J. Wei, Z. Guo, and C.-H. Lu, 2011: Land-atmosphere coupling strength in the Global Forecast System. *J. Hydrometeor.*, **12**, 147-156, doi: 10.1175/2010JHM1319.1.

Science and Technology Infusion Climate Bulletin
NOAA's National Weather Service
38th NOAA Annual Climate Diagnostics and Prediction Workshop
College Park, MD, 21-24 October 2013

Climate Mean, Variability and Dominant Patterns of the Northern Hemisphere Wintertime Mean Atmospheric Circulation in the NCEP CFSv2

Peitao Peng and Arun Kumar
Climate prediction Center, NECP/NOAA, College Park, Maryland
Bhaskar Jha
INNOVIM, LLC, Greenbelt, Maryland

ABSTRACT

In this study, the climate mean, variability, and dominant patterns of the Northern Hemisphere (NH) wintertime mean 200 hPa geopotential height (Z200) in a CMIP and a set of AMIP simulations from the NCEP CFSv2 are analyzed and compared with the NCEP/NCAR reanalysis. For the climate mean, it is found that a component of the bias in stationary waves characterized with wave trains emanating from the tropics into both the hemispheres can be attributed to the precipitation deficit over the Maritime continent. The lack of latent heating associated with the precipitation deficit may have served as the forcing of the wave trains (Fig. 1).

For the variability of the seasonal mean (Fig. 2), both the CMIP and AMIP successfully simulated the geographical locations of the major centers of action, but the simulated intensity is generally weaker than that in the reanalysis, particularly for the center over the Davis Strait-southern Greenland area. It is also noted that the simulated action center over Aleutian Islands was southeastward shifted to some extent. The shift was likely caused by the eastward extension of the Pacific jet. Differences also existed between the CMIP and the AMIP simulations, with the center of actions over the Aleutian Islands stronger in the AMIP and the center over the Davis Strait-southern Greenland area stronger in the CMIP simulation.

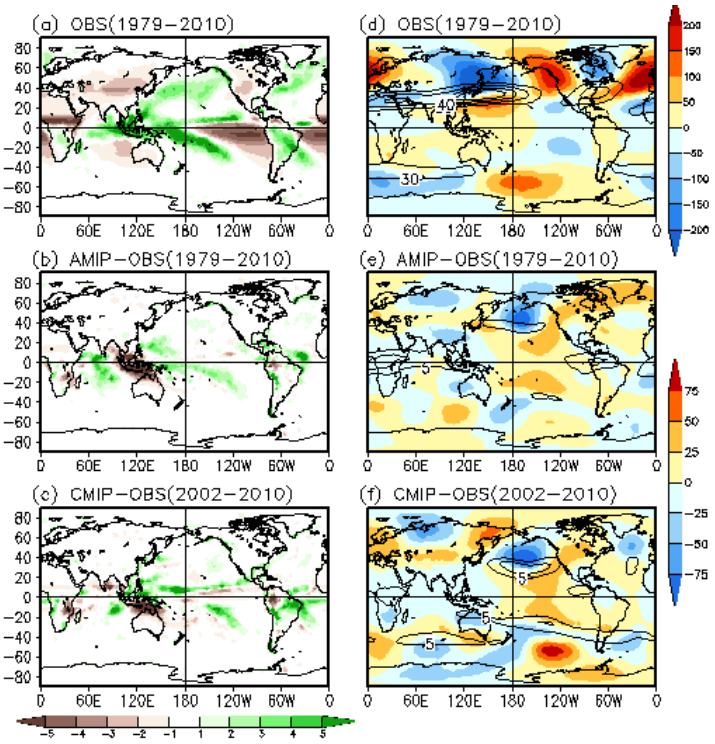

Fig. 1 Climate mean of the zonally asymmetric DJF precipitation rate (mm/day) (left column) and eddy 200 hPa height (m) (right column): The upper row is for the climate of observation over 1979-2010, the middle row is for the bias of AMIP runs from the observation over the same period, and the bottom row is for the bias of CMIP run over 2002-2010. The contours with the height fields are the climate mean of 200 hPa zonal wind (U200) in observation (panel d) and model bias for AMIP and CMIP runs (panel e and f). With m/s unit, the contour levels for U200 climate are 30, 40, 50 and 60, for U200 bias are 5, 10, and 15.

Correspondence to: Peitao Peng, Climate prediction Center, NECP/NOAA, College Park, Maryland;
E-mail: peitao.peng@noaa.gov.

In the mode analysis, the El Nino-Southern Oscillation (ENSO) teleconnection pattern (Fig. 3) in each dataset was first removed from the data, and a rotated EOF (REOF) analysis was then applied to the residual. The purpose of this separation was to avoid possible mixing between the ENSO mode and those generated by the atmospheric internal dynamics. It was found that the simulated ENSO teleconnection patterns from both model runs well resembled that from the reanalysis, except for a small eastward shift. Based on the REOF modes of the residual data, six dominant modes (Figs. 4-6) of the reanalysis data had counterparts in each model simulation, though with different rankings in explained variance and some distortions in spatial structure. By evaluating the temporal coherency of the REOF modes between the reanalysis and the AMIP, it was found that the time series associated with the equatorially displaced North Atlantic Oscillation (ED_NAO) in the two datasets were significantly correlated, suggesting a potential predictability for this mode.

This paper has been submitted to the Climate Dynamics and in revision.

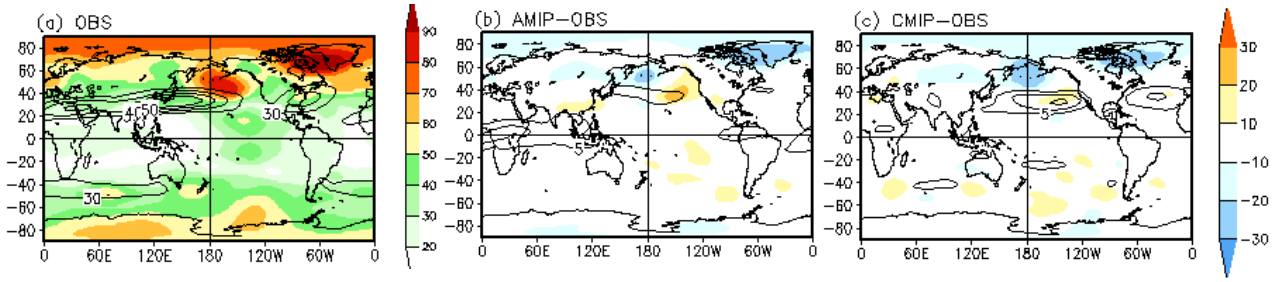

Fig. 2 Standard deviation of DJF mean Z200 (m): (a) total quantity of the observation; (b) AMIP run minus observation; (c) CMIP simulation minus observation. The contours, with the same levels and unit as that in Fig. 1, are for the corresponding climate mean U200. The results are based on the data from the whole period of each dataset.

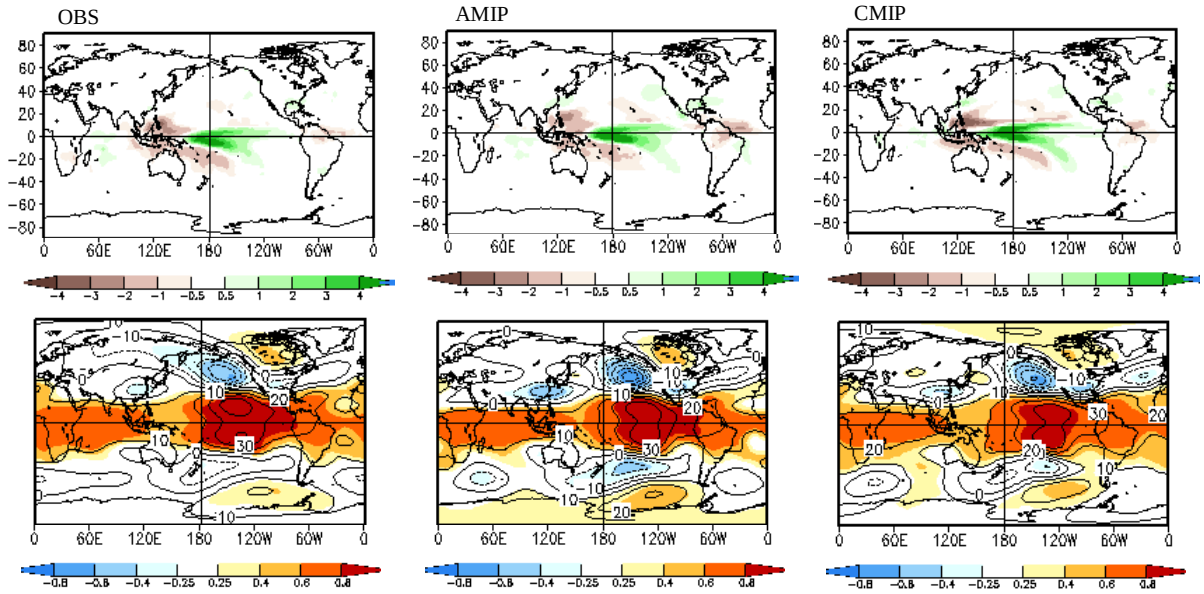

Fig. 3 Regression patterns of DJF mean precipitation rate (mm/day) (upper row) and 200 hPa height (m) (lower row) to the Nino3.4 SST index for observation (left column), AMIP data (middle column), and CMIP data (right column). For the height patterns, the contours are for regression and shading for correlation, with contour interval of 10m, and shaded areas passing the 95% significant level. The data periods are the same as that in Fig. 2.

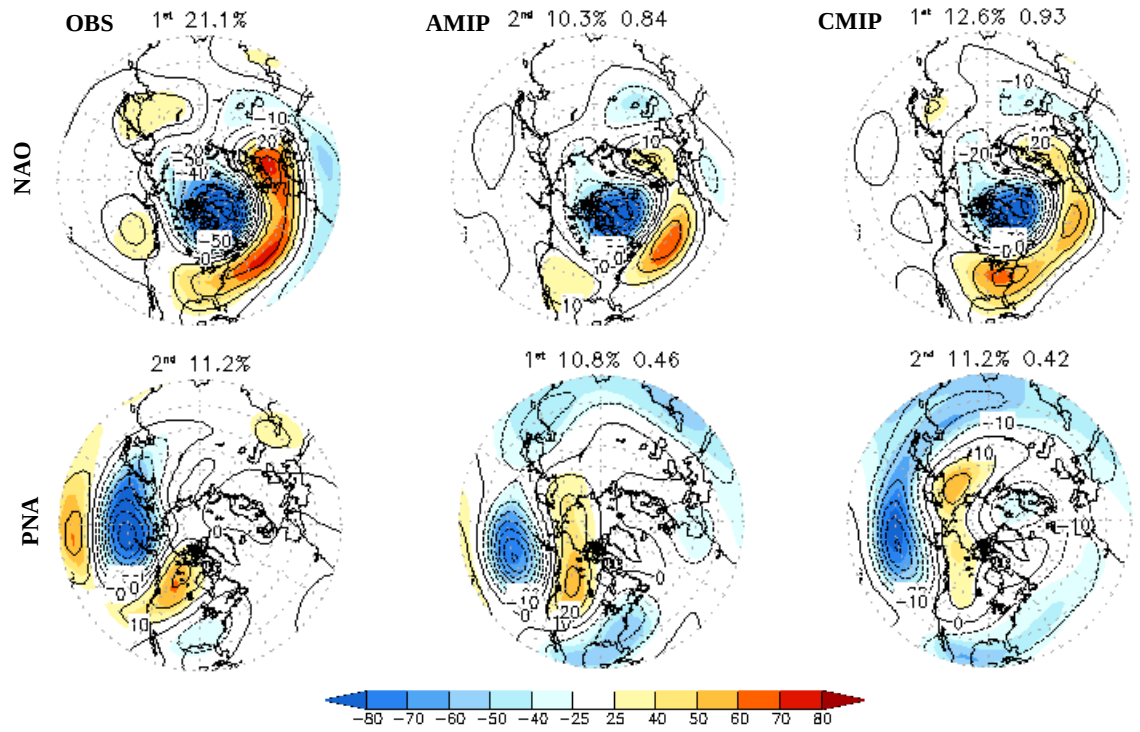

Fig. 4 NAO (upper row) and PNA (lower row) patterns of DJF Z200 for the observation (left column), AMIP runs (middle column) and CMIP run (right column). The patterns are obtained by regressing/correlating Z200 total fields to the rotated principal components (RPCs) of the Z200 residuals (with ENSO related variability removed) over the NH domain (20ºN-90ºN). The contours with interval of 10 m are for regression, and shading (%) for correlation. On the top of each penal, the numbers give the ranking, explained variance (%), and the spatial correlation between the pattern from model and that from observation, respectively.

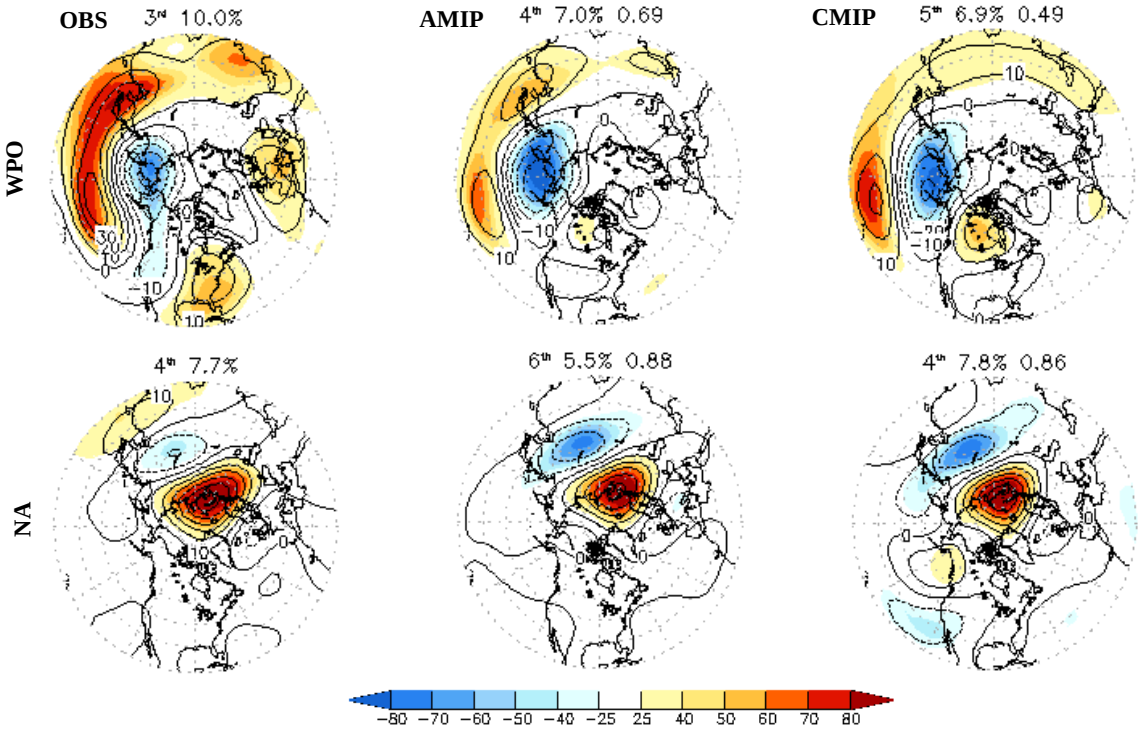

Fig.5 As in Fig.8, but for WPO and NA patterns.

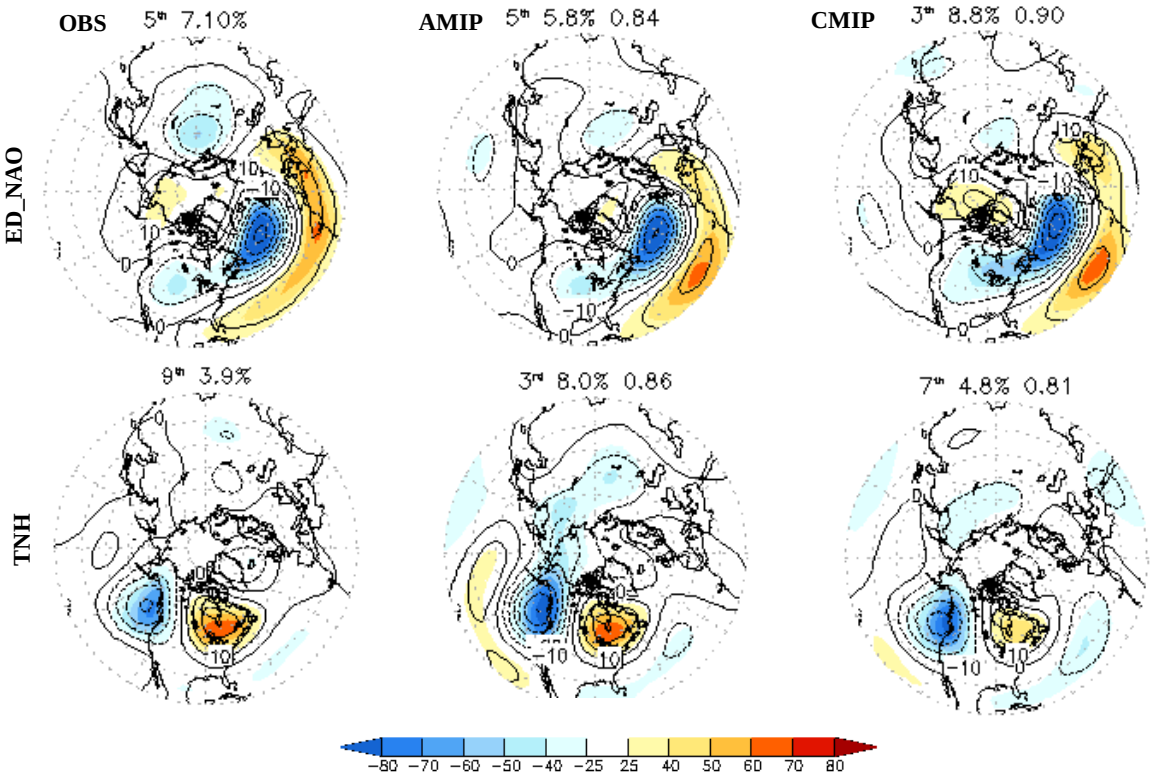

Fig.6 As in Fig.8, but for ED_NAO and TNH patterns.

Science and Technology Infusion Climate Bulletin
NOAA's National Weather Service
38th NOAA Annual Climate Diagnostics and Prediction Workshop
College Park, MD, 21-24 October 2013

NMME Year 2: Verification of Real-time Monthly-mean Forecasts

Emily J. Becker, Huug van den Dool, and Qin Zhang
Climate Prediction Center, NCEP/NWS/NOAA, MD
Malaquias Peña
Environmental Modeling Center, NCEP/NWS/NOAA, MD

1. Introduction

The North American Multi-Model Ensemble (NMME) is a forecasting system consisting of coupled global circulation models from U.S. and Canadian modeling centers (Kirtman *et al.*, 2013). August, 2013, marked two years of real-time NMME forecasting, with forecast data delivered on-time by all modeling centers and posted by the 9th of each month. Real-time and archived forecast graphics from Aug. 2011 – present are available at www.cpc.ncep.noaa.gov/products/NMME. Hindcast and forecast data is archived at the International Research Institute for Climate and Society (IRI), accessible at iridl.ldeo.columbia.edu/SOURCES/Models/NMME/.

NMME forecasts during the first two years focused on monthly-mean 2m surface temperature (T2m), precipitation rate (prate), and sea-surface temperature. Additional environmental variables were added in Year 2, and further additions, as well as intra-seasonal forecasts, are in development. NMME forecast fields are global, and produced at a 1°-longitude by 1°-latitude resolution. Forecast leads and number of ensemble members vary by model; during Year 2 of NMME real-time forecasting, the multi-model ensemble included 79 members. Table 1 contains the models involved in NMME Phase I, and more details on the models and forecasting structure can be found in Kirtman *et al.* 2013. Monthly mean and 3-month average seasonal forecast graphics are published by the CPC in deterministic and probabilistic formats: anomalies for each model's forecast are departures from that model's climatology, and the multi-model ensemble was created with equal weighting for all models.

TABLE 1 Models included in the NMME. The first part of each model's name is the center where it was produced.

Model	Hindcast	Ensemble Size	Lead Times	Forecast
NCEP-CFSv1	1981-2009	15	0-8 Months	Aug 2011 – Oct 2012
NCEP-CFSv2	1982-2010	24 (28)	0-9 Months	Aug 2011 – present
GFDL-CM2.2	1982-2010	10	0-11 Months	Aug 2011 – present
IRI-ECHAM4-a	1982-2010	12	0-7 Months	Aug 2011 – Jul 2012
IRI-ECHAM4-f	1982-2010	12	0-7 Months	Aug 2011 – Jul 2012
CMC1-CanCM3	1981-2010	10	0-11 Months	Aug 2012 – present
CMC2-CanCM4	1981-2010	10	0-11 Months	Aug 2012 – present
NCAR-CCSM3.0	1982-2010	6	0-11 Months	Aug 2011 – present
NASA-GEOS5	1981-2010	10	0-9 Months	Aug 2011 – present

Hindcast ensembles were run for all NMME models from all initial months for approximately 30 years. The hindcast database allows for both calibration of the forecasts and an assessment of average skill. For example, Fig. 1 shows the anomaly correlation (AC) of the prate multi-model ensemble for the July-August-

Correspondence to: Emily J. Becker, Climate Prediction Center, NCEP/NWS/NOAA, 5830 University Research Court, College Park, MD 20740-3818; E-mail: emily.becker@noaa.gov.

September (JAS) period, from June initial conditions. Over the hindcast period, some skill is found over the western half of the United States, including portions of the region affected by the North American Monsoon. As prate is a notoriously difficult field to forecast, even limited skill is welcome.

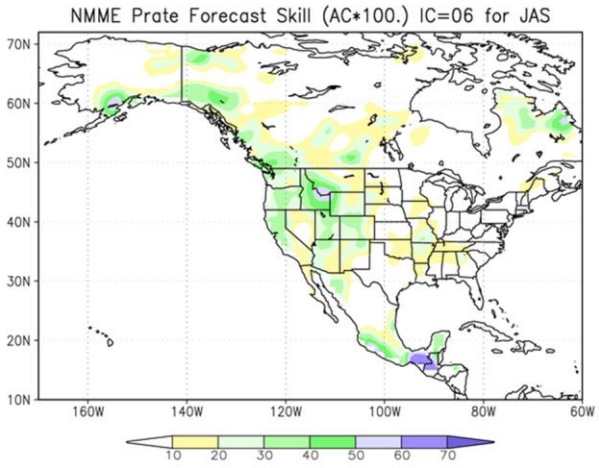

Fig. 1 Anomaly correlation for the NMME multi-model ensemble prediction of precipitation rate for the July-August-September period, from June initial conditions, based on hindcast data. ACs are multiplied by 100.

2. Assessment

With two years of operation under our belts, we can look back to see how well the NMME forecasts have performed. Figure 2 depicts the anomaly correlations for bias-corrected seasonal T2m and prate forecasts, area-averaged over North America, all land north of 15°N (Greenland is not included), averaged for each of the first two years of the project. T2m forecasts were verified against the station observation-based GHCN+CAMS (Fan and van den Dool, 2008), and prate forecasts against the CPC global daily Unified Rainguage Database (URD, Xie *et al.*, 2010). ACs are the average of the "leads 1 – 3" seasons from all the initial conditions in the year. For example, the leads 1 – 3 seasons from January initial conditions are FMA, MAM, and AMJ. The averages over the 5 available seasonal leads (not shown) are similar to the ACs in Figure 2. This is a sample of the real-time verification analysis, which covers both monthly and seasonal forecasts from August, 2011, available at www.cpc.ncep.noaa.gov/products/NMME/verif/.

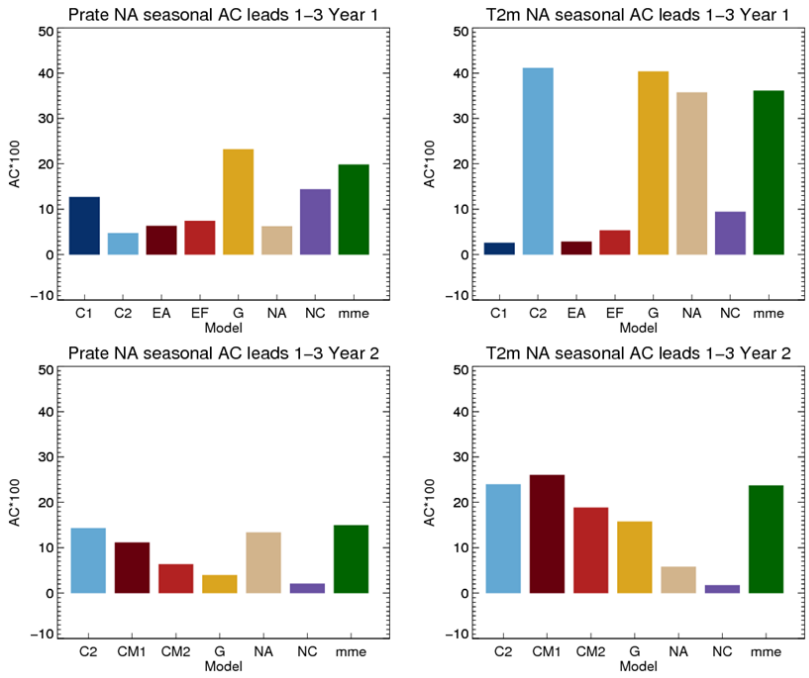

Fig. 2 Area-average North American prate (left) and T2m (right) anomaly correlations for NMME operational Year 1 (top row) and Year 2 (bottom row). Label key: C1=CFSv1, C2=CFSv2, EA=ECHAMa, EF=ECHAMf, G=GFDL, NA=NASA, NC=NCAR, CM1=CMC1, CM2=CMC2. The green bar, "mme", indicates AC for the 7-model (Year 1) or 6-model (Year 2) ensemble mean.

Year 1, August 2011 – July 2012 (top row), includes seven models and the multi-model ensemble mean (mme). The ACs shown are for the ensemble mean of each model and the mme. The models show a wide range of success in forecasting during Year 1, especially in the T2m field. While the mme score is not always the highest among the models, it is consistently among the highest; this held true when other regions were examined (not shown.)

The Year 1 period featured some remarkable climate extremes, including the record heat and "flash drought" of July, 2012, in the central North American continent. The NMME monthly-mean ensemble forecast for July indicated a likelihood of hot and dry conditions as far out as five months in advance, contributing to the relatively high pattern correlations found in Year 1. The record high temperatures over much of the United States and southern Canada in March, 2012,

were suggested by the NMME some months in advance, as well, although the spatial extent of this event was underestimated.

Year 2, August 2012 – July 2013, was a more challenging year for the NMME forecasting system in North America. ACs for Year 2 forecasts, SON 2012 – JJA 2013, are shown in Fig. 2, lower row. CFSv1 is not included in these results, although it did contribute to the mme until October, 2012. In June, 2013, the NMME indicated an increased probability of above-average precipitation during July-August-September in the southwestern United States (Fig. 3). While the verification period for this forecast was not complete at the time of writing, through late September much of this region was showing 90-day average precipitation rates of 150-200% of normal.

Obviously, two years of forecasts and a handful of specific events cannot be generalized to an overall statement of skill, and this assessment lacks an attribution component that could help diagnose why the models captured some events and not others. However, it is still worthwhile to take stock of our results, to understand how the NMME is contributing to long-lead climate forecasting. With some encouraging results thus far, we can look forward to further refinements to the system as it develops over the next few years.

This work has been published in CLIVAR Exchanges / VAMOS! Newsletter in 2013.

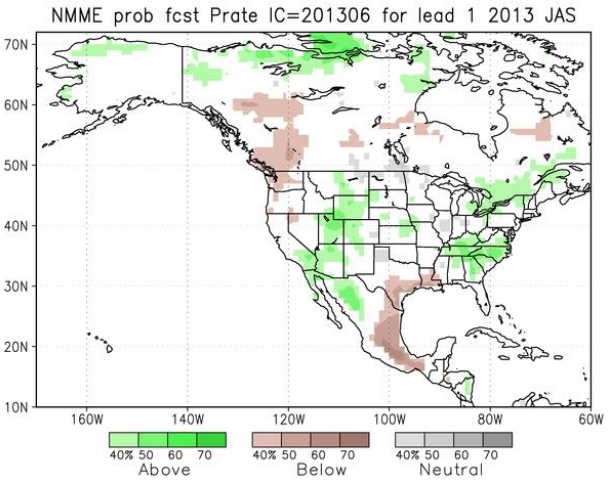

Fig. 3 NMME tercile-based prate probability forecast for July-August-September 2013, made in June 2013, using 79 ensemble members from six models. Above and Below contours show when one class has >38% of ensemble members, and the opposite class is below 33%. In the case that Above is >38% and Near-neutral is >33%, Above will be shown. This is the same for Below. Gray contours show when >38% of ensemble members fall in the "Neutral" tercile, and both A and B are below 33%. White areas show where no one class is dominant: either all terciles are under 38%, or both Above and Below are over 38%.

References

Becker, E., 2013: The Real-time North American Multi-Model Ensemble Turns 2. CLIVAR Exchanges No. 63 / VAMOS! Newsletter No. 9, 6-9.

Fan, Y., and H. van den Dool, 2008: A global monthly land surface air temperature analysis for 1948-present. *J. Geophys. Res.*, **113**, D01103, doi:10.1029/2007JD008470.

Kirtman, B. P., D. Min, J. M. Infanti, J. L. Kinter, D. A. Paolino, Q. Zhang, H. van den Dool, S. Saha, M. P. Mendez, E. Becker, P. Peng, P. Tripp, J. Huang, D. G. DeWitt, M. K. Tippett, A. G. Barnston, S. Li, A. Rosati, S. D. Schubert, Y.-K. Lim, Z. E. Li, J. Tribbia, K. Pegion, W. Merryfield, B. Denis and E. Wood, 2013: The US national multi-model ensemble for intra-seasonal to interannual prediction. *Bull. Amer. Meteor. Soc.*, **94**, in press.

Xie, P., M. Chen, and W. Shi, 2010: CPC unified gauge analysis of global daily precipitation. To be submitted to *J. Hydrometeor*.

5. DEVELOPING APPLICATIONS

Science and Technology Infusion Climate Bulletin
NOAA's National Weather Service
38th NOAA Annual Climate Diagnostics and Prediction Workshop
College Park, MD, 21-24 October 2013

A Different Kind of Guidance for Climate Adaptation Planning

Rachael G. Jonassen
George Washington University, SEAS/EMSE, Washington, DC
Marina Timofeyeva
Climate Services Division, NOAA/NWS, Silver Springs, MD

1. Background

Efforts to mitigate anthropogenic emissions of greenhouse gases have failed to prevent acceleration in emissions, rising concentrations in the atmosphere, and increasing acidification of the oceans. Because of the impasse in negotiations, emphasis on adaptation has grown in recent years. Mandates for adaptation planning exist at international, national, and local levels. Organizations such as the World Bank, and related international financing organizations, now fund significant efforts at adaptation planning and adaptation actions through vehicles such as the Green Climate Fund and the Adaptation Fund. The Green Climate Fund may expend $100B per year by 2020. The US government, through Executive Order, requires federal agencies to develop and implement adaptation plans. Certain public stock exchanges require listed companies to report their climate risks and the Securities and Exchange Commission has issued guidance on such reporting. Many in the private sector develop climate change adaptation plans and an industry is growing around demands for climate change adaptation services.

2. Climate science

To plan correctly for adaptation, an organization must first identify the risks it faces. For this purpose, those involved frequently refer to the results of General Circulation Models (GCMs) that use boundary conditions including possible future atmospheric concentration of greenhouse gases (representative concentration pathways, or RCPs). The newest model results were produced in the Coupled Model Inter-comparison Project phase five (CMIP5), which implemented experiments to support the Intergovernmental Panel on Climate Change (IPCC) Fifth Assessment Report (AR5). These model results represent the world's best estimate of what might happen under various possible scenarios of mitigation success (or failure). CMIP5 GCM results for IPCC AR5 vary widely in the magnitude of climate change projected using the various RCPs. The climate modeling community does not attempt to, nor does it advocate, assignment of likelihoods to any of these outcomes.

3. The problem

Climate modelers do not advocate use of CMIP results for adaptation planning. Indeed, they caution against such applications since they have no basis for determining which projection is most likely. CMIP5 and AR5 groups carefully label GCM results 'projections' of what might happen to distinguish them from 'predictions' of what will happen. CMIP5 results are not predictions (most likely outcomes) and are not designed for adaptation planning. Despite this limitation, and in the absence of alternatives, the adaptation community frequently (almost invariably) draws upon CMIP projections to characterize future climate to which adaptation planning then responds.

This unintended application of CMIP results is further compromised by another simplification, which results from the nearly incomprehensible plethora of CMIP results. Adaptation planners select particular scenarios; they nearly invariably do not consider the full suite. Examples abound in the literature of adaptation planning based on AR4 and CMIP3 results, which used a different set of boundary conditions (SRES scenarios). Most adaptation exercises draw upon one or two, and at most three SRES scenarios. Insidiously,

Correspondence to: Rachael G. Jonassen, Engineering Management and Systems Engineering, George Washington University, 1776 G Street, N.W., Washington, DC 20052; E-mail: rachaelj@gwu.edu.

these analyses come to be taken for what adaptation is needed, rather than adaptation that might be needed if that scenario holds.

Conditional projections cannot serve as ‘best science’ for climate adaptation planning, which depends upon risk analysis informed by at least ordinal-scale impact likelihoods. Adaptation efforts should be directed to an expected future, not a future whose likelihood is unknown. Such an expected future is, by definition, a prediction; adaptation needs prediction.

4. NOAA’s role and responsibility

NOAA's CPC climate predictions do not extend to time periods relevant to climate adaptation. Experimental decadal forecasts do not demonstrate skill and remain research topics with distant prospects of utility. NOAA's GFDL provides GCM projections for IPCC that are conditioned on RCPs and designed to support climate mitigation policy. Recently developed online analytical tools (LCAT) from the Climate Services Division support modeling of NCDC observational data but eschew predictive applications. Thus, adaptation decisions lack NOAA predictions, although NOAA's climate goal specifically includes support for climate adaptation decisions.

5. A fundamental barrier

Meteorological tradition requires demonstrated skill to accept a prediction method. Climatology has inherited a meteorological tradition for determination of predictability that is inappropriate to, and inadequate for, the societal challenge of adapting to climate change. The requirement for demonstrable skill in a conditional analysis of a transient non-linear system where long lead predictions are needed fails the test of utility. The existing system of conditional projections was created for, and is well suited to, informing policy decisions about mitigation. It fails to address the challenge of adaptation and the very failure of mitigation actions necessitates reexamination of the projection/skill paradigm. If climate science cannot inform our expectations, what can?

6. An option

Meteorology is not the only science that makes predictions in the context of saving life and property. For example, seismologists forecast earthquake risk from recorded seismicity, mapped records of fault behavior, and strain dynamics. Prediction is inherent in the scientific enterprise, though traditions of valid prediction differ between disciplines (e.g. medicine, engineering, seismology, cosmology). Although the traditions differ fundamentally and are not interchanged, each demonstrates service to society. The projection/skill paradigm is unsuited for the task of adaptation, yet the demands for adaptation press upon science. A scientific response would consider the possibility of a different, more useful, paradigm. Creating a new paradigm may be informed by metasystematic examination of existing prediction traditions in the full spectrum of scientific and technical fields (such as the seismology example) to ensure the dialogue is disencumbered of dominant forces inadvertently limiting discourse and options. Such dialogue is needed now and, consistent with its climate goal, NOAA should lead.

Science and Technology Infusion Climate Bulletin
NOAA's National Weather Service
38th NOAA Annual Climate Diagnostics and Prediction Workshop
College Park, MD, 21-24 October 2013

The Prediction of Extreme Agrometeorological Indices Using the Canadian Meteorological Centre's Medium Range Forecasts

Aston Chipanshi[1], and Hai Lin[2]

[1]*Agriculture and Agri-Food Canada, Science and Technology Branch, Regina, Saskatchewan*
[2]*Atmospheric Numeric Weather Prediction Research, Environment Canada, Dorval, Quebec*

1. Introduction

The overarching objective of this work was to develop practical indicators, methods, and procedures for monitoring and analyzing agrometeorological extremes that significantly influence crop and/or livestock production in agricultural regions of Canada. Because of Canada's extreme northern location, agriculture lies at the fringe of ideal conditions. As a result, extreme weather conditions can quickly assume disaster proportions. The economic loss due to extreme weather events is always substantial. In 2001 and 2002 for example, Canada's GDP fell some $5.8B due to extreme drought (Wheaton *et al.* 2005) and in 2010, excessive flooding led to unseeded acres, resulting in insurance claims of about $956 Million (Public Safety Canada 2011). We therefore sought to develop some key indicators that can inform the industry about the weather related risks over time frames associated with managing an agricultural activity. We considered water, heat and wind related extreme events and developed agrometeorological indices that can be linked directly to agriculture operations. This work was partly influenced by the world-wide interest in reporting climate extremes (Peterson and Manton 2008). In total, twelve indices were developed as discussed below. Predictions were made at daily to monthly time frames which closely coincide with the planning window of most agricultural activities during the growing season.

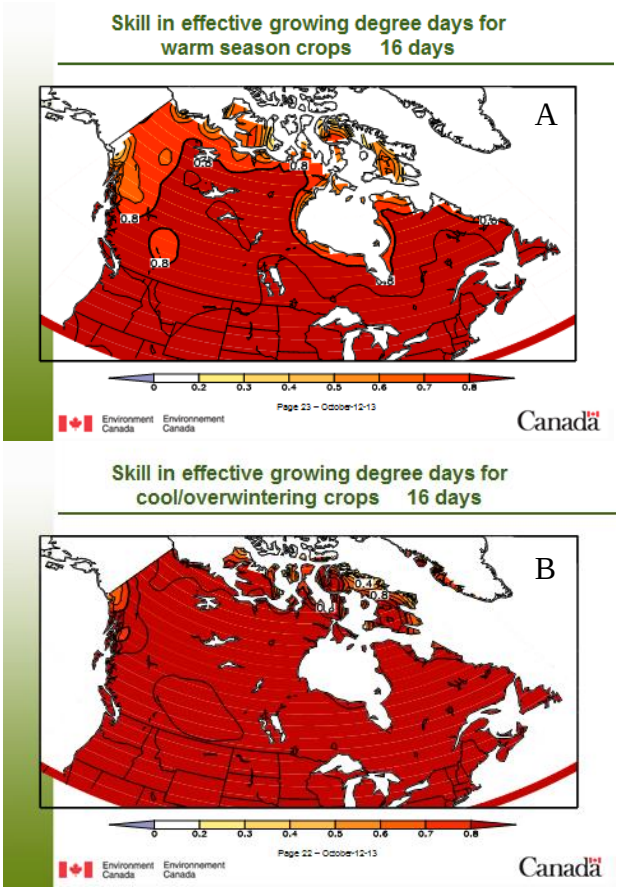

Fig. 1 Skill in predicting the effective growing degree days for A) warm and B) cool season crops across Canada.

2. Methodology and data

A phased approach was taken to develop, test and forecast agrometeorological indices across Canada's agricultural landscapes. In phase 1, the occurrence of extreme agrometeorological indices, their trends and variability were analyzed (Qian *et al*. 2010). In phase 2, improvements were made to the extreme indicators by defining the indices in terms of the critical thresholds by major crops. Phase 3 consisted of calculating and validating the indices in hindcast mode using forecast data sets from the Canadian Meteorological Centre's medium range and seasonal forecasts. This step was critical because it involved assessing the forecast skill. The last step involved communicating the forecast of indices to the agriculture sector on an experimental basis as part of building an integrated agroclimate monitoring system that includes near real time reporting and forecasting of agrometeorological indices.

Correspondence to: Aston Chipanshi, Agriculture and Agri-Food Canada, Science and Technology Branch, Regina, Saskatchewan; E-mail: aston.chipanshi@agr.gc.ca.

In all, twelve agrometeorological extreme indicators from heat, water and wind sub-climatic themes were investigated as follows:

Heat based indices

i) *Effective Growing Degree Days (EGDD)* - Growing Degree Days were calculated using 5°C and 10°C as the baseline for cool and warm season crops respectively. The growing season was defined using the Biometeorological time scale (Baier and Robertson, 1968). Daily EGDD = (Tmax+Tmin)/2.

ii) *Crop Heat Units (CHU)* - Although similar to EGDDs, the maximum and minimum temperature are defined differently. The maximum temperature uses 10ºC as the base and 30ºC as the ceiling. The minimum temperature uses 4.4ºC as the base. Thus, Ymax = (3.33 (Tmax-10)) - (0.084 (Tmax-10.0) ^{2}) and Ymin = (1.8 x (Tmin - 4.4)). Daily CHU = (Ymax + Ymin)/2.

iii) *Number of Frost-Free Days (NFFD)* - Frequency of days above the frost temperature (-2ºC for cool and 0ºC for warm season crops respectively).

iv) *Number of Ice Free Days (NIFD)* - Frequency count of days with a minimum temperature below the frost temperature (-2ºC for cool and 0ºC for warm season crops respectively). The T thresholds for herbaceous and woody crops are much lower.

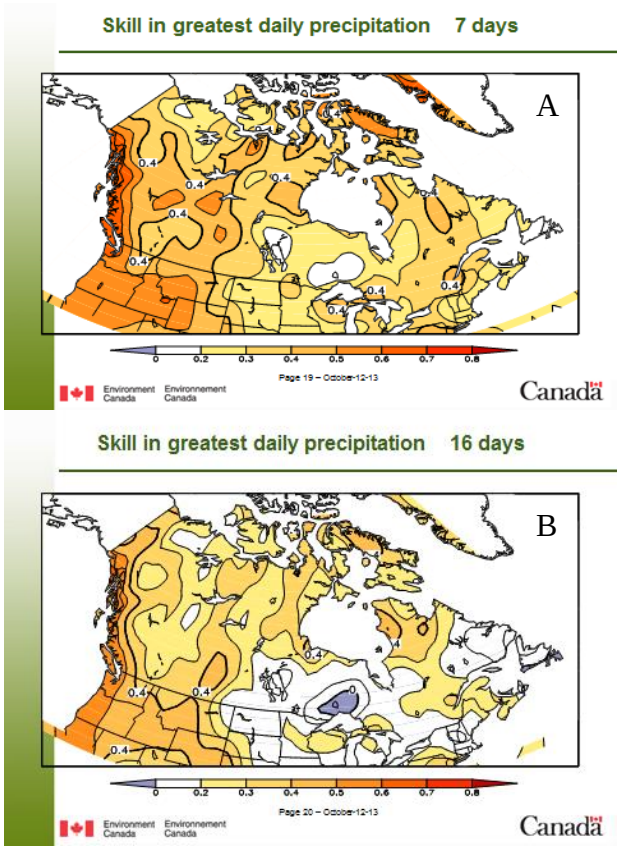

Fig.2 Skill in predicting the greatest 7 –day (A) and 16- day (B) precipitation across Canada.

v) *Days of Cool Wave (DCW)* - A frequency count of days with a minimum temperature below the cardinal minimum temperature (5ºC and 10ºC for cool and warm season crops respectively).

vi) *Days of Heat Wave (DHW)* - Frequency count of days with maximum temperature above the maximum cardinal temperature (30ºC and 35ºC for cool and warm season crops respectively).

Water based indices

i) *Greatest Daily Precipitation (P1D)* - the greatest daily precipitation over the period of analysis.

ii) *Greatest 10-Day Precipitation (P10D)* - the greatest 10 day precipitation total in a 2-week period.

iii) *Seasonal Water Deficit (SWD=P-PE)* - the difference between total precipitation (P) and evapotranspiration (PE).

Wind based indices

i) Maximum Daily Wind speed (MDWS) - the maximum wind speed reached per day.

ii) Number of Strong Wind Days (NSWD) - Frequency of days with an average wind speed > 30km h^{-1}.

iii) Number of Drying Days - Frequency of days with an average wind speed > 30km h^{-1} and maximum temperature > 30ºC.

Homogenized climate data from Environment Canada (Vincent *et al.* 2009) were used to calculate trends, variability and change in agrometeorological indices over a period of 60 to 100 years across Canada (depending on station history length). To calculate the forecast skill, hindcast data were obtained from the Global Ensemble Prediction System (GEPS) covering 2009 to 2011. The GEPS has been in operation since 1996 (with many upgrades) and consists of the Global Environmental Multiscale (GEM) model, a global

Gaussian grid of 600×300 km, 40 levels and top at 2hPa, 30 minute time step, 16 day integration, disturbed physical parameterizations and Kalman Filter initialization (Houtekamer *et al.* 2009).

3. Results

Skill of Agrometeorological Indices - We examined the predictability of the indices by calculating the Heidke Skill Score (HSS) which compares the proportion of correct forecasts to a no skill random forecast Hyvärinen (2014).

Energy based indices - The energy and temperature - based indices were realistically forecast over Canada. At most locations, the skill score was in excess of 70% correct (Fig. 1).

Water (precipitation) based indices - The precipitation based indices exhibit a relatively high forecast skill in western Canada at both 7 and 16- day time frames (Fig. 2). In central and eastern Canada, the skill score drops at the 16-day timeframe and degrades even further at the monthly time frame (data not shown).The temporal drop in skill is caused by the growth of initial errors in the model. Spatially, the difference in skill can be partially explained by the consistency of the forcing factors during the period under study (April to September). It has been shown that western Canada is influenced by the Madden-Julian Oscillation and ENSO-like forcing factors more than eastern Canada during spring through summer (*e.g.*, Lin *et al.* 2010).

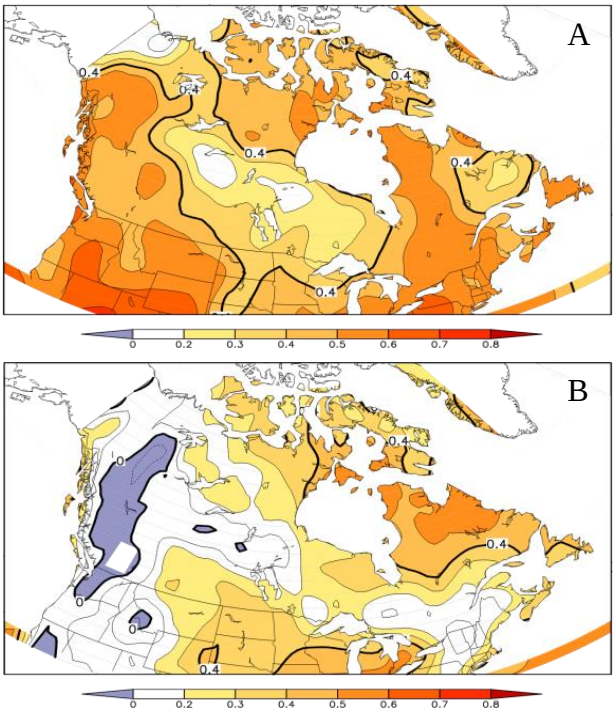

Fig.3 Skill in daily maximum wind speed (A) and the number of strong winds (B) at the 7-day time frame.

Wind based indices -The skill of predicting the wind-based indices has significant spatial differences: the maximum daily wind speed is best forecast in western and eastern Canada, with a relatively low skill in central Canada; the number of strong wind days is more reliable in eastern and central Canada, with a low skill in western Canada (Fig.3). Like the water based indices, the skill in the wind based indices drops at longer time frames in the future.

Real time reporting of the extreme agrometeorological indices - The 12 grometeorological indices are updated daily and e-posted on a public website: http://collaboration.cmc.ec.gc.ca/science/rpn/sages/.

The weekly and bi-weekly forecasts have a spatial resolution of 60 km while the monthly forecasts have a resolution of about 200 km. The intent for posting these products is to encourage the evaluation of the evolving weather related risks so that corrective actions can be taken. In some instances, the products may show opportunities which those involved in activities that are sensitive to the mapped extreme indices may react to. In the examples (Fig. 4) drawn from the 2013 growing season, the greatest 10-day precipitation total between October 14 and 27 (A) and the Number of Frost Free Days (B) between October 14 and 20, were showing ideal harvesting conditions and this information is timely to make plans to take machinery in the field.

Similar maps exist for other indices at the time frames discussed above.

References

Baier, W. and G. W. Robertson, 1968: The performance of soil moisture estimates as compared with the direct use of climatological data for estimating crop yields. *Agric. Meteorol.*, **5**, 17-31.

Houtekamer, P. L., H. L. Mitchell, and X. Deng, 2009: Model error representation in an operational Ensemble Kalman Filter, *Mon. Wea. Rev.*, **137**, 2126-2143.

Hyvärinen, O., 2014: A probabilistic derivation of Heidke Skill Score. *Wea. Forecasting*, **29**, 177–181. doi: http://dx.doi.org/10.1175/WAF-D-13-00103.1

Lin, H., G. Brunet, and R. Mo, 2010: Impact of the Madden-Julian Oscillation on wintertime precipitation in Canada. *Mon. Wea. Rev.*, **138**, 3822-3839.

Peterson, T. C., and M. J. Manton, 2008: Monitoring changes in climate extremes: A tale of international collaboration. *Bull. Amer. Meteor. Soc.*, **89**, 1266–1271. doi: http://dx.doi.org/10.1175/2008BAMS2501.1

Public Safety Canada, 2011: Canadian disaster database http://www.publicsafety.gc.ca/prg/em/cdd/index-eng.aspx. Accessed: December, 2012.

Qian, B., X. Zhang, K. Chen, Y. Feng, T. O'Brien, 2010: Observed long-term trends for agroclimatic conditions in Canada. *J. Appl. Meteor. Climatol.*, **49**, 604–618. doi: http://dx.doi.org/10.1175/2009JAMC2275.1

Vincent, L. A., E. J. Milewska, R. Hopkinson, and L. Malone, 2009: Bias in minimum temperature introduced by a redefinition of the climatological day at the Canadian synoptic stations. *J. Appl. Meteor. Climatol.*, **48**, 2160-2168. doi: http://dx.doi.org/10.1175/2009JAMC2191.1.

Wheaton, E., V. Wittrock, S. Kulshreshtha, G. Koshida, C. Grant, A. Chipanshi, B. Bonsal with P. Adkins, G. Bell, G. Brown, A. Howard, and R. McGregor, 2005: Lessons learned from the Canadian drought years of 2001 and 2002: Synthesis Report. Technical Report Prepared for Agriculture and Agri-Food Canada. Saskatchewan Research Council (SRC) Publication No. 11602—46E03, 30pp.

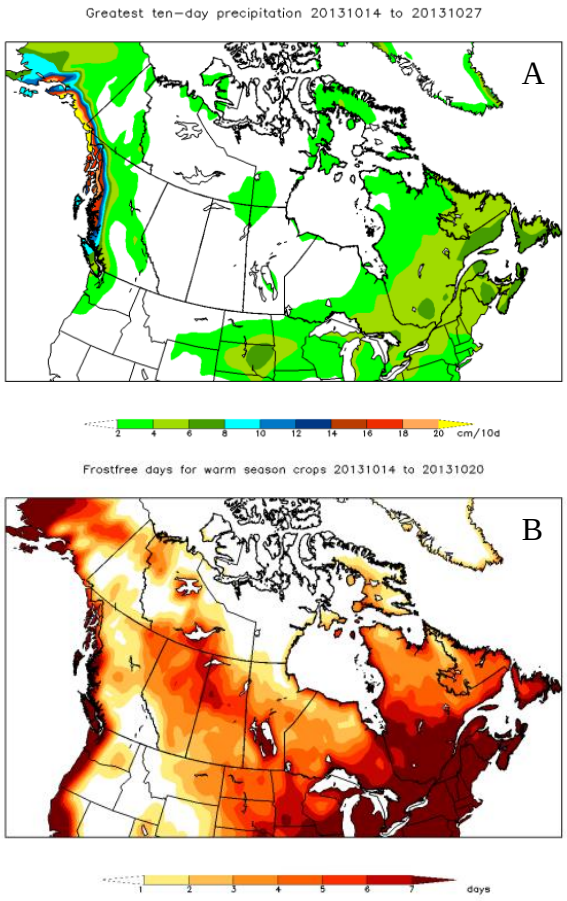

Fig 4 Predicted greatest 10-day precipitation total (A) and number of frost free days for warm season crops (B) on October 1, 2013.

Science and Technology Infusion Climate Bulletin
NOAA's National Weather Service
38th NOAA Annual Climate Diagnostics and Prediction Workshop
College Park, MD, 21-24 October 2013

Toward an Interannual to Decadal Local Sea Level Forecasting Service

Hans-Peter Plag

Climate Change and Sea Level Rise Initiative (CCSLRI), Old Dominion University, Norfolk, VA

1. Introduction

Climate change is likely to lead to a significant rise in Global Sea Level (GSL) with potentially devastating impacts on coastal cities and settlements (*e.g.*, Rowley et al. 2007, Edwards 2008, Hallegatte 2012, Hallegatte *et al.* 2013, Horton *et al.* 2014). The societal and economic impacts would be felt globally. Recent successive events show that the costs of single sea-level related disasters are increasing and exceeding $100 Billion. In many urban coasts, an accelerated Local Sea Level (LSL) rise is presently causing mounting adaptation costs (*e.g.*, Atkinson *et al.* 2013). The recent extreme events (*e.g.*, tropical cyclones Katrina, Sandy, and Haiyan) are demonstrating the high risks for urban coasts associated with storm surges and hurricanes. Spatial variability in LSL (*e.g.*, Plag 2006, Ezer 2013) will amplify any increase in GSL on regional scales. Acceleration in LSL rise is also spatially variable, and some regions already exhibit significant non-linear changes (*e.g.*, at the U.S. East Coast, Sallenger et al. 2012, Ezer *et al.* 2013, Kopp 2013). In a recent report of the National Research Council's Committee on Abrupt Climate Change, the risk for rapid climate change impacts is emphasized (NRC 2013). In particular, the uncertain response of the large ice sheet to climate change (*e.g.*, Little *et al.* 2013; see also the discussion in Plag and Jules-Plag 2013, and the reference therein) introduces the possibility of a rapid GSL rise. The rate of change in global temperature observed in the last, and projected for the current century is much greater than those documented for many past millennia (Marcott *et al.* 2013), and the projected changes classify as "abrupt changes." Under these conditions, rapid sea level changes cannot be excluded.

Projections of GSL and LSL on century time scales are highly uncertain, and recent risk assessments demonstrate that presently future LSL variations are not predictable on century time scales (Plag and Jules-Plag 2013, and the reference therein). The large uncertainty in the plausible range of LSL trajectories and their Probability Density Functions (PDFs) reduces the value of these long-term assessments for risk management. Even the upper end of the range of plausible future LSL trajectories is highly uncertain (Horten *et al.* 2014) . Importantly, the trajectories do not account for the risk of abrupt climate change. The range of plausible GSL trajectories resulting from the still unpredictable response of the large ice sheets to climate change is often displayed for GSL trajectories at the end of the 21st Century (Figure 1), giving the false impression that the large range of plausible trajectories can only develop on century time scales. However, there is no scientific basis to exclude rapid contributions from the ice sheets on decadal to multi-decadal time scales, opening the

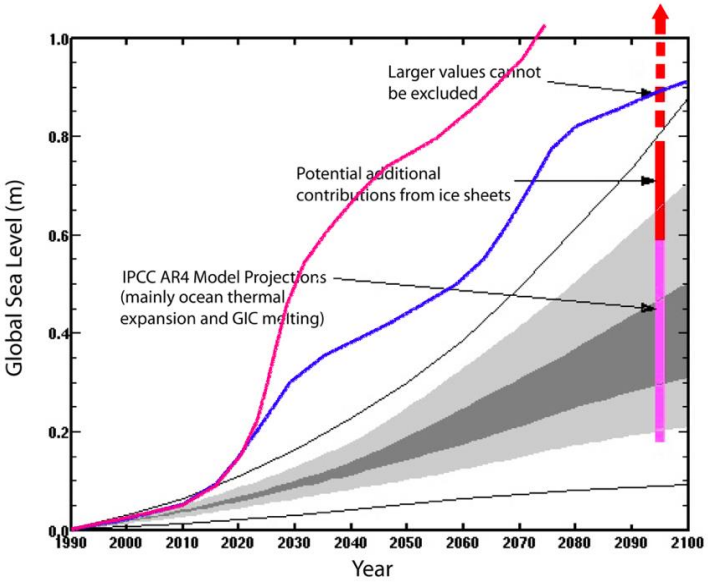

Fig. 1 Plausible 21st Century trajectories of GSL cover a wide range at the end of the present century, with possibly much higher trajectories indicated for the later part of the 21st Century (red arrow). However, rapid increases caused by rapid melting of parts of the large ice sheets are possible over the next decades, and trajectories like the red and blue one cannot be excluded. Modified from Church *et al.* (2010).

Correspondence to: Hans-Peter Plag, Climate Change and Sea Level Rise Initiative (CCSLRI), Old Dominion University, Norfolk, VA; E-mail: hpplag@odu.edu.

possibility for low-probability, high impact rapid increases in GSL already in the near future. Such a rapid rise would have devastating consequences for the growing urban coasts, including coastal mega cities. In fact, observations of the ice sheets during the last 10 years have repeatedly surprised glaciologists and earth scientists with large and accelerating melting rates (Velicogna and Wahr 2005, 2006) that exceeded what was considered likely, or even possible, a few years earlier.

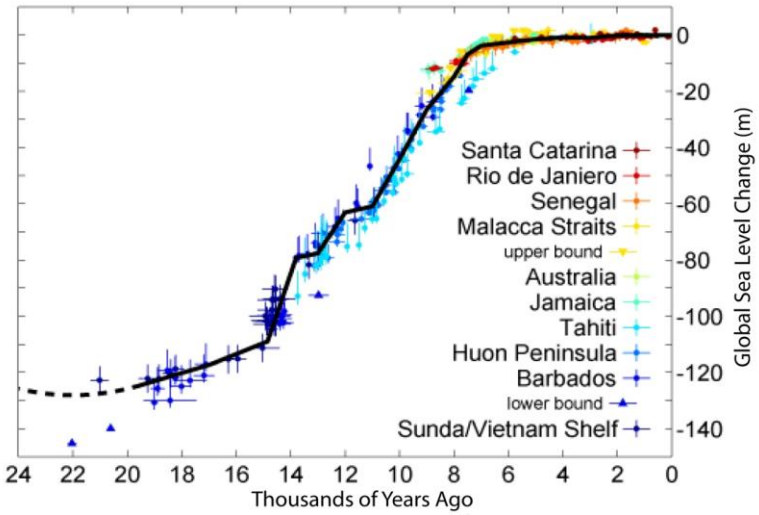

Fig. 2 GSL for the last 24,000 years. During the last 6,000 years, GSL has been exceptionally stable with changes on the order of 0.1 m per century. Human civilizations have not experienced larger rates, which has created a normalcy bias toward the belief that GSL is inherently stable.

Considering the high costs of adaptation and potential disasters caused by coastal hazards, both over and under-protection/adaptation can be very costly and challenging for national economies. Adaptation taking into account a potential rapid LSL rise is economically expensive, culturally difficult to communicate, and legally and politically difficult to implement. Our civilization has a normalcy bias caused by more than 6,000 years of experience with a relatively stable GSL, which created the general concept that sea level does not change significantly through the life time of a human being or even on time scales of several centuries (Figure 2). During the existence of human civilization, typical GSL changes were on the order of 0.1 m per century. It is difficult to communicate that climate change might cause GSL to change much faster than any of the changes human civilizations have experienced. Even on local scale, LSL has been very stable except for a few areas where coastal subsidence or rapid land uplift caused changes discernible withing a typical human lifespan. However, paleo data for the last 800,000 years (Hansen *et al.* 2008) shows that changes on the order of 5 m per century are possible, and changes on the order of 1 to 2 m per century are normal (Plag and Jules-Plag 2013). Due to large spatial variability of LSL, this translated into a PDF for LSL with changes on the order of 3 m per century still having high probabilities, while much larger changes cannot be excluded.

GSL displays interannual to decadal variability on the order of centimeters (Figure 3)[1]. This variability has been related to atmosphere-ocean modes and to changes in land water storage (Fasullo *et al.* 2013). The interannual to decadal variability shows large spatial variability, which can amount to up to 0.20 m over two decades, not accounting for additional contributions from local vertical land motion. Partly, the variability is caused by internal ocean processes and partly by interaction with the water cycle and the atmosphere (Meyssignac and Cazenave 2012). At time scales of 50 years, spatial variability

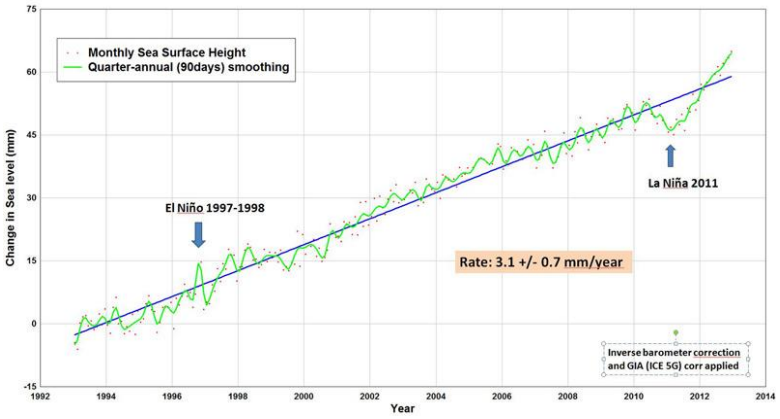

Fig. 3 GSL variations determined from satellite altimetry for the period 1993 to 2013. Note that Fasullo *et al.* (2013) attribute the dip in the GSL curve around 2010.5 to the flooding in Australia after a prolonged drought.

[1] From http://www.space.dtu.dk/english/Research/Scientific_data_and_models/Sea-Level-Change; accessed on 2013/10/02.

can be as large as 0.15 m (Plag, 2006; Meyssignac *et al.*, 2012).

2. Need for interannual to decadal LSL projections

In many coastal locations, small changes in mean LSL can significantly change inundation risk and the frequency and magnitude of flooding (Atkinson *et al.* 2013). A rapid LSL rise would amplify risks and the ensuing disasters could challenge our civilization. During the last deglaciation, rapid LSL altered coast lines within decades. However, during that time, large-scale built environment was absent, and with much lower populations, humans could easily adopt to shifting coast lines. Today, with substantial built environment and crucial infrastructure in coastal zones, rapid changes in coast lines and increased inundation risks during storm surges would be economically and environmentally devastating. Recently, several city managers have indicated that "early warnings" for a rapid LSL rise with lead times of five to fifteen years would provide actionable information for decision makers (*e.g.*, Timothy Reeder 2009, personal communication), and they have asked for the establishment of a decadal LSL forecasting service. Considering the normalcy bias resulting from a very unusual period of stable GSL and the extremely high risk associated with a rapid LSL rise, predictions on decadal time scales are needed to inform timely adaptation and to provide early warning in case there is on onset of rapid changes (Plag *et al.* 2010; Showstack 2013).

Having the ability to reliably predict seasonal to decadal LSL variations would allow for timely detection of the onset of a low-probability, high-impact rapid GSL rise and enable an "early warning system" required to facilitate mitigation and adaptation where and when necessary. Earth observations will be able to identify major ice masses that enter a state of instability, and for these masses, predictive capabilities for their disintegration trajectories need to be developed. Based on such disintegration predictions, LSL could then be forecast with the same time horizon as ice sheets, if a validated ice-ocean-solid-Earth model is available. Likewise, ocean observations will be able to detect the onset of major changes in ocean circulation and heat content affecting GSL and LSL, and validated atmosphere-ocean models will be able to forecast the further development on seasonal to decadal time scales.

Predictive capabilities need to be assessed quantitatively before actionable interannual to decadal predictions can be made available as decision support. No single Earth system model is currently available that can accurately predict past, present, or future LSL changes, and it is unlikely that such a model will become available in the near future. Moreover, some underlying processes (including future greenhouse gas emissions; effects of human "re-engineering" of the planet on climate; response of ice sheets and glaciers to global warming) likely will remain unpredictable on century time scales for a long time to come.

In order to assess our predictive capabilities, it is important to answer three specific science questions: (1) At what time scales does predictability break down for the individual processes contributing to LSL changes? (2) Which of these processes have the potential to cause rapid LSL rise? (3) With what lead time could the onset of a rapid LSL rise be detected, given the limited predictability of several contributing processes?

3. Local sea level equation

The definition of LSL and a cumulative equation for LSL are given in Box 1. LSL as defined there is the quantity directly related to potential impacts of climate change and LSL rise in a given coastal area. GSL is the average of LSL taken over the surface of the oceans. With this definition, changes in GSL equal changes in the Global Ocean Volume (GOV).

Coastal LSL is the result of global, regional and local-scale Earth system processes, which alter sea surface height, land surface height, or both (*e.g.* Plag 2006). These processes include mass relocation in ice sheets, glaciers, land water storage, and oceans; deformation of the solid Earth and gravity field changes caused by the mass relocation; changes in ocean heat storage and ocean currents; changes in atmospheric circulation; tectonic processes; and local coastal subsidence caused by natural and anthropogenic processes. In many locations, detrended LSL exhibits interannual to interdecadal variability exceeding 20 cm, and intraseasonal variability and changes in the seasonal cycle add to LSL variability.

Earth system models available today are not capable of modeling all LSL forcing processes and predicting LSL changes. However, the scientific understanding of the link between individual global, regional and local processes and LSL changes is well developed. Therefore, a local approach can be used to model LSL changes. To accomplish this, we separate LSL into a high-frequency and a low-frequency part and provide cumulative equations for each part, expressing LSL variations as a sum of contributions from the various processes (eqs. (3) and (4) in Box 1).

BOX 1: Cummulative Local Sea Level Equation

We define LSL as the height h of the sea surface above the underlying surface of the solid Earth, i.e.

$$h(\lambda,\theta,t) = \begin{cases} r_1(\lambda,\theta,t) - r_0(\lambda,\theta,t) & : \text{ in the ocean} \\ 0 & : \text{ on land ,} \end{cases} \tag{1}$$

where r_0 and r_1 are the geocentric positions of the sea floor and sea surface, and λ and θ the geographical longitude and latitude, respectively (Plag, 2006). Variations $\xi(t) = h(t) - h_0$ of LSL are the result of variations in r_0 and r_1.

We separate the equation describing LSL into a high-frequency and a low-frequency part:

$$\xi(t) = \xi_{\mathrm{hf}}(t) + \xi_{\mathrm{lf}}(t) \tag{2}$$

with the separation at a period of 2 months (Plag, 2006). For the assessment of impacts, the combined effects of these two parts are important. The high frequency part ξ_{hf} can be written as:

$$\xi_{\mathrm{hf}}(t) = \xi_{\mathrm{waves}}(t) + \xi_{\mathrm{tidal}}(t) + \xi_{\mathrm{atmos}}(t) + \xi_{\mathrm{seiches}}(t) + \xi_{\mathrm{tsunami}}(t), \tag{3}$$

where we have omitted the location dependence. Here we will only consider the low-frequency part ξ_{lf}, which can be written as:

$$\begin{aligned} \xi_{\mathrm{lf}}(\vec{x},t) = {} & S(\vec{x},t) + C(\vec{x},t) + F(\vec{x},t) + A(\vec{x},t) + I(\vec{x},t) + G(\vec{x},t) + T(\vec{x},t) + \\ & P(\vec{x})(t-t_0) + V_0(\vec{x})(t-t_0) + \delta V(\vec{x},t) \end{aligned} \tag{4}$$

where t is time, t_0 an arbitrary time origin, $\vec{x}$ a point on Earth's surface, and ξ is given relative to an arbitrary zero level (Plag, 2006). The processes included in eq. (4) are S: steric changes, C: ocean circulation, F: freshening due to melting of sea and land ice, A: atmospheric forcing, I: mass changes in the large ice sheets, G: mass changes in the continental glaciers, T: mass changes in the terrestrial hydrosphere, P: post-glacial rebound, V_0: secular vertical land motion others than postglacial rebound, δV: non-linear vertical land motion.

Equation 4 illustrates the complex nature of low-frequency LSL variations as the result of processes in the global water and energy cycles merged with geodynamic processes and, recently, anthropogenic activities. The processes separate into two large groups, namely those that are mainly volume changes of the ocean water (and thus affect GOV but not Global Ocean Mass (GOM) and those that are associated with significant mass redistribution in the global water cycle (and thus may also affect GOM).

The link between mass redistributions, including mass exchanges between the oceans and other reservoirs in the global water cycle, is given by the mass-LSL equation detailed in Box 2. Eq. (5) has been applied extensively to studies of LSL changes caused by the ice ages and the subsequent Post-Glacial Rebound (PGR, see Mitrovica *et al.* 2010, and the references therein). Main focus has been on the viscous part and the determination of the radial viscosity profile of the Earth mantle. There are still considerable inter-model differences in predictions of present-day PGR signals in LSL, surface displacements, geoid, and rotation (*e.g.*,

BOX 2: Local Sea Level Changes Caused by Mass Redistribution

Processes involving redistribution of mass in the water cycle all are associated with viscoelastic-gravitational effects on LSL, leading to very distinct spatial and temporal patterns of LSL variations caused by these processes. The governing equation that links mass redistribution to LSL variations ξ (first introduced by Farrell & Clark, 1976) can be written as:

$$\xi(\vartheta,\lambda,t) = c(t) + \int_{-\infty}^{t}\int_{0}^{\pi}\int_{0}^{2\pi} G(\vartheta,\lambda,\vartheta',\lambda',t-t') \tag{5}$$

$$\frac{\mathrm{d}}{\mathrm{d}t'}\left\{O(\vartheta',\lambda',t')\rho_{\mathrm{W}}\xi(\vartheta',\lambda,t') + \left[1-O(\vartheta',\lambda',t')\right]\rho_{\mathrm{L}}\eta(\vartheta',\lambda,t')\right\}\sin\vartheta'\mathrm{d}\lambda'\mathrm{d}\vartheta'\mathrm{d}t',$$

where ϑ, λ, and t are co-latitude, longitude, and time, respectively, ρ_{W} and ρ_{L} are the densities of the ocean water and the load on land (water or ice), respectively, G is the Green's function for LSL, O the ocean function, defined to be one over ocean and zero over land, and η the accumulated ice load change due to mass added or removed from land. $c(t)$ is determined such that mass is conserved. ξ as defined by eq. (5) is a continuous continuation of LSL onto the continents, and the true LSL has to be defined as $\widehat{\xi} := O\,\xi$. The mass-LSL equation (5) assumes instantaneous distribution of the water in the global ocean and is appropriate at seasonal to longer time scales (see Plag, 2006, and the reference therein). Over the last two decades, eq. (5) has been augmented by several groups (e.g. Milne et al., 1999; Mitrovica & Milne, 2003; Kendall et al., 2005).

Chambers *et al.* 2009), which originate mainly in differences in ice history and the treatment of rotational effects. Using eq. (5) to describe the relation between present-day mass changes and LSL so far has been restricted to a few examples (*e.g.*, Plag and Juettner 2001; Mitrovica *et al.* 2001; Plag 2006; Mitrovica *et al.* 2009; Bamber *et al.* 2009).

Major mass redistribution in the global water cycle can result from significant mass loss from ice sheets, ice caps, and glaciers. Net ice-mass depletion of land-based ice will add to net water mass in the ocean unless it is intercepted by surface water or terrestrial storage reservoirs. The mass loss is accomplished by direct climate forcing (through changes in precipitation, melt rate, *etc.*) and by dynamic changes (*e.g.*, subglacial sliding, iceberg calving) that can be indirectly and non-linearly influenced by climate. Dynamic changes can act to accelerate mass loss from glaciers and ice sheets, but generally not to retard it. If these mass changes are known sufficiently, for example, from model predictions, then the resulting LSL variations can be calculated using eq. (5).

Predictions of GSL from land ice sources depend critically upon numerical simulations and require knowledge of atmospheric and oceanic forcing as well as geometric landscape boundary conditions. While significant progress has been made in ice sheet numerical modeling capacity, robust operational models do not yet exist for prediction (Libscomb *et al.* 2009). Chief among obstacles to be overcome are a lack of knowledge of the processes of subglacial sliding (boundary slip) and iceberg calving. Solutions to these problems and limitations are being sought, and in the meantime, predictions based on climate proxies and approximations of dynamics (*e.g.*, Pfeffer *et al.* 2008) provide temporary "placeholder" solutions.

4. A modular, coupled Earth system model for LSL

Equation 4 can be implemented in a modular, coupled model representing the relevant Earth system processes and ensuring consistency between these processes. Fig. 4 displays the main modules of a modeling framework for LSL changes. Ideally, all individual modules would be at the same level of internal complexity and fully coupled, representing all interactions between the four main modules. Most Atmosphere-Ocean General Circulation Models (AOGCMs) include a reasonably well developed coupled atmosphere and ocean

system, but the physical processes for ice sheets, glaciers, sea ice, biosphere, land use changes, and land water storage are not sufficiently represented. Advanced land water storage models such as the Global Land Data Assimilation System (GLDAS) account for hydrological feedbacks in detail and provide high-resolution water storage predictions. Empirical models for ice sheets and glaciers based on recent observations are likely to provide better results than physical models, which have not reached a high degree of predictive capabilities. Similarly, separate sea ice models forced by climate model output might get the best modeling of the sea ice extent. Considering these diverse state-of-the-art-models, it is of advantage to develop the modular model depicted in Fig. 4 as an extendable and scalable framework, in which the individual modules successively can be improved and couplings can be added as they are better understood. By allowing for maximum usage of all available information, with some processes better constrained by observations and models and other processes less constrained, the modular approach provides the basis for assessing in detail the uncertainties, including their spatial variability.

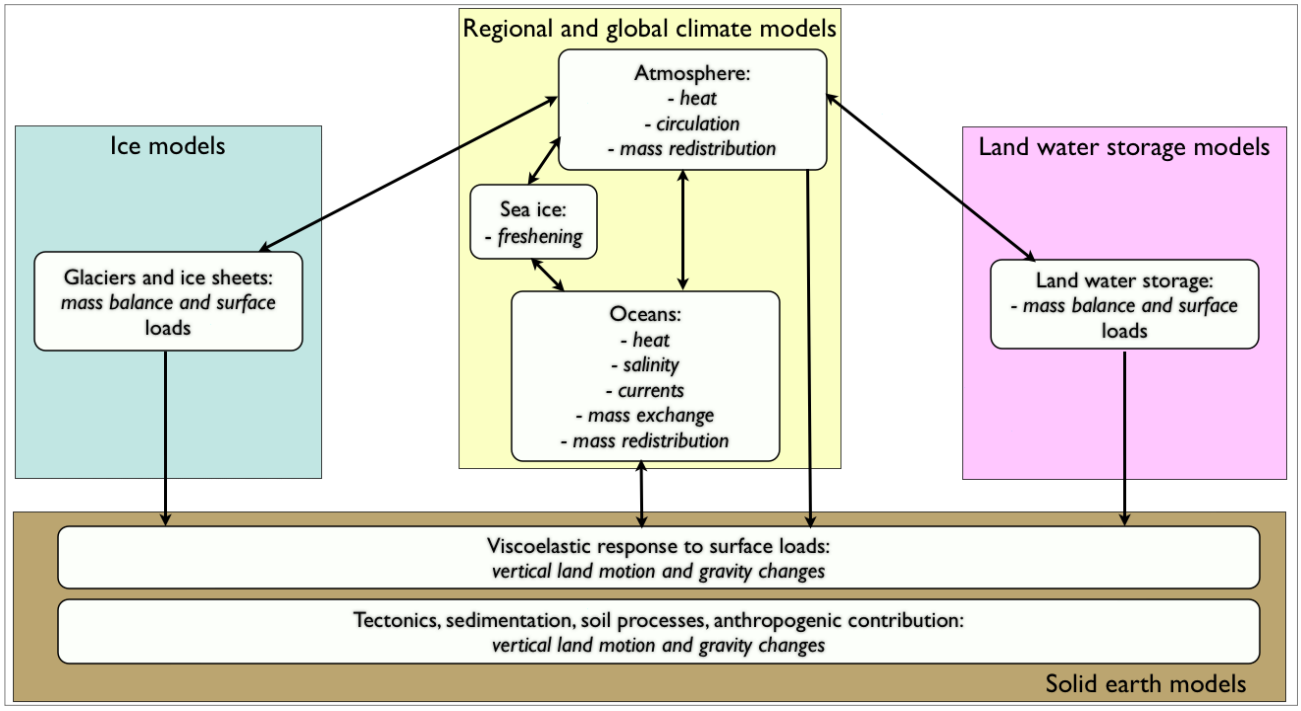

Fig. 4 Structure of the modular LSL modeling framework. The upper three boxes are modules representing the fluid envelope of the solid Earth. Mass exchanges of the ocean with land ice and land water storage represent the main mass fluxes. Heat exchange with the atmosphere contributes to steric changes of the ocean and impacts currents. Mass redistribution in the fluid envelope loads the solid Earth and leads to mass redistribution in the ocean. The arrows represent couplings between the modules including mass fluxes, heat exchange, surface forces, and gravitational forces.

5. Discussion

A scalable modular Earth system modeling framework for LSL changes can be used to study the predictability of LSL on intraseasonal to interdecadal time scales. Continuous observations of key components of the Earth system (*e.g.*, the ice sheets, ice caps and major glaciers, ocean currents, ocean temperature, land water storage, sea surface height changes, vertical land motion) and a combination of global and regional system models that assimilate these observations provide a basis for forecasts of short-term (years) and intermediate (decades) LSL changes. This system modeling framework is currently under implementation. Modules of the system modeling framework will include (1) global models (atmosphere and oceans, ice sheets, glaciers, continental hydrosphere), (2) regional models for steric effects, (3) local models for vertical land motion, and (4) physical models to convert global processes into local effects. The modular system model will provide a framework for data assimilation and model integration. In order to improve

predictive capabilities, assimilation of observations on global to regional scales (*e.g.*, gravity field, Earth rotation, sea surface heights) will constrain models, while regional and local observations (*e.g.*, InSAR, GNSS, ground observations) will inform specific processes. The system model ensures global consistency for key Earth system variables, including mass and momentum conservation. The modular nature of the system enables rapid integration of progress made in any of the modules by the project team or by other groups working on relevant models.

The seasonal to decadal LSL variability (see Section1) observed by satellite altimetry for more than two decades and by tide gauges for more than 50 years can be used to assess the predictive capabilities of models for the processes that force these LSL variations. There is considerable uncertainty in the relative contribution of the various processes that cause the spatial variability at interannual to decadal time scales and the extent to which models have predictive capabilities for this variability.

The modules of the system modeling framework will be validated by comparing hindcast predictions of LSL changes with observations from 1950 to present. Special attention will be given to the increasing level of significance of processes, such as ice dynamics, that have become important now but were less active in the past. The validation will be set up such that it supports a full assessment of the predictive capabilities of individual modules as well as the integrated system, and provides quantified uncertainties. This will provide feedback on the predictive capabilities of individual modules, including global to regional climate models.

References

Atkinson, L. P., T. Ezer, and E. Smith, 2013: Sea level rise and flooding risk in Virginia. *Sea Grant Law and Policy Journal*, **5**, 3--14.

Bamber, J. L., R. E. M. Riva, B. L. A.Vermeersen, and A. M. LeBrocq, 2009: Reassessment of the potential sea-level rise from a collapse of the West Antarctic ice sheet. *Science*, **324**, 901-903, doi: 10.1126/science.1169335.

Chambers, D., J. Famiglietti, I. Velicogna, and R. S. Nerem, 2009: The global water cycle 2003-2008: Implications for long-period sea level change. *Geophys. Res. Abstracts*, **11**, EGU2009-10107.

Church, J., T. Aarup, P. Woodworth, W. Wilson, R. Nicholls, R. Rayner, K. Lambeck, G. Mitchum, K. Steffen, A. Cazenave, G. Blewitt, J. Mitrovica, and J. Lowe, 2010: Sea-level rise and variability: Synthesis and outlook for the future. *Understanding Sea-Level Rise and Variability*. J. Church, P. L. Woodworth, T. Aarup, S. Wilson, Eds., Wiley-Blackwell, 402-419.

Edwards, R., 2008: Sea levels: science and society, *Progress in Physical Geography*, **32**, 557--574.

Ezer, T., 2013: Sea level rise, spatially uneven and temporally unsteady: Why the U.S. East Coast, the global tide gauge record, and the global altimeter data show different trends. *Geophys. Res. Lett.*, **40**, 5439–5444, doi:10.1002/2013GL057952.

Ezer, T., L. P. Atkinson, W. B. Corlett, and J. L. Blanco, 2013: Gulf Stream's induced sea level rise and variability along the U.S. mid-Atlantic coast. *J. Geophys. Res. Oceans*, **118**, 685–697, doi:10.1002/jgrc.20091.

Farrell, W. E. and J.A. Clark, 1976: On postglacial sea level. *Geophys. J. R. Astron. Soc.*, **46**, 647--667.

Fasullo, J. T., C. Boening, F. W. Landerer, and R. S. Nerem, 2013: Australia's unique influence on global sea level in 2010–2011. *Geophys. Res. Lett.*, **40**, 4368—4373, doi: 10.1002/grl.50834.

Hallegatte, S., 2012: Economics: The rising costs of hurricanes. *Nature Clim. Change*, **2**, 148—149, doi: 10.1038/nclimate1427.

Hallegatte, S., C. Green, R. J. Nicholls, and J. Corfee-Morlot, 2013: Future flood losses in major coastal cities. *Nature Clim. Change*, **3**, 802-806, doi: 10.1038/nclimate1979.

Hansen, J., M. Sato, P. Kharecha, D. Beerling, V. Masson-Delmotte, M. M. Pagani, Raymo, D. L. Royer, J. C. Zachos, 2008: Target atmospheric CO2: Where should humanity aim? *The Open Atmospheric Science Journal*, **2**, 217-231.

Horton, B. P., S. Rahmstorf, S. E. Engelhart, and A. C. Kemp, 2014: Expert assessment of sea-level rise by ad 2100 and ad 2300. *Quaternary Science Reviews*, **84**, 1-6, doi: 10.1016/j.quascirev.2013.11.002.

Kendall, R. A., J. X. Mitrovica, and G. A. Milne, 2005: On post-glacial sea level - II. Numerical formulation and comparative results on spherically symmetric models. *Geophys. J. Int.*, **161**, 679--706.

Kopp, R. E., 2013: Does the mid-Atlantic United States sea level acceleration hot spot reflect ocean dynamic variability? *Geophys. Res. Lett.*, **40**, 3981–3985, doi:10.1002/grl.50781.

Lipscomb, W., R. Bindschadler, E. Bueller, D. Holland, J. Johnson, and S. Price, 2009: A community ice sheet model for sea level prediction. *Eos, Trans. Am. Geophys. Union*, **90**, 23.

Little, C. M., N. M.Urban, and M. Oppenheimer, 2013: Probabilistic framework for assessing the ice sheet contribution to sea level change. *Proc. Nat. Academy Sciences USA*, **110**, 3264--3269.

Marcott, S. A., J. D. Shakun, P. U. Clark, and A. C. Mix, 2013: A reconstruction of regional and global temperature for the past 11,300 years. *Science*, **339**, 1198-1201.

Meyssignac, B. and A. Cazenave, 2012: Sea level: A review of present-day and recent-past changes and variability. *J. Geodynamics*, **58**, 96–109.

Meyssignac, B., M. Becker, W. Llovel, and A. Cazenave, 2012: An assessment of two-dimensional past sea level reconstructions over 1950--2009 based on tide gauge data and different input sea level grids. *Surv. Geophys,* doi:10.1007/s10712—011--9171--x.

Milne, G. A., J. X. Mitrovica, and J. L. Davis, 1999: Near-field hydro-isostasy: the implementation of a revised sea-level equation. *Geophys. J. Int.*, **139**, 464--482.

Mitrovica, J. X. and G. A. Milne, 2003: On post-glacial sea level: I. General theory. *Geophys. J. Int.*, **154**, 253--267.

Mitrovica, J. X., N. Gomez, and P. U. Clark, 2009: The sea-level fingerprint of West Antarctic Collapse, *Science*, **323**, 753-756, doi: 10.1126/science.1166510.

Mitrovica, J. X., M. E. Tamisiea, J. L. Davis, and G. A. Milne, 2001: Recent mass balance of polar ice sheets inferred from patterns of global sea-level change. *Nature*, **409**, 1026--1028.

Mitrovica, J. X., M. E. Tamisiea, E. R. Ivins, L. L. A. Vermeersen, G. A. Milne, and K. Lambeck, 2010: Surface mass loading on a dynamic earth: Complexity and contamination in the geodetic analysis of global sea-level trends, *Understanding Sea-Level Rise and Variability*, J. Church, P. L. Woodworth, T. Aarup, and S. Wilson, Eds., Wiley-Blackwell, 285--325.

National Research Council, 2013: Abrupt impacts of climate change: Anticipating surprises. Washington, D.C., The National Academies Press.

Pfeffer, W. T., J. T. Harper, and S. O'Neel, 2008: Kinematic constraints on glacier contributions to 21st-century sea-level rise. *Science*, **321**, 1340-1343, doi: 10.1126/science.1159099.

Plag, H.-P., 2006: Recent relative sea level trends: an attempt to quantify the forcing factors. *Phil. Trans. Roy. Soc. London*, **A**, **364**, 1841--1869.

Plag, H.-P., and S. Jules-Plag, 2013: Sea-level rise and coastal ecosystems. *Vulnerability of Ecosystems to Climate*, R. A. Pielke Sr., T. Seastedt, and K. Suding, Eds., vol. **4** of Climate Vulnerability: Understanding and Addressing Threats to Essential Resources, Elsevier, 163-184.

Plag, H.-P. and H.-U. Juettner, 2001: Inversion of global tide gauge data for present-day ice load changes. *Proceedings Second Int. Symp. on Environmental Research in the Arctic and Fifth Ny-Alesund Scientific Seminar 23-25, February 2000, NIPR, Tokyo*, O. Watanabe, and T. Yamanouchi, Eds., Special Issue, No. 54, Memoirs of the National Institute of Polar Research, 301-317.

Plag, H.-P., J. Adegoke, M. Bruno, R. Christian, P. Digiacomo, L. McManus, R. Nicholls, and R. van de Wal, 2010: Observations as decision support for coastal management in response to local sea level changes. *Proceedings of OceanObs'09: Sustained Ocean Observations and Information for Society (Vol. 2)*, Venice, Italy, 21-25 September 2009, J. Hall, D. E. Harrison, and D. Stammer, Eds., ESA Publication WPP-306. doi:10.5270/OceanObs09.cwp.69.

Rowley, R. J., J. C. Kostelnick, D. Braaten, X. Li, and J. Meisel, 2007: Risk of rising sea level to population and land area, *Eos, Trans. Am. Geophys. Union*, **88**, 105, 107.

Sallenger, A. H., K. S. Doran, and P. A. Howd, 2012: Hotspot of accelerated sea-level rise on the Atlantic coast of North America, *Nature Climate Change*, **2**, 884–888, doi:10.1038/nclimate1597.

Showstack, R., 2013: Concern about abrupt climate changes prompts call for early warning system. *EOS, Trans. Am. Geophys. Union*, **94**, 498-499, doi: 10.1002/2013EO510003.

Velicogna, I. and J. Wahr, 2005: Greenland mass balance from GRACE, *Geophys. Res. Lett.*, **32**, L18505, doi:10.1029/2005GL023955.

Velicogna, I. and J. Wahr, 2006: Measurements of time-variable gravity show mass loss in Antarctica. *Science*, **311**, 1754-1756.

Science and Technology Infusion Climate Bulletin
NOAA's National Weather Service
38th NOAA Annual Climate Diagnostics and Prediction Workshop
College Park, MD, 21-24 October 2013

Analysis of Oceanic Precipitation before the Satellite Era

Thomas M. Smith[1, 2], Phillip A. Arkin[2], and Li Ren[1]

[1]*Cooperative Research Program, NOAA/NESDIS/STAR*

[2] *Earth System Science Interdisciplinary Center / Cooperative Institute for Climate and Satellites-Maryland*

1. Introduction

Satellite-based analyses are critical for climate analyses because of their ability to sample globally with much higher frequency than is possible using in situ observations. The satellite measurements most important for long records of global precipitation include those from infrared and microwave instruments. The Global Precipitation Climatology Project (GPCP, Adler *et al.* 2003) combines bias-adjusted satellite-precipitation estimates with the available in situ measurements to produce a monthly global analysis beginning 1979. Before 1979 satellite data are not adequate for quantitative global analysis and here we refer to 1979 as the beginning of the satellite era.

Before the satellite era there were many island and land in situ precipitation measurements, allowing for a fairly comprehensive land analysis back to 1900 or earlier. However, there are almost no oceanic precipitation measurements for that period. Oceanic precipitation is a critical component of the Earth's hydrologic cycle because the oceans cover roughly 70% of the surface and because oceanic variations influence those over land. A better understanding of oceanic precipitation for a period longer than the satellite era would improve understanding of global climate variations, including the influence of global temperature changes on precipitation.

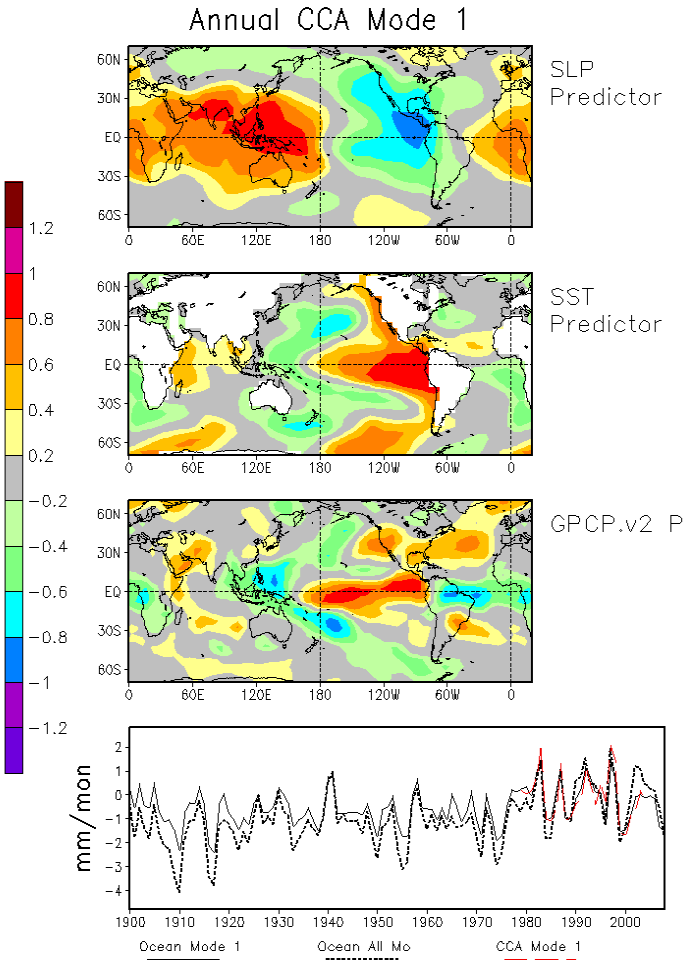

Fig. 1 First CCA spatial predictor and GPCP predictand spatial pattern (upper 3 panels) and the CCA and reconstruction time series for ocean areas for the 1st and all 8 CCA modes used (lower panel).

Reconstructions of global precipitation have been developed. Reconstructions are extended analyses of relatively sparse data using statistics produced using data from a shorter but densely-sampled period. The GPCP data provide roughly 30 years of data that have been used to analyze global precipitation beginning 1900. A series of reconstructions were produced by the authors, with knowledge gained from each used to improve subsequent reconstructions (Smith *et al.* 2008, 2009, 2010, 2012). Here we give a summary of some aspects of the ocean-area precipitation analysis and how reliable it is in the pre-satellite period.

Correspondence to: Thomas M. Smith, NOAA/STAR/SCSB and CICS/ESSIC University of Maryland, 5825 University Research Court, Suite 4001, College Park, MD 20740; E-mail: tom.smith@noaa.gov.

2. Results

The most recent reconstruction method begins with a canonical correlation analysis (CCA) to estimate annual precipitation anomalies from annual SST and SLP predictors. That step was found to better represent annual large-scale oceanic variations. The first CCA mode shows that much of the variance from this analysis is ENSO like, but including additional modes enhances multi-decadal variations in the ocean-area CCA (Fig. 1). Ocean area CCA output is combined with annual gauge anomalies and used to estimate annual global anomalies by fitting those data to a set of spatial modes.

The spatial modes used to combine annual CCA and gauge data are annual Empirical Orthogonal Function (EOF) covariance modes. Modes not adequately sampled would be removed, although including CCA data means that under-sampling of modes never occurs. As an example, the first (main ENSO) annual mode is shown along with the time series from GPCP, from GHCN gauges alone, and from combined gauge and CCA inputs (Fig. 2). Note that most of this mode's variations can be reconstructed for the historical period using either gauges alone or gauges combined with CCA output, although the multi-decadal signal is a little stronger when CCA output are included.

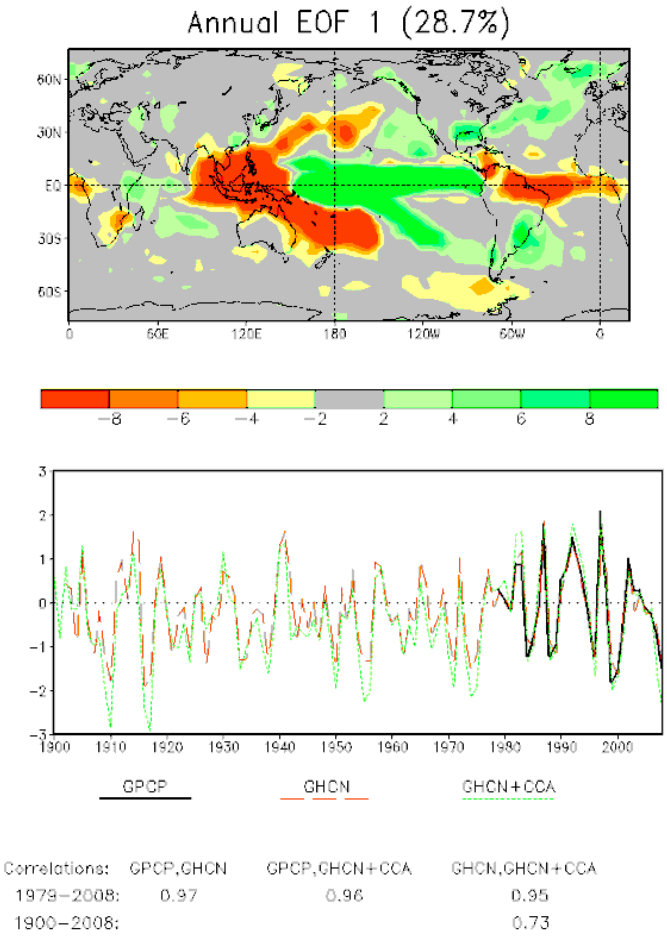

Fig. 2 First covariance EOF of GPCP annual anomalies and the time series from GPCP along with reconstructed time series for gauges alone (GHCN) and gauges + CCA over ocean areas. Correlations for the time series are also given.

The annual estimate is adjusted by analyzing monthly anomaly increments from the annual average. For this step we use gauge monthly anomaly increments and a set of monthly increment spatial modes. The sum of annual and monthly increments defines the monthly reconstruction. In some versions the monthly gauge anomalies are statistically re-injected to reduce differences from gauges in regions where gauges are available.

Cross-validation analyses are used to help show the reliability of the analysis in historical periods. For these test analyses the GPCP data are analyzed using the reconstruction method. Data for the analysis year are removed for computing statistics and data are subsampled using historical sampling masks. Comparisons to the full GPCP give an indication of reliability. An additional test of the reconstruction reliability is the reconstruction of model output from a reanalysis model that incorporates observed SST and SLP. Results from both of these tests show that the reconstruction is capable of resolving large scale oceanic variations on interannual and longer time scales, but it is less reliable for small regions and shorter time scales.

Global-average results were compared to CMIP5 coupled model output by Ren *et al.* (2013). Although there is a lot of spread among the various models, the global model mean is similar to the reconstruction (Fig. 3). The reconstruction is more variable than the model mean since interannual variations are filtered out of the mean. Over the oceans both the model mean and reconstruction indicate a gradual increase until about 1960, followed by a flat or slight decrease period until about 1980, followed by an increasing global averages.

Disclaimer. The contents of this presentation are solely the opinions of the authors and do not constitute a statement of policy, decision, or position on behalf of NOAA or the U.S. Government.

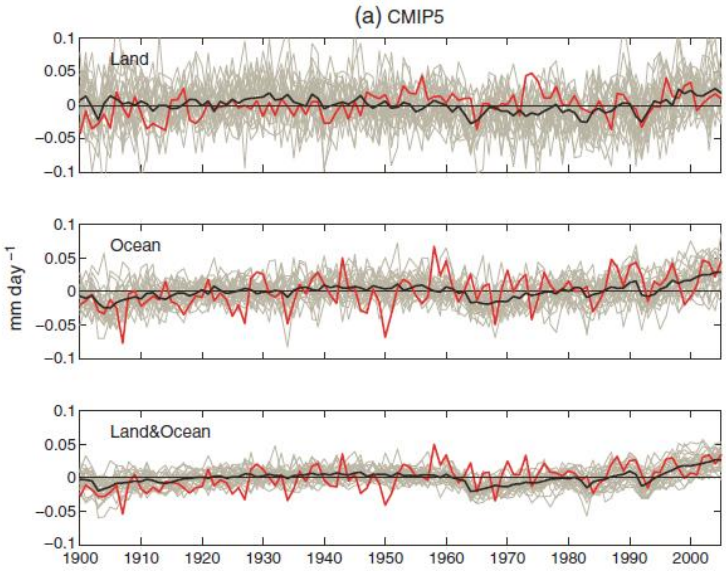

Fig. 3 Global averages over land, oceans and all areas from CMIP5 coupled-model precipitation (grey lines), the model mean (thick black line) and reconstruction (thick red line).

References

Adler, R.F., G.J. Huffman, A. Chang, R. Ferraro, P.-P. Xie, J. Janowiak, B. Rudolf, U. Schneider, S. Curtis, D. Bolvin, A. Gruber, J. Susskind, P. Arkin, and E. Nelkin, 2003: The version-2 Global Precipitation Climatology Project (GPCP) monthly precipitation analysis (1979-presient), *J. Hydromet.*, **4**, 1147-1167.

Ren, L., P.A. Arkin, T.M. Smith, and S.S.P. Shen, 2013: Global precipitation trends in 1900-2005 from a reconstruction and coupled model simulations. *J. Geophys. Res.*, **118**, 1-11, doi:10.1002/jgrd.50212.

Smith, T. M., M. R. P. Sapiano, and P. A. Arkin, 2008: Historical Reconstruction of Monthly Oceanic Precipitation (1900-2006), *J. Geophys. Res.*, **113**, D17115, doi:10.1029/2008JD009851.

Smith, T. M., P. A. Arkin, and M. R. P. Sapiano, 2009: Reconstruction of near-global annual precipitation using correlations with sea surface temperature and sea level pressure. *J. Geophys. Res.*, **114**, D12107, doi:10.1029/2008JD011580.

Smith, T.M., P.A. Arkin, M.R.P. Sapiano, C.-Y. Chang, 2010: Merged statistical analyses of historical monthly precipitation anomalies beginning 1900. *J. Climate*, **23**, 5755-5770.

Smith, T.M., P.A. Arkin, L. Ren, and S.S.P. Shen, 2012: Improved reconstruction of global precipitation since 1900. *J. Atmos. Ocean Tech.*, **29**, 1505-1517.

Science and Technology Infusion Climate Bulletin
NOAA's National Weather Service
38th NOAA Annual Climate Diagnostics and Prediction Workshop
College Park, MD, 21-24 October 2013

Hydrologic and Climatologic Conditions that Shape Groundwater Resources in Utah and the Great Basin

Kirsti A. Hakala[1], Shih-Yu Wang[1, 2], and Jin-Ho Yoon[3]

[1]*Department of Plants, Soils, and Climate, Utah State University, Logan, UT*
[2]*Utah Climate Center, Utah State University, Logan, UT*
[3]*Pacific Northwest National Laboratory, Richland, WA*

1. Introduction

In Utah, the declining trend of groundwater levels, combined with the rapid growth of urban population and water withdrawal, are already a cause for concern for water planners throughout the state. Previous research has identified a significant link between the region's hydroclimate to Pacific Ocean sea surface temperature anomalies (SSTA). Using this link, from which the SSTA impact extends to groundwater, we use the Community Earth System Model (CESM) to diagnose and predict groundwater levels for potential future climate scenarios. The CESM performs well in replicating both the seasonal cycle and the quasi-decadal oscillation (QDO) teleconnection (Wang *et al.* 2011) for Utah's groundwater level variations. In addition, the CESM was chosen for a focused analysis, as groundwater is not a standard output from the Coupled Model Intercomparison Project Phase 5 (CMIP5). Building upon such model capability, this study analyzes the effects of greenhouse gas (GHG) on groundwater level change. The results indicate a troubling future for groundwater over the Great Basin and Utah in particular.

2. Data/methodology

Groundwater levels over northern Utah were recorded using 400 active wells that were obtained from the

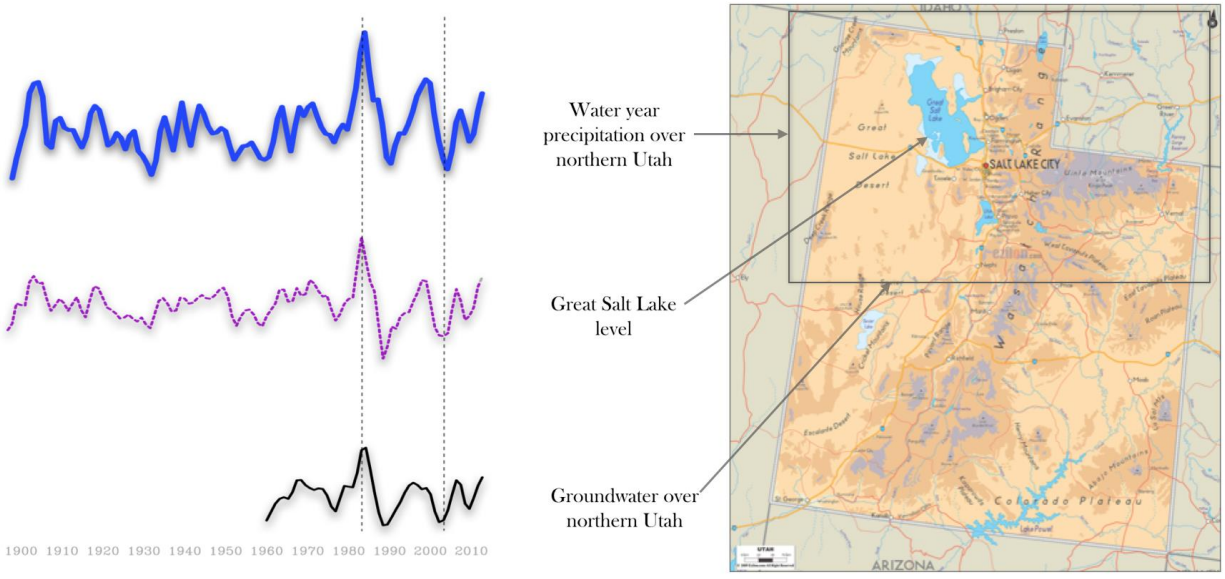

Fig. 1 Observed precipitation, plotted on top, oscillates in tandem with GSL level (tendency) and northern Utah groundwater (tendency). Dashed lines were provided to highlight the consistency in oscillations. A map of Utah is provided to the top with arrows designating the location of the GSL and the region of northern Utah.

Correspondence to: Kirsti Hakala, Department of Plants, Soils, and Climate, Utah State University, 4820 Old Main Hill, Logan, UT 84322-4820; Email: kirsti.hakala2@gmail.com.

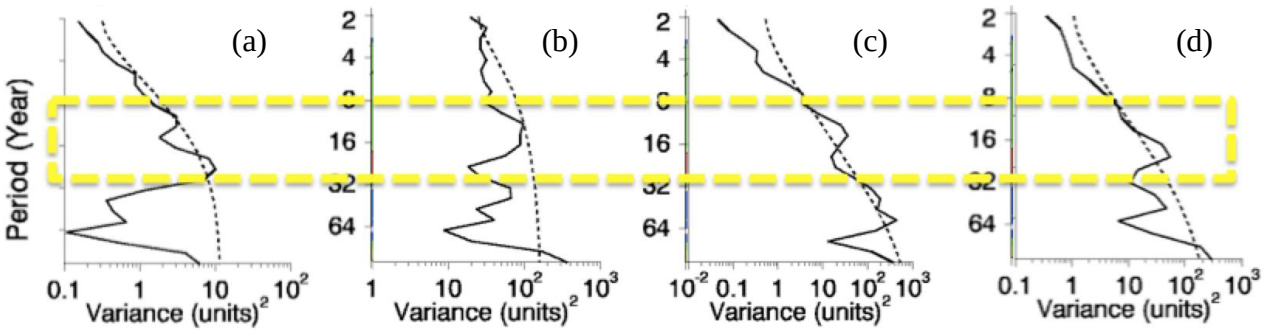

Fig. 2 Wavelet spectral analysis was performed on (a) modeled groundwater, (b) modeled precipitation, (c) observed GSL, and (d) observed groundwater. A prominent spike can be seen at the 10-15 year frequency throughout all datasets. This strong coherence throughout all datasets exemplifies the CESM's ability to replicate the predominant climate oscillations in the region.

United States Geological Survey (USGS) Active Groundwater Level Network[1, 2], with data since 1960. These wells are measured at least once within the past 13 months, primarily during the spring. Springtime groundwater levels were standardized prior to averaging among the 400 wells. Other datasets include: station-derived, monthly Global Precipitation Climatology Centre (GPCC) dataset at a 1° horizontal resolution (Schneider *et al.* 2013); the Great Salt Lake (GSL) surface elevation[3]. Outputs from the CESM version 1 were generated by the Pacific Northwest National Laboratory (PNNL) at a resolution of 2.5° long. × 1.875° lat. The CESM was chosen for its noted ability to simulate the ENSO evolution and precursors. We used the Historical Experiments of the CESM that were initialized at 1850 under preindustrial conditions and added with external forcings of aerosol, GHG, and natural – volcanic eruptions and solar cycle.

3. Results

The average groundwater level over northern Utah exhibits variability that fluctuates at a quasi-decadal frequency. In order to understand the hydrological forcing that leads to the observed periodicity of groundwater levels, we plotted observed precipitation alongside the tendency of the GSL level (*i.e.* current year minus the previous year) and the tendency of groundwater level over northern Utah, shown in Figure 1. It is noted that fluctuations in the precipitation are in good agreement with the tendency of GSL level and groundwater. Figure 1 also shows a pronounced quasi-decadal frequency within all observed data sets (10-15 year time period). This variability in precipitation, reflected by the alternating dry and wet spells, is particularly pronounced after the 1960s. The pervading quasi-decadal variability shown in all observational data suggests a potential for decadal climate prediction.

The unique timescale of 10-15 years, observed in the datasets discussed above, echoes an emerging Pacific climate mode – the Quasi-Decadal Oscillation (QDO) – described in a growing number of articles focusing on low-frequency variability in the Pacific SST (*e.g.* Allan 2000; Tourre *et al.* 2001; White and Tourre 2003; White and Liu 2008; Wang *et al.* 2011). The Pacific QDO alternates between warm/cool status in the central equatorial Pacific near the NINO4 region (160°E-150°W, 5°S-5°N), and features distinctive phases in atmospheric circulation perturbations.

The CESM output of groundwater levels and precipitation are analyzed next; the CESM appears to replicate the QDO, as is shown in the wavelet spectral analysis in Figure 2. Results show a strong coherence between CESM output and observational data, which alludes to the model's ability to pick up the predominant climate oscillations in the region. CESM model years cannot be directly compared to observational years, and thus wavelet spectral analysis provides an insightful way to diagnose the model.

[1] Utah Water Science Center of the USGS, Active Groundwater Level Network, 1930-present. http://ut.water.usgs.gov/ (July 28, 2012).
[2] http://groundwaterwatch.usgs.gov/default.asp
[3] http://waterdata.usgs.gov/nwis

Building upon the CESM's noted ability to replicate the QDO and teleconnection patterns, we then analyzed modeled groundwater, from 1850 to 2005, with the ensemble historical runs shown in Figure 3. CESM runs for greenhouse gas forcing (GHG), aerosol (AERO), natural (NAT) and all forcing (ALL) were compared to identify each forcing's effects on groundwater. Each CESM ensemble is comprised of two members with the exception of the ALL ensemble, which consists of four members. Results show the effect of NAT, AERO and ALL forcing is oscillatory with the last half a century showing a steady increase in groundwater. In contrast, the effect of GHG on groundwater shows a persistent drying tendency throughout the last 80 years. This suggests that the system may initially be able to cope with an influx of GHG up to a point, but resilience is limited and groundwater will eventually be depleted by continued increases in GHG.

Figure 3 shows CESM historical groundwater in two separate time periods: (a) 1960-2005 and (b) 1850-2005. The overall drying effect of GHG can be seen by the steady decrease in groundwater in both plots. It can be seen in Figure 3b that around 1928, GHG has destabilized the hydro-climatic system and groundwater decreases steadily thereafter. For future scenarios, we then utilized CESM's representative concentration pathways (RCP) simulations to depict the outcome of groundwater behavior. The RCP simulations begin in year 2006 and projections are carried out to year 2100. RCP simulations are initialized with new levels of CO2 and therefore do not directly carry over from any particular historical run. RCP4.5 represents a specific concentration of CO2 in the atmosphere defined as stabilization without overshoot pathway to 4.5 W/m2 (~650 ppm CO2), reaching stabilization after year 2100. RCP8.5 represents a higher concentration of CO2, defined as rising radiative forcing pathway leading to 8.5 W/m2 (~130 ppm CO2) by year 2100. Figure 4 shows the ensemble run of RCP4.5 and RCP8.5, each consisting of two members, for groundwater. Results show that the higher levels of CO2 in RCP8.5 cause a greater decrease in groundwater level over time, resulting in an

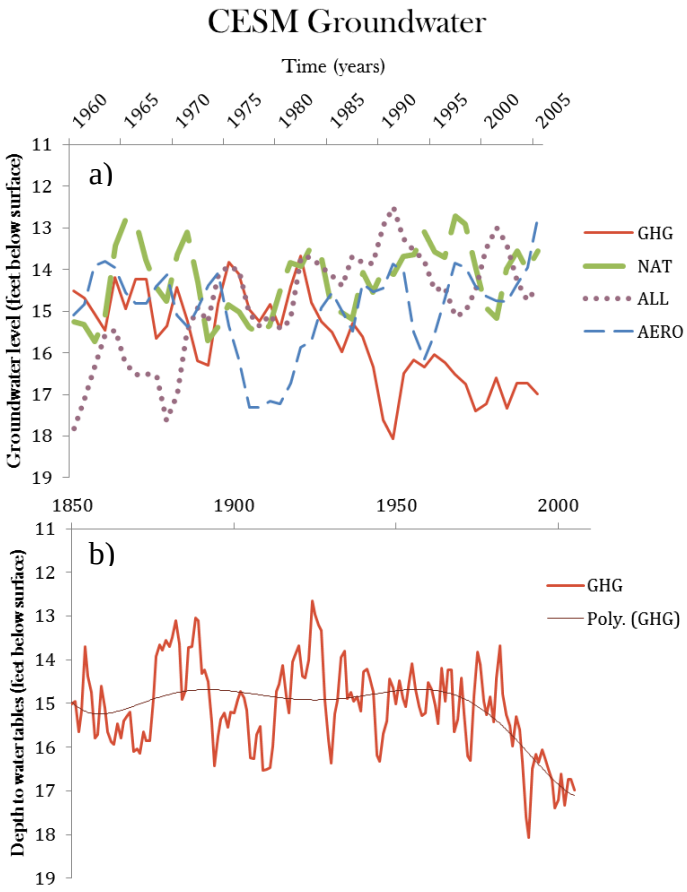

Fig.3 a) CESM historical groundwater is plotted above from 1960-2005. The plot shows the ensemble runs for GHG, NAT, ALL, and AERO forcing. Each ensemble run is the average of two members, with the exception of ALL forcing, which has four members. b) CESM groundwater is plotted above from 1850-2005. This plot isolates the ensemble run for GHG for the longer time period so as to highlight the decreasing trend in groundwater that begins in the late 1920's.

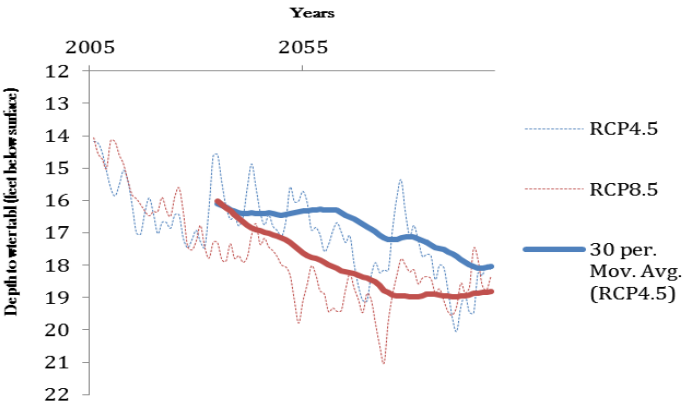

Fig.4 CESM – RCP ensemble 4.5 (blue) and RCP ensemble 8.5 (red) of groundwater are depicted above. Each ensemble is the average of two members.

approximate five-foot drop in groundwater level by year 2100. RCP4.5 also shows a decreasing trend in groundwater level, with an approximate one-foot difference between the two simulations by year 2100.

4. Concluding remarks

In Utah, groundwater is the source of 58 percent of public supply use and is a vital contributor for irrigation when surface water resources are depleted late in the growing season. According to the USGS Annual Groundwater Conditions Report for 2013 (Burden *et al.* 2013), the total estimated withdrawal of water from wells in Utah during 2012 has increased about 215,000 acre-feet from 2011 usage and 145,000 acre-feet more than the 2002-2011 average annual withdrawal. This increase in withdrawal resulted mostly from increased irrigation and public-supply use. As discussed in this paper, groundwater resources in Utah and the Great Basin are already susceptible to depletion by the effects of GHG. This issue is then exacerbated by the increasing trend in water withdrawal for irrigational and public-supply purposes. Therefore, research on the predictive nature of groundwater resources is vitally important and the increase of GHG in the atmosphere can have a direct influence on this drought-prone region. This research hopes to pave the way for the utilization of long-term prediction of groundwater and strives to inspire the need for better water management in light of the changing climate.

References

Allan, R., 2000: ENSO and climatic variability in the last 150 years. *El Niño and the Southern Oscillation: Multiscale Variability, Global and Regional Impacts*, H. F. Diaz, and V. Markgrav, Eds., Cambridge Univ. Press, 3–56.

Burden, C. B, and Co-authors, 2013: Groundwater conditions in Utah, spring of 2013. Cooperative Investigations Report No. 54, Utah Department of Natural Resources, 132 pp. http://ut.water.usgs.gov/publications/GW2013.pdf

Schneider, U., A. Becker, P. Finger, A. Meyer-Christoffer, M. Ziese, and B. Rudolf, 2013: GPCC's new land surface precipitation climatology based on quality-controlled in situ data and its role in quantifying the global water cycle. *Theoretical and Applied Climatology*, **115**, 1-26.

Tourre, Y., B. Rajagopalan, Y. Kushnir, M. Barlow, and W. White, 2001: Patterns of coherent decadal and interdecadal climate signals in the Pacific Basin during the 20th century. *Geophys. Res. Lett.*, **28**, 2069-2072.

Wang, S.-Y., and R. R. Gillies, L.E. Hipps, and J.Jin, 2011: A transition-phase teleconnection of the Pacific quasi-decadal oscillation. *Clim Dyn.*, **36**, 681-693.

White, W. B., and Y. M. Tourre, 2003: Global SST/SLP waves during the 20th century. *Geophys. Res. Lett.*, **30**, 53-51 - 53-54.

White, W. B., and Z. Liu, 2008: Resonant excitation of the quasi-decadal oscillation by the 11-year signal in the Sun's irradiance. *J. Geophys. Res.*, **113**, 1-16.

Science and Technology Infusion Climate Bulletin
NOAA's National Weather Service
38th NOAA Annual Climate Diagnostics and Prediction Workshop
College Park, MD, 21-24 October 2013

Observed Linkages between the Northern Annular Mode/North Atlantic Oscillation, Cloud Incidence, and Cloud Radiative Forcing

Marina Timofeyeva, Barbara Mayes Boustead, Victor Murphy, and Fiona Horsfall
NOAA's National Weather Service

Annette Hollingshead
Innovim, LLC, Greenbelt, MD

1. Why decision support services?

The National Oceanic and Atmospheric Administration (NOAA) Next Generation Strategic Plan (2010)[1] identified four societal challenges that have been translated into NOAA long-term goals:

- Climate Adaptation and Mitigation – An informed society anticipates and responds to climate and its impacts.
- Weather-Ready Nation – Society is prepared for and responds to weather-related events.
- Healthy Oceans – Marine fisheries, habitats, and biodiversity are sustained within healthy and productive ecosystems.
- Resilient Coastal Communities and Economies – Coastal and Great Lakes communities are environmentally and economically sustainable.

Although climate is a cross-cutting theme in all four societal challenges, the first two most directly address developing NOAA climate information and products that are usable for decision support. For example, NOAA's National Weather Service (NWS) Strategic Plan (2011)[2] states a goal on enhancing climate service as a part of the Weather-Ready Nation goal. Becoming a Weather-Ready and Climate-Smart Nation implies building community resilience to extreme weather and long-term changes. The critical issue in achieving this goal is a need to move from serving products to serving decision support, i.e. to provide what people really need.

2. Climate-weather linkages

The centerpiece of decision support services includes advancing preparedness and planning for extreme weather and water events that can be achieved through understanding and effective use of information on weather-climate linkages. Climate variability and change often "drive" weather and water events. For example, El Niño/Southern Oscillation impacts temperature and precipitation in many parts of United States. Global climate change impacts the local climate with a recognizable seasonal and spatial variability (Livezey *et al*., 2007). Understanding local climate drivers of weather and water events as well as ability to incorporate this information in weather forecasting process at local level are critical for developing decision support services.

3. Partnership

Developing background scientific methods for decision support service relies on NWS partnership with NOAA climate research offices, academia, and other partners in climate services such as state climatologists, who may represent either state university or state government institutions. NWS draws on the available scientific expertise and data for understanding climate variability and change impacts on local and regional weather and water elements. Delivery of decision support service depends on extensive network of partners

[1] NOAA Next Generation Strategic Plan 2010. http://www.ppi.noaa.gov/ngsp/
[2] NOAA's NWS Strategic Plan 2011. http://www.nws.noaa.gov/sp/

Correspondence to: Marina Timofeyeva, NOAA's National Weather Service, 1325 East-West Hwy, SSMC2 Room 13344, Silver Spring, MD 20910; E-mail: marina.timofeyeva@noaa.gov.

representing local government, emergency managers, natural resources oversight organizations and local communities.

4. Local Climate Analysis Tool (LCAT)

The new Local Climate Analysis Tool (LCAT, Figure 1), introduced in NWS operations in July 2013, highlights the effort to increase effectiveness of climate-related decision support service development and delivery. LCAT provides the most scientifically sound method and data for application in local climate studies. LCAT allows a user to answer questions like: Is the local temperature changing in my town, and how fast does the change occur? What is the relationship between El Niño/Southern Oscillation and precipitation in my town? Does the behavior of drought spell change over time? LCAT is linked from the NOAA climate portal (http://www.climate.gov) or directly at http://nws.weather.gov/lcat/. LCAT can be used for environmental applications, community planning, event preparedness, and natural resource management decisions.

Fig. 1 Functions and features of Local Climate Analysis Tool.

5. Second generation of NWS version of Automated Climate Information System (xmACIS)

The second generation of NWS version of Automated Climate Information System (xmACIS2) has been released in May 2013. The xmACIS2 interface provides near real-time mining of climate data records from the NWS weather observation system, as archived by NOAA National Climate Data Center, and is enhanced with data mining capabilities by the Northeast Regional Climate Center. Compared to the previous version, xmACIS2 includes additional features for multiple station data mining, a larger suite of climate statistics, and new data selection and reporting options. NOAA internal users can access xmACIS2 at http://xmacis.rcc-acis.org/. The public can access xmACIS data information either by using NOAA Online Weather Data (NOWData, Figure 2) at http://www.nws.noaa.gov or by contacting a climate focal point in their local NWS Weather Forecast Office.

6. User support

To enhance climate information application, the NWS tools are enhanced with training modules, consisting of help documentation and dynamic interpretation statements. For example, the LCAT Learn section consists of eleven online audio-visual tutorials covering an introduction to LCAT, background of LCAT data, scientific methodologies recommended for local climate studies, and LCAT applications in NWS climate services operations including decision support service. By developing support features for operational NWS uses, with explanations of the scientific background and best practices for methodology in local climate studies, LCAT enhances our ability to create linkages to climate information in decision support services.

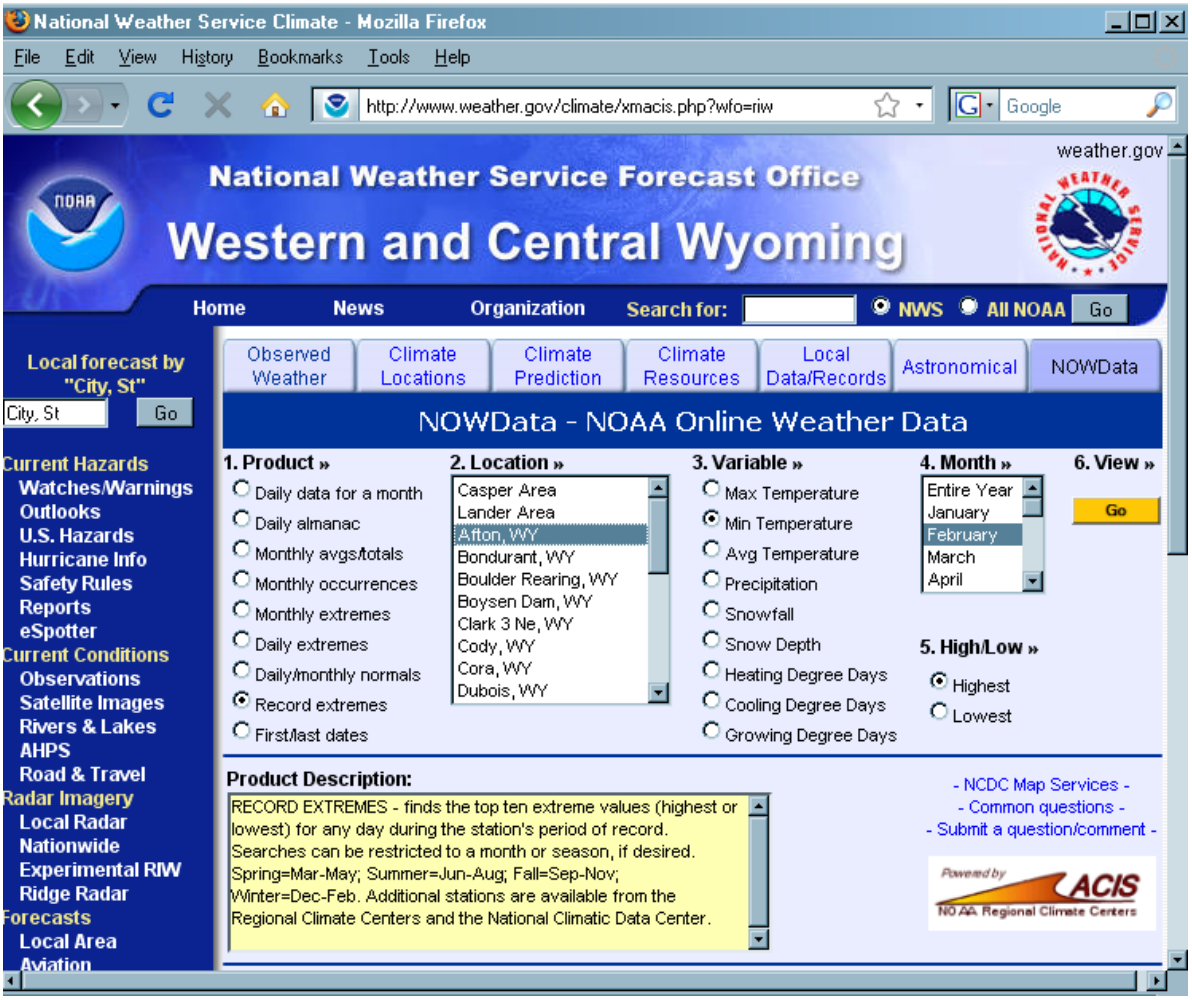

Fig. 2 NOWData features

References

Livezey, R.E., K.Y. Vinnikov, M.M. Timofeyeva, R. Tinker, and H.M. van den Dool, 2007. Estimation and Extrapolation of Climate Normals and Climatic Trends. Journal of Applied Meteorology and Climatology, Vol 46, pp. 1759-1776.

Science and Technology Infusion Climate Bulletin
NOAA's National Weather Service
38th NOAA Annual Climate Diagnostics and Prediction Workshop
College Park, MD, 21-24 October 2013

Jaziku - Statistical Inference Software for the Teleconnections Analysis

Corredor Llano X., and Sánchez Rodríguez I. C.

Institute of Hydrology, Meteorology and Environmental Studies (IDEAM), Bogotá, Colombia

1. Introduction

In geographical terms, Colombia is within the Torrid Zone[1], this means that the temperature decreases with altitude and by the presence of the training Andes mountains, Colombia has a variety of climates. According to Snow J. W. (1976), Colombia "is an island in the middle of three oceans", the author refers to that besides the influence of the Pacific and Caribbean oceans, Colombia receives moisture from the Amazon basin. In the Colombian territory the trade winds converge from north-east and south-east and from the convergence of the trade winds is made a belt of low pressure known as the Intertropical Confluence Zone (ITCZ), which causes large upswings that favor the formation of clouds, causing abundant rainfall. The meridional oscillation of the ITCZ which results in the annual cycle of surface temperatures as a result of insolation effect is the most important physical mechanism to explain the annual cycle of rainfall in Colombia.

However, multiple studies have shown the influence of several phenomena of climate variability in the climate of Colombia (Montealegre 2009) and taking into account that in recent years, multiple studies has reported an increase in the frequency and intensity of these phenomena with the extreme categories, are increasingly the sectors, communities and regions vulnerable to these changes. Consequently it's required to have better and adapted tools, for forecasting changes in the climate of our country and thus help in making decisions for the prevention.

Therefore, currently the seasonal rainfall forecast turns out to be an important item in the planning of the different social and economic sectors of Colombia. As part of the products of working group "Weather and Climate" of the Meteorology branch of the IDEAM (Institute of Hydrology, Meteorology and Environmental Studies - Colombia), is used the composite analysis methodology proposed by National Oceanic and Atmospheric Administration (NOAA)[2], facilitated by Jaziku software.

2. Jaziku

There are multiple methods that can be used for seasonal forecast (such as results of dynamic models, statistical models, *etc.*) and among these, there is a statistic methodology proposed in the article "Creating a Local Climate Product Using Composite Analysis" (by NOAA[2]), this is based in composite analysis. In the original proposal of this methodology are used spread sheets that make this process to be tedious, with possible human errors and impractical for robust studies with many time series, which also produced human errors in the process. Jaziku born as a tool to systematize this process and as the need for own tool and adapted software for own needs but with the advantage of being a free and open source software and therefore can be improved and adapted for different purposes, for example, could be corrected, improved, adapted and implemented by anyone, institutions or weather service.

The Jaziku software was designed to find relationships through composite analysis methodology between the time series of the dependent variables (observed meteorological variable) with the index that represents the phenomenon of climate variability (independent variables)[3].

---

[1] Geographic Universal Atlas and Colombia, Oceano Editorial, 1994. ISBN 847764782 8. Barcelona España. 100 pp.
[2] NOAA and UCAR. Creating a local climate product using composite analysis - Print version of webcast - (on line). 1997-2010:COMET Website at http://meted.ucar.edu/, 1997.
[3] Jaziku is statistical inference software for the teleconnections analysis, (version 0.6.1). (2013) IDEAM, Colombia. Jaziku is a free and open source software GPLv3. http://hg.ideam.gov.co:8000/meteorologia/jaziku/summary.

Correspondence to: Corredor Llano X., Institute of Hydrology, Meteorology and Environmental Studies (IDEAM), Bogotá, Colombia; Email: xcorredorl@unal.edu.co.

2.1 Modules

• Data analysis – homogeneity: Evaluates the trend of the series, outliers, multiyear climatology, and several statistics for the time series and presents the results of parametric tests of homogeneity analysis. Such results are for example: Test Mann-Whitney-Wilconxon, F-test or T-test. Respect to the descriptive statistics, are: sample size, minimum, mean, median, standard deviation, kurtosis, coefficient of variation and variance of the series[3].

• Climate: In "Jaziku - climate", the software produces the climatology of the behavior of the dependent variable under the phases associated with the phenomena represented by the independent variable. Generates a series of average values according to the chosen time resolution (Quarter, two months, month, 15days, 10days or 5 days) and generate contingency tables (NOAA and UCAR 1997), which become more probable scenarios of response the dependent variable under the categories (phases) of the phenomenon . Subsequent to the calculation of the most likely scenarios of variation of dependent variable in the module "Jaziku-Climate", the software uses the probability values of the phenomenon represented by the independent variable

• Forecast: In the forecast module is used the total probability theorem to calculate the probability that the dependent variable to be in any category. For these step are required the probabilistic predicted values for each of the categories of the independent variable (which in the case of ENSO are facilitated by physical and statistical models of IRI "International Research Institute for Climate and Society"[4]) and then is used the conditional probability taken of contingency tables (Wilks 1995).

2.2 Software development and program structure

Jaziku run and work only with one file in format csv called "runfile", this file is where are the settings of all options to run Jaziku (see Figure 1). The time series are of dependent an independent variable, are in plain text with the data organized chronologically. Jaziku runs in command line interface (CLI), is developed in Python language[5] with some libraries and software as support to make some statistical formulas (Scipy[6] and Numpy[7]), graphics (Matplotlib[8]), interpolation (HPGL[9]), maps (NCL[10]) and manipulate images (PIL[11]).

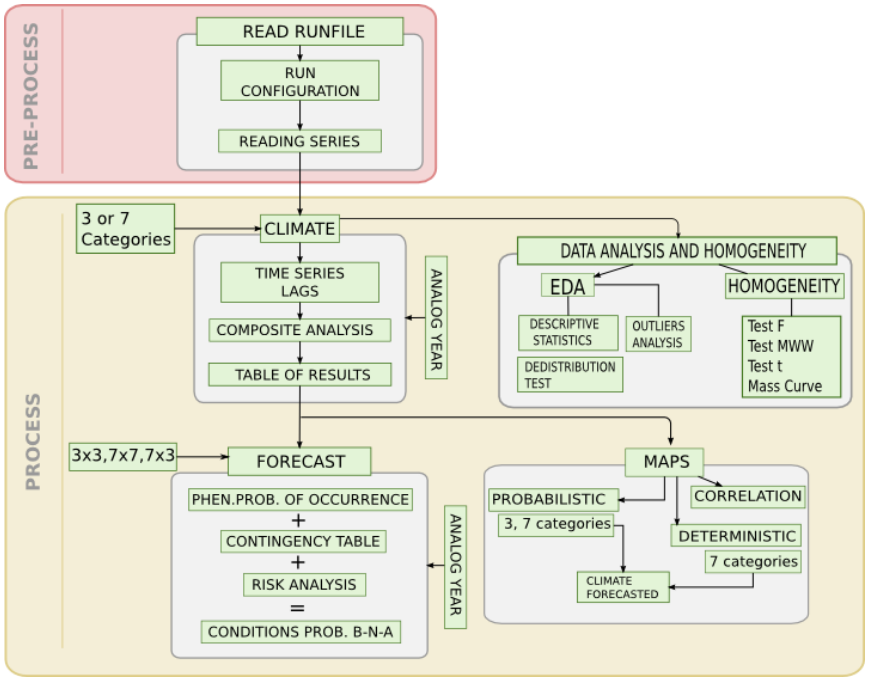

Fig. 1 General scheme of Jaziku run process.

[4] International Research Institute for Climate and Society.
url: http://iri.columbia.edu/climate/ENSO/currentinfo/QuickLook.html.
[5] Python Programming Language, Python Software Foundation, version 2.7. Available at http://www.python.org.
[6] Scipy, Open source scientific tools for Python, License: BSD-new, url: http://www.scipy.org
[7] Numpy, Fundamental package for scientific computing with Python, License: BSD-new, url: http://www.numpy.org.
[8] Matplotlib is a plotting library for Python. License: matplotlib-licence, url: http://matplotlib.org.
[9] HPGL stands for High Performance Geostatistics Library. License: BSD, url: http://hpgl.aoizora.org.
[10] NCL, NCAR Command Language, Copyright (C) 2013 University Corporation for Atmospheric Research. The use of this software is governed by a License Agreement. See http://www.ncl.ucar.edu/ for more details.
[11] PIL, Python Imaging Library, Alex Clark and Contributors, License: PIP-license,
url: http://pillow.readthedocs.org/en/latest/.

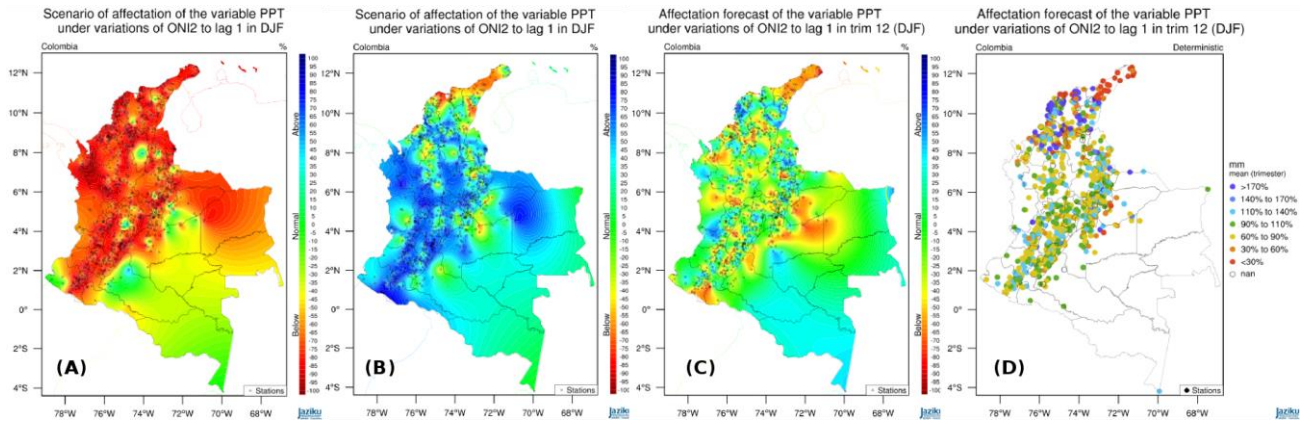

Fig. 2 These are some examples outputs of Jaziku, the first two graphs show the most likely scenarios of rainfall variation under El Niño (A) and La Niña (B) for Colombia. The following two graphs show the special forecast of precipitation for Colombia in the DJF trimester, probabilistic (C) and seven categories (D).

Jaziku is a free and open source software (GPLv3 license), and therefore can be improved and adapted for different purposes, for example, could be corrected, improved, adapted and implemented by anyone, institutions or weather service, but always preserving and respecting the copyright and software licensing agreements.

Jaziku started its development from 2011 and continues being developed. The actual version control system of code of Jaziku is: http:// hg.ideam.gov.co:8000/meteorologia/jaziku/summary. The actual mailing list is: https://groups.google.com/forum/#!forum/jaziku

3. Specific uses and applications

- Currently Jaziku is used for exploratory data analysis, to detect changes in the homogeneity of the time series and analysis of outliers

- Each month the maps of composite analysis results of climate module are used operationally to verify the response of precipitation under the observed conditions the El Niño phenomenon and these are used as the most likely scenarios for risk prediction (Fig. 2, A and B).

- Taking also the results of the composite analysis methodology of climate module, is possible to explore the influence of different climate variability phenomena for specific areas of interest, for example for the agricultural sector or areas of biodiversity protection

- Based on predicted probabilities of IRI models for the El Niño phenomenon and using the forecast module, each month is made a seasonal forecast of rainfall in Colombia (Fig. 2 C and D). These results add to other methodologies (dynamic models and analysis canonical correlation, for example).

- Currently is being explored the skill of the methodology for seasonal forecast of precipitation in Colombia.

4. Conclusions

- Jaziku has helped and facilitated the elaboration of exploratory data analysis, detection of teleconnections and seasonal forecast, so it becomes a tool for multiple applications

- Jaziku even being a young software and still developing, shows great methodological robustness, given the fact that it is based primarily on an existing methodology which has proved very useful in the climatology field.

- Is important for develop of the Jaziku software, to have feedback of its use in other institutions and users.

Acknowledgements. The authors express their gratitude to IDEAM and SIGOT for giving all information necessary for the development of this work, and to Gloria León Aristizabal (Met.), Franklyn Ruíz Murcia (McS. Phy.) and all professionals of the "Weather and Climate group" of IDEAM for their continued feedback and suggestions.

References

Montealegre J. E Bocanegra, 2009: Study of climatic variability of precipitation in Colombia associated with oceanic and atmospheric processes and large-scale meso: Final report of the activities carried out under contract to provide services in IDEAM 022-2009. Institute of Hydrology, Meteorology and Environmental Studies, IDEAM - Directorate of Meteorology, page 54.

Snow, J. W., 1976: The climate of northern South America. Climates of Central and South America, W. Schwerdtfeger, Ed., *Elsevier*, 295–403.

Wilks, D. S., 1995: Statistical methods in the atmospheric sciences: An introduction. *Academic Press*, ISSN 0127519653 9780127519654, 467 pp.

Science and Technology Infusion Climate Bulletin
NOAA's National Weather Service
38th NOAA Annual Climate Diagnostics and Prediction Workshop
College Park, MD, 21-24 October 2013

Developing a Framework to Incorporate Climate Information and Climate Change Projections in Water Planning for Texas

D. Nelun Fernando[1, 2, 3] and Rong Fu[2]

[1] *Visiting Scientist Programs, University Corporation for Atmospheric Research, Boulder, CO*
[2] *Department of Geological Sciences, Jackson School of Geosciences, University of Texas, Austin, TX*
[3] *Water Science and Conservation, Texas Water Development Board, Austin, TX*

1. Introduction

The report summarizes some key aspects of climate research designed and undertaken to support decision-making in the water planning sector in Texas. The research was carried out during a UCAR PACE (University Corporation for Atmospheric Research - Postdocs Applying Climate Expertise) postdoctoral fellowship where the PACE Fellow worked with the Texas Water Development Board (TWDB) and the University of Texas at Austin to improve current understanding of the predictability of flash droughts over the southern Great Plains and how climate projections could be incorporated in water availability modeling.

2. Water planning and drought management in Texas

Climate information is needed at two timescales for planning purposes. The first is the short-term timescale where drought information can be provided to the state Drought Preparedness Council [1]. The second is the long-term timescale feeding into the State Water Plan [2] that addresses water needs over the next 50 years within the state. This plan is updated every five years.

Given the magnitude and extent of the 2011 drought event over Texas and its rapid intensification over the late-spring of 2011, much emphasis was given to understanding factors that led to the drought taking on the characteristics of a "flash drought" and to developing a summer drought early warning indicator to support drought management through the Texas Drought Preparedness Council. The possibility for using climate information for long-term water planning was investigated at a purely exploratory basis because climate change projections are not, as yet, factored into water resources planning in Texas.

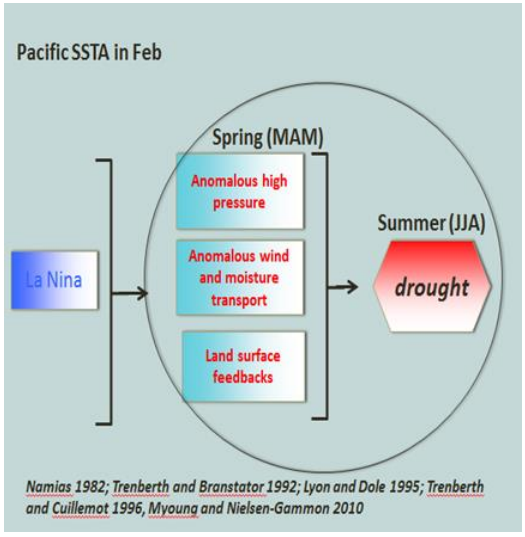

Fig. 1 Physical mechanisms known to drive summer drought over the US Great Plains.

3. Summer drought early warning indicator

"Flash" droughts refer to those droughts that intensify rapidly in spring and summer, coupled with strong increase of summer extreme temperatures, such as those that occurred over Texas in 2011 and the Great Plains in 2012. Climate models failed to predict these "flash" droughts in 2011 and 2012 and are ambiguous in projecting their future changes, largely because of models' weakness in predicting summer rainfall and soil moisture feedbacks. By contrast, climate models are more reliable in simulating changes of large-scale circulation and

[1] www.txdps.state.tx.us/dem/CouncilsCommittees/droughtCouncil/stateDroughtPrepCouncil.htm
[2] http://www.twdb.texas.gov/waterplanning/swp/index.asp

Correspondence to: D. Nelun Fernando, Department of Geological Sciences, Jackson School of Geosciences, University of Texas at Austin, Austin, TX 78712; E-mail: nelun.fernando@jsg.utexas.edu.

warming of temperatures during winter and spring seasons. Prior drought research based on observational data indicates that severe-to-extreme summer drought events over Texas are preceded by dry springs (Fernando *et al.*, 2013). Thus, we propose to develop and test a physical climate indicator of the risk of "flash" droughts in summer by using the large-scale circulation and land surface conditions in winter and spring based on observed relationships between these conditions and their underlying physical mechanisms established by previous observations and numerical model simulations (Figure 1).

Figure 2 shows a prototype drought indicator averaged over the US southern Great Plains (90-110˚W, 24-40˚W), indicating "flash" drought risk during June-August (JJA) based on climate information in April of each year for the period of 1951-2011. The prototype indicator was developed by regressing JJA percent normal rainfall with April geopotential height anomalies, the difference between April temperature at 700 hPa and April surface dewpoint, and the cumulative difference between precipitation and evaporation from November to April. The indicator (blue bars) generally match observed drought events in JJA, especially the multi-year strongest drought events, such as those in 1950s, mid-1960s and after 2006, especially 2011. The prototype indicator missed three summer drought events in 1978, 80 and 84. We find that the prototype process-based statistical model demonstrates considerable potential for an early warning indicator of summer flash droughts. This indicator is based on anomalous climate conditions and land surface characteristics in the spring.

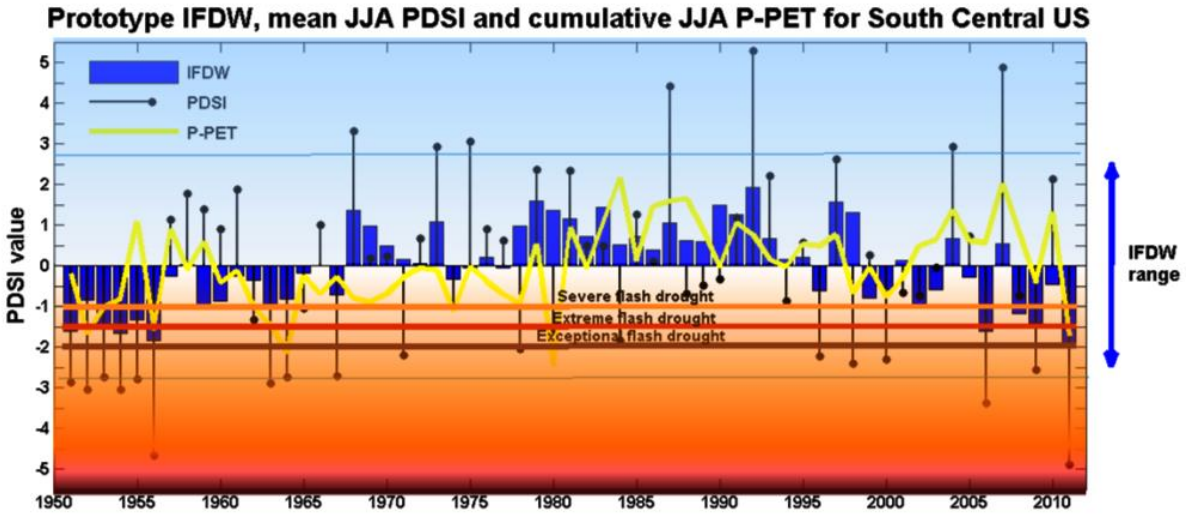

Fig. 2 Prototype drought hindcast (1951-2011) over the Southern Great Plains.

4. Climate information for long-term water planning

Surface water supply in Texas is heavily reliant on reservoir water storage. There are 176 reservoirs in the state representing approximately 70% of the water supply in the state. Water planning in the state of Texas comes under the aegis of the Texas Water Development Board. Water Availability Models (known as WAM) that use naturalized stream flow, pan evaporation and water rights as input to form the basis of water planning in the state. The WAM models are used to assess firm yield at all reservoirs in the state. Firm yield of a reservoir is the amount of water that can be supplied without system failure under a repeat of the worst drought conditions experienced by the state during the 1950s drought-of-record.

We approach the issue of how climate change might affect the availability of surface water by asking the question: "How might climate change affect the sensitivity of reservoir firm yield?" There is a mismatch between the information needs of WAM model users and the format in which climate change information is presently available. We propose a framework by which climate change projections could be incorporated into WAM models if, in the near future, the Texas Water Development Board is mandated by the Texas Legislature to incorporate climate change in water resource planning.

As the first step, we will explore the empirical relationship between naturalized flow in 14 rivers and rainfall over these river basins over the historical period. Second, we will explore the empirical relationship between pan evaporation and potential evaporation. Third, we will obtain ranges of possible naturalized flows and pan evaporation in the mid- and late-21st centuries using rainfall and evapotranspiration from the CMIP5 RCP4.5 and RCP8.5 projections and the empirical relationships obtained in steps 1 and 2. We will then use these ranges to estimate the sensitivity of reservoir firm yield in all 14 river basins. As a preliminary step, we applied the framework to the Brazos river basin using quadrangle precipitation and pan evaporation from the TWDB [3], potential evaporation from NCEP CDAS1 and naturalized flow at the outflow station of the Brazos. Naturalized flow refers to streamflow where anthropogenic influences on the river basin have been factored out. The outflow station is one of the control points at which naturalized flow is entered into the WAM model. We first aggregated all data to the annual time step and checked the annual naturalized flow and pan evaporation for normality. If they were non-normally distributed, we used a box-cox transformation to normalize the data. Next, assuming a linear relationship between precipitation and (normalized) naturalized flow and evaporation, we used linear regression analysis to derive the beta values for each parameter. We next obtained projected mean values of naturalized flow and pan evaporation over the Brazos basin for 2021-2050 using RCP4.5 and RCP8.5 projected rainfall and potential evaporation from the CCSM4 model.

References

Fernando, D. N., R. Fu, K. C. Mo, B. R. Scanlon, R. Solis, L. Yin, A. Bowerman, and R. Mace, 2013: Factors influencing the persistence of ENSO-led winter rainfall deficits into late-spring and early-summer over Texas. NOAA Climate Prediction Science and Technology Digest, January 2013, 103-106. http://issuu.com/climatesti/docs/37cdpwdigest.

[3] http://www.twdb.texas.gov/surfacewater/conditions/evaporation/index.asp

APPENDIX

Workshop Photos

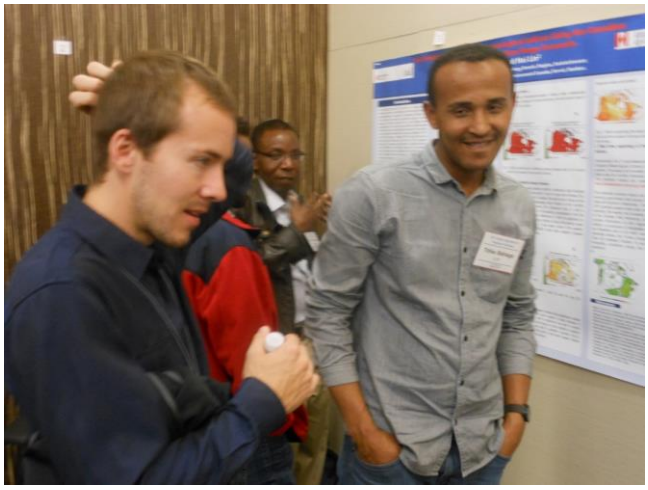

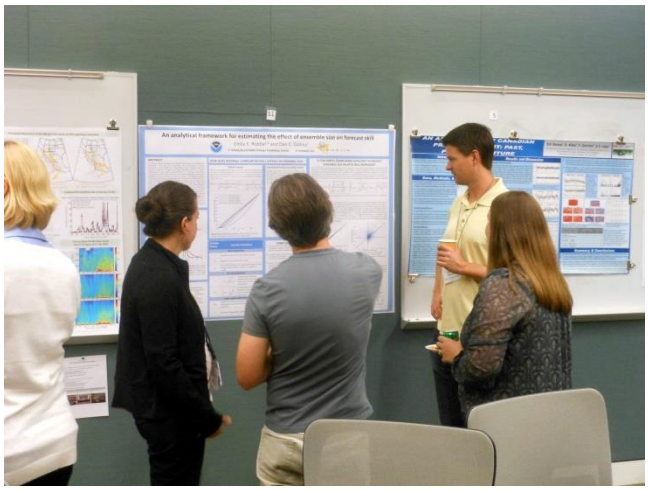

Workshop Photos

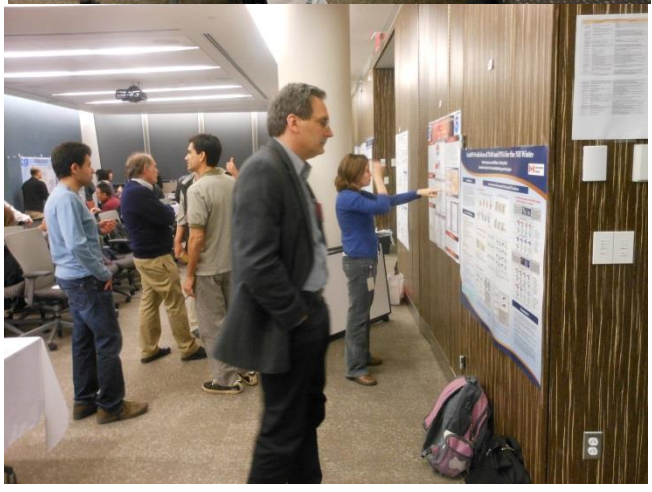

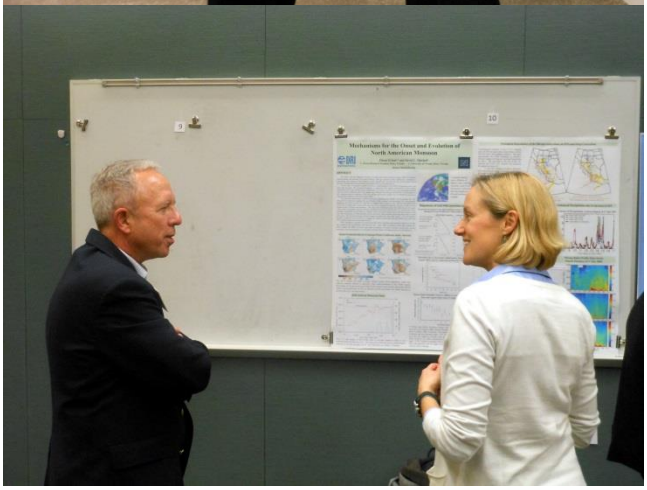

NWS Science and Technology Infusion Climate Bulletin

Featured Special Collections

(http://www.nws.noaa.gov/ost/climate/STIP/Collections.htm)

Climate Prediction Science and Technology Digest

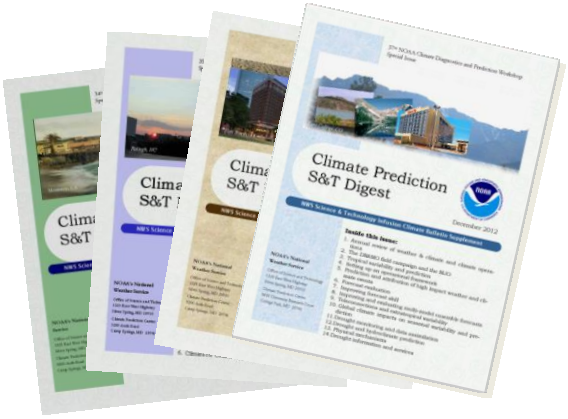

1. 37th Climate Diagnostics and Prediction Workshop
2. 36th Climate Diagnostics and Prediction Workshop
2. 35th Climate Diagnostics and Prediction Workshop
3. 34th Climate Diagnostics and Prediction Workshop
4. 33rd Climate Diagnostics and Prediction Workshop

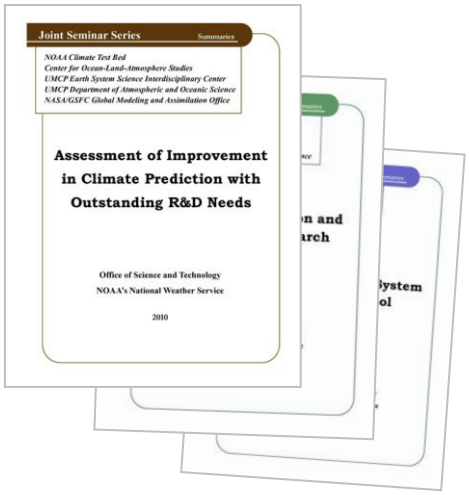

NOAA Climate Test Bed Joint Seminar Series Extended Summaries Collection Volume

1. Unified Modeling, Seamless Prediction and Integrated Services (2010-2011)
2. Assessment of Improvement in Climate Prediction with Outstanding R&D Needs (2009-2010)
3. Research to Operation and Operation to Research (2008-2009)
4. CFS as a Prediction System and Research Tool (2007-2008)

S&T Infusion Lecture Series & Notes

1. Notes about CPC's seasonal prediction
2. Uncertainty and Ensemble Forecast